The Catalytic Cycle of the Nucleotide-Binding Domain of the ABC-Transporter HlyB

Dissertation
zur Erlangung des Doktorgrades
der Naturwissenschaften

vorgelegt beim Fachbereich 14
der Johann Wolfgang Goethe - Universität
in Frankfurt am Main

von

Jelena Zaitseva

aus Moskau

Frankfurt (2005)
(D 30)

Vom Fachbereich………………………………………………………………….der

Johann Wolfgang Goethe - Universität als Dissertation angenommen.

Dekan : ...

Gutachter : ...

Datum der Disputation: ...

Fachbereich 14

der

Johann Wolfgang Goethe - Universität

Der Bewerber ...

hat heute das Promotionsverfahren im Fach

...

mit der Gesamtnote ...

abgeschlossen.

Die einzelnen Prüfungsleistungen wurden wie folgt bewertet :

Dissertation: ………………………………….

Disputation: ……………………………...

Das Recht zur Führung des Doktortitels wird nicht durch diese Bescheinigung, sondern erst durch die Aushändigung der Urkunde erworben.

Frankfurt am Main, den ...

(Siegel)

Der Dekan

(Unterschrift)

(Siegel der Universität)

Der Fachbereich ...

der

Johann Wolfgang Goethe - Universität

verleiht

Jelena Zaitseva

aus Moscau

den Grad eines Doktors der Naturwissenschaften

(Dr. phil. nat.)

im Fach 14

nachdem er in ordnungsgemäßem Promotionsverfahren

durch die Arbeit

The catalytic cycle of the nucleotide-binding domain of

the ABC-transporter HlyB

und eine öffentliche Disputation

seine wissenschaftliche Befähigung erwiesen hat.

Die Promotionsleistung wurde mit

(Gesamtnote)

beurteilt.

Frankfurt am Main, den (Datum der Disputation)

(Siegel)

Der Dekan

(Unterschrift)

The Catalytic Cycle of the Nucleotide-Binding Domain of the ABC-Transporter HlyB

by

Jelena Zaitseva

Submitted to the Institute of Biochemistry, the Johann Wolfgang Goethe-University of Frankfurt in partial fulfillment of the requirements for the degree of Doctor of Philosophy

Date

Summary

Nucleotide-binding domains (NBDs), roughly 27 kDa in size, are conservative components of the large family of ABC (ATP-binding cassette) transporters, which includes importers, exporters, and receptors. NBDs or ABC-ATPases supply energy for the translocation of a vast variety of substrates across biological membranes. Despite their hydrophilic sequence, many NBDs tend to aggregate and precipitate in solution upon isolation from the complete transporter. The conditions stabilizing an extremely labile NBD component of the *E.coli* HlyA transporter, HlyB-NBD, were developed. As a result, the pure highly concentrated enzyme was protected from precipitation for months that allowed screening of the unlimited crystallization conditions in the presence of different substrates and performance of the reproducible functional assays. HlyB-NBD was characterized in regard to its uncoupled ATPase activity, oligomeric state, and stability in solution. Comparative analysis of protein stability and ATPase activity in various buffers suggested an inverse relationship between the two. Kinetic analysis of ATPase activity revealed ATP-induced protein dimerization. Gel-filtration experiments with the wild type protein and H662A-mutant of HlyB-NBD provided further evidence of protein dimerization in the presence of ATP. The crystal structures in post- and pre-hydrolysis nucleotide-bound states of HlyB-NBD were determined at 1.6Å and 2.5Å resolution, respectively. While the hydrolytically deficient H662A mutant of HlyB-NBD was crystallized as a stable dimer in the presence of ATP or ATP-Mg^{2+}, with two nucleotide molecules sandwiched between the two monomers, the same protein was shown to be a monomer in the ADP-loaded state. The wild type protein failed to develop crystals with bound ATP, yet formed ADP-bound crystals identical to those of the H662A-mutant. The X-ray structures of HlyB-NBD in various states of the hydrolytic cycle and the functional studies of the enzyme have provided an opportunity to characterize enzyme-substrate complexes and protein-protein interactions between the NBD subunits in great detail. Comparison of the nucleotide-free, the ADP-, and the ATP-loaded states revealed oligomeric and conformational changes of the protein upon substrate binding and resulted in a molecular picture of the catalytic cycle. The correlated results of the structural and functional investigations of HlyB-NBD are discussed with relation to the mechanism of action of ABC transporters.

Acknowledgements

The completion of this dissertation would not have been possible without help and support of numerous people. First of all, I would like to thank my thesis adviser Robert Tampé. His generous invitation to visit Germany almost 5 years ago gave me a unique opportunity to see all the people in the lab and have informal conversations with them, to present my previous work and have a genuine scientific discussion with my future colleagues. I am also thankful to Robert Tampé for his support, his advice, and his guidance throughout the course of my stay at Frankfurt University.

I owe an enormous debt of gratitude to my co-adviser Lutz Schmitt, whose integral view on research, overly enthusiasm, stimulating suggestions, and encouragement helped me all the time during experimental work and writing of this thesis. I would also like to acknowledge Lutz Schmitt for his immense willingness to share his knowledge, skills, time, and his expertise.

I would like to express my sincere gratitude to Barry Holland for his seminal work on HlyB, who provided me with invaluable guidance and vital feedback on the project.

My special thanks go to Lutz Schmitt, Nils Hanekop, Alexander Wiedenmann, Robert Ernst, Robin Klemm, and Carsten Horn for their tremendous help with my adjustment to a new place, a new life style, and a new working environment. I am very grateful to Lutz and Nils, who always had time to help me with all the problems I encountered in my everyday life and science. I would also like to extend my gratitude to Renate Guntrum, Alexander Wiedenmann, Robert Ernst, Robin Klemm, and Stefan Jenewein for truly enjoyable atmosphere they fostered both in and out of the lab and for being my very good friends and the best colleagues I would ask for. I simply cannot put into words my appreciation of all of you, who made me feel truly home in a foreign country.

I would like to thank Christine Le Gal, Susanne Heintke, Martynas Gavutis, and Rupert Abele for their indispensable assistance with the thesis submission. I am also grateful to all other members of the group: Hans Bäumert, Gerhard Spatz-Kümbel, Eckhard Linker, Chris van der Does, Eva Janas, Christoph Kyritsis, Ramunas Valiokas, Stanislav Gorbulev, Silke Hutschenreiter, Min Chen, Chiara Presenti, Christian Kolbe, Karin Busch, Dirk Schaible, Claudia Detje, Joachim Koch, Jennifer Strunk, Matthias Hofacker, Meike Herget, Simone Gompf, Stephanie Becker, Peter Lamken, Suman Lata, Eva Jaks, Annett Reichel, Pia Müller, Gudrun Illig, Silke Beismann-Driemeyer. I want to thank you for many valuable and

Abbreviations

A_{280}	absorbance at 280 nm
ABC	ATP-binding cassette
ADA	N-2-Acetamidoiminodiacetic acid
ADP	adenosine-5'-diphosphate
AmoRe	Alliance for Mindanao Off-grid Renewable Energy, crystallization package for molecular replacement
AMP	adenosine-5'-monophosphate
AMP-PNP	adenosin-5'-[β, γ-imido]-triphosphate
ARP/warp	Automated Refinement Procedure for refining protein structures
ATP	adenosine-5'-triphosphate
2'-Br-ATP	2'-bromo-adenosine-5'-triphosphate
8-Br-ATP	8-bromo-adenosine-5'-triphosphate
ATPγS	adenosine 5'-[γ-thio]-triphosphate
CAPS	cyclohexylaminoethanesulfonic acid
CHES	3-[cyclohexylamino]-propanesulfonic acid
CHAPS	3-[(3-Cholamidopropyl)-dimethylammonio]-1-propane sulfonate
CNS	Crystallography and NMR System, a program designed to perform phasing, density modification, and refinement of macromolecules
DENZO	crystallographic program for auto-indexing, refinement and integration
DDM	dodecyl-β-D-maltoside
DNA	deoxyribonucleic acid
DTT	dithiothreitol
EDTA	ethylenediaminetetraacetic acid
EPMR	a program that finds crystallographic molecular replacement solutions using an evolutionary search algorithm
HEPES	N-2-Hydroxyethylpiperazine-N'-2-ethanesulfonic acid
Hly	haemolysin
HlyB-NBD	haemolysin B nucleotide-binding domain
HMW	high molecular weight
IR	isomorphous replacement
LDAO	lauryldimethylamine-N-oxide
MAD	multi-wavelength anomalous dispersion

MAR CCD	the MarCCD camera is 2D detector driven by a software running under linux (RedHat distribution)
MEGA-10	decanoyl-N-methylglucamide
MFP	membrane fusion protein
β-ME	β-mercaptoethanol
MERLOT	an integrated package of computer programs for the determination of initial models of crystal structures using the molecular replacement technique
MIR	multiple isomorphous replacement
MLPHARE	a program for maximum likelihood heavy atom refinement and phase calculation in multi-wavelength anomalous dispersion
MOSFLM	a program for visualization, indexing and integrating single crystal diffraction data from area detectors
MOLREP	automated crystallographic program for molecular replacement
MR	molecular replacement
MWCO	molecular weight cut-off
NBD	nucleotide-binding domain
NCS	non-crystallographic symmetry
O	a program for model building using electron density maps and model manipulation
OD_{600}	optical density of cell suspension at 600 nm
OG	octyl-β-D-glucopyranoside
OMP	outer membrane protein
PDB	protein data bank
PHASES	a package of computer programs designed to compute phase angles for diffraction data from macromolecular crystals
PIP	di-μ-iodobis(ethylenediamine)diplatinum (II)
Procheck	programs to check the stereochemical quality of protein structures in model analysis
R value	the standard crystallographic factor, which is simply the average fractional error in the calculated amplitude compared to the observed amplitude
RANTAN	direct method module for determination of heavy atom positions in a macro-molecule structure or to determine a small molecule structure
REFMAC	macromolecular refinement crystallographic program
rmsd	root mean square deviation
RSPS	a program to determine heavy atom positions from derivative difference Patterson maps in multiple isomorphous replacement
SAD	single-wavelength anomalous diffraction

SCALA   a program to scale together multiple observations of reflections and to merge multiple observations into an average intensity

SCALEPACK   a program designed for data merging and scaling

SDR   structurally diverse region

SDS   sodium dodecyl sulfate

SDS-PAGE   sodium dodecyl sulfate-polyacrylamide gel electrophoresis

SeMet   seleno-methionine

Sharp   Experimental phasing of macromolecular crystal structures

SHELXL   a program for structure refinement

SHELXM   a program for phase refinement and for position location of the anomalously scattered atoms in MAD experiments

SHELXS   a program for structure solution by Patterson and direct methods in crystal structure determination from single-crystal diffraction data

SIGMAA   a crystallographic program to improve Fourier coefficients using calculated phases

SIR   single isomorphous replacement

SIRAS   single isomorphous replacement with anomalous signal

Solve   an automated crystallographic structure solution for MIR and MAD

TAMM   tetrakis (acetoxymercuri) methane

TLS   TLS refinement - one of the approaches to model anisotropic displacements in macromolecular refinement program

TMD   transmembrane domain

TNP   2'(or 3')-O-(2,4,6-trinitrophenyl)-

TNT   a program package which is used to "refine" models of macromolecules

Tris-HCl   Tris-hydroxymethyl-aminomethane

Tricine   N- {Tris [hydroxymethyl] methyl}glycine

wt   wild type protein

Xfit   a map fitting and molecular modeling program to display or manipulate models and fit to electron density

Xheavyr   a program for refinement of the heavy atom positions by a systematic correlation search and phase calculation

Xhercules   a program to search for heavy atom sites by application of Patterson correlation

Single letter codes for amino acids were used.

Table of Contents

Chapter 1   Introduction

Chapter 2   Materials and Methods

**Chapter 3   Purification of HlyB-NBD and search for the conditions
supporting highly concentrated pure substrate-free protein in
solution**

Chapter 7 Functional characterization and ATP-induced dimerization of the isolated HlyB-NBD

Chapter 8   Conformational and oligomeric changes of HlyB-NBD within the ATP-hydrolytic cycle

Publications

Arising from work in this thesis

Zaitseva, J., Holland, I. B., and Schmitt, L. (2004). The role of CAPS buffer in expanding the crystallization space of the nucleotide-binding domain of the ABC transporter haemolysin B from *Escherichia coli. Acta Crystallogr D Biol Crystallogr 60*, 1076-1084.

Zaitseva, J., Jenewein, S., Jumpertz, T., Holland, I. B., and Schmitt, L. (2005). H662 is the linchpin of ATP hydrolysis in the nucleotide-binding domain of the ABC transporter HlyB. *Embo J 24*, 1901-1910.

Zaitseva, J., Jenewein, S., Wiedenmann, A., Benabdelhak, H., Holland, I. B., and Schmitt, L. (2005). Functional characterization and ATP-induced dimerization of the isolated ABC-domain of the haemolysin B transporter. *Biochemistry 44*, 9680-9690.

Zaitseva, J., Jenewein, S., Oswald, C., Jumpertz, T., Holland, I. B., and Schmitt, L. (2005). A molecular understanding of the catalytic cycle of the nucleotide-binding domain of the ABC transporter HlyB. *Biochem Soc Trans 33, part* 5, 990-995.

Hanekop, N., Zaitseva, J., Jenewein, S., Holland, I. B., and Schmitt, L. (2005). Molecular insights into the mechanism of ATP hydrolysis by the NBD of the ABC-transporter HlyB. *FEBS Lett.* In Press.

Zaitseva, J., Oswald, C., Jumpertz, T., Jenewein, S., Wiedenmann, A., Holland, I. B., and Schmitt, L. (2005). A structural analysis of hinges, springs, and inherent asymmetry required for functional activity of an ABC ATPase domain. *Manuscript in preparation*.

Index of Figures

Index of Tables

Chapter 1

Introduction

1.1. General mechanisms of transport across the cell membrane

Cells utilize a wide range of membrane transport mechanisms to obtain specific nutrients from the environment and to expel various molecules to the outside. The transport mechanisms fall into three major categories: passive diffusion, facilitate diffusion, and active transport. Passive diffusion allows molecules to freely pass the membrane. Facilitate diffusion utilizes specific membrane proteins to accomplish transport processes. Both diffusions depend on the concentration gradient developed between inside and outside of the cell and always proceed down the gradient. In the case of active transport, the transported molecules may be moved against their concentration gradient. This process requires energy, usually in the form of ATP, and a transmembrane carrier-protein. The energy may be used directly or indirectly. Primary active transporters directly utilize energy to cause conformational changes in membrane proteins (or protein complexes) leading to the transportation of the molecule through this protein. Secondary active transport uses energy to establish a gradient of ions (protons, sodium-ions) across the membrane, and then uses this gradient to pump the molecules in or out of the cell.

1.2. Secretion systems in Gram-negative bacteria

In order to interact with their host, pathogenic strains of *E.coli* need to secrete some virulence factors which can modify the metabolism of host cells, contributing to disease. Since *E.coli* is a Gram-negative bacterium, this secretion process involves the crossing of both the inner and the outer membrane. Gram-negative bacteria use mainly five secretion mechanisms called Type I, Type II, Type III, Type IV and Type V secretion systems (Figure 1) (China and Goffaux, 1999; Hueck, 1998; Lee and Schneewind, 2001;
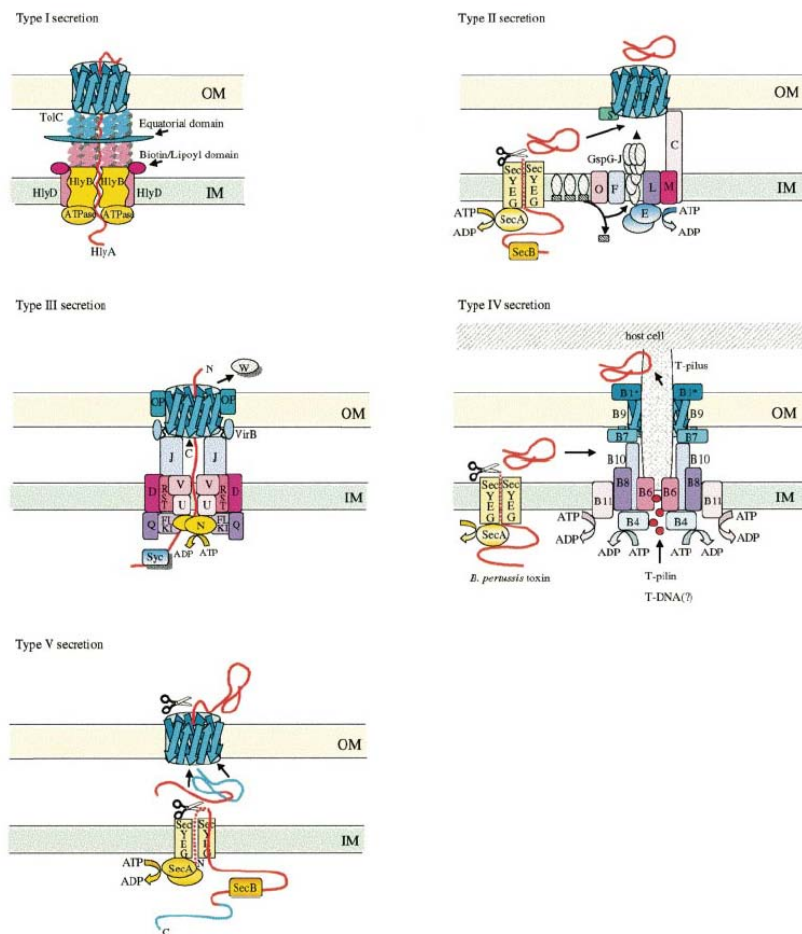
Figure 1. Main secretion mechanisms in Gram-negative bacteria
Drawing reprinted from (Sharff *et al.*, 2001).

Sharff *et al.*, 2001). All those types of secretion belong to the primary active transporters, utilizing energy of ATP. In the Type I secretion system (Koronakis and Hughes, 1996), the secretion machinery is composed of three proteins forming a channel through the inner and outer membranes. It is a one-step mechanism without periplasmic intermediate. The secretion signal is present in the C-terminal region of the secreted protein but without proteolytic cleavage. In *E.coli* the first discovered and the best-studied Type I secreted protein is haemolysin A (HlyA). In Type II and Type V secretion systems, the crossing of the inner membrane involves the Sec machinery with the cleavage of about 30 amino acid N-terminal hydrophobic sequence. The presence of such a signal sequence in the exported protein serves as an indication of the Sec-dependent transport. The crossing of the outer membrane involves the formation of a pore either by other proteins (Type II) or by the C-terminal region of the protein (Type V). Type II secretion systems are primarily used by Gram-negative bacteria for the secretion of extracellular degradative enzymes (Russel, 1998). Members of the IgA

proteases are secreted by Type V secretion pathway (Henderson and Nataro, 2001). The Type III secretion system involves at least 20 proteins including cytoplasmic, inner membrane and outer membrane proteins (Hueck, 1998). Most of the protein components are inner membrane proteins. This system is also Sec-independent, like the Type I pathway, and seems to not include distinct periplasmic intermediates of the secreted proteins. Yet, separation of the inner membrane export from the outer membrane secretion can be achieved by mutation of the outer membrane protein and results in accumulation of the transported protein in the periplasm (Charkowski *et al.*, 1997). The originality of this system is the ability to inject the secreted effector molecules into the cytosol of the host cells. Such a system is found in attaching and effacing *E.coli* and in diffusely adhering *E.coli*. The fourth mechanism of secretion is involved in conjugal transfer of plasmids, T-DNA transfer into the plant cells, and secretion of the protein pathogens. Although the virulence factors that are exported by these transporters can be either nucleic acid or protein, the general mechanism of transport appears to be similar for members of this family. Type IV transporters are Sec-dependent and produced by several bacterial pathogens such as *Agrobacterium tumefaciens*, *Bordetella pertussis*, *Helicobacter pylori* and *Legionella pneumophila*. (Burns, 2003; Christie and Vogel, 2000).

1.3. *Characterization of HlyA toxin from E.coli*

HlyA is a secreted protein virulence factor observed in certain uropathogenic strains of *E.coli* (Hacker *et al.*, 1983). The secretion process is mediated by the Sec-independent Type I mechanism. HlyA binds to and lyses mammalian cell membranes and, at lower concentrations, perturbs cell signal transduction and release of inflammatory mediators. It is one of a family of membrane-active toxins of similar mechanism. The family includes, among others, the leukotoxins of *Pasteurella* and *Actinobacillus* and the bifunctional adenylate cyclase hemolysin of *Bordetella pertussis* (Coote, 1992; Lobo and Welch, 1994; Menestrina *et al.*, 1994). These homologous toxins produced by Gram-negative bacteria are known as RTX (repeats in toxin) toxins. A repetitive glycine- and aspartate-rich nine amino acid sequence, the distinguishing structural feature for which the toxin family is named, creates a Ca^{2+}-binding motif. In HlyA there are between 11 and 17 such repeats (Stanley *et al.*, 1998). Binding of Ca^{2+} (one calcium ion per repeat) initiates formation of short β-strands organized
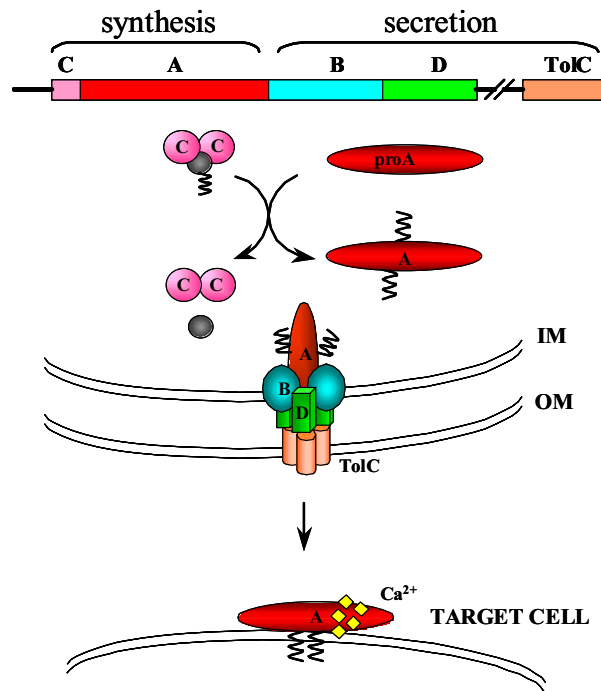
Figure 2. Haemolysin synthesis, maturation, and export by *E. coli*

IM, inner membrane; OM, outer membrane. The *hlyA* gene encodes inactive prohaemolysin, which is activated by HlyC. HlyA is secreted by a type I process. Ca^{2+} binds to the glycine-aspartate-rich repeats of the toxin externally before interacting with the mammalian membrane.

Drawing adapted from (Stanley *et al.*, 1998).

in an unusual "spring-like" structure called a parallel β-barrel or β-superhelix (Baumann *et al.*, 1993). Calcium binding is an absolute requirement for cytotoxic activity (Boehm *et al.*, 1990) and occurs outside bacteria following export.

The toxin arises from the expression of the *hlyCABD* gene cluster located on either the bacterial chromosome or the conjugative plasmids (Figure 2). The *hlyA* gene product is nontoxic prohaemolysin (proHlyA), which is converted intracellularly to mature toxin, HlyA, by the action of the *hlyC* gene product, HlyC (Nicaud *et al.*, 1985). HlyC is required for transfer of a fatty-acyl group from acyl-acyl carrier protein (acyl-ACP) to proHlyA, converting it to HlyA, which is secreted into the medium by the action of HlyB, HlyD, and TolC (Hardie *et al.*, 1991; Issartel *et al.*, 1991; Trent *et al.*, 1998). The nature of HlyC-dependent modification was shown to be an internal acylation of the ε-amino groups of lysine residues 564 and 690 of proHlyA , with saturated 14- (68%), 15- (26%), and 17- (6%) carbon

4

amide-linked side chains. Thus, HlyA activated *in vivo* consists of a heterogeneous family of up to nine different covalent structures (Lim *et al.*, 2000). Acylation is not essential for secretion of the toxin (Ludwig *et al.*, 1987). The possible role of the HlyA acylation is an increase in the affinity of a protein to a host membrane. Protein lipidation is also important in the regulation of protein-protein interactions, which could enhance interactions either between HlyA and components of a host signal transduction pathway to influence cytokine production or between HlyA monomers to bring about oligomerization during pore formation (Stanley *et al.*, 1998). The mechanism of cell lysis by HlyA is not clear. It has been shown that a HlyA toxin associated with the target membrane seems to occupy only one of the membrane phospholipid monolayers, i.e. it is not a transmembrane protein (Soloaga *et al.*, 1999).

1.4. HlyA transporter as a member of ABC protein superfamily

Secretion of the 107 kDa protein toxin HlyA in *E.coli* is mediated by a dedicated transporter utilizing ATP-binding and hydrolysis (Holland *et al.*, 2003; Juranka *et al.*, 1992; Koronakis *et al.*, 1995). This Sec-independent, Type I protein translocation machinery is composed of the outer-membrane porin-like protein TolC, the membrane-fusion protein HlyD, and HlyB, a member of the ABC (ATP-binding cassette) transporter family (Figures 2 and 3). HlyD and HlyB assemble a stable inner-membrane complex in the absence of TolC and
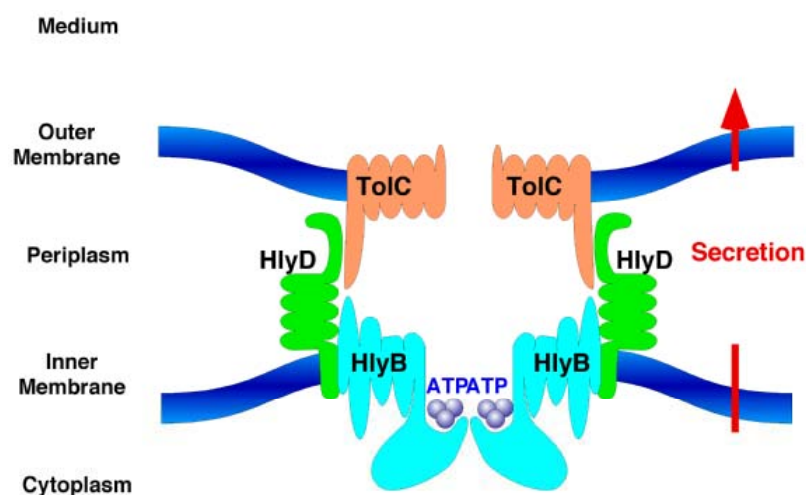
Figure 3. Schematic presentation of HlyA transporter
Drawing reprinted from (Holland *et al.*, 2003).

substrate. Both engage HlyA, inducing the inner-membrane complex to contact TolC, concomitant with conformational changes in all three exporter components. Protein complex assembly and substrate recruitment occur without ATP hydrolysis, by substrate-induced, reversible bridging of the inner-membrane translocase to the outer membrane export pore (Thanabalu *et al.*, 1998).

TolC and its homologues are the common outer-membrane components of a wide variety of efflux pumps that are involved in the export of chemically diverse molecules ranging from large protein toxins, such as HlyA, to small toxic compounds, such as antibiotics. TolC family members thus play important roles in conferring pathogenic bacteria with both virulence and multidrug resistance. These pumps assemble reversibly in a transient process that brings together TolC or its homologue, an inner-membrane-associated periplasmic component, an integral inner-membrane translocase and the substrate itself. TolC can associate in this fashion with a variety of different partners to participate in the transport of diverse substrates (Sharff *et al.*, 2001). The high resolution structure of TolC indicates that three TolC protomers assemble to form a continuous solvent-accessible 'channel-tunnel' over 140 Å long that spans both the outer membrane and periplasmic space (Figure 4) (Koronakis *et al.*, 2000). An alpha-helical transperiplasmic tunnel is embedded in the bacterial outer
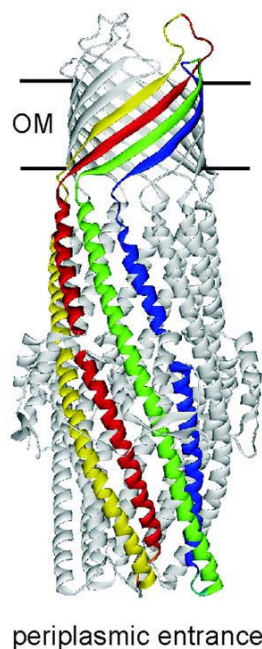
Figure 4. The structure of TolC (Koronakis *et al.*, 2000)
OM, outer membrane.
Drawing reprinted from (Andersen *et al.*, 2002)

membrane by a contiguous beta-barrel channel, providing a large exit duct for diverse substrates. The dense packing of the 12 tunnel-forming alpha-helices closes the periplasmic entrance of the pore, which can be re-opened by an 'iris-like' mechanism when recruited by substrate-engaged proteins in the cytosolic membrane (Andersen *et al.*, 2002; Koronakis *et al.*, 2001).

The inner membrane complex of HlyA exporter comprises a dimeric ATPase (HlyB) and the trimeric 478-residue adaptor protein (HlyD), which contacts TolC during substrate-triggered recruitment. **HlyD** has a large periplasmic domain (amino acid residues 81-478) linked by a single transmembrane helix to a small N-terminal cytosolic domain (1-59). This N-terminal region appears to play an important role in binding of HlyA and transduction of the substrate binding signal directly to the HlyD periplasmic domain to trigger recruitment of TolC and assemble the Type I export complex (Balakrishnan *et al.*, 2001; Pimenta *et al.*, 1999).

Haemolysin B (**HlyB**) is another inner membrane protein component of the haemolysin transporter, which belongs to the family of ABC transporters (Higgins, 1992; Higgins *et al.*, 1986). Composed of 707 amino-acid residues HlyB molecule represents a fusion of the N-terminal hydrophilic portion (amino-acids 1-150) followed by a hydrophobic transmembrane region (150-450) and the cytosolic C-terminal ATP-binding cassette. According to various topology prediction programs, the hydrophobic domain contains 5-7 membrane-spanning alpha-helices (SOSUI system (Mitaku); Tmpred (Hofmann and Stoffel, 1993); "DAS" - transmembrane prediction server (Cserzo *et al.*, 1997)) (Figure 5).

1.5. ABC-transporters

ABC (ATP-binding cassette) transporters are found in all organisms and compose one of the largest protein superfamily (Higgins, 1992; Higgins *et al.*, 1986). They participate in translocation of vast variety of substrates across the membrane. The size of the transported molecules (allocrites) varies from small molecules, such as ions, amino-acids and sugars, to large protein toxins, with their nature ranged from extremely hydrophobic to very hydrophilic. In prokaryotes and archaea ABC-transporters import or export their allocrites, while in eukaryotes they were identified only as exporters. Members of the ABC family play an important role in variety of physiological processes and have high medical relevance. In bacteria the members of the family are associated with virulence (Blight *et al.*, 1994), antibiotic resistance (Mendez and Salas, 2001) and nutrients uptake (Ames *et al.*, 2001;
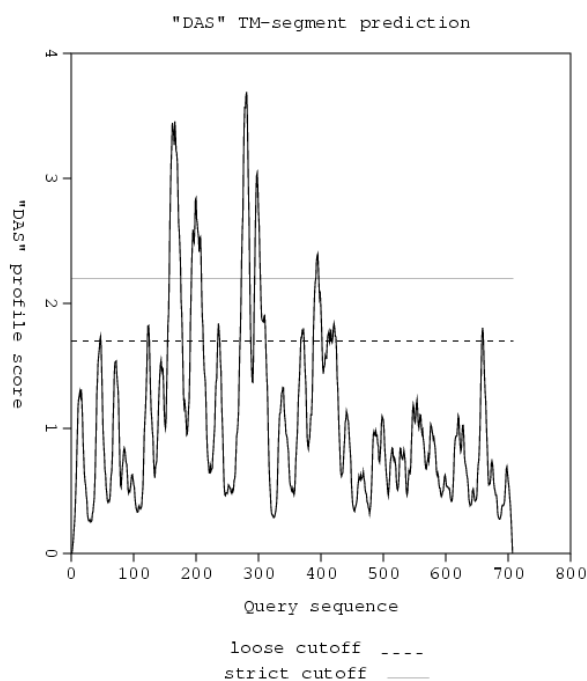
Figure 5. The DAS curve for HlyB (Cserzo *et al.*, 1997)

Dense Alignment Surface (DAS) method, predicting transmembrane segments in an integral membrane protein, is based on low-stringency dot-plots of the query sequence against a collection of non-homologous membrane proteins using a special scoring matrix.
TM, transmembrane.

Barroga *et al.*, 1996; Davidson *et al.*, 1992); in humans they are linked to many disorders, such as inherited retinal diseases (Biswas-Fiss, 2003; Sun and Nathans, 2001), cystic fibrosis (Annereau *et al.*, 2003; Csanady and Gadsby, 1999), suppression of the immune response (Abele and Tampe, 2004; Schmitt and Tampe, 2000) and drug resistance in cancer cells (Gottesman and Pastan, 1993; Kruh *et al.*, 2001; Litman *et al.*, 2001; Sauna *et al.*, 2001).

Typically ABC-transporters are composed of at least four modules: two soluble nucleotide-binding domains/subunits (NBD) or ABC-ATPases and two hydrophobic domains/subunits (Holland and Blight, 1999). ABC-domains provide energy for the substrate translocation, and membrane-spanning domains form the pathway for the specific substrate. Various combinations of those modules constitute the whole functional transporter. All four domains can be fused into single polypeptide (some eukaryotic transporters: MDR (Chang *et al.*, 1997) and CFTR (Riordan *et al.*, 1989)) or be represented by separate subunits (some bacterial transporters: HisQMP$_2$J (Ames *et al.*, 2001) and MalFGK$_2$E (Davidson *et al.*, 1992)). In some ABC transporters, however, domains can be fused to each other in a different manner: in the *E. coli* ribose transporter two fused NBDs form the energizing part of the complex (Barroga *et al.*, 1996); in *E. coli* and *A. pleuropneumoniae* iron-hydroxamate transporters the

8
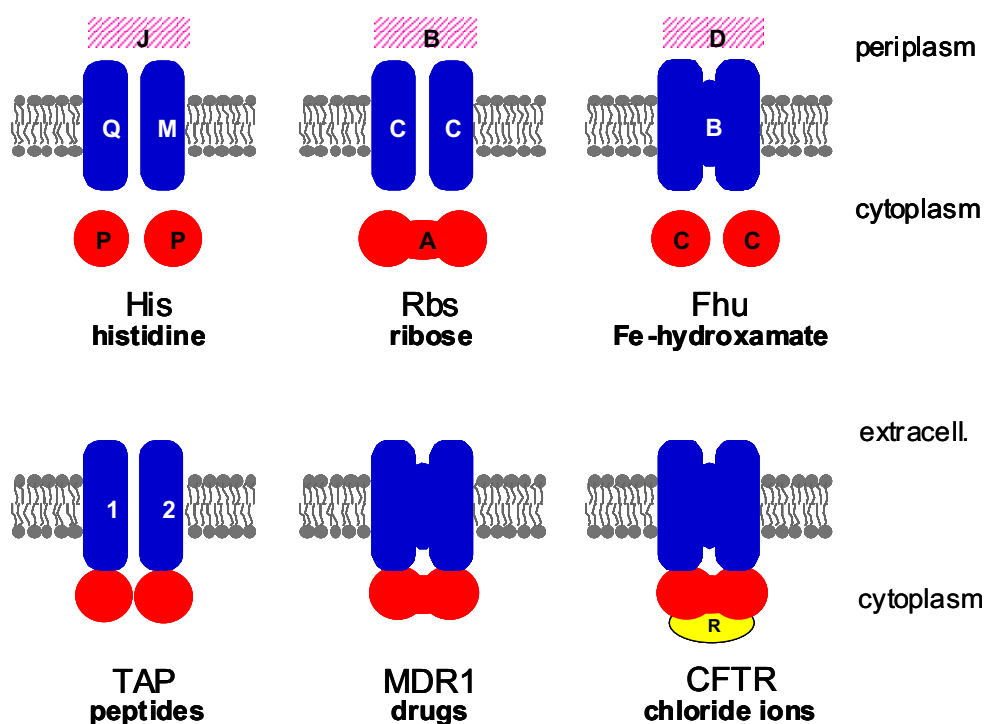
Figure 6. Composition of ABC-transporters

Blue, transmembrane components; red, NBDs; pink stripped, periplasmic substrate-binding proteins; yellow, regulatory subunit of CFTR. His, Rbs, Fhu, TAP, MDR, and CFTR correspond to a histidine, ribose, Fe-hydroxamate, Transporter Associated with antigen Presentation, MultiDrug Resistant protein and chloride channel protein Cystic Fibrosis Transmembrane Regulator transporters, respectively. The translocated substrates are indicated under the name of the transporter.

Drawing reprinted from (Schmitt and Tampe, 2000).

membrane components are combined into one protein (Groeger and Koster, 1998; Mikael *et al.*, 2002) in *Lactococcus lactis* LmrA and in *H. sapiens* TAP1/TAP2 a single polypeptide contains one transmembrane domain and one NBD (Poelarends *et al.*, 2002; Schmitt and Tampe, 2000) (Figure 6). By its structural organization, HlyB also belongs to this last group, which is called "half-size" ABC-transporters.

Transmembrane domains (TMD) presumably form a translocation pore in the membrane. They share little sequence similarity and are specific to every ABC-transporter, what makes the comparative analysis of the various membrane ABC-subunits challenging. Extreme hydrophobicity of these proteins/domains also hampers their functional and structural characterization. According to the hydropathy analysis the presence of 6-10 α-helical segments for each domain was predicted, making total of a 12-20 stretches for the transmembrane pore of the complete transporter. The common feature of the bacterial membrane-spanning subunits of ABC importers is a conservative 'EAA'-motif (EAA-X_3-G-

X_9-I-X-LP) in one of their predicted cytoplasmic loop, which most likely provides communication between NBD and TMD (Hunke *et al.*, 2000; Mourez *et al.*, 1997; Steinke *et al.*, 2001). Such loop may represent a general interface between ABC- and membrane-spanning subunits/domains (Locher *et al.*, 2002), since the local sequence similarities and the functional relevance between the 'EAA'-motif, the fourth intracellular loop of CFTR protein, and the first cytoplasmic loop in drug exporters exist (Cotten *et al.*, 1996; Currier *et al.*, 1992; Locher *et al.*, 2002). Significant variations in size and primary sequence of the membrane components presumably reflect their accommodations to the specific allocrite being translocated across the membrane.

In contrast to the TMDs, **nucleotide-binding domains** of different unrelated ABC transporters demonstrate significant sequence conservation (see Chapter 1.7).

To survive in the media with extreme low concentration of nutrients or other vital components, such as maltose, ribose, vitamin B_{12}, and iron, bacteria developed high affinity uptake systems that belong to the family of ABC transporters. These systems include additional protein constituents along with the core four domains, such as substrate binding proteins and specific outer-membrane receptors in Gram-negative bacteria. The former can be attached to the membrane of Gram-positive bacteria via lipid modifications at the N-terminus or freely diffuse in the periplasm of Gram-negative bacteria. While the cell surface receptors translocate allocrites across the outer membrane, the substrate binding proteins bind allocrites and deliver them to the specific membrane associated ABC-complexes. Maltose-, histidine-, and hydroxamate-uptake systems are the examples of the 'periplasmic binding protein dependent' ABC transporters in *E.coli* (Figure 6) (Davidson and Chen, 2004; Holland, 2003; Linton and Higgins, 1998).

1.6. *Structures of the full-length ABC-transporters*

Structures of four full-length ABC-transporters in the absence of nucleotides and substrates were reported recently. The first one, MsbA (a lipid A flippase) from *E.coli*, appeared to be very controversial (Chang and Roth, 2001) (Figure 7B). The protein structure was solved in the presence of non-ionic detergent n-dodecyl-α-D-maltoside at a resolution of 4.5 Å. MsbA is assembled as a homodimer with one transmembrane domain and one nucleotide-binding domain fused in each subunit. An additional intracellular domain bridging TMD and NBD was identified in MsbA (Figure 7 A, B). Each transmembrane domain is composed of 6 membrane-spanning α-helices, which is consistent with the prediction by
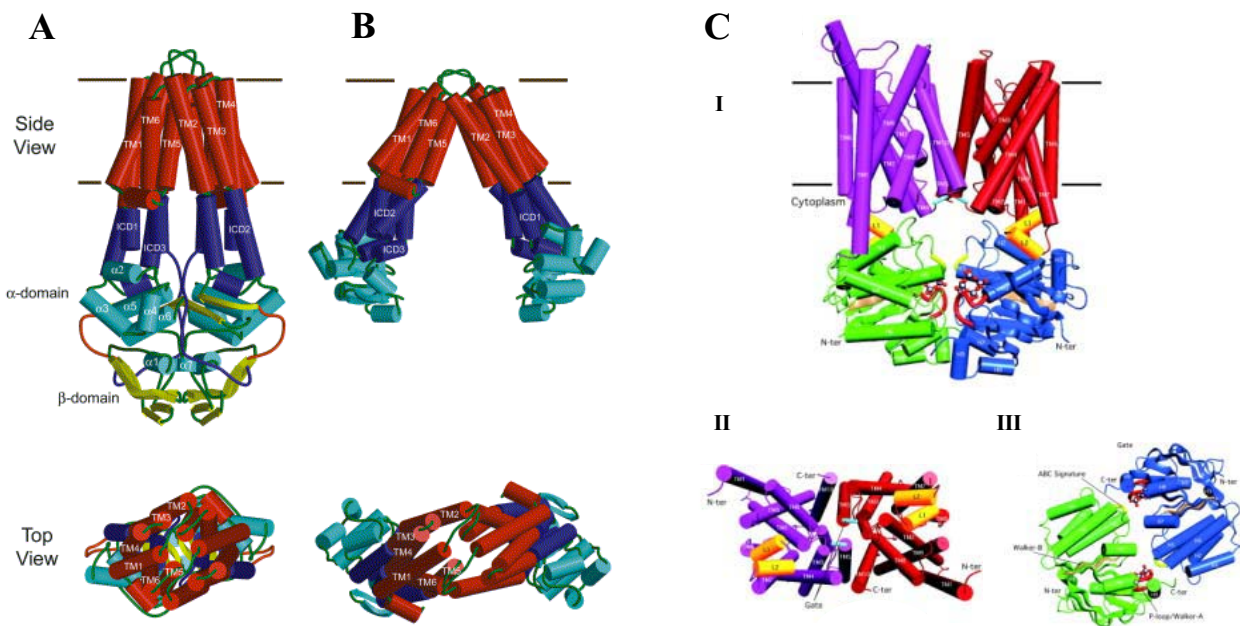
Figure 7. Structures of the full-length ABC transporters

Black lines indicate the approximate location of the cell membrane with periplasm above and the cytoplasm below the lines.

A. MsbA from *Vibrio Cholerae*: side view of homodimeric VC-MsbA and view from the extracellular side, perpendicular to the membrane. The transmembrane domain, intracellular domain, and nucleotide-binding domain are colored red, dark blue, and cyan, respectively. The transmembrane and NBD α-helices are indicated by cylinders and the connecting loops are shown in green. The loop connecting the α and β domains of the NBD is shown in orange. β-Sheets are drawn as ribbons and highlighted in light green.

B. MsbA from *E.coli*: the corresponding side and top views of the transporter.

C. Vitamin B_{12} transporter (BtuCD) from *E.coli* composed of 2 membrane-spanning BtuC subunits (purple and red) and 2 nucleotide-binding domains BtuD (bright green and blue). α-Helices are drawn as cylinders and β-Sheets as ribbons. The cyclotetravanadate molecules, located in the ATP-binding sites, are depicted in ball-and-stick. Cytoplasmic loop (yellow) of the membrane BtuC subunit folded into two short L1 and L2 helices interacts with BtuD. The gate region of the transmembrane part of the transporter is shown in light blue.

    I.   Side view of the transporter.
    II.   View onto the cytoplasmic face of the membrane BtuC subunits.
    III.   Bottom view onto NBD dimer from the same side as in II.

Drawing reprinted from (Chang, 2003) and (Locher *et al.*, 2002).

11

hydropathy analysis. Two tilted TMDs form a chamber with 25 Å opening to the cytoplasm. This unusually large chamber seems to be locked from the extracellular face of the membrane. The MsbA structure revealed a dimeric organization of the transporter and was somewhat similar to the low resolution structures of two eukaryotic ABC multidrug transporters, P-glycoprotein and MRP1 (Blott *et al.*, 1999; Rosenberg *et al.*, 1997). Yet, it didn't accommodate many existing experimental data and was not readily adaptable to the structures and mechanism of action of other ABC transporters. The apparent discrepancies include distantly located NBDs and the closed conformation of the chamber on the extracellular surface (Blott *et al.*, 1999; Bolhuis *et al.*, 1996; Loo and Clarke, 1996; Rosenberg *et al.*, 1997). The following structure of MsbA from *Vibrio cholerae*, solved in the presence of either dodecyl-β-D-maltoside or tridecyl-β-D-maltoside, differed from MsbA-*E.coli* in orientation of nucleotide binding domains and, according to the author, reflected the closed conformation of the transporter (Chang, 2003) (Figure 7A). One more X-ray crystal structure at 4.2 Å of MsbA from *Salmonella typhimurium* had just been published (Reyes and Chang, 2005), which expected to be in a post-hydrolysis state of transporter with ADP-Mg and vanadate bound in one of the two nucleotide-binding sites. Based on the structural studies of MsbA, it was postulated that NBDs undergo through the cycles of association and dissociation, pushing and pulling the corresponding transmembrane domains of ABC transporters during the transport cycle (Chang and Roth, 2001). A similar mechanism was suggested for other ATP-binding cassette transporters based on their structural and biochemical studies (Chen *et al.*, 2003; Davidson, 2002; Thomas and Hunt, 2001).

Another model was proposed as a result of the structural studies of an ABC transporter mediating vitamin B_{12} uptake, BtuCD (Locher *et al.*, 2002) (Figure 7C). The crystal structure at 3.2 Å resolution of the *E.coli* vitamin B_{12} full-length importer (solubilized in dodecyl-*N,N*-dimethylamineoxide) is composed of two ATP-binding cassettes (BtuD) and two membrane-spanning subunits (BtuC). The BtuC subunits provide 20 transmembrane helices grouped around a translocation pathway that is closed to the cytoplasm whereas the dimer-like arrangement of the BtuD subunits resembles the ATP-bound form of the Rad50 DNA repair enzyme. The two ABC cassettes bury only 740 $Å^2$ between them, which is rather small for a specific dimer contact surface. The buried interfaces between each pair of BtuC-BtuD subunits and between the two BtuC subunits are ~1500 $Å^2$ and ~1800 $Å^2$, respectively. At the center of the heterotetramer, below the predicted membrane surface and exposed to the cytoplasm, a giant water-filled channel crosses the flat face of the transporter. As a consequence, each subunit only contacts its two immediate neighbors and has no interface with the remaining,

diagonally positioned subunit. Since the BtuCD structure revealed two ABC domains directly contacting each other, the authors suggest an ATP binding to the shared interface between two ABC-subunits will induce their dimerization with ATP molecules sandwiched between the conservative Walker A and signature motives of the monomers. Based on the structures of nucleotide/substrate-free BtuCD and the dimeric ATP-bound states of the DNA repair enzyme Rad50, the isolated E171Q-MJ0796 ABC subunit (Smith *et al.*, 2002b) (Chapter 1.7) and MalK (Chen *et al.*, 2003) (Chapter 1.7) the common mechanism for all ABC importers and exporters was postulated, assuming direct coupling of ATP hydrolysis to the release of the substrate on the outside. In the case of importers, the `substrate' would correspond to the tightly attached binding protein, while the true substrate (translocated molecule / allocrite) would slip through the translocation channel in an earlier stage of the transport cycle. Exporters of hydrophilic molecules (such as antigenic peptides) may expose a substrate binding pocket where the water-filled, cytoplasmic channel between the four subunits is present in BtuCD (Locher, 2004; Locher and Borths, 2004).

The structure of BtuCD, which reconciles with the structural data for various NBDs (see below) and immense amount of biochemical knowledge, significantly contributed to our understanding of general architecture and subunit interaction in the family of ABC transporters (Locher *et al.*, 2002). However, lack of information on BtuCD structure in the presence of nucleotides and/or allocrites leaves many open questions regarding the mechanism of ATP-hydrolysis and coupling of ATPase activity to transmembrane transport of the allocrite.

1.7. *Nucleotide-binding domain, an energizing component of ABC transporters*

Nucleotide-binding components or ABC-ATPases, roughly 27 kDa in size, are very conservative components of the large family of ABC membrane proteins, which includes importers, exporters, and receptors. NBDs energize a translocation of vast variety of substrates (allocrites) across biological membranes. Molecules to be transported recognize their own transporter, bind and induce its conformational changes, resulting in activation of ATPase component, which in turn initiates opening of the transport pathway (Holland and Blight, 1999).

ABC-ATPases of different ABC-transporters contain highly conserved regions, such as the Walker A, the Walker B, the signature motif, a glutamine residue in the Q-loop, a histidine residue in the His-loop, and an aspartate residue in the D-loop (Figure 8). Despite their hydrophilic sequence, many NBDs readily associate with the membranes and demonstrate extreme instability in solution upon isolation from the complete transporter. Even though large quantities (at least few mg per liter of culture) of soluble NBDs can be overexpressed and purified by means of an affinity His-tag attached either to C-terminus or N-terminus, in many cases a problem emerges immediately after purification. Many isolated and purified ABC-domains tend to precipitate in solution, especially in the concentrations required for structural studies (Kerr *et al.*, 2003; Nikaido *et al.*, 1997; Smith *et al.*, 2002b).

A possible explanation for NBD instability in solution might be the disruption of native protein-protein interactions upon separation of the components from a fully assembled transmembrane complex. The protein instability makes crystallization as well as functional assays very challenging. Employment of some additives seems to improve the solubility of nucleotide-binding components after purification. To protect the ABC-constituent of the histidine permease (HisP) from precipitation, glycerol and ATP were added to the purified protein (Nikaido *et al.*, 1997). MJ0796 ABC from *Methanococcus jannaschii* formed amorphous precipitate in the absence of ADP-Mg^{2+} (Yuan *et al.*, 2001). It was found possible to resolubilize precipitated E171Q mutant protein of MJ0796 ATPase with 1M arginine-HCl (Smith *et al.*, 2002b). To increase the solubility of MalK, ABC of *Salmonella typhimurium* maltose transporter, octyl-β-D-glucopyranoside and dodecyl-β-D-maltoside detergents were successfully employed (Schmees *et al.*, 1999). However, the presence of ATP/ADP in protein solution could interfere with functional assays and hamper crystallization in the presence of other substrates. Detergents and high concentration of arginine, in general, could also cause complications in crystallization screens and a biochemical analysis of proteins. Due to the inherent unstable nature of the isolated HlyB-NBD, only freshly purified protein was available for crystallization, and its concentration had to be kept below a certain level. A similar effect has also been observed for other purified NBDs (Janas *et al.*, 2003; Kerr *et al.*, 2003). Thus, the problem of protein solubility sets serious limitations for the functional and structural analysis of isolated ABC subunits.

Availability of a stable protein solution at concentrations of 20 mg/ml and higher, in one of the common buffers and in the absence of detergents and substrates would be highly desirable for further studies of isolated NBDs. Such a stock solution would allow to greatly extend investigations of isolated NBD-domain, thus making it possible to test the interaction
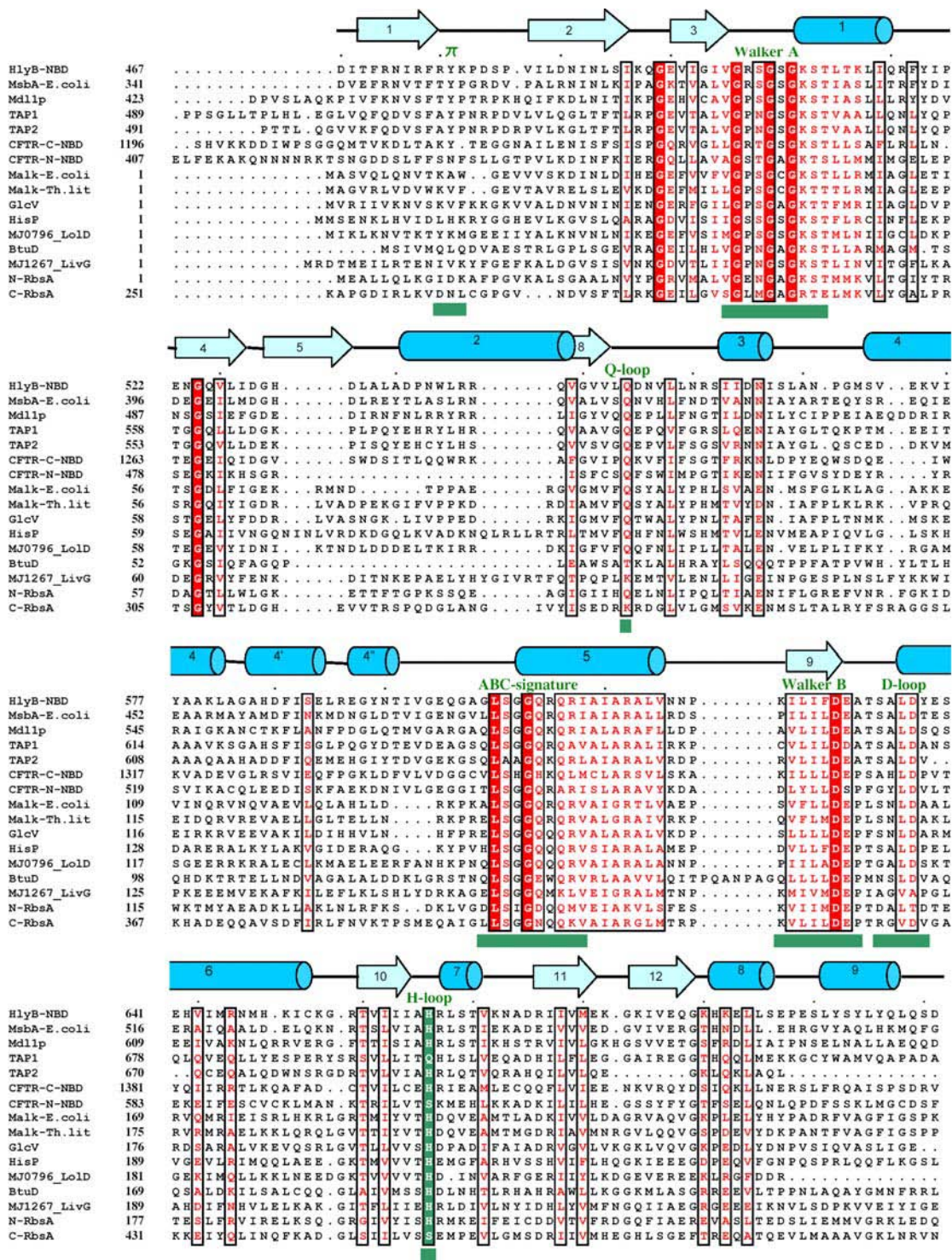
Figure 8. Sequence/structural alignment of HlyB-NBD with that of other ABC-proteins

The alignment was performed using ClustalW (www.ebi.ac.uk/clustalw). Important conserved motifs are underlined and indicated above the sequences in green. The conserved amino-acid residues designated by red color. Secondary structure elements derived from the HlyB-NBD structure (Schmitt *et al.*, 2003) are indicated above the sequence and named according to HisP nomenclature (Hung *et al.*, 1998). A conservative histidine, which was replaced by an alanine to produce H662A HlyB-NBD mutant protein, is highlighted in green.

of the protein with various substrates in numerous buffers with no limitation on protein concentration.

Isolated nucleotide-binding domains proved to be effective in determination of the detailed crystal structure of the ABC-ATPases of the transporters (Diederichs *et al.*, 2000; Gaudet and Wiley, 2001; Hung *et al.*, 1998; Karcher *et al.*, 2005; Karpowich *et al.*, 2001; Lewis *et al.*, 2004; Scheffel *et al.*, 2005; Schmitt *et al.*, 2003; Verdon *et al.*, 2003a; Yuan *et al.*, 2001). The crystal structure of NBD monomer is composed of three subdomains, an F1-ATPase like one, and two specific for ABC subdomains, one of them is predominantly α-helical and another a β-antiparallel sheet (Karpowich *et al.*, 2001) (Figure 9-I). However, the overall shape of an ABC-ATPase/domain is more convenient to represent by an L-shaped molecule with two arms (Figure 9-II, III). Arm I contains the conserved Walker A and B motives as well as the D- and the H-loop, arm II – the signature motif or C-loop, while the Pro-loop and the Q-loop are located on the interface between two arms (Hung *et al.*, 1998; Kerr, 2002; Schmitt *et al.*, 2003) (Figure 9). These studies have revealed remarkable structural conservation of various isolated NBDs despite huge diversity of translocated substrates (Schmitt and Tampe, 2002). That allows one to postulate a common mechanism of ATP-binding/hydrolysis for ABC transporters with different functions.

An important achievement in this area was determination of the crystal structure of ATPase subunits with bound nucleotides. Some of the NBDs were crystallized with ADP in the binding pocket (Gaudet and Wiley, 2001; Karpowich *et al.*, 2001; Verdon *et al.*, 2003a; Yuan *et al.*, 2001), visualizing the nucleotide-binding site of ATPases and a post-hydrolysis state of enzyme. Crystallization of the isolated NBDs with bound ATP/or pyrophosphate demonstrated dimerization of two ATPase subunits (Chen *et al.*, 2003; Diederichs *et al.*, 2000; Hung *et al.*, 1998; Smith *et al.*, 2002b) (Figure 10). While the nature of the obtained dimers in the protein crystals was questionable, dimerization of mutant NBDs was detected by many other techniques, such as fluorescence binding experiments (Smith *et al.*, 2002b), gel-filtration (Janas *et al.*, 2003; Moody *et al.*, 2002; Verdon *et al.*, 2003b) and analytical centrifugation (Moody *et al.*, 2002). Analysis of ATPase activity of the wild type NBDs also supported the notion of ATP-induced dimerization, although the complete functional dimerization has never been shown by ATPase assays (Janas *et al.*, 2003; Nikaido *et al.*, 1997). Functional interaction of two MalK monomers in result of ATP-hydrolysis was also detected with vanadate-catalyzed photocleavage experiments (Fetsch and Davidson, 2002). According to the majority of the collected biochemical data for ABC-components, the ATP-bound dimer structures of the isolated E171Q-MJ0796 ABC subunit (Smith *et al.*, 2002b) and
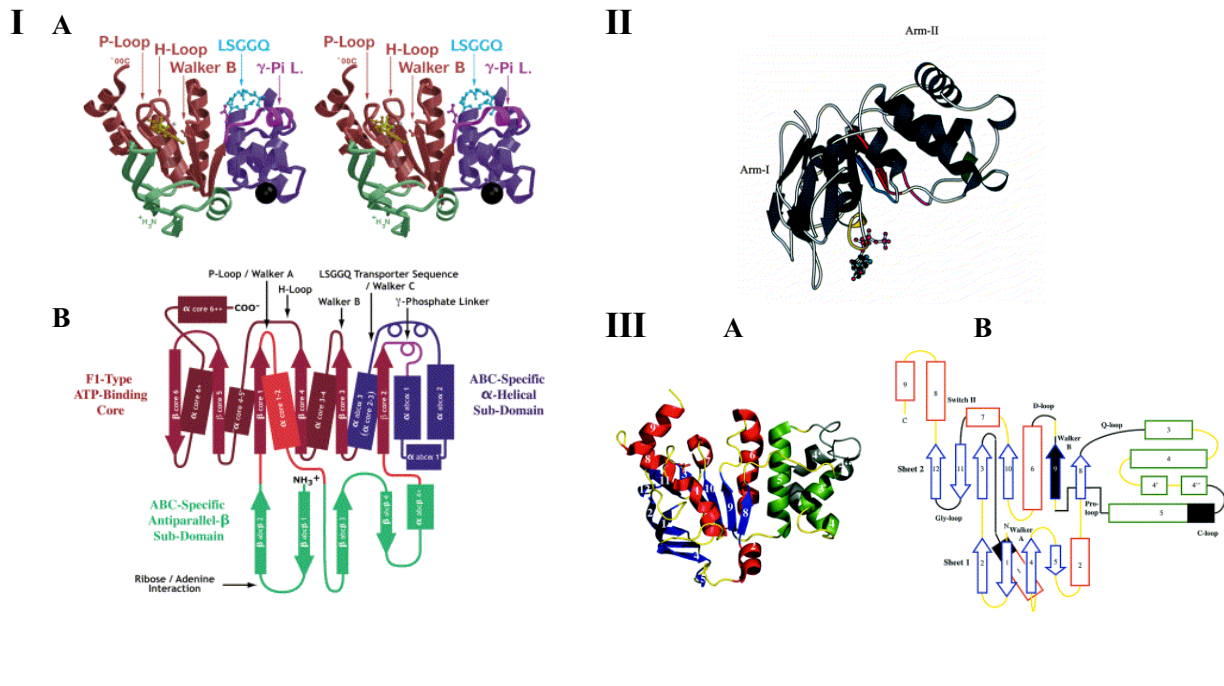
Figure 9. Structure and subdomain organization of a monomeric nucleotide-binding domain

I. MJ1267 ATP Binding Cassette protein. The F1-type ATP binding core subdomain is shown in red, the ABC subdomain-α is shown in blue, the ABC subdomain-β is shown in green (Karpowich *et al.*, 2001).

A. A stereo ribbon diagram with the "LSGGQ" transporter sequence (signature sequence) highlighted in cyan. A γ-phosphate linker (Q-loop) is colored in magenta. The base and the ribose of the nucleotide are shown in orange, the phosphates are shown in yellow, and the Mg^{2+} counterion is shown in gray. The black sphere represents the Hg used for phasing at the N109C position.

B. A topology diagram with the rectangles represents α-helices, the circles represent 3_{10} helices, and the arrows represent β-strands.

II. HisP (Hung *et al.*, 1998; Kerr, 2002). The figure is displayed with the program Molscript (Kraulis, 1991).

The two arms of the monomeric domain are indicated. α-Helices are shown as ribbons, and β-strands are displayed as arrows. Bound ATP is displayed in ball-and-stick format. The conserved NBD motifs are shown in yellow (Walker A), magenta (Q-loop), green (signature motif), red (Walker B), and blue (H-loop). Coordinates obtained from 1BOU dataset at the Protein Data Bank (Hung *et al.*, 1998).

III. **HlyB-NBD** with two domains/arms (Schmitt *et al.*, 2003). The α-helices and β-strands in arm I are colored red and blue, respectively. Arm II composed of α-helices is colored green. The loops are in yellow.

A. A ribbon representation of HlyB-NBD. The sulphate ion is shown in ball-and-stick representation.

B. Topology diagram with the conservative motives highlighted in black. The Walker B motif is extended and includes D-loop.
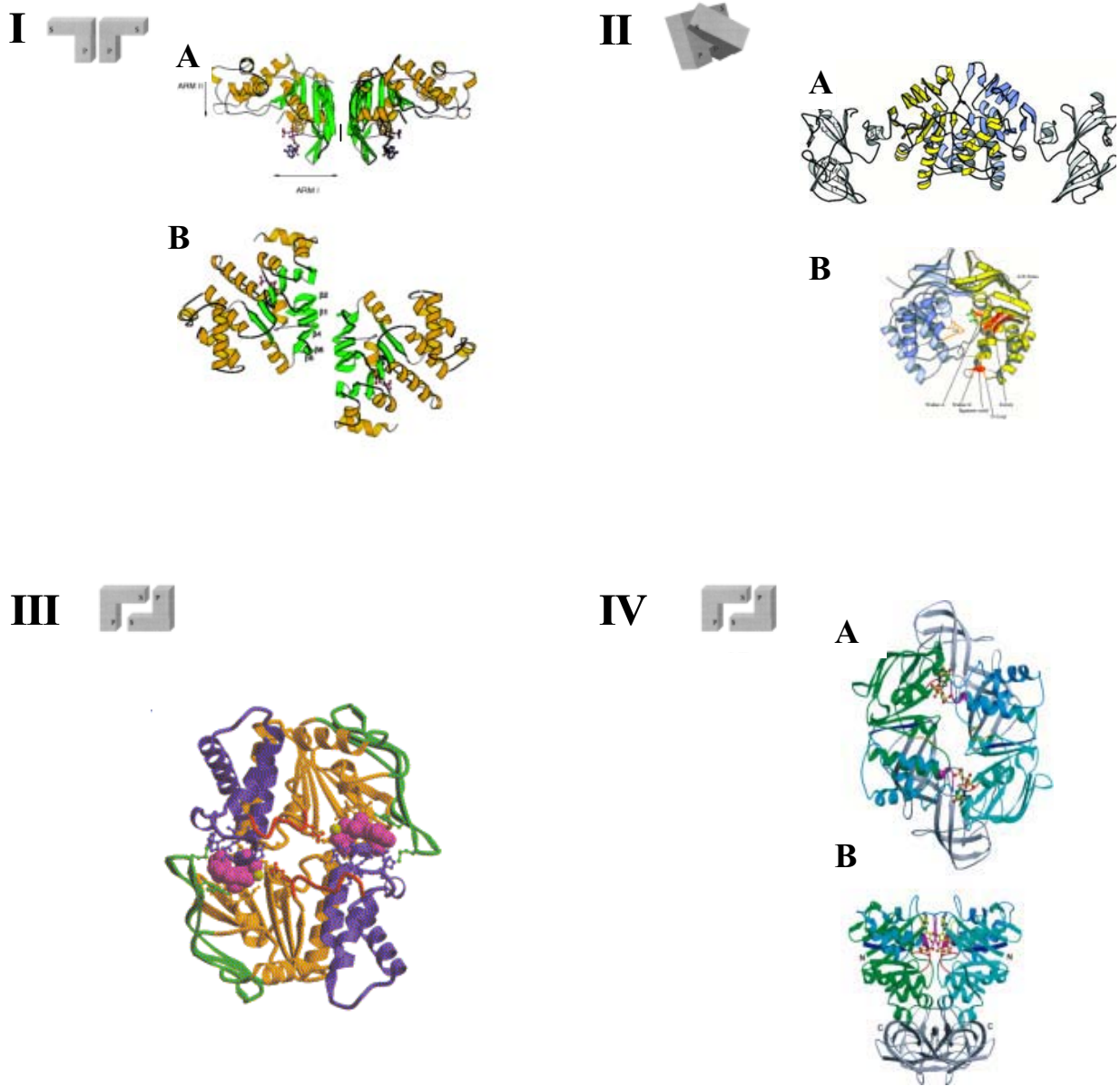
Figure 10. Ribbon presentations of the various dimeric NBD structures along with schematic representations of the NBD dimers (Kerr, 2002)

L-shapes represent the NBD, while 'S' and 'P' refer to the signature motif and the phosphate-binding loop (Walker A) respectively.

I. HisP with bound ATP from *Salmonella typhimurium* (Hung *et al.*, 1998).

II. MalK with bound pyrophosphate from *Thermococcus litoralis* (Diederichs *et al.*, 2000).

III. E171Q mutant of the MJ0796 ABC with bound ATP from *Methanococcus jannaschii* (Smith *et al.*, 2002b);

IV. MalK with bound ATP from E*scherichia coli* (Chen *et al.*, 2003).

Drawing reprinted from (Hung *et al.*, 1998), (Diederichs *et al.*, 2000), (Smith *et al.*, 2002b), (Chen *et al.*, 2003), and (Kerr, 2002).

MalK (Chen *et al.*, 2003) reflect the most functionally relevant dimeric structures along with the corresponding conformational changes in protein upon ATP-binding. The conservative glutamate in Walker B motif (E171 in MJ0796 ABC subunit, E504 in BmrA, and E631 in HlyB) was proposed to be a general catalytic base for ATP hydrolysis (Orelle *et al.*, 2003; Smith *et al.*, 2002b), yet, our work and mutational studies for some ABC transporters seem to not support this statement (Sauna *et al.*, 2002; Tombline *et al.*, 2004; Urbatsch *et al.*, 2000; Zaitseva *et al.*, 2005a).

1.8. *Motivations and aims of the thesis*

The overall aim of this thesis is to gain an insight into the mechanism involved in the activity of ABC transporters. Although many intensive studies of whole ABC-complexes and their isolated NBD-components were done (Davidson and Chen, 2004; Holland *et al.*, 2003; Kerr, 2002), we are still far from understanding their mechanism of action. A key aspect of the presented research is to obtain detailed structural information on the various intermediate functional states of one particular ABC protein, HlyB-NBD, and to characterize its complete cycle of ATP hydrolysis. At the moment, only single structural snapshots for the most structures of NBD components are available. Four ABC-ATPases were crystallized and their structures were solved in two or more intermediate states: MJ1267 ABC from *Methanococcus jannaschii* (nucleotide-free and ADP-Mg^{2+}-bound (Karpowich *et al.*, 2001; Yuan *et al.*, 2001)), MJ0796 ABC from *Methanococcus jannaschii* (ADP-Mg^{2+}- and ATP-bound (Yuan *et al.*, 2001; Smith *et al.*, 2002b), MalK from *Escherichia coli* (nucleotide-free and ATP-bound: (Chen *et al.*, 2003)), and GlcV from *Sulfolobus solfataricus* (nucleotide-free, ADP-Mg^{2+}- and AMP-PNP- Mg^{2+}-bound states (Verdon *et al.*, 2003a)). However, none of ABC-ATPase proteins provides enough structural knowledge to derive a complete ATP hydrolytic cycle for one NBD.

The research will resolve the following questions: (1) is the NBD dimer architecture a universal characteristic of all ABC transporters, importers, and exporters and why two NBD subunits are necessary for the transporter function, (2) what kind of conformational changes in the HlyB-NBD are associated with ATP binding/hydrolysis and protein dimerization, (3) what are the specific features of HlyB-NBD in terms of activity, stability in solution, and structural details, and (4) what are the common features of various NBD proteins? The study is also aimed at identification of the catalytically active amino acids in the active site of the

enzyme that will clarify the mechanism of ATPase activity / allocrite transport in ABC-transporters.

Previous genetic and biochemical studies of ABC-transporters demonstrated that all members of this family contain two NBD components, which serve as a molecular engine to power transport of various substances across the membrane. Yet, structural studies exhibited different dimer architectures for the NBD importers, raising question about the biological relevance of these dimers (Hung *et al.*, 1998; Diederichs *et al.*, 2000; Smith *et al.*, 2002b; Chen *et al.*, 2003). At the same time, no structural and functional information on dimerization of the isolated NBDs of ABC exporters was available. Thus, our other goal is to detect the functionally relevant dimerization of ABC subunits in a course of ATP binding/hydrolysis and confirm these studies with structural analysis.

Thus, the overall objective is to provide valuable data on the mechanism of ATP-hydrolysis and accompanying conformational/oligomeric alterations in the NBD component of ABC transporters and to aid in establishing a more accurate model for energizing the transport process in ABC-transporters. A combination of structural data with biochemical analysis in the work will supply important information that would significantly enhance our knowledge on ABC transporters, allow to interpret the functioning of various ABC transporters and to better understand the negative effects of ABC-transporter's mutations in humans.

Chapter 2

Materials and methods

2.1. Over-expression and purification of the wild type HlyB-NBD and its mutants

The construction of the pPSG122 plasmid carrying the *hlyB-NBD*-gene under control of arabinose-inducible promoter was described (Benabdelhak et al., 2005) (Figure 11).
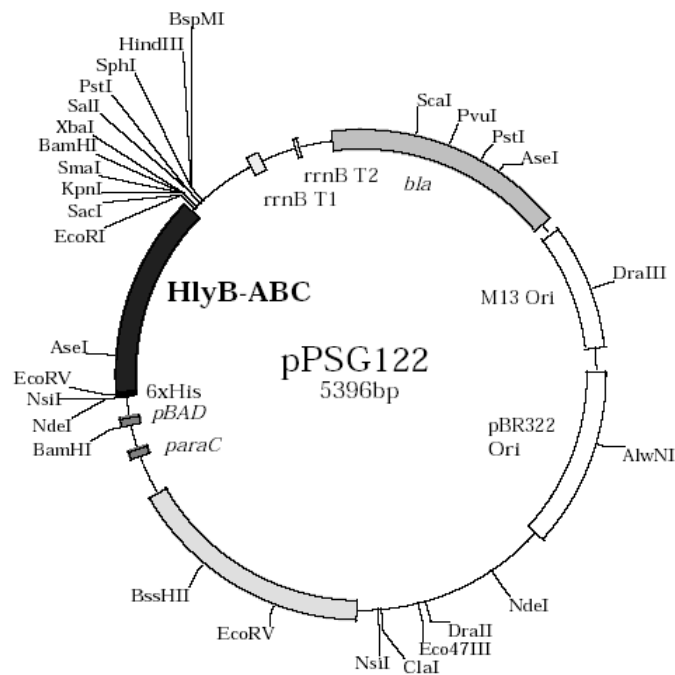
Figure 11. The pPSG122 plasmid (Benabdelhak *et al.*, 2005) for HlyB-NBD over-expression derived from the cloning vector pBAD-GFPuv (CLONTECH Laboratories, Inc. (Crameri *et al.*, 1996)).

The pPSG122 plasmid carries gene "bla" to produce beta-lactamase, which confers resistance of bacteria to ampicillin.

The *hlyB-NBD*-gene encodes the C-terminal ABC-domain of HlyB (D^{467}-D^{707}) with a 6-His-tag attached to the N-terminus of the protein, which is named either HlyB-NBD. The His-tagged 28 kDa HlyB-NBD protein was produced and purified as described (Schmitt et al., 2003) with some adjustments in order to improve protein yield and stability. Since every single step in a large-scale over-expression and purification proved to be essential for the quantity and quality of the produced proteins (Kerr et al., 2003; Wang et al., 2003), a detailed protocol of HlyB-NBD isolation for the structural studies is described below (Figure 12).

DH5α-cells freshly transformed with pPSG122 were grown overnight at 37°C in the presence of ampicillin (100 mg/L). The next morning new LB media with ampicillin was inoculated 1:100 with the overnight culture and grown at 37°C until an OD_{600} of 0.8 (about
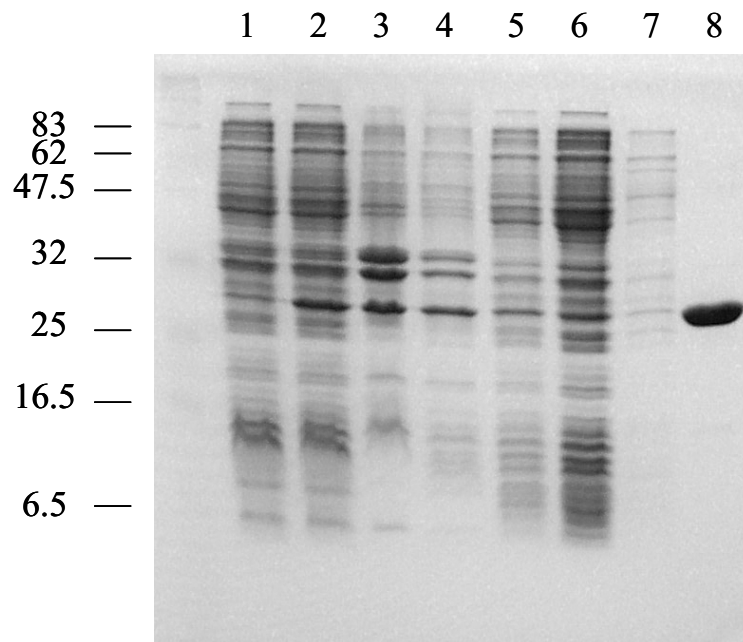
Figure 12. Over-expression of HlyB-NBD, its presence in various cell fractions, and main stages of HlyB-NBD purification from the soluble fraction.

Analysis was performed using 12.5% SDS-PAGE gels stained with Coomassie brilliant blue R-250. All samples were boiled in the SDS-loading buffer for 5 min. in the presence of β-ME. Cell fractionation was performed according to the method described in Chapter 2.1.

The molecular weight of the standard proteins in kDa is shown on the left. 1, whole cell extract before induction; 2, whole cell extract after induction; 3, inclusion bodies and cell debris; 4, membrane fraction; 5, soluble proteins; lanes 6-7, flow-through fractions from Zn^{2+}-chelating column (see Figure 13 for details); 8, pure HlyB-NBD

3 hours). The culture was further transferred to a 20°C-shaker. Over-expression of the protein was induced at an OD_{600} of 1.0-1.1 (30 min. after the transfer) by the addition of 0.002% L-arabinose. Cells were grown at 18°C for 3-5 h and then collected by spinning in a Sorvall RC 3C Plus centrifuge at 4°C for 30 min at 4500xg (H6000A rotor).

The following purification steps were performed at 4°C. Cells were resuspended in buffer A (25 mM sodium phosphate, pH 8.0, 20% glycerol, 100 mM KCl, 10 mM imidazole) and lysed by three passes through a French pressure cell at 16,000 psi. The lysed cell suspension was centrifuged at 42,000 rpm (125,000xg) for 1-2 h in a Beckman L-70 ultracentrifuge (70Ti rotor) to pellet unbroken cells, cell debris, protein inclusion bodies, and membranes. The clarified supernatant, obtained from 2 L of culture, was applied onto a Zn^{2+}-charged 5ml-Chelating Hi-Trap column (Pharmacia) that had been equilibrated with buffer A. The column was further washed with approximately 20 CV (100 ml) of the same buffer. The protein was eluted with a linear gradient of imidazole (10-300 mM) in buffer A (30 CV, total volume 150 ml) (Figure 12, 13). Fractions with pure HlyB-NBD were combined and concentrated to 1-1.5 ml with an Amicon Ultra-15 Centrifugal Filter Unit (10,000 MWCO).

A Hi-Load 16/60 Superdex 200 column (Pharmacia) was equilibrated with buffer B (10 mM CAPS-NaOH, pH 10.4, 20% glycerol). The protein after metal-ion-chelating purification, concentrated by ultrafiltration, was loaded onto the gel-filtration column. A major peak was eluted with Buffer B at about 80 ml, which corresponded to the monomeric size of protein (Figure 14). Fractions with pure HlyB-NBD were combined and concentrated to 1-5 ml (about 5 mg/ml protein) with an Amicon Ultra-15 Centrifugal Filter Unit (10,000 MWCO). In some cases visible protein precipitation started at this point. Adjustment of CAPS concentration and pH to 100 mM and 10.4, respectively, was necessary to stabilize the protein solution and was accomplished by the addition of 0.5 M stock solution of CAPS pH 10.4. A completely clarified sample was further concentrated to 20-50 mg/ml. This HlyB-NBD solution in 100 mM CAPS-Na-buffer pH 10.4 and approximately 16% glycerol was directly used for crystallization trials or exchanged into buffer with lower CAPS content immediately before crystallization (Chapter 4.1). The typical yield was about 7-10 mg of the purified and homogeneous HlyB-NBD from 1 L of cell culture.

The quality of protein was routinely estimated by SDS-PAGE (Laemmli, 1970). In order to visualize S-S-dimer formation, if any, and to separate the monomer and dimer species on SDS-PAGE, samples of fractions after gel-filtration were not heated in SDS-PAGE sample buffer, neither β-Mercaptoethanol (β-ME)/Dithiothreitol (DTT) was added at that step (for SDS-PAGE see also Chapter 2.5). Protein concentration was determined by ultraviolet
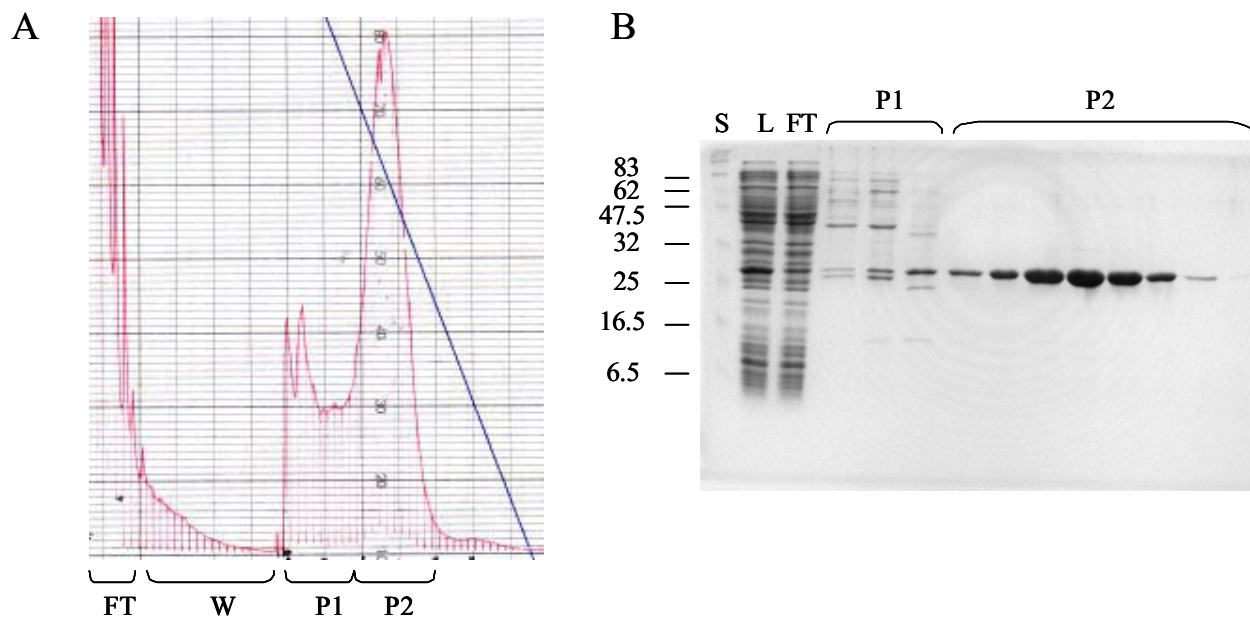
Figure 13. HlyB-NBD purification on a Zn^{2+}-Chelating Hi-Trap column (Pharmacia)

S, molecular weight standard, kDa; L, the sample loaded on the column (supernatant after ultracentrifugation); FT, flow-though; W, washing unbound proteins; P1, the first protein peak eluted with a linear (10-300mM) imidazole gradient from the column; P2, second protein peak eluted by imidazole gradient from the column.

A. Elution profile of protein monitored by the absorbance at 280nm

B. SDS-PAGE analysis of the corresponding column fractions stained with Coomassie brilliant blue R-250. All samples were boiled in SDS-loading buffer for 5 min. in the presence of β-ME.
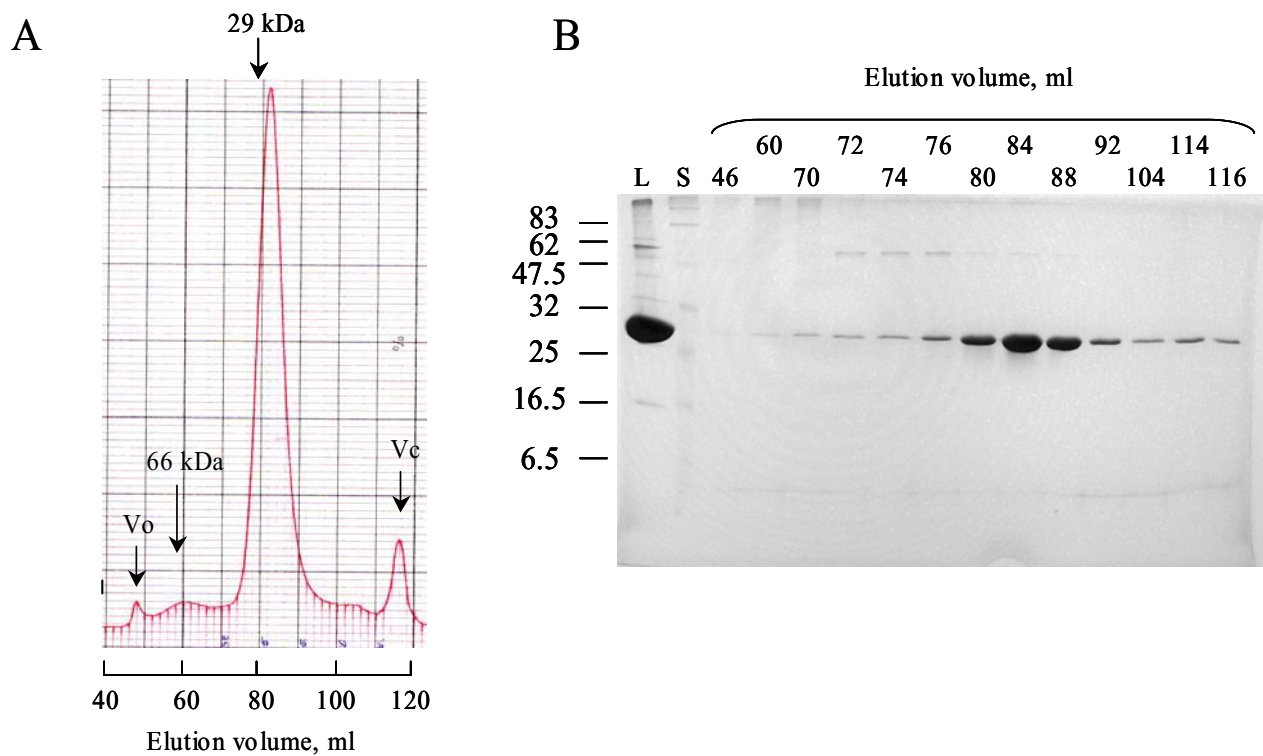
Figure 14. HlyB-NBD purification on a Hi-Load 16/60 Superdex 200 column (Pharmacia Biotech)

A. Elution profile of protein monitored by the absorbance at 280nm. Vo, the void volume; Vc, the column volume; 66 kDa, elution volume of the standard protein BSA; 29 kDa, elution volume of the standard protein carbonic anhydrase.

B. SDS-PAGE analysis of the corresponding column fractions stained with Coomassie brilliant blue R-250. All samples were mixed with SDS-loading buffer without further treatment (no boiling, no β-ME). L, the sample loaded on the column (combined and concentrated fractions after chelating column); S, molecular weight standard, kDa; the numbers 46-116 represent the column fraction number, equivalent to the elution volume, ml.

absorbance at 280 nm (molar extinction coefficient 15,400 M^{-1} cm^{-1} (Stoscheck, 1990)) and by the BCA protein assay (Smith et al., 1985; Wiechelman et al., 1988).

The same procedure was utilized for purification of HlyB-NBD H662A- and E631Q mutant proteins. The H662A protein was over-expressed from pPSG122 plasmid modified by site-directed mutagenesis (Benabdelhak et al., 2005). To generate the E631Q mutation plasmid pPSG122 was used as a template. The mutation was introduced using the ligase chain reaction (LCR) according to the protocol of the manufacturer (Stratagene). After successful amplification, a plasmid encoding HlyB-NBD E631Q was transformed into DH5α cells and sequenced to confirm the correct mutation.

2.2. Optimization of the soluble HlyB-NBD over-expression

Various modifications of the protein over-expression protocol were employed to optimize the yield of soluble HlyB-NBD. Variations included:
- Bacterial strains: DH5α and BL21DE3;
- Growing the pre-culture from freshly transformed bacterial colonies and from the colonies stored on LB-ampicillin-plates in a refrigerator up to 1 month;
- Growing pre-culture and the preparative batch at various temperatures ($+18^{o}C$ - $+37^{o}C$);
- Starting points of protein induction with arabinose, OD_{600} (0.6-1.6);
- Inductor concentrations (0.002% - 0.06);
- Induction times (1 hour – overnight).

The bacterial culture with over-expressed HlyB-NBD was pelleted in a Sorvall RC 3C Plus centrifuge at 4°C for 25-30 min at 4500xg (H6000A rotor,). Cells were resuspended in buffer A and lysed by three passes through a French pressure cell at 16,000 psi. The lysed cell suspension was centrifuged at 28,000 x g for 30 min. at $4^{o}C$ to pellet unbroken cells, cell debris and protein inclusion bodies. The clarified supernatant was transferred to the ultracentrifuge tube. The membrane fraction was pelleted at 110,000xg - 125,000xg for 1-2 hr. at $4^{o}C$ in Beckman L-70 ultracentrifuge. The supernatant after ultracentrifugation represents the soluble protein fraction.

The most optimal protocol for over-expression of the soluble wild type HlyB-NBD is described above in Chapter 2.1. Figure 12 represents a typical cell fractionation of the

bacterial culture resulting this protocol and general scheme of HlyB-NBD purification, both assessed by SDS-PAGE.

2.3. Over-expression and purification of the SeMet substituted HlyB-NBD H662A protein

The pPSG122 plasmid carrying H662A-mutation in *hlyB-NBD*-gene (Benabdelhak et al., 2005) was transformed into BL21 (DE3) cells[1] that are not auxotrophic for methionine. To overcome the problem of methionine incorporation, of methionine biosynthesis, and of slow growth due to the presence of toxic SeMet, the following precautions were undertaken. A freshly transformed single colony was grown at 37°C in 100 ml LB media in the presence of ampicillin (100 mg/L) for 6 hours until an OD_{600} of 0.3-0.4. Cell culture then was collected by centrifugation at 4°C for 10-15 min. at 4500xg. The cell pellet was stored overnight at 4°C. The next morning the cell pellet was resuspended in 2 ml of minimal media and inoculated into pre-warmed 2 L of minimal media. Minimal media contained 1x M9 salts supplemented with 0.8% glycerol, 2 mM $MgSO_4$, 40 µg/ml ampicillin, 0.1 mM $CaCl_2$ and 10 µg/ml thiamine (5x stock solution of M9 salts included 42.5 g Na_2HPO_4-$2H_2O$, 15 g KH_2PO_4, 2.5 g NaCl, 5 g NH_4Cl, and H_2O in 1 L volume). For the most optimal growth and aeration the culture was grown in four 2-liter flasks, 0.5 L of culture per flask, at 37°C for 7.5-8 h to an OD_{600} of 0.5-0.6. Then culture was transferred to 18°C shaker for the further growth and simultaneous cooling. A mixture of L-amino acids was added after 30 minutes [per liter of culture: 60 mg of L-SeMet (or 120 mg L- and D-SeMet) as 10 mg/ml solution, 50 mg each of leucine, isoleucine, and valine as 10 ml of a 5 mg/ml solution and 100 mg each of lysine, threonine, and phenylalanine as 10 ml of a 10 mg/ml solution]. After another 15 min., protein expression was induced by the addition of 0.002% arabinose and the culture was grown overnight at 18°C.

The first purification step on a metal-chelating column was performed as described for the non-substituted protein. For the successful crystallization of SeMet HlyB-NBD H662A in the presence of ATP, the protein required a gel-filtration step being modified according to the procedure described below. Combined and concentrated fractions (6-7 mg protein in 0.4-0.5

---

[1] An attempt to express and overproduce SeMet-substituted protein in DH5α-cells was not successful.

ml obtained from 2 L of culture) after a Zn^{2+}-charged 5ml-Chelating Hi-Trap column (Pharmacia) were twice diluted with gel-filtration buffer C (50 mM malonate pH 5.6, 20% glycerol, 100 mM sodium acetate), then ATP and ß-ME were added to the final 2 mM and 10 mM concentrations, respectively. After overnight incubation on ice the protein was subjected to the chromatography on a Hi-Load 16/60 Superdex 200 column (Pharmacia Biotech) equilibrated with gel-filtration buffer C. Fractions with HlyB-NBD H662A were combined and concentrated to 1.5-2 ml (about 3 mg/ml protein) with an Amicon Ultra-15 Centrifugal Filter Unit (10,000 MWCO). Then ATP and ß-ME were added to the concentrated protein to 2 mM and 2-5 mM concentrations, respectively. A typical yield was 3-4 mg of protein per liter of cell culture.

2.4. Drop assay for protein stability

HlyB-NBD was purified by Zn^{2+}-chelating chromatography and concentrated to 1-2 mg/ml in the previously used elution buffer, 20 mM Tris-Cl, pH 8.0, 100 mM KCl, about 150 mM imidazole (Kranitz et al., 2002). 1-2 µl of freshly purified protein with tracing amount of precipitation was mixed with 1-2 µl of the tested solution on a microscope glass slide at the room temperature. The immediate effect of the added component was inspected with a light microscope and monitored for several minutes. Changes in the turbidity of protein solution were qualitatively assessed.

2.5. Stability screening for extended time

To check the long-term stability of HlyB-NBD, a slight modification of the droplet assay was performed in microtiter plates and by micro-dialysis. Promising solutions, selected by the droplet assay, were mixed in a 1:1 ratio with the protein (50-100µl of 1 mg/ml) in wells of microtiter plates and incubated at various temperatures for a few days. Changes in the turbidity of the tested samples were monitored by absorbance at 600 nm.

Alternatively, protein stability was tested by micro-dialysis. 50-100 µl of 1 mg/ml HlyB-NBD were dialyzed against the chosen buffer at 4°C overnight. The degree of precipitation in the samples was qualitatively assessed and compared to the control (the initial protein dialyzed against 20 mM Tris-Cl, pH 8.0, 100 mM KCl, 150 mM imidazole).

The final protein solutions were analyzed by SDS-PAGE (Laemmli, 1970). The samples were diluted with SDS sample buffer and loaded onto 12.5-14% SDS polyacrylamide gel. The same samples were compared after heating at 100°C for 5 min. with 200 mM β-ME and without previous treatment. Protein bands were visualized by staining with Coomassie Brilliant Blue R-250 (Andrews, 1981).

2.6. ATPase activity

ATPase assay for the pure protein stored on ice in 100 mM CAPS, pH 10.4, 20% glycerol up to 2-3 weeks was performed as described (Zaitseva et al., 1996) with the following modifications. The dependence of ATP hydrolysis on buffer and pH was measured at room temperature in 100 mM buffering component, 20% glycerol, 1 mM ATP, 10 mM $MgCl_2$, and 5 µg/50 µl (3.6 µM) protein. The protein was first pre-diluted from storage buffer into water solution of glycerol and ATP (pH of ATP stock solution was adjusted with NaOH to 7.5-8.0). Tested buffer was added immediately before the start of the reaction (see Chapter 7.1 for the details on protein pre-dilution). The assay was initiated by the addition of $MgCl_2$.

ATPase activity as a function of enzyme concentration was assayed in 100 mM HEPES-Na pH 7.0, 20% glycerol, 1 mM ATP and 10 mM $MgCl_2$ with protein concentrations varying from 0.1 to 5 µg per 50 µl solution (72 nM-3.6 µM). The protein was pre-diluted in 20% glycerol and 1 mM ATP water solution. The reaction was started by addition of HEPES pH 7.0, $MgCl_2$, 1 mM ATP, and 20% glycerol.

To collect data for ATP hydrolysis by HlyB-NBD at varying ATP concentrations, protein solution was first pre-diluted into 20% glycerol and aliquoted. After the addition of the corresponding amounts of ATP, the reaction was initiated with HEPES pH 7.0, $MgCl_2$ and glycerol to provide desired assay conditions: 100 mM HEPES, pH 7.0, 20% glycerol, 10 mM $MgCl_2$ and 0.01-1 mM ATP.

The level of protein ATPase activity was found to be inversely related to the concentration of $MgCl_2$ in the range 1-10 mM (data not shown). The same phenomenon was also observed for the ATP-binding subunit of the histidine permease (Nikaido et al., 1997) and for the soluble domain of the ABC transporter Atm1 (Chen and Cowan, 2003). Still the highest concentration of 10 mM $MgCl_2$ was used in order to maintain the same concentration of free Mg^{2+} in the assay. Reactions of ATP hydrolysis were run at room temperature for a period of time ranging from 1 min to 2 h, depending on the detected level of ATPase activity.

50 µl aliquots were taken at the appropriate times and the reaction was stopped by 350 µl of 20 mM H_2SO_4. The concentration of inorganic phosphate in the final solution was determined by colorimetric method (Baykov et al., 1988). Absorbance was measured at 620 nm in microtiter plates 10-20 min. after the addition of 100 µl dye [0.096% (w/v) malachite green, 1.48% (w/v) ammonium molybdate and 0.173% (w/v) Tween-20 in 2.36 M sulfuric acid]. The fresh working dye solution has to be prepared on the day of use by rapid mixing of 250 µl 7.5% ammonium molybdate and 1 ml of the concentrated dye solution followed by the addition of 20 µl 11% Tween-20 (Bio-Rad). The concentrated dye solution, which is stable at least for a year at room temperature, is prepared by the slow addition of 60 ml H_2SO_4 to 300 ml H_2O, followed by cooling to room temperature, then 0.44 g malachite green (Sigma) was added. All measurements were made at the linear rate of product formation (Pi) over time. Calibration of free phosphate concentration was performed with Na_2HPO_4 in the working assay solution. All proper controls (time zero, no protein, and no ATP) were taken into account and subtracted, if necessary.

2.6.1. Theory of enzyme kinetics

2.6.1.1. Michaelis-Menten theory for protein enzymes

Enzymes are extraordinarily efficient and selective biological catalysts that accelerate chemical reaction. They achieve their effect by temporarily binding to the substrate and, in doing so, lowering the activation energy needed to convert it to a product. Enzymatic reactions are 10^3 to 10^{17} times faster than the corresponding uncatalyzed reactions. The rate at which an enzyme works is influenced by several factors: the concentration of substrate molecules, the concentration of the enzyme, the temperature, pH, and the presence of inhibitors (Fersht, 1999).

For many enzyme reactions the rate (V, velocity) varies with the substrate concentration, [S]. The rate is defined as the number of moles per unit time, which is a measure of enzyme activity. At low substrate concentration the rate or velocity is almost proportional to substrate concentration. At high substrate concentrations, the velocity is not linear with the concentration and rate approaches a maximum velocity called V_{max}. When the amount of enzyme is much less than the amount of substrate, the reaction is pseudo first order.

The effect of enzyme concentration on reaction velocity in pseudo first-order reaction can be demonstrated by their linear dependence. The more enzyme present, the faster the reaction.

In 1913 Michaelis and Menten described the reaction rate and specificity for a simple one-site reaction. Here is a simplified representation of their theory. Michaelis and Menten divided the process of the conversion of a substrate S into a product P into two steps as shown:

$$E + S \underset{k_{-1}}{\overset{k_1}{\rightleftharpoons}} ES \xrightarrow{k_2} E + P$$
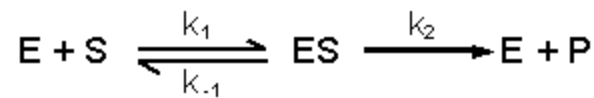
where E, ES, S, and P are the concentrations of enzyme, substrate-enzyme complex, substrate, and product, respectively. The terms k_1, k_{-1}, and k_2 are rate constants for, respectively, the association of substrate and enzyme, the dissociation of unaltered substrate from the enzyme, and the dissociation of product (altered substrate) from the enzyme.

The first reaction step describes the binding of the substrate to the enzyme (catalyst) and the constant K_m corresponds to the *dissociation constant* of the equilibrium under conditions where the product formation is very slow compared to the dissociation process of the substrate. K_m equals the substrate concentration at half maximal reaction rate $V_{max}/2$. In this case K_m is an approximation for the dissociation constant and thus describes the *affinity* of the substrate for the enzyme. For more complex reactions the constant reflects the dissociation equilibrium of all substrates bound to the enzyme.

$$\frac{(k_{-1} + k_2)}{k_1} = K_M$$

The second reaction step describes the *catalytic rate* or the rate of product formation and referred to as the turnover number k_{cat}. The turnover rate is defined as the *maximal number of product P per active site per unit time*.

The Michaelis-Menten kinetic is valid only under *saturation* conditions, i.e., when the concentration of substrate S is much larger than the enzyme concentration. The maximal reaction rate V_{max} describes a *steady-state equilibrium* of the reaction catalyzed by the enzyme. The steady-state equilibrium is an important concept in biochemistry because many enzyme catalyzed reactions run at saturation and the product often is removed from the reaction site so as to render the reaction irreversible.

The saturation conditions of an enzymatic catalysis, where the substrate concentration exceeds the enzyme concentration, for all practical purposes, means that the Michaelis-Menten kinetic is valid only for *initial rates* because with time the substrate gets depleted and

we no longer deal with an excess of substrate over enzyme. In addition, product P can affect the reaction, and this is indeed a major mechanism in the control of biochemical reactions. The product can often bind to the enzyme and at a site *other* than the active site influence its activity. This is called *feed-back control*, which can be positive or negative feed back, stimulate or inhibit the formation of P. Slow denaturation of the enzyme over time is another reason for the use of initial rates of velocity.

An enzyme can be also characterized by its *substrate specificity*. The ratio k_{cat} / K_m defines a measure of the catalytic efficiency of an enzyme-substrate pair. It refers to the properties and reactions of free enzyme and free substrate. The theoretical limit for k_{cat} / K_m is set by the rate constant of the initial complex formation (ES) and cannot be faster than the diffusion controlled interaction of substrate and enzyme. The specificity of an enzyme is therefore a measure of the specificity of an enzyme for competing substrates or of competing enzymes for a single substrate.

Thus, Michaelis-Menten equation describes a simple enzymatic reaction:

$$[E] + [S] \underset{k_2}{\overset{k_1}{\rightleftharpoons}} [ES] \xrightarrow{k_3} [E] + [P]$$
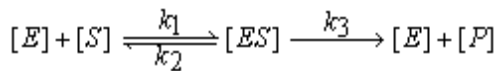
$$\frac{d[ES]}{dt} = 0 \qquad \text{steady-state approximation}$$

$[P] = 0$ \qquad at time zero

$$V = \frac{d[P]}{dt} = k_3 \times [ES]$$

$[E_{total}] = [E] + [ES]$

$V_{max} = \mathbf{k_3} [E_{total}]$

$$K_m = \frac{k_2 + k_3}{k_1} = [S]_{1/2}$$

at $V = (1/2) V_{max}$

$$\frac{V}{V_{max}} = \frac{[S]}{[S] + K_m} \qquad \text{Michaelis-Menten equation}$$

K_m and V_{max} for an enzyme-catalyzed reaction can be measured in several ways. Both values can be obtained by analysis of initial velocities at a series of substrate concentrations and a fixed concentration for the enzyme. In order to obtain reliable values for the kinetic constants, the [S] point must be spread out both below and above K_m to produce a hyperbola.

It is difficult to determine either K_m or V_{max} directly from a graph of initial velocity versus concentration because the curve approaches V_{max} asymptotically. However, using a suitable computer program, accurate values can be determined by fitting the experimental results to the equation for the hyperbola.

2.6.1.2. Cooperativity for the oligomeric protein

However, single protein enzymes are rare. Many enzymes are *protein complexes*. Protein complexes are often referred to as *oligomeric* proteins. Oligomeric proteins are composed of *subunits*, with the subunits being individual polypeptide chains. Protein complexes have defined *quaternary structural symmetries,* if they are *homo*-oligomeric protein complexes where all subunits are identical. The quaternary symmetry are *pseudo-symmetries* if the complex is a *hetero*-oligomer. Homo- and hetero-oligomeric compositions allow for an additional regulatory hierarchy at the cellular, tissue, or organism level, where different combinations of subunits of heteromeric complexes, due to cell specific gene expression, often show minute, yet important differences in enzyme activity. Protein complexes provide *structural and functional variability* through combinatorial effects of subunits that cannot be achieved by single polypeptides (of course they could be large, multi-domain proteins, where each domain adopts the function of a subunit). The most significantly, protein oligomerization enables *cooperativity* between multiple binding sites, a property referred to as *allostery* or allosteric regulation of enzymes (yet again, single polypeptide, multi-domain proteins show allosteric behavior). In general, cooperative interactions occur when ligands bind to proteins or protein complexes. If the binding of ligands is *regulated by different ligands at sites other than an active site*, then we call this *allosteric interaction*. Ligands function as effectors or modulators at different sites in the protein. If the ligands are identical, this is known as homotropic effect, if they are different, it is known as heterotropic effect.

In contrast to the hyperbolic plot, which is expected of non-allosteric enzymes, one of the common characteristics of an allosteric enzyme is that it shows a sigmoidal plot when the velocity is plotted against substrate concentration. The Hill equation describes this dependence:

$$[E] + n \times [S] \underset{k_2}{\overset{k_1}{\rightleftharpoons}} [ES_n] \xrightarrow{k_3} [E] + n \times [P]$$
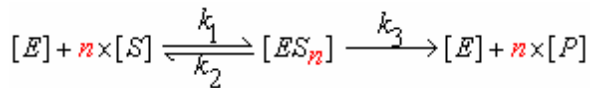
$$\frac{d[ES_n]}{dt} = 0 \qquad \text{steady-state approximation}$$

$[P] = 0$ at time zero

$$V = \frac{d[P]}{dt} = n \times k_3 \times [ES]$$

$[E_{total}] = [E] + [ES_n]$

$V_{max} = \mathbf{n\ k_3}\ [E_{total}]$

$$K_m = \frac{k_2 + k_3}{k_1} = [S]_{1/2}$$

at $V = (1/2)\ V_{max}$

$$\frac{V}{V_{max}} = \frac{[S]^h}{[S]^h + K_m^h} \qquad \text{Hill equation}$$

where **h** = Hill coefficient, and n = number of the substrate binding sites

In the Hill equation the substrate, S, and the constant $K_{0.5}$ are raised to a power, *h*, which is called the Hill coefficient. The constant $K_{0.5}$ is very similar to the Michaelis constant in that it represents the substrate concentration, which gives a velocity equal to half the maximal velocity. The value of the Hill coefficient gives us a measure of the degree of substrate cooperativity. If it were equal to one, of course, it would effectively disappear from the equation which would then be the same as the Michaelis equation with $K_{0.5}$ equal to K_m. Thus, a value of *h* equal to one means that there is no cooperativity and the graph is hyperbolic. An increasing value of *h*, however, will show an increasingly sigmoidal curve showing positive cooperativity for the substrate. A value less than one shows negative cooperativity.

The graph (Figure 15) shows that curve is a typical hyperbolic plot at h=1, while the h=2 and h=4 lines are clearly sigmoidal. These are typical plots showing positive substrate cooperativity, with cooperativity increasing as the Hill coefficient rises. The h=0.5 curve, showing negative cooperativity, is less easy to distinguish from a normal hyperbolic plot but, by comparing the two, it has a faster initial rise and tails off much more sharply. All lines are
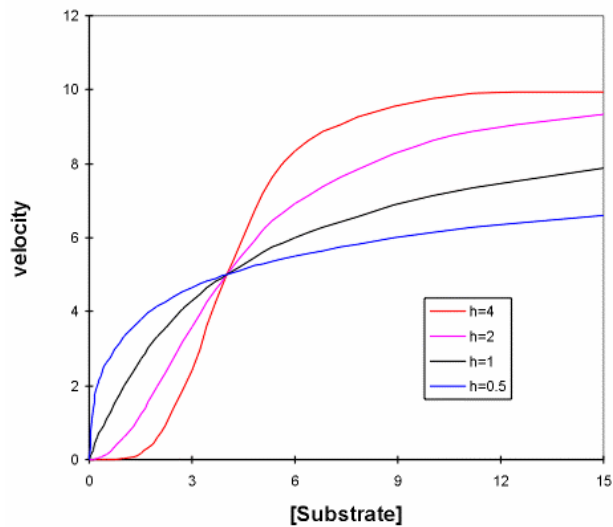
Figure 15. Effects on the *V/S* plot of values of *h* from 0.5 to 4.
In each case the enzyme has a V_{max} of 10 units and a $K_{0.5}$ of 4 units.

heading towards the same maximal velocity and, as they share the same $K_{0.5}$, they all cross at the same point.

There are two main models to account for allosterism; the *concerted or symmetry* model of Monod, Jacob and Wyman (Monod et al., 1965), and the *sequential* model of Koshland (Koshland et al., 1966). Basically these represent two extremes. The major difference between the two models is that the symmetry model allows only one type of conformation to be present in a molecule, whereas Koshland's model allows for mixed, or hybrid, molecules with more than one conformation of subunit to coexist. In other words, each subunit exists in two (or more) conformations T and R and the change from T to R states may occur in unison (MWC model) or sequentially (Koshland model). One major differenc between the models is that the sequential one assumes that the binding of the ligand *induces* the conformational change in the subunit, while the symmetry model proposes that T and R conformations are in equilibrium whether ligands are bound or not. Some experimental systems are best fit by one model, others by the other.

2.7. Analytical gel filtration

20-50 mg/ml stock solution of HlyB-NBD (or H662A-mutant) in 100 mM CAPS pH 10.4, 20% glycerol was diluted to 1-1.9 mg/ml (36-68 µM) into the buffer of interest and incubated in the presence of additives (salts or nucleotides), if necessary. After 1-hour incubation on ice, 50 µl samples were subjected to size exclusion chromatography to assess the stability and/or oligomeric state of the protein. The samples were injected onto Superdex 75 PC 3.2/30 gel filtration column (Pharmacia Biotech) equilibrated with an appropriate buffer at +8°C and were run at 50-75 µl/min. Protein elution from the column was monitored by measuring absorbance at 280, 290 and 295 nm. Fractions (75 µl) were collected and protein content was estimated by SDS-PAGE, if necessary. Elution volumes (in ml) were compared to those of molecular weight standards: BSA (66 kDa), carbonic anhydrase (29 kDa), and lysozyme from hen egg white (14.6 kDa). All experimental buffers contained 20% glycerol to protect the protein from precipitation.

2.8. Crystallization, data collection, and structure alignment

Initial screening was performed with the Hampton Research Crystal Screen and Crystal Screen 2 solutions (Hampton Research, Laguna Niguel, USA). HlyB-NBD and the mutant proteins were crystallized by a hanging-drop vapor diffusion technique at 4°C. Drops were usually set up in 1:1 precipitant to protein ratio. 5-50 mg/ml protein solution in the storage buffer, 100 mM CAPS-Na-buffer pH 10.4, 20% glycerol, was used for crystallization. If necessary, the protein in the storage buffer was diluted with 20-30% glycerol and further concentrated on the Centricon-10 device to reduce CAPS concentration in the starting protein solution (Chapter 4.1). Since SeMet-substituted HlyB-NBD H662A protein didn't produce crystals from the standard storage buffer, it was purified in 50 mM malonate pH 5.6, 20% glycerol, 100 mM sodium acetate, 2 mM ATP and 5 mM ß-ME (Chapter 2.3). The resulting protein solution concentrated to 3 mg/ml was used to obtain diffraction-quality crystals (Chapter 4.2.1.1). Detailed protocols of crystallization of HlyB-NBD and its derivatives are described in Chapter 4. Structure determination of the ADP- and ATP-bound proteins is described in Chapters 5 and 6, respectively.

Initial data collection was performed in-house using a Rigaku X-ray generator with CuKα radiation and an R-AXIS IV image plate at 100 K. Data sets were collected either at beamline BW-6 (DESY, Hamburg, Germany) or at the Advanced Swiss Light Source (Paul Scherer Institute, Villigen, Switzerland) equipped with a MAR CCD. All data sets were processed with DENZO and scaled with SCALEPACK (Otwinowski and Minor, 1997) or processed and scaled with d*TREK (Pflugrath, 1999).

Structural alignments of proteins were performed either with LSQMAN (Kleywegt, 1996) or with the "magic fit" function in the program Swiss-PDB viewer (Kaplan and Littlejohn, 2001). All structure figures were prepared using PyMOL (pymol.sourceforge.net). A662 of the refined structure of HlyB-NBD H662A was replaced *'in silico'* by histidine to obtain the wild type protein situation. After manual adjusting the side chain rotamer orientation of His662, the resulting model was energy-minimized using the GROMOS96 force field (van Gunsteren and Berendsen, 1990) to reduce model bias.

2.8.1. *Theory of protein crystallization*

Protein crystallization occurs when the concentration of protein in solution is greater than its limit of solubility and so the protein is in a supersaturated state. Once a solution is saturated, solid material starts to form. If the molecules come together in a random arrangement, they do not occupy the closest packed space and consequently form an unordered, amorphous precipitate. However, if the molecules come together in an ordered array, they pack together in a much smaller space. Thus, the proper packing uses less space and is also of lowest energy, which is always the most stable condition. As it happens, this ordered array pattern repeats itself regularly in three dimensions, and the crystal is the macroscopic object we see as a result (McPherson, 1999). However, the incoming molecules need a little time to align themselves properly at the surface of a growing crystal in order for the crystal to continue to grow nicely, hence the need for slow crystallization. If the solution becomes over-saturated so that solid forms quickly, the incoming molecules do not have time to align properly with the result that one obtains small crystals that are usually poorly formed.

Crystals start growing be a process called "nucleation". Nucleation can either start with the protein molecules themselves (unassisted nucleation), or with the help of some solid matter already in the solution (assisted nucleation). The central point of crystallization theory is that nucleation of a crystal is enhanced in the vicinity of a metastable critical point between

two metastable liquid phases. The physical intuition behind this model is that the critical nucleus is wetted by the dense protein solution, which lowers the surface tension between the liquid and crystal thereby reducing the free energy barrier to nucleation. Based on this model, a systematic approach to crystallization consists of first mapping the phase diagrams of protein as a function of many variables: temperature, ionic strength, protein concentration, precipitant concentration, and pH. In addition, there may be one or more buffers and additives. Also, the history of the protein sample may affect crystallization and can be treated as a variable.

Since the probability of nucleation increases with increasing supersaturation, the more supersaturated the protein solution, the greater the likelihood that a critical nucleus will form. This is represented on a phase diagram by dividing the supersaturated zone into regions of increasing probability of nucleation and precipitation. The phase diagram (Figure 16) for a typical protein shows zones for crystal nucleation, growth, and precipitation.
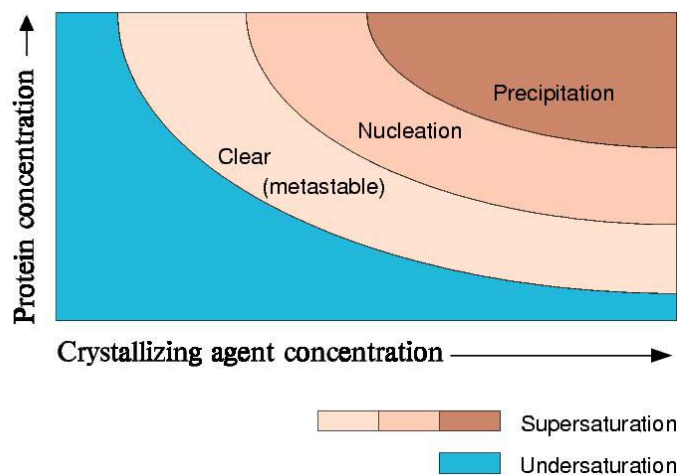
Figure 16. The phase diagram plots the solubility curve of a protein.

The horizontal axis shows the parameter being varied (here precipitant concentration) and the vertical axis shows the protein concentration.

2.8.1.1. Shapes and structures of crystals

There are many ways to categorize a crystal. The one most common method is to group them according to their crystalline structure or lattice:

There are seven crystal lattice systems:

1. **Cubic or Isometric** – they are not always cube shaped; they can also be octahedrons (eight faces) and dodecahedrons (10 faces)
2. **Tetragonal** - similar to cubic crystals, but longer along one axis than the other, forming double pyramids and prisms
3. **Orthorhombic** - like tetragonal crystals except not square in cross section (when viewing the crystal on end), forming rhombic prisms or dipyramids (two pyramids stuck together)
4. **Hexagonal** - six-sided prisms. When you look at the crystal on-end, the cross section is a hexagon
5. **Trigonal** - possess a single 3-fold axis of rotation instead of the 6-fold axis of the hexagonal division
6. **Triclinic** - usually not symmetrical from one side to the other, which can lead to some fairly strange shapes
7. **Monoclinic** - like skewed tetragonal crystals, often forming prisms and double pyramids

This is a very simplified view of crystal structures. In addition, the lattices can be primitive (only one lattice point per unit cell) or non-primitive (more than one lattice point per unit cell). Combining the 7 crystal systems with the 2 lattice types yields the 14 Bravais Lattices (named after Auguste Bravais, who worked out lattice structures in 1850).

Another classification of all crystals is based on their chemical/physical properties. There are four types of crystals: covalent crystals, metallic crystals, ionic crystals, and molecular crystals. Molecular type of crystals contains recognizable molecules within their structure that are held together by non-covalent interactions, like van der Waals forces or hydrogen bonding. The crystals of the molecular type tend to be soft and have lower melting points. Protein crystals belong to that last type.

2.8.1.2. Protein crystallization

Requirements to the protein being crystallized:

1. Purity (homogeneity and monodispersity), which can be assessed, for example, by size-exclusion chromatography, SDS-PAGE, and dynamic light scattering
2. Native conformation that can be evaluated by activity and/or spectrophotometric methods such as circular dichroism spectroscopy
3. Stability during crystallization
4. Relatively high concentration, typically 10 mg/ml or higher

Successful conditions are difficult to predict *a priori*; however, experimental works suggests that many proteins and complexes behave similarly (McPherson, 1985) leading to the use of standard screens based on successful crystallization conditions for other proteins. Typically, these screens do not exhaustively cover all possible combinations of precipitant, pH, and additives, but sample this "crystallization space" sparsely, and are known as sparse matrix factorial strategies (Carter and Carter, 1979; Cudney et al., 1994; Doudna et al., 1993; Jancarik and Kim, 1991). The use of dynamic light scattering to identify favorable protein samples and starting buffer conditions can decrease the necessary search space, because molecules that are monodisperse in non-saturating conditions tend to readily yield crystals, while polydisperse and aggregating samples are less likely to yield crystals (Ferre-D'Amare and Burley, 1994). This technique can be used to rapidly scan for pH ranges, additives, and cofactors that tend to improve the solubility of the protein in solution. Hampton research (http://www.hamptonresearch.com) designed few reagent kits to provide a highly effective and rapid screening method for the crystallization of macromolecules. They include combinations of pH, salts, and precipitants. The three categories of precipitants are utilized: salts, polymers, and organic solvents.

Once protein crystals are obtained, usually an optimization of the crystallization conditions is required to improve the quality of the crystal for the best possible diffraction pattern. Screening around the conditions that give microcrystals or imperfect crystals is done by varying precipitate concentration, pH, protein concentration, temperature, crystallization method, and additives (glycerol, detergents, divalent metals, low molecular weight organic solvents). Sometimes the separation of the phases of crystal nucleation and growth is required to control protein crystallization and obtain diffraction-quality crystals. Methods to achieve that are seeding (Bergfors, 2003), changing temperature, and diluting microbatch drops after pre-incubation (Saridakis et al., 2002).

There are two different categories of seeding based on the size of the seeds (Bergfors, 2003):

1. Microseeding – transfer of submicroscopic seeds, too small to be distinguished individually

2. Macroseeding – transfer of a single crystal, usually 5-50 µm

and four different ways of using seeding :

1. Homogeneous seeding. The seeds are used to grow crystals of the same lattice and symmetry from an identical macromolecule

2. Heterogeneous seeding (Cross-Seeding). The seeds are used to grow crystals of the same lattice and symmetry from a different, but usually very similar macromolecule (such as a mutant)

3. Homogeneous epitaxial seeding. The seeds are used to grow crystals of a different lattice and symmetry from an identical macromolecule

4. Heterogeneous epitaxial seeding. The seeds are used to grow crystals of a different lattice and symmetry from a different macromolecule e.g. the nucleation of protein crystals on cellulose fiber impurities in the drops

2.8.1.3. Methods for protein crystallization

The following methods are utilized for protein crystallization:

1. Vapor Diffusion - in a vapor diffusion experiment small volumes of precipitant and protein are mixed together and the drop is equilibrated against a larger reservoir of solution containing precipitant or another dehydrating agent. A vapor diffusion experiment could be performed either as a hanging, sitting, or sandwich drop (Figure 17).

2. Batch - in batch crystallization the precipitant and protein are mixed directly under oil (Figure 18).

3. Dialysis – in a dialysis crystallization experiment, protein is equilibrated against a larger volume of precipitant through a dialysis membrane (Figure 19).

A. Sitting drop

grease & coverslip (or tape)

protein 2µl + reservoir 2µl H_2O

reservoir ~1m l

B. Hanging drop

protein 2µl + reservoir 2µl   coverslip & grease

H_2O

reservoir ~1m l

C. Sandwich drop

protein 10µl reservoir 10µl   coverslips   grease

H_2O

reservoir ~1m l
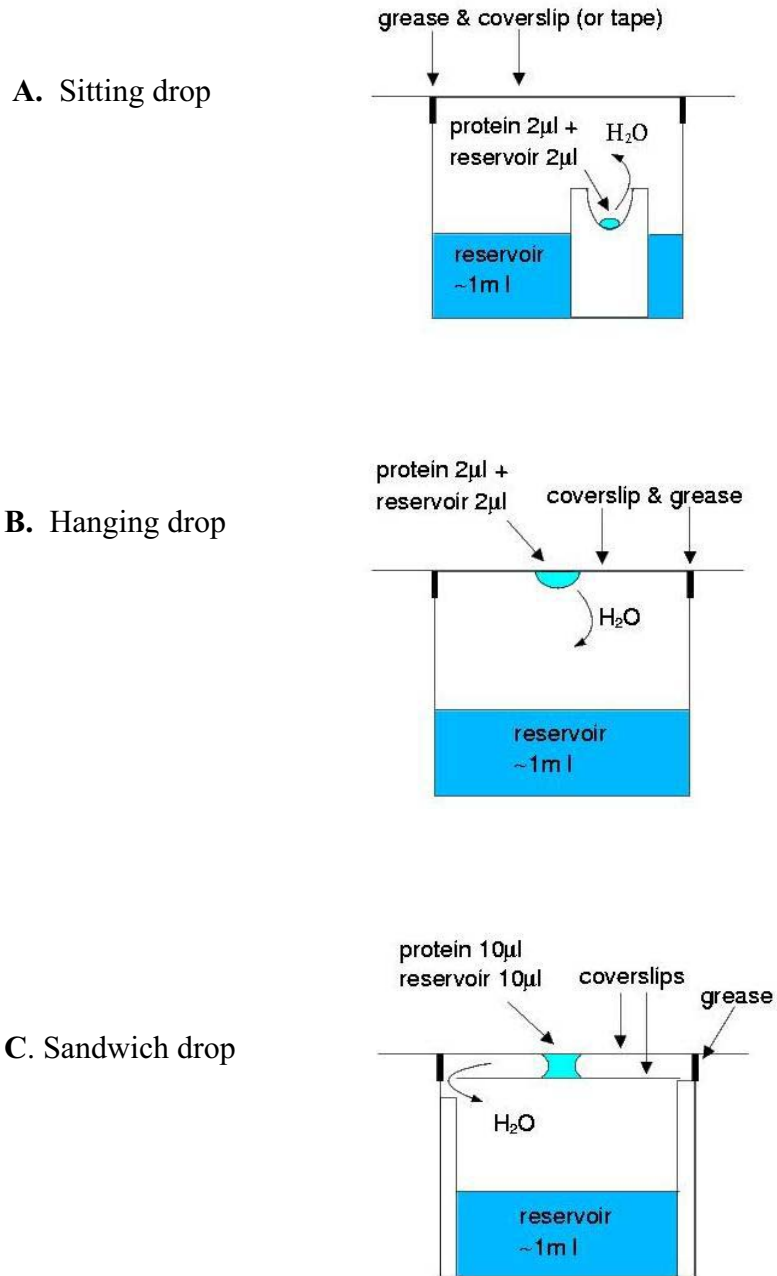
Figure 17. Vapor diffusion.
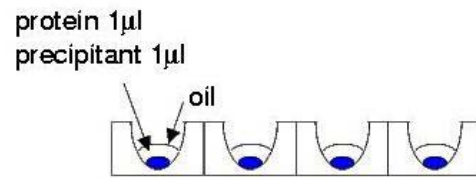
Figure 18. Batch crystallization.
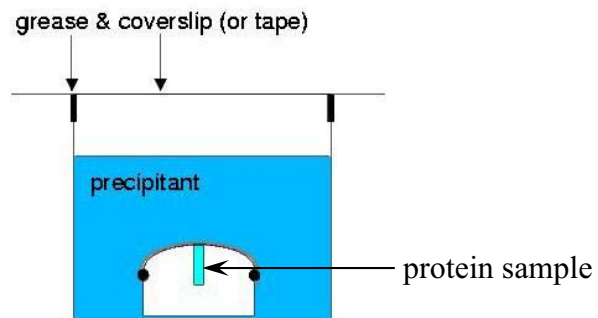
Figure 19. Crystallization by dialysis.

2.8.2. Theory of crystallography

X-ray crystallography is an experimental technique that exploits the fact that X-rays are diffracted by crystals. X-rays have the proper wavelength (in the Ångström range, $\sim10^{-10}$ m) to be scattered by the electron cloud of an atom of comparable size. The diffracted X-rays are scattered by the crystal at a certain angle. The further backwards the X-rays scatter, the higher the resolution of the data set. The extent to which the crystal diffracts determines how fine a detail can be actually distinguished in the final model of the structure. High resolution is thus desirable. Knowing the wavelength, λ, and the diffraction angle of a reflection, θ, its resolution d can be easily calculated:

$$d = \frac{1}{2}\left(\frac{\lambda}{\sin\theta}\right)$$

This is just a reformulation of the famous Bragg equation (Drenth, 1999):

$$\lambda = 2d\sin\theta$$

In a macromolecular X-ray diffraction experiment a small protein crystal is placed into an intense, monochromatic X-ray beam and the diffracted X-rays are collected with, for example, an area detector. It is advantageous to cool the crystals to temperatures of liquid nitrogen (around 100 K), primarily to prevent radiation damage, but also to improve resolution and to reduce disorder in a protein structure. The diffraction pattern consists of reflections of different intensity, and a lot of patterns need to be collected to cover all necessary crystal orientations. As a result, single crystal X-ray diffraction experiments provide direct information about the crystallographic unit cell and symmetry as well as experimental intensities, which can be converted into amplitudes for eventual electron density map generation into which atomic structures can be built. The phasing information that is required for generating these maps, however, cannot be obtained directly. Techniques for phasing utilize either information derived computationally from related structural models, when available, or information derived indirectly from systematic perturbations of the intensities. These perturbations are generated by the addition of atoms possessing many electrons and large scattering power or the presence of atoms whose scattering is influenced by absorption phenomena. Importantly, these sources of phasing information can be used

additively and with computational density modification techniques to generate the best possible initial maps for interpretation and model building.

In order to reduce radiation damage to crystals of biological macromolecules, various techniques of cryocrystallography (Rodgers, 1994) are successfully employed. The crystals are immersed in mother liquor containing a cryoprotectant that enables them to be flash-cooled in a liquid nitrogen stream without the formation of crystalline water. Cryocooling of crystals enables high intensity synchrotron radiation to be used for characterizing initial small crystals, unique crystals that are difficult to grow, as well as for atomic resolution data collection. Data collected are processed using standard software, including DENZO/SCALEPACK (Otwinowski and Minor, 1997) and MOSFLM/SCALA (Collaborative computational project, 1994), for integrating the intensities of the diffracted X-rays and for converting the intensities to crystallographic structure factors.

Thus, based on the diffraction pattern obtained from X-ray scattering of the periodic assembly of molecules or atoms in the crystal, with additional phase information an electron density can be reconstructed. A model is then progressively built into the experimental electron density, refined against the data and the result is a quite accurate molecular structure.

2.8.2.1. *Methods to obtain initial experimental phases:*

1. Isomorphous Replacement: Multiple (MIR) and Single with Anomalous Signal (SIRAS)
2. Anomalous Dispersion: Multi-wavelength (MAD) and Single wavelength (SAD)
3. Molecular Replacement (MR)

2.8.2.1.1. Isomorphous Replacement

The concept of isomorphous replacement phasing is based on the fact that the structure factor, F (hkl), for a certain reflection, hkl, is a simple summation of all individual atomic scattering contributions. Heavy atoms such as transition metals, lanthanides, uranium, gold, mercury salts, even noble gasses under pressure, can quite successfully be soaked into crystals through solvent channels and frequently bind to the well-defined sites in the native protein. Such a protein crystal is then called a heavy atom derivative (crystal). Based under the assumption that the derivative crystal retains its structure (i.e., is in fact isomorphous) one

should be able to derive some information on the structure factor amplitudes for the heavy metal from the differences between the derivative and the native dataset.

In practice, at least one native and 2 crystals soaked with heavy metal solution must be available. The theory is based on 2 assumptions: a) ideal isomorphism and b) exact heavy atom positions, neither of which is perfectly met, for practical and experimental reasons in the first case and for theoretical reasons in the second. So, another derivative may be necessary to improve the quality of the phases. The method is therefore called MIR, Multiple Isomorphous Replacement.

Multiple Isomorphous Replacement (MIR) and Single Isomorphous Replacement with Anomalous Signal (SIRAS) are two methods for providing the needed phasing information by introducing heavy atoms into isomorphous crystals. MIR and SIRAS are performed using crystal soaks or co-crystallization of protein domains and complexes with heavy atoms. For DNA-bound complexes, replacement of thymidines with 5-iodouridines has frequently been used as a phasing technique. For particularly large complexes for which single metal sites are unlikely to provide substantial phasing information, using metal clusters, such as di-μ-iodobis(ethylenediamine)diplatinum (II) nitrate (PIP) and tetrakis(acetoxymercuri)methane (TAMM), is employed to obtain stronger difference information. The advantage of SIRAS methods over MIR is that only a single derivative is required to solve the phase problem (Guan et al., 1998). These techniques may be of particular importance for crystals that are too radiation-sensitive to survive a full multiwavelength (MAD) experiment. Alternatively, data collected can be rapidly converted into a MAD experiment (see Chapter 2.8.2.1.2 below). The positions of heavy atom sites must be identified for phasing techniques, and the positions of initial derivatives can be identified from isomorphous or anomalous difference Patterson maps either through direct inspection or through automated search methods implemented in Solve (Terwilliger and Berendzen, 1999), CNS (Brunger et al., 1998), XHercules (McRee, 1999), or RSPS (Collaborative computational project, 1994). Phasing from these sites and refinement of heavy atom parameters can be performed by Solve, Sharp (Fortelle and Bricogne, 1997), MLPHARE (Otwinowski, 1991), XHeavy (McRee, 1999), or PHASES (Furey and Swaminathan, 1997), depending on the particular experimental constraints. Additional derivatives and weaker derivative sites can be identified automatically or manually through difference Fourier methods, which are far more sensitive than Patterson methods and retain the same origin for all positions.

2.8.2.1.2. Anomalous Dispersion

Multiple-wavelength Anomalous Dispersion (MAD) and Single wavelength Anomalous Dispersion (SAD) experiments are the alternative to MIR and SIR examples, which exploit anomalous dispersion effects and which are proven powerful phasing techniques. Typical anomalous scatters can be endogenous metal ions, such as Zn^{2+} (Hosfield et al., 1999), 5-bromouridines incorporated into protein-DNA complexes, and, most commonly, selenium atoms biosynthetically incorporated into proteins as selenomethionine residues (Hendrickson et al., 1990; Van Duyne et al., 1993).

MAD experiments use the abrupt variation of the structure factor of the anomalous scatterer (expressed as f' and f'') near an absorption edge, while SAD or SIRAS experiments are best performed at a wavelength where f'' is at a maximum, e.g. at a "white line" (Figure 20). While
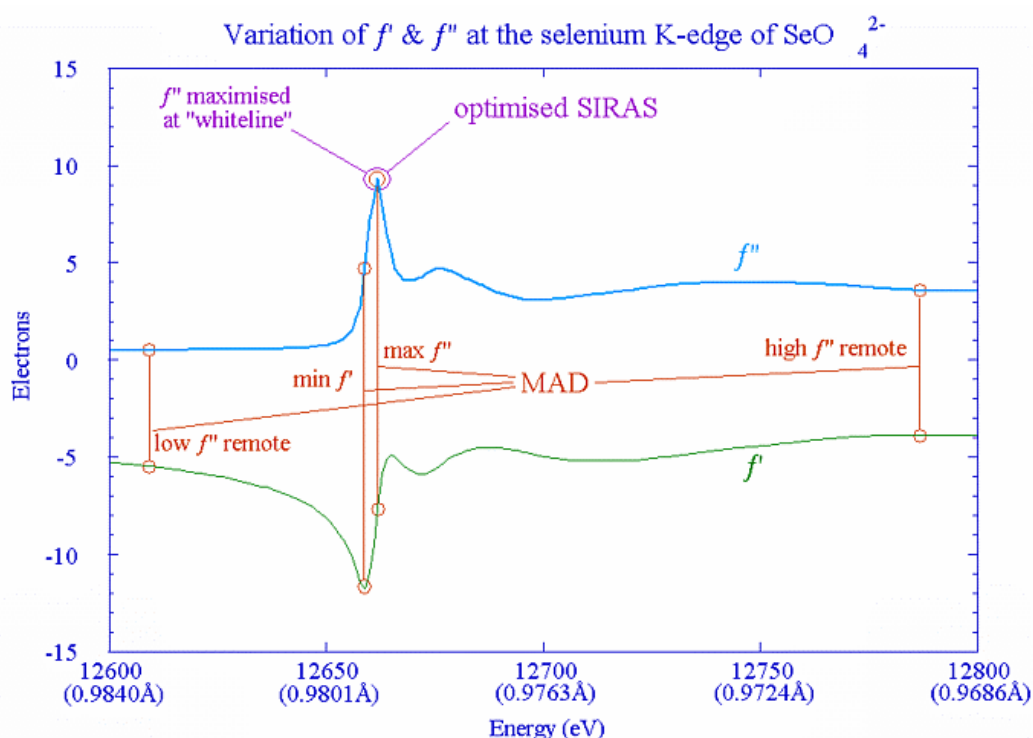
Figure 20. X-ray absorption spectroscopy.

Excitation of atoms of selenium in a material by X-rays of energy close to an absorption edge of selenium. The amount of absorption (or the associated fluorescence or photoelectron yield following absorption) is measured as a function of the incident photon energy. The imaginary components, f'', are shown in the upper curve and the real components, f', are in the lower curve.

IR (isomorphous replacement) methods involve soaking (or co-crystallization) the native crystals in solutions of heavy metal reagents, the most popular vehicle of anomalous dispersion is selenomethionine (SeMet), which is introduced into proteins in place of normally occurring methionine by genetic engineering (Dauter, 2002). Production of the SeMet derivatives usually provides highly isomorphous SeMet crystals; yet, incomplete incorporation of SeMet is possible. Another complication is that protein yields are usually greatly reduced and SeMet is oxidation sensitive. Another prerequisites for SeMet expression include sufficient amount of native Met in protein: as a rule of thumb, one SeMet can phase about 15 kDa protein. However, the phasing power of SeMet in a MAD experiment – in contrast to MIR - strongly depends on the resolution and as in the case of MIR is connected to the flexibility of this amino acid in the crystal lattice.

Exploiting anomalous dispersion often demands special experimental conditions: wavelength tunability, narrow bandpass, as well as the detectors to record diffraction data and absorption edges. Multiwavelength Anomalous Dispersion (MAD) and Single wavelength Anomalous Dispersion (SAD) techniques make it possible to determine a phase set from data collected from a single crystal with anomalously scattering atoms (Hendrickson and Ogata, 1997), so isomorphism is exact in comparison to MIR (due to the use of a single crystal and therefore guaranteed). Generation of diffraction-quality crystals makes it possible to solve structures with one crystal using the tunable wavelength capacity for the rapid structure determination and, in principle, allows to avoid lengthy, systematic searches of heavy atom soaks or heavy atom co-crystallizations. MAD and SAD also provide an elegant technique for approaching systems that suffer severe lack of isomorphism with heavy-atom derivatives and shifts in unit cell changes due to freezing. As for MIR methods, a number of manual and automated techniques can be used to identify the positions of anomalous scatterers. Additionally, important recent advances in direct methods for phasing have solved the anomalous scattering substructure of a crystal from intensity information from MAD experiments (Uson and Sheldrick, 1999). The requirements of measuring X-ray data extending to atomic resolution does not hold for these substructure determinations, and it is sufficient that the resolution be higher than the separation between anomalous scatters so they can be treated as individual atoms. SHELXS (Sheldrick, 1990) and RANTAN (Yao, 1981) allow the anomalous ΔF data to be treated as the amplitudes generated from a substructure of just the anomalous scatterers, though the information content is lower as the true scattering from the substructure is only approximated by the observed ΔF data and the deviations are treated as a noise. A more powerful technique utilizes dual real-space/reciprocal-space

algorithms implemented in SHELXM (Sheldrick, 1998) and Shake-N-Bake (Weeks and Miller, 1999) that have phased entire proteins of over 1000 atoms *ab initio* and have successfully located large numbers of anomalous scatters (more than 60 per asymmetric unit) that cannot be located manually and are problematic for standard automated approaches.

2.8.2.1.3. Molecular Replacement

Molecular replacement (MR) provides a third technique for obtaining the needed phasing information. Briefly, MR uses a structure of a homologous protein as a starting model, does mathematical rotations and translations to orient model in lattice and, once statistically well-placed, uses it as an initial phase estimate. Once initial phases are obtained a protein model is fitted into the initial electron density map (the actual and sometimes marginal experimental reality).

Thus, the goal in MR is to orient and position the search model such that it coincides with the position of the unknown protein in the crystal. This is depicted in the Figure 21. MR has a high probability of success for enzyme/DNA and protein/protein complexes, for which the structure of one protein component is known, and for the homologous enzyme structures, in which the amino acid sequence identity between the target and search molecules is near 30%, or in structural words: the rmsd of the C-alpha coordinates has to be below 2 Å.
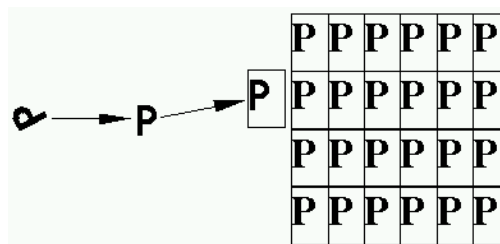
Figure 21. Schematic presentation of the search model in molecular replacement

Orientation and position of the known structure of the protein "**P**" such that it corresponds with the unknown structure in the crystal of a related protein "**P**" (Hazes, 2003).

The following MR programs AMoRe (Navaza, 1994), CNS (Brunger et al., 1998), MOLREP (Vagin and Teplyakov, 2000), and MERLOT (Fitzgerald, 1988) break up the six-dimensional search into a three-dimensional rotation search in Patterson space followed by a three-dimensional translational search in real space. For highly symmetric systems, the general locked-rotation search will be performed with GLRF to simultaneously reduce the rotational space to be searched and increase the signal-to-noise ratio of the rotational hits (Tong and Rossmann, 1997). For difficult MR problems, the program EPMR (Kissinger et al., 1999) is used which uses a genetic search algorithm to efficiently search all six dimensions simultaneously, or the phased translation function can be applied (Read and Schierbeek, 1988), which unambiguously solves the translation problem with phases from even a poor single heavy atom derivative. With MR techniques, a single native data set is sufficient for structure determination even if heavy atoms or anomalous scatters are not present.

2.8.2.2. *Model Building and Refinement*

Model building and crystallographic refinement involves interactive cycles of manual interpretation of electron density followed by automated refinement of the model against experimental and stereochemical restraints. Maps used for manual interpretation can be generated either entirely from experimental phasing information, from Fourier transforms of model phases applied to experimental amplitudes, or through a combined phase set generated from both experimental and model sources. Optimization of the models against the diffraction amplitudes can be performed by applying stereochemically-restrained least-squares refinement in CNS (Brunger et al., 1998), TNT (Tronrud et al., 1987), SHELXL (Sheldrick, 1996), or REFMAC (Collaborative computational project, 1994). CNS also combines refinement against X-ray terms with molecular dynamics under a simulated-annealing protocol to escape local potential surface minima. For ultra-high resolution structures greater than 1.5 Å resolution, refinement can be carried out with the SHELXL program, which employs an explicit, rather than fast, Fourier transform, and enables the anisotropic B-factors of individual atoms to be determined and refined when sufficient experimental parameters exist to constrain the refinement. At resolutions below 2 Å, the ARP/wARP package (Perrakis et al., 1997) can also be used to automatically build models using an iterative reciprocal space structure factor refinement with automated real-space model building. Refinement strategy and electron-density map fitting can be guided by cross validation by monitory the free R

value to prevent over-refinement and to evaluate the effects of any non-crystallographic symmetry restraints (Brunger, 1993). Examination of simulated-annealing omit maps (Hodel et al., 1992) that reduce the effect of model bias on electron density have to be performed regularly. Partial model phase combination with SIGMAA weighting (Read, 1986) can improve the maps at later stages. Model building into electron density with interactive graphics can utilize variety of program such as XFit ((McRee, 1999) or O (Jones et al., 1991). Stereochemistry of resulting models can be evaluated with Procheck (Laskowski et al., 1993) and potential problem areas inspected for manual rebuilding.

Chapter 3

Purification of HlyB-NBD and search for the conditions supporting highly concentrated pure substrate-free protein in solution

3.1. Dependence of protein stability on pH

Previously, the purification and crystallization of the HlyB-NBD were performed either in Tris-buffer or in phosphate buffer (Kranitz *et al.*, 2002). However, protein concentrated above 1 mg/ml tended to precipitate in Tris-buffered solution (10 mM Tris-Cl pH 8.0, 100 mM KCl) in a few hours, forming tiny white flakes. In an attempt to optimize the purification scheme, Tris-buffer was replaced with phosphate buffer (10 mM sodium phosphate pH 8.0, 100 mM KCl) for HlyB-NBD isolation (Benabdelhak *et al.*, 2003; Schmitt *et al.*, 2003). The selection of phosphate buffer allowed concentrating the soluble HlyB-NBD up to 10 mg/ml. Even though the protein did not precipitate in phosphate buffer immediately, only freshly purified protein was used for crystallization trials because of the more reliable results (the older protein solution usually didn't produce crystals). In 24-48 hours of storage on ice HlyB-NBD eventually precipitated from phosphate containing solution at protein concentrations about 10 mg/ml, with the precipitation rate directly related to the protein concentration. As a result of crystallization of freshly purified protein in the presence of ATP, sodium phosphate and lithium sulfate, crystals of HlyB-NBD diffracting to 2.6 Å were obtained (Kranitz *et al.*, 2002; Schmitt *et al.*, 2003). The protein structure was solved (Schmitt *et al.*, 2003) and the ATP-binding site was found to be occupied by a sulfate or a phosphate ion. The extensive efforts to crystallize nucleotide-bound states of HlyB-NBD were not successful. The possible reasons could be protein instability in purification buffer and reduced affinity of the enzyme to nucleotides in the presence of free inorganic phosphate in the mother liquor.

To improve solubility of the isolated HlyB-NBD and to avoid free inorganic phosphate in protein solution, pH-dependence of protein stability was evaluated first in different buffers.

A simple screening test was employed to assess effect of various pH and buffers on protein stability. Slightly turbid solution of pure HlyB-NBD in Tris-buffer at approximately 1 mg/ml was subjected to the drop assay against buffers listed in Table 1 with pH range of 4.65-10.4 (see Chapter 2.4).

Number	Buffer composition	pH value
1	200 mM sodium acetate	4.65
2	200 mM sodium citrate	5.1
3	200 mM sodium malonate	5.6
4	200 mM ADA	6.5
5	200 mM ADA	7.0
6	200 mM HEPES	7.2
7	50 mM sodium phosphate, 100 mM KCl	8.0
8	200 mM Tris-HCl	8.0
9	10 mM Tris-HCl, 100 mM KCl, 150 mM imidazole	8.0
10	100 mM Tris-HCl, 2 M ammonium sulfate	8.0
11	200 mM Tricine-HCl	8.1
12	200 mM CHES	9.3
13	200 mM CAPS	10.4

Table 1. Buffers used in the drop assay

The buffer with the lowest pH, 200 mM Acetate-Na pH 4.65, seemed to induce precipitation, compared to the control (10 mM Tris-Cl pH 8.0, 100 mM KCl, 150 mM imidazole). Two buffers appeared to reverse protein aggregation: phosphate buffer (50 mM sodium phosphate pH 8.0, 100 mM KCl) and the buffer with the highest tested pH, 200 mM CAPS-Na pH 10.4. Addition of either buffer visibly clarified a turbid protein solution. All the other buffers seemed to have the same effect as 10 mM Tris-Cl pH 8.0, 100 mM KCl, 150 mM imidazole, causing no significant changes in the amount of precipitated protein. The phosphate buffer was not evaluated further, as this buffer had been used in the structure determination of the nucleotide-free state of the HlyB-NBD (Schmitt *et al.*, 2003). Therefore, all subsequent experiments were continued with the CAPS buffer as the preferred alternative to the phosphate-buffer system.

To verify the effect of CAPS on the protein stability, freshly purified HlyB-NBD in the elution phosphate buffer (10 mM sodium phosphate pH 8.0, 100 mM KCl and approximately 150 mM imidazole) was subjected to a size-exclusion chromatography step in the presence of CAPS pH 10.4. It was feasible to attain 25 mg/ml protein concentration and

retain HlyB-NBD solubility in 25 mM CAPS, pH 10.4, 100 mM KCl. However, the next day the concentrated protein solution had already formed a precipitate.

3.2. Protein stability in different buffers

For further screening of conditions ensuring HlyB-NBD stability, a number of supplements were tested in various concentrations by the drop assay, this time starting from a turbid solution of 20-25 mg/ml protein in 25 mM CAPS buffer pH 10.4, 100 mM KCl. Those supplements included β-ME, DTT, glycerol, ATP, ADP, EDTA, various salts such as potassium chloride, sodium chloride, magnesium chloride, lithium sulfate, ammonium sulfate, sodium acetate, and sodium citrate, and detergents such as deoxycholic acid, taurocholic acid, CHAPS, OG, LDAO, MEGA-10, and DDM.

The addition of glycerol or ATP resulted in partial clarification of the turbid protein solutions in 25 mM CAPS, pH 10.4, 100 mM KCl. However, the most significant improvement in protein solubility was detected upon the introduction of higher CAPS concentrations as an individual component. Various combinations of the above ingredients produced an even greater effect on the solubility of HlyB-NBD. For example, simultaneous addition of ATP and glycerol dissolved most of the precipitated protein, albeit in a not very reproducible manner. The strongest effect of the supplements on HlyB-NBD solubility was observed in the presence of CAPS and glycerol. A cloudy protein suspension was visibly clarified upon the addition of these components, resulting in an absolutely transparent appearance to the solution within a few minutes. Salts of divalent metals seemed to induce precipitation. All other tested components had no noticeable effect.

The stability of the HlyB-NBD was also tested by microtiter plate assay and dialysis (Chapter 2.5) against buffers 6, 8, 9, 11, 12, and 13 (see Table 1) with and without 20% glycerol for extended times at $+4^{o}C$. Micro-dialysis was performed against 10-fold-diluted tested buffers (6, 8, 11, 12, 13) and compared to 10 mM Tris-Cl pH 8.0, 100 mM KCl, and 150 mM imidazole. Again, a CAPS buffer with glycerol exhibited the best protein solubility. CAPS alone was not that effective. Glycerol proved to be the stabilizing ingredient in all cases, partially protecting the protein from precipitation.

After the dialysis or microtiter-plate assay, samples were analyzed by SDS-PAGE. No degradation products were observed in the tested protein solutions by SDS-PAGE, although high molecular weight (HMW) aggregates were observed in some samples. Duplicate samples

of the NBD were examined to compare total protein amount and the dimer/monomer ratio as well as the presence of aggregates. Thus, before loading for SDS-PAGE analysis, the protein solution under test was either boiled following the addition of β-ME and SDS-sample buffer or directly mixed with the latter without heating and omitting β-ME. SDS-PAGE analysis without boiling/β-ME demonstrated that significant amount of protein from the turbid samples migrated at the relative size of the HlyB-NBD dimer. The molecular weight of these 56 kDa-bands was reduced to that of monomeric protein in the SDS-PAGE gel in the presence of β-ME. Apparently, the formation of intermolecular disulfide bridges through the single cysteine (Cys652) of HlyB-NBD monomers serves as an indication of protein denaturation. A direct correlation between the amount of S-S dimers detected by SDS-PAGE and the level of protein precipitation was observed in the assayed samples. The lowest ratio of dimer to monomer was observed in CAPS-glycerol samples.

Based on the results of all screening procedures, 10 mM CAPS-NaOH pH 10.4, 20% glycerol was chosen for the last step of HlyB-NBD purification, the size-exclusion chromatography (see Chapter 2.1 and Figure 14) as the most efficient buffer for protein stabilization. However, the pH of HlyB-NBD solution started to decline to neutral during protein concentration in the gel-filtration buffer, leading to the protein precipitation. Addition of 500 mM CAPS-Na pH 10.4 to the protein solution completely eliminated the problem. Thus, for the concentrated HlyB-NBD the pH and CAPS concentration had to be adjusted to 10.4 and 100 mM, respectively. Furthermore, 100 mM CAPS pH 10.4 with 20% glycerol proved to be superior for the long-term storage of the pure HlyB-NBD at high concentrations. No precipitation or aggregation was observed in a 20-50 mg/ml protein solution stored for 2-4 months on ice in that buffer. Moreover, the ABC-domain of HlyB was found to be suitable for crystallization for at least a month after purification when maintained in CAPS-glycerol on ice.

3.3. Disulfide dimers as a monitor for protein denaturation over time

Freshly purified protein in 100mM CAPS pH 10.4, 20% glycerol usually demonstrated more than 99% monomeric protein content when analyzed by SDS-PAGE omitting the treatment with a reducing agent. However, the percentage of the disulfide HlyB-NBD dimers increased progressively during storage of the protein on ice, even though no visible precipitation was observed (Figure 22). In 18 days the amount of dimer had reached 5-20% of the total protein and 20-50% was converted to the inactive S-S dimeric species in two months,

as estimated by either SDS-PAGE (Figure 22) or SEC (data not shown). Surprisingly, no protein precipitation was observed in 100mM CAPS pH 10.4 and 20% glycerol, even when SDS-analysis detected up to 50% of the disulfide dimer from the total HlyB-NBD. The HlyB-NBD eventually precipitated upon 3-6-month storage on ice, forming white fluffy flakes. The addition of reducing agents such as β-ME and DTT protected the protein from disulfide bridging of monomers, but didn't appear to extend the storage life of the isolated HlyB-NBD. Besides, the uncoupled ATPase activity of protein from β-ME-containing stock solution seemed to decline faster during storage when compared to HlyB-NBD stock without any additives (data not shown).
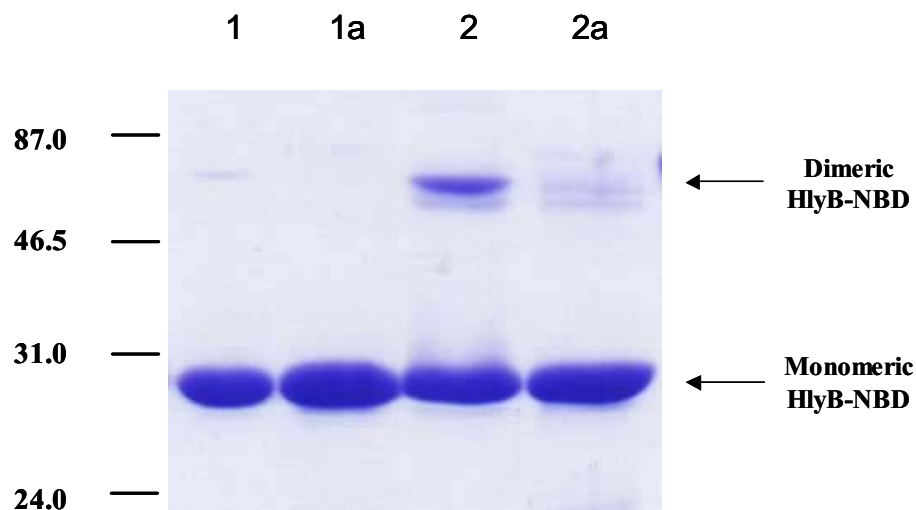
Figure 22. SDS-PAGE analysis of the purified HlyB-NBD stored at 4 °C in 100 mM CAPS pH 10.4, 20% glycerol

Approximately 2.5μg of protein was loaded per lane and subjected to SDS electrophoresis. 1, freshly purified protein without boiling and treatment with β-ME; 1a, the same as 1 but boiled and treated with β-ME prior to analysis; 2, two and a half month old protein without boiling and treatment with β-ME; 2a, the same as 2 but boiled and treated with β-ME prior to analysis.

3.4. The ATPase activity of the NBD is reversibly inactivated in the CAPS buffer

In order to evaluate the oligomeric state of HlyB-NBD in the storage buffer, one-week-old protein was subjected to gel filtration on a Superdex 75 column in 100 mM CAPS pH 10.4 and 20% glycerol. The protein appeared to run according to its monomeric size (Figure 23). The injected sample was eluted as a relatively sharp peak coinciding with a 29 kDa protein, carbonic anhydrase, which was run in the same buffer for column calibration. The slight asymmetry of the peak (Figure 23) indicates the presence of a higher molecular weight species in the sample. This is likely to be attributed to disulfide protein dimers, since small amount of dimers can be detected in the one-week-old sample by SDS-PAGE analysis.
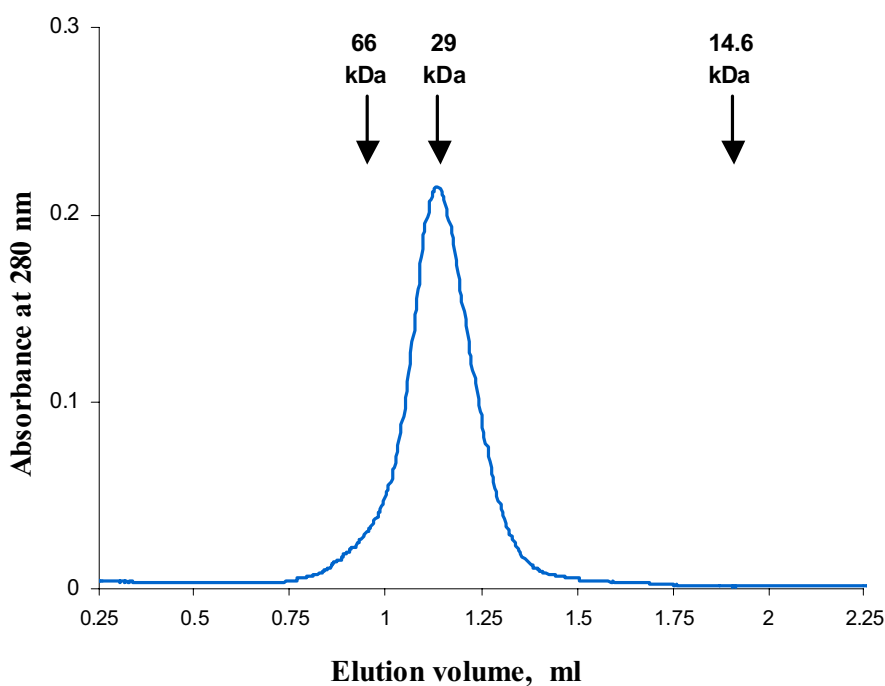
Figure 23. Analytical size-exclusion chromatography of the one-week-old HlyB-NBD in 100 mM CAPS pH 10.4, 20% glycerol

The protein was eluted according to its monomeric size, 28 kDa. The column was calibrated with standard proteins in the same buffer.

Unexpectedly, HlyB-NBD was found to be completely inactive as ATPase in the CAPS-containing storage buffer (Figure 24). However, activity was fully restored by protein dilution into a conventional assay buffer. Figure 24 shows the time-dependent ATPase activity of HlyB-NBD in 100 mM HEPES-Na pH 7.0, 20% glycerol following an approximately 700-fold dilution from the storage buffer 100 mM CAPS-Na pH 10.4, 20% glycerol. Thus, HlyB-NBD exposure to high pH (CAPS buffer pH 10.4) inactivated the protein only temporarily, shifting the ABC-domain to a 'sleeping mode' and protecting it from denaturation. The significantly improved stability of HlyB-NBD in the storage buffer made it possible to perform highly reproducible ATPase assays up to two weeks after protein purification. In three weeks, the ATPase activity still corresponded to 90% of that of freshly
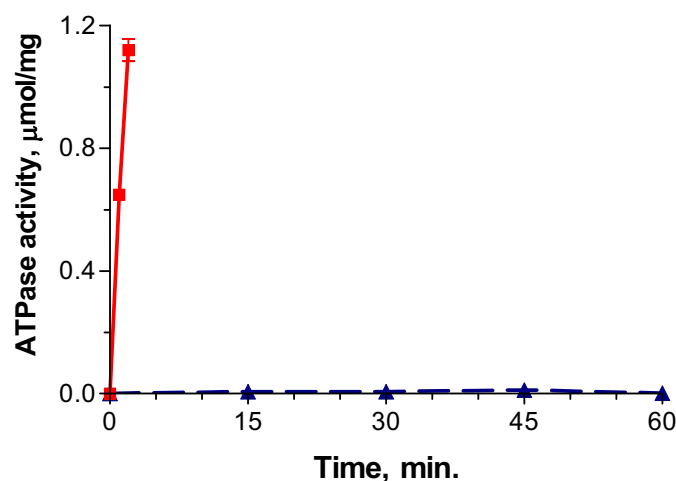
Figure 24. Time dependent ATPase activity of the purified HlyB-NBD in two different buffers, CAPS pH 10.4 and HEPES pH 7.0

Protein from the storage buffer, 100 mM CAPS pH 10.4 and 20% glycerol, was diluted for ATPase assay into 100 mM CAPS pH 10.4, 20% glycerol, 1 mM ATP, and 10 mM $MgCl_2$ (final protein concentration 14.4 μM, triangles, blue line) or the standard assay buffer, 100 mM HEPES pH 7.0, 20% glycerol, 1 mM ATP, and 10 mM $MgCl_2$ (final protein concentration 3.6 μM, squares, red line). No steady-state ATPase activity was detected over a time period of 120 min. in CAPS buffer in the aforementioned conditions. No ATPase activity was detected in CAPS buffer at the lower protein concentration, 1.44 μM, either (not shown). Data points are the average of three independent experiments.

purified protein, when tested in 100 mM HEPES-Na pH 7.0, 20% glycerol assay buffer (data not shown). In contrast, while HEPES buffer pH 7.0 with 20% glycerol was found to be the most optimal assay buffer supporting high level of HlyB-NBD activity immediately upon protein dilution, the prolonged incubation of the enzyme in this buffer caused a concentration dependent protein precipitation, which significantly reduced the rate of the observed ATPase activity by HlyB-NBD (Chapter 7).

A possible explanation for the effect of CAPS pH 10.4 on HlyB-NBD stability and activity could be structural modifications of the protein accompanying the change in pH. For example, in case of the retinol-binding protein, pH-induced structural changes were reported, resulting in the rearrangement of salt bridges, hydrogen bonds, the network of the solvent molecules, alteration of charge distribution on the protein surface, changes in flexibility in some regions of the protein and in the volume of the internal substrate-binding cavity (Calderone *et al.*, 2003). Similar structural alterations might take place in the case of HlyB-NBD upon switching to high pH. Elevation of pH above the theoretical isoelectric point (pI = 8.9, as calculated with the ExPASY server; http://ca.expasy.org/tools/pi_tool.html) of HlyB-NBD will change close-range electrostatic interactions and alter hydrogen bonds and salt bridges in the protein. On the one hand, the predicted modifications could potentially contribute to the conformational stability of the protein, making the whole molecule structure more rigid. On the other hand, these structural rearrangements could limit protein flexibility, modify van der Waals surfaces and the charge distribution, resulting in a lowered affinity for ATP and/or an inability to cleave ATP. The aforementioned effect of CAPS buffer could also be explained by an interaction between CAPS and the protein at one or more potential low-affinity binding sites. Surprisingly, the chemically highly related CHES with buffering capacity in a somewhat lower pH range (pKa = 9.3) failed to improve HlyB-NBD solubility. This makes us believe that the high pH, not protein-CAPS interactions, has a major impact on protein stability. However, we cannot rule out the significance of the chemical structure and the ability to maintain constant pH in more basic regions, a combination that makes CAPS buffer unique for our studies.

Chapter 4

Crystallization of HlyB-NBD and its mutants with various nucleotides, data collection and phasing

4.1.   HlyB-NBD crystallization

The use of the nucleotide-free HlyB-NBD maintained in the "sleeping" CAPS storage buffer, 100 mM CAPS pH 10.4, 20% glycerol, permitted screening of crystallization conditions with different substrates: ATP, ADP, AMP-PNP, TNP-ATP, TNP-AMP, ATPγS, 2'-Br-ATP and 8-Br-ATP. However, since high buffer concentration, 100 mM CAPS, in the storage buffer could be a potential problem for protein crystallization, the buffer can be exchanged for 1-10 mM CAPS pH 10.4, 20-30% glycerol by simple dilution into 20-30% glycerol solution and further concentration by ultrafiltration. Extreme care had to be employed to avoid protein precipitation during the buffer exchange. Immediate addition of substrates, if necessary, is an example of possible protein stabilization at the low concentration of CAPS. Instant utilization of the final CAPS-deficient HlyB-NBD solution was also preferable for the successful crystallization. Maintaining a constant low temperature of 4°C was also very important for protein stability.

HlyB-NBD with bound ADP was crystallized at 4°C in the presence of ATP (interestingly, Mg^{2+} was not required for crystallization; it seems that a tracing amount of divalent metals in water-based protein/crystallization solutions was sufficient for ATPase activity of the protein) or ADP in hanging drops containing 1μl protein solution (25 mg/ml in 70 mM CAPS pH 10.4, 30% glycerol, 10 mM ATP or 10 mM ADP) and 1μl well solution (100 mM Tris pH 8.0, 10% PEG 6000, 5% MPD). Crystal plates fused together usually appeared the next day and continued to grow to the full size over 7-10 days (Figure 25A). The largest crystals obtained were 450 μm x 350 μm x 30 μm. Crystals were directly flash-frozen in liquid nitrogen and diffracted to 1.6 Å at the Advanced Swiss Light Source (Villigen, Switzerland) (Figure 25B and Table 2). Identically shaped crystals were also obtained from
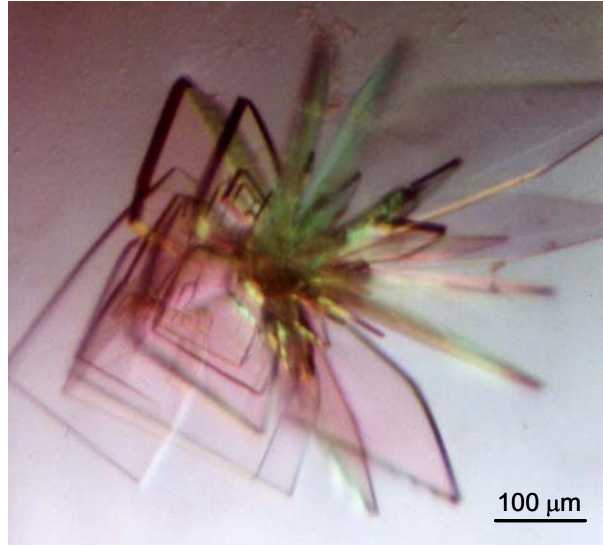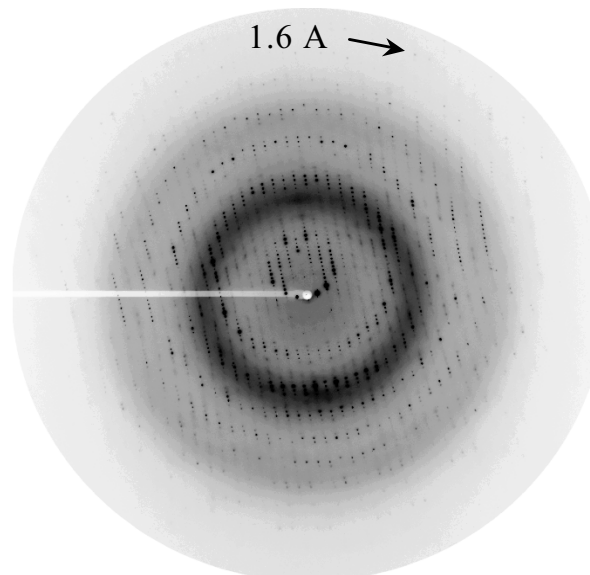
Figure 25. Crystals of the wild type HlyB-NBD with bound ADP. The HlyB-NBD H662A protein produced crystals of the same shape.

A. Crystals of HlyB-NBD with bound ADP. The hanging drops contained 1 μl protein solution (25 mg/ml in 70 mM CAPS pH 10.4, 30% glycerol, 10 mM ATP or 10 mM ADP) and 1 μl well solution (100 mM Tris, pH 8.0, 10% PEG 6000, 5% MPD).

B. The X-ray diffraction pattern of HlyB-NBD crystals with bound ADP obtained at the Advanced Swiss Light Source (Villigen, Switzerland).

Table 2. Summary of the crystallographic analysis and data-set collection of the ADP-bound states of the wild type HlyB-NBD and its H662A- and E631Q-mutants

Resolution limits are based on I/σ (I) statistics. Values in parentheses refer to the highest resolution shell (1.65-1.6 Å for the wild type, 1.76-1.7 Å for H662A protein, and 1.95-1.9 Å for E631Q protein). Data sets were scaled and processed with DENZO and SCALEPACK (Otwinowski and Minor, 1997).

	Wild type	**His662Ala**	**Glu631Gln**
Space group	C2	C2	C2
Cell constants at 100 K			
a, b, c [Å]	180.37, 34.84, 37.82	180.16, 34.77, 38.1	178.57, 34.75, 37.52
α, β, γ [°]	90, 98.41, 90	90, 98.58, 90	90, 97.97, 90
Wavelength [Å]	1.005	1.005	1.005
Resolution [Å]	20 – 1.6	20 – 1.7	20 – 1.9
Mean redundancy	10.9	12.2	6.9
Completness [%]	90.5 (69.5)	99.2 (88.5)	94.1 (88.1)
I/σ	14.7 (2.1)	26 (3.2)	10.8 (2.3)
R_{sym} [%]	8.8 (25.4)	6.2 (16.3)	4.9 (27.7)

Refinement

R_F [%]	19.2 (26.8)	20.5 (24.0)	20.2 (29.7)
R_{free} [%]	23.1 (36.6)	24.0 (32.0)	25.0 (30.1)
Rmsd bond length [Å]	0.013	0.015	0.013
bond angle [°]	1.434	1.498	1.414
Average B-factor [Å^2]	30.2	25.1	37.0

Ramachandran plot

Most favored [%]	93.5	93.0	92.0
Allowed [%]	5.6	6.0	7.1
Generously allowed [%]	0.9	0.9	0.9

Model content

Protein residues	466-707	465-707	465-707
Ligands	ADP	ADP	ADP
Water molecules	176	246	128

protein solutions containing ATP/Mg2+ and ADP/Mg2+. No crystals appeared from solutions containing ATP/EDTA, ATPγS, or AMP-PNP with and without Mg^{2+}. The structure of the wild type HlyB-NBD with bound ADP was solved by molecular replacement using nucleotide-free structure of HlyB-NBD (Schmitt et al., 2003) (Chapter 5).

In an attempt to crystallize HlyB-NBD in the ATP-bound state, crystals were produced at 4°C by mixing 1μl protein solution (40 mg/ml in 8 mM CAPS pH 10.4, 30% glycerol, 10 mM ATP, 0.8 mM EDTA) and 1μl well solution (100 mM citrate-Na pH 5.6, 30% PEG 4000, 0.2 M Ammonium Sulfate) using the hanging-drop vapor diffusion technique (Figure 26). However, the shape of the crystals and growth conditions closely resembled those of the previously reported nucleotide-free state of the HlyB-NBD (Schmitt et al., 2003). Alternatively, long rod crystals were grown in hanging drops at 4°C from the same protein solution and 2 M malonate-Na, pH 6.0-6.2 as a precipitant (McPherson, 2001) (Figure 27).
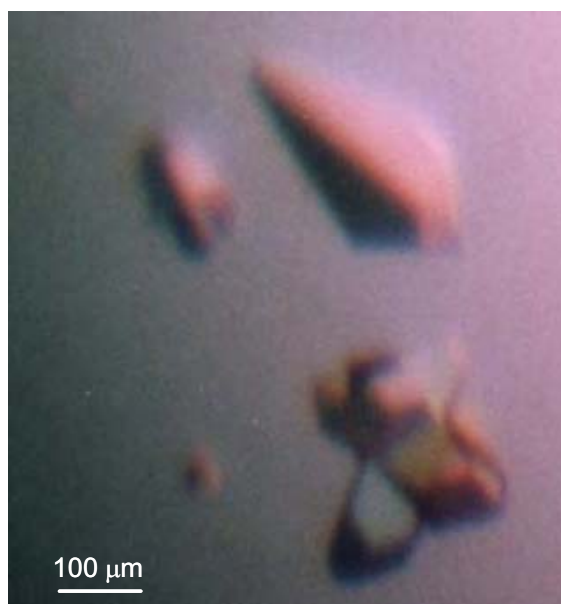
Figure 26. Crystals of HlyB-NBD grown in the presence of ATP and EDTA in 'citrate buffer pH 5.6'

Hanging drops contained 1 μl 40 mg/ml HlyB-NBD in 8 mM CAPS pH 10.4, 30% glycerol, 10 mM ATP, 0.8 mM EDTA and 1 μl well solution (100 mM citrate-Na pH 5.6, 30% PEG 4000, 0.2 M ammonium sulfate).
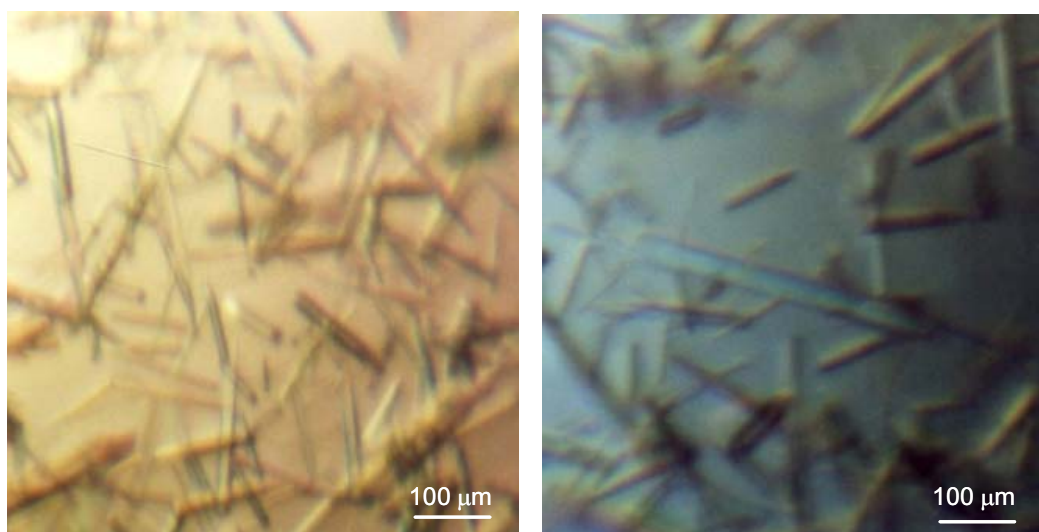
Figure 27. Crystals of HlyB-NBD in the presence of various substrates and without substrates in 2M Malonate pH 6.0

Crystals were produced by mixing 1 µl protein (40 mg/ml, in 8 mM CAPS pH 10.4, 30% glycerol, 10 mM ATP, 0.8 mM EDTA) and 1 µl well solution (2 M malonate-Na, pH 6.0-6.2).

Thoroughly washed in crystallization buffer, latter crystals were dissolved, ran on SDS-PAGE-gel, and identified with Coomassie stain as the expected 28 kDa protein. However, this type of crystals was easily reproduced in the presence of ADP and AMP-PNP as well as in the absence of nucleotides. In addition, both types of crystals (Figures 26, 27) failed to bind TNP-ATP and TNP-ADP, as demonstrated by their inability to absorb the yellow color of the fluorophore. Therefore, we considered both crystal forms as resembling the nucleotide-free state of the protein and they were not further evaluated.

Screening of different crystallization conditions by the hanging-drop vapor diffusion technique revealed further crystal types formed in the presence of ATP at 4°C: 30 mg/ml HlyB-NBD in 60 mM CAPS pH 10.4, 35% glycerol, 10 mM ATP and 20 mM MgCl2 was mixed in a 1:1 ratio with 100 mM Tris-Cl pH 8.0, 2 M Ammonium Sulfate and 10% DMSO (Figure 28). The formation of these crystals was observed only upon pre-incubation of protein with ATP. Neither ADP, nor AMP-PNP, nor ATPγS supported crystal growth under the above conditions. Crystals produced under the same conditions with the addition of 50 µM

TNP-ATP were colored opalescent yellow. Inclusion of 50 µM TNP-AMP in the droplet did not lead to accumulation of color in protein crystals, suggesting the specific binding of the fluorescent analog of ATP, not AMP, to the protein under these conditions. However, those crystals only diffracted to 4.5-5 Å even at a synchrotron beamline. Thus, these crystals were not suitable for collection of the high-resolution data, and were not further evaluated.
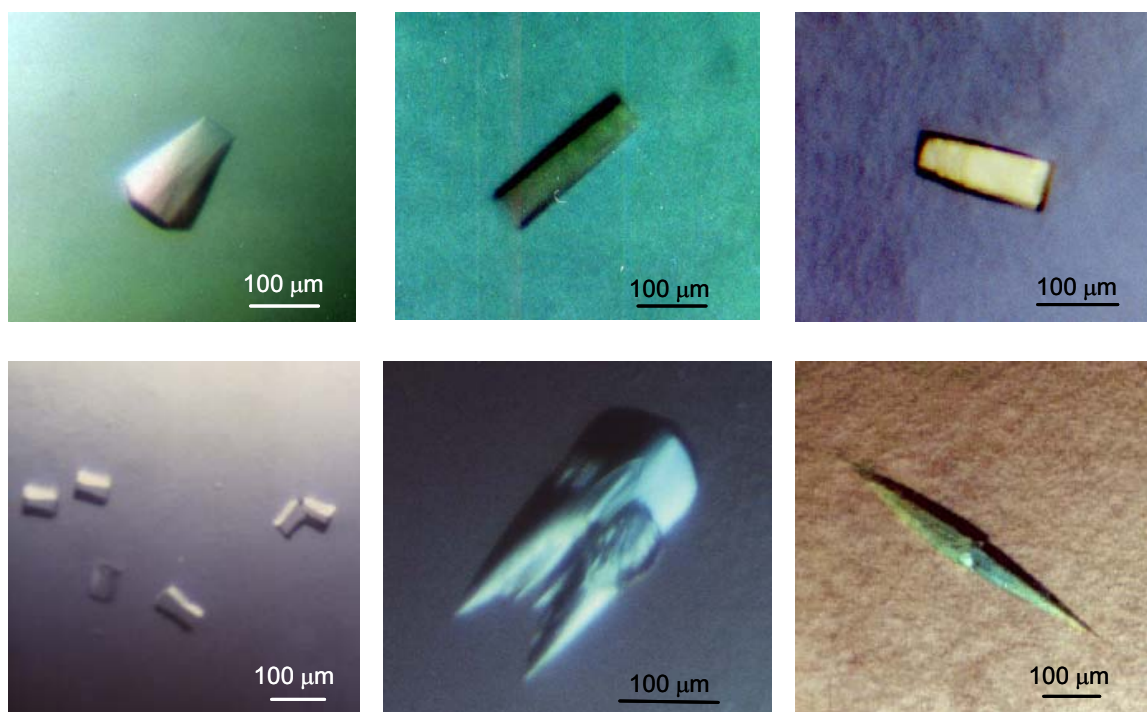
Figure 28. Crystals of HlyB-NBD grown in the presence of Mg^{2+}-ATP

30 mg/ml HlyB-NBD in 60 mM CAPS pH 10.4, 35% glycerol, 10 mM ATP and 20 mM $MgCl_2$ was mixed in a 1:1 ratio with 100 mM Tris-Cl, pH 8.0, 2 M ammonium sulfate, and 10% DMSO in the hanging drops.

4.2 Crystallization of the HlyB-NBD H662A- and E631Q-mutant proteins

Having had no success in obtaining crystals of wild type HlyB-NBD with ATP and ATP analogs (AMP-PNP, TNP-ATP, ATPγS), which diffracted to high resolution even using the optimized conditions described here, we considered the employment of HlyB-NBD mutants in order to extend our screening efforts of the various functional states of the ABC domain. Crystallization and determination of the high-resolution structure of the MJ0796 NBD from *Methanococcus jannaschii* carrying the E171Q mutation has proved the importance of mutant proteins in elucidation of the transporter reaction cycle (Smith *et al.*, 2002b). This structure was the very first example of the biologically relevant dimer, whose structure was supported by the majority of the accumulated data for the members of ABC-transporter family. While extensive biochemical and genetic studies of different ABC transporters previously suggested ATP-induced dimerization of the NBD-components in the reaction cycle (Ambudkar et al., 1999; Hopfner *et al.*, 2000; Sharma & Davidson, 2000), the detection of the ATP-bound dimers of the isolated NBDs proved to be extremely difficult. High-resolution structures for the various wild type ABC proteins demonstrated different models of NBD dimerization upon nucleotide binding (Chapter 1.7). The only one of them, the ABC-component of *E.coli* maltose transporter, MalK, shows the same dimer interface as MJ0796-NBD-E171Q. The crystal structure of MalK revealed the closed ATP-bound dimeric conformation of the protein with two ATP molecules sandwiched between the monomers (Chen *et al.*, 2003). However, the MalK nucleotide-free structure also maintained the dimer conformation owing to the extensive contacts between the MalK-specific C-terminal regulatory domains. Since MalK represents a rare case of the pre-formed NBD dimer observed upon isolation from the transmembrane domains, employment of the mutant NBDs seems to be indispensable for the study of the complete reaction cycle of the ABC transporters.

4.2.1   HlyB-NBD H662A

Mutation of a conserved histidine (His-662) to alanine in HlyB-NBD completely eliminated its ability to hydrolyze ATP (Chapter 7 Figure 71), whilst preserving its ATP-binding capability (Chapter 7, (Zaitseva *et al.*, 2005b)). The same effect on replacement of a conserved histidine (His-211) was reported for HisP, the ATP-binding subunit of

histidine permease from *Salmonella typhimurium* (Nikaido and Ames, 1999). Crystals of H662A-HlyB-NBD in the presence of ATP were obtained by the hanging-drop vapor diffusion technique at 4°C in 3-5 days after mixing 1µl protein solution (10 mg/ml in 1 mM CAPS pH 10.4, 30% glycerol, 2 mM ATP) and 1µl reservoir solution (100 mM malonate pH 5.6, 10% PEG MME 5500, 0.25 M sodium acetate). Protein was also successfully crystallized in the presence of ATP and Mg^{2+}: 1µl protein solution (4-6 mg/ml in 2 mM CAPS pH 10.4, 30% glycerol, 100 mM $MgCl_2$, 2 mM ATP) was mixed with 1µl reservoir solution (95 mM malonate pH 5.7, 9.5% PEG MME 5500, 0.24 M sodium acetate, 5% isopropanol) to set-up hanging-drop crystallization. Crystals continued to grow for 2-3 weeks, reaching a maximum size of 250 µm x 50 µm x 50 µm for the single crystals. Diffraction data were collected to 2.5 Å on the flash-frozen crystals at beamline BW-6 (Figure 29 and Table 3). Native Patterson analysis revealed the presence of a dimer of dimers or a tetramer in the asymmetric unit. Initial attempts to solve the structure of the ATP-Mg^{2+} bound HlyB-NBD H662A by molecular replacement using the nucleotide-free structure of the HlyB-NBD (Schmitt *et al.*, 2003) failed. In order to solve the phase problem, crystals were grown from seleno-methionine substituted protein under conditions slightly different from those used for the wild type protein (Chapter 4.2.1.1). Eventually the structure of HlyB-NBD H662A mutant with ATP-Mg^{2+} in the binding site was solved by the combination of SAD and MR (Chapter 6). HlyB-NBD H662A with ATP-Mg^{2+} served as a model to solve the structure of H662-HlyB-NBD with bound ATP by molecular replacement (Chapter 6).

The H662A mutant protein also produced crystals under similar conditions with 8-Br-ATP instead of the ATP. Yet, no crystals appeared upon 2'-Br-ATP substitution for ATP.

The H662A-HlyB-NBD protein formed crystals with ADP that were identical in shape to those of the wild type enzyme obtained under exactly the same conditions (Figure 25), except that the H662A mutant required the exclusive presence of ADP to produce this type of crystals. As expected, the space groups of H662A mutant and the wild type protein were identical and the unit-cell parameters were rather similar (Table 2). Data from the crystals were collected at the Advanced Swiss Light Source (Villigen, Switzerland) and BW-6 (DESY, Hamburg, Germany) (Table 2). The structure of H662A mutant of HlyB-NBD with bound ADP was solved at 1.7 Å resolution by molecular replacement using nucleotide-free structure of HlyB-NBD (Schmitt *et al.*, 2003) (Chapter 5).
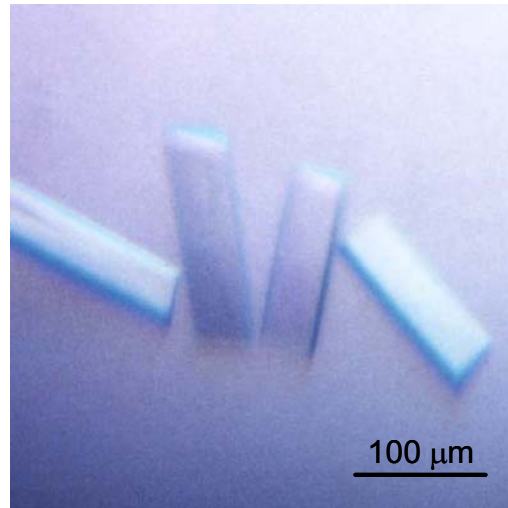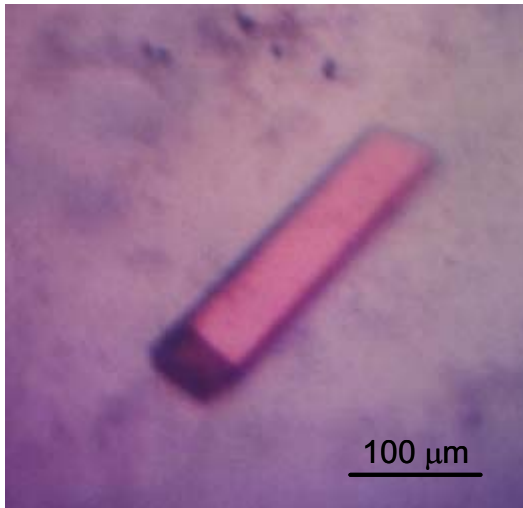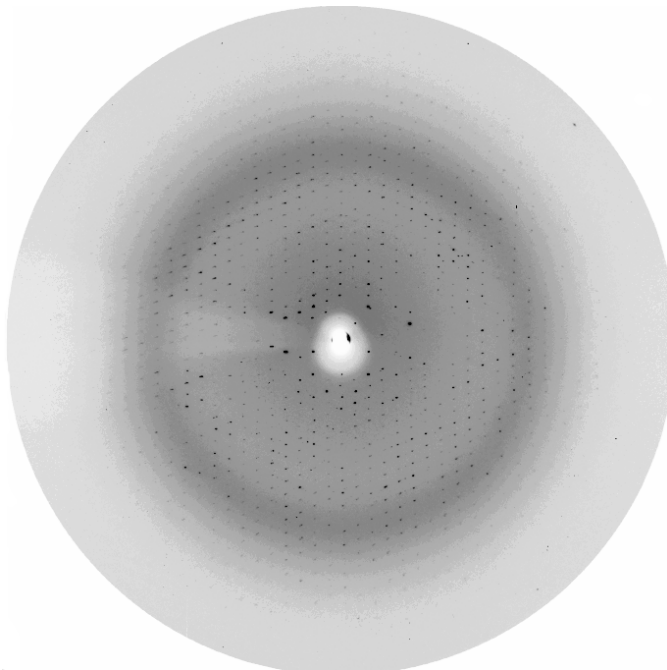
Figure 29. Crystals of HlyB-NBD H662A with bound ATP

A. Crystals of HlyB-NBD H662A with bound ATP were obtained by mixing
1 μl protein, 10 mg/ml in 1 mM CAPS pH 10.4, 30% glycerol, 2 mM ATP, and
1 μl reservoir solution, 100 mM malonate-Na pH 5.6, 10% PEG MME 5500,
0.25 M sodium acetate.

B. Oscillation photograph of HlyB-NBD H662A crystals obtained at the beamline
BW-6 (Hamburg, Germany). Protein was crystallized in the presence of ATP.
Further detailes are given in Table 3.

Table 3. Summary of the crystallographic analysis and data-set collection of HlyB-NBD H662A with ATP-Mg^{2+} and with ATP

Crystal parameters and data collection statistics come from (Otwinowski and Minor, 1997). Refinement statistics were derived from REFMAC5 (Murshudov *et al.*, 1997) and Ramachandran analysis was performed using PROCHECK (Laskowski *et al.*, 1993). Values in parentheses correspond to the highest resolution shell.

Ligand	ATP-Mg^{2+}	ATP
Space group	P2$_1$	P2$_1$
Cell constants at 100 K		
a, b, c [Å]	44.926, 194.917, 63.706	44.56, 195.17, 63.23
α, β, γ [°]	90, 110.68, 90	90, 110.85, 90
Wavelength [Å]	1.05	1.05
Resolution [Å]	20–2.5 (2.56–2.50)	20–2.6 (2.65–2.60)
Mean redundancy	6.8	10.2
Completeness [%]	99.4 (99.8)	96.4 (93.2)
I/σ	23.4 (2.8)	12.1 (3.2)
R$_{sym}$ [%]	5.3 (40.1)	5.7 (19.3)
Refinement		
R$_F$ [%]	21.9 (31.3)	21.1 (27.3)
R$_{free}$ [%]	26.4 (37.1)	27.9 (37.1)
Rmsd bond length [Å]	0.006	0.007
bond angle [°]	1.037	1.085
Average B-factor [Å^2]	51.1	62.3
Ramachandran plot		
Most favored [%]	91.1	90.0
Allowed [%]	8.9	8.7
Generously allowed [%]	0.1	0.9
Forbidden region [%]	0.1	0.4
Model content		
Protein	964 residues	964 residues
Ligands	4 ATP	4 ATP
	4 Mg^{2+}	-
Water molecules	172	197

4.2.1.1. SeMet HlyB-NBD H662A with ATP-Mg^{2+}

SeMet-substituted protein required a different crystallization solution and some adjustments to the crystallization set-up and to the purification protocol (Chapter 2.3**).** Crystals were grown at 4°C by the hanging-drop vapor diffusion technique (Figure 30). Droplets were composed of 1 µl protein (3 mg/ml in 50 mM malonate pH 5.6, 20% glycerol, 100 mM sodium acetate, 2 mM ATP, and 5 mM ß-ME) and 1.5-2 µl crystallization solution (100 mM ADA pH 5.6, 15% PEG 8000, 0.2 M Mg acetate). Crystals usually appeared the next day and were used when they were between 2 days and 1 month old.

Crystals were flash-frozen in a stream of liquid nitrogen. In contrast to the wild type protein, seleno-methionine substituted crystals could be scaled equally well in P2$_1$ (R$_{sym}$= 9.6%) and C222$_1$ (R$_{sym}$= 9.8%). A subsequent twinning test (Padilla and Yeates, 2003) revealed that the seleno-methionine crystal was a perfect pseudo-merohedral twin ($\alpha\sim$ 0.496). Nevertheless, it was possible to obtain a molecular replacement solution from this crystal using the catalytic and helical domain of the nucleotide-free structure of the HlyB-NBD (Schmitt *et al.*, 2003) simultaneously as search models in MOLREP (Vagin and Teplyakov, 2000). The solution obtained was subsequently used as a template for molecular replacement of the 'native' data set using AmoRe (Navaza, 1994). The initial solution was refined using REFMAC5 (Murshudov *et al.*, 1997) employing TLS-grouped refinement (Winn *et al.*, 2001), followed by repetitive rounds of manual rebuilding into 2Fo-Fc and 1Fo-Fc maps using O (Jones *et al.*, 1991). In the initial state of refinement, strict non-crystallographic symmetry (NCS) was applied to all four monomers, which was released in the last four cycles of rebuilding and refinement. The final model consists of a dimer of dimers in the asymmetric unit (964 residues), four ATP, four Mg^{2+}, and 172 water molecules, which were determined using ARP/wARP (Lamzin, 1993) at a threshold of 3.5σ and manually checked for the appropriate density. Refinement statistics and model geometry are given in Table 3.
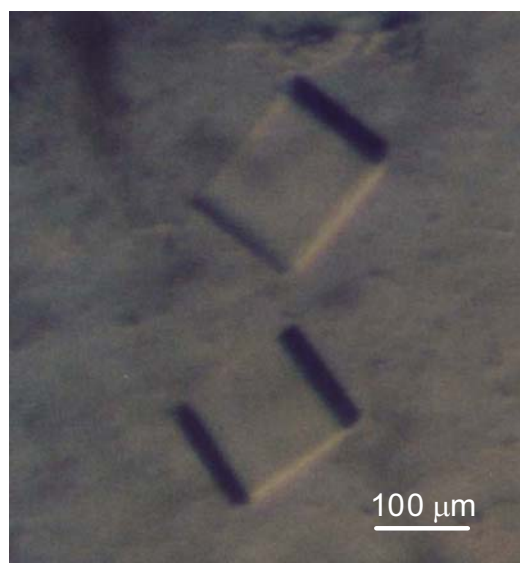
Figure 30. Crystals of SeMet HlyB-NBD H662A with bound Mg^{2+}-ATP

Crystals of SeMet-HlyB-NBD H662A with bound Mg^{2+}-ATP were obtained by mixing 1 µl protein (3 mg/ml in 50 mM malonate pH 5.6, 20% glycerol, 100 mM sodium acetate, 2 mM ATP and 5 mM ß-ME) and 1.5-2 µl crystallization solution (100 mM ADA pH 5.6, 15% PEG 8000, 0.2 M Mg acetate).

4.2.2. *HlyB-NBD E631Q*

While the E171Q mutation completely abolished ATPase activity of MJ0796 NBD (Moody *et al.*, 2002), HlyB-NBD E631Q carrying an equivalent mutation was capable to hydrolyze ATP, though at the significantly reduced rate. The modified enzyme demonstrated an approximately 30-fold reduction of ATPase activity compared to the wild type HlyB-NBD (Figure 31). Setting up crystallization trials of HlyB-NBD E631Q with ATP yielded protein crystals with bound ADP. Crystals were produced by mixing of 1µl protein, 20 mg/ml in 10 mM CAPS pH 10.4, 30% glycerol, 10 mM ATP, and 1µl well solution, 100 mM Tris-Cl pH 8.0-8.5, 10% PEG 6,000, 5% MPD (Figure 32). Usually crystals/needles appeared the next day or even in a few hours after set-up and continued to grow for 1-2 weeks. The same crystallization conditions produced similar in shape protein crystals in the presence of 10 mM ADP and 3 mM EDTA in 10-14 days after set-up. Interestingly, the shape of the ADP-bound

E631Q crystals resembled one of the ATP-bound H662A mutant, while crystallization conditions were identical to those where ADP-bound form of H662A or the wild type HlyB-NBD was obtained. Data from the crystals were collected at the Advanced Swiss Light Source (Villigen, Switzerland) and BW-6 (DESY, Hamburg, Germany) (Table 2). The structure of E631Q enzyme with ADP in the nucleotide-binding pocket was solved at 1.9 Å resolution by molecular replacement using nucleotide-free structure of HlyB-NBD (Schmitt *et al.*, 2003) (Chapter 5).
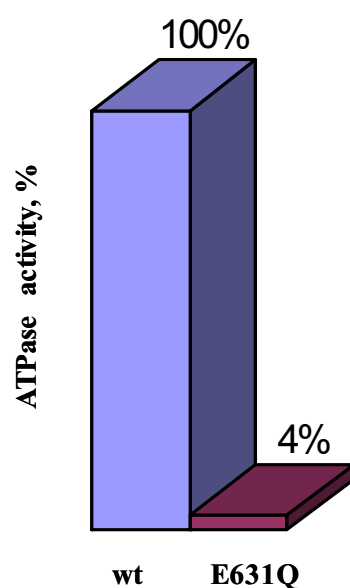
Figure 31. ATPase activity of the purified wild type HlyB-NBD protein and its E631Q mutant

ATPase activity of proteins was measured at room temperature at 3.6 μM enzyme concentration in 100 mM HEPES pH 7.0, 20% glycerol, 1 mM ATP and 10 mM $MgCl_2$. ATPase activity of HlyB-NBD E631Q mutant (magenta bar, 4%) is expressed as percent from the wild type enzyme (blue bar). Data points are the average of three independent experiments.
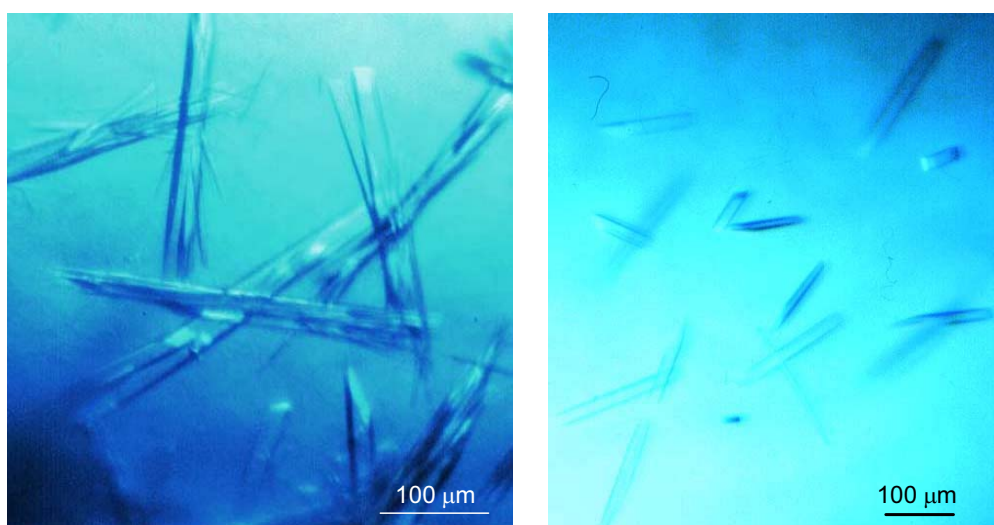
Figure 32. Crystals of HlyB-NBD E631Q with bound ADP

Crystals were produced by mixing of 1 μl protein, 20 mg/ml in 10 mM CAPS pH 10.4, 30% glycerol, 10 mM ATP, and 1 μl well solution, 100 mM Tris-Cl pH 8.0-8.5, 10% PEG 6,000, 5% MPD.

4.3. Conclusions

To obtain the detailed information on the intermediate states of HlyB-NBD in the ATP hydrolytic cycle, the wild type protein and its H662A- and E631Q-mutant proteins were crystallized in the ADP-bound states (Zaitseva *et al.*, 2004; Zaitseva *et al.*, 2005c). The wild type protein and its mutants produced the crystals diffracting to 1.6 Å-1.9 Å. The phase information for all three proteins with bound ADP was obtained by molecular replacement (MR), using the known structure of apo-HlyB-NBD (Schmitt *et al.*, 2003).

The protein was also crystallized in the ATP- and ATP-Mg^{2+}-bound states. Crystals of H662A-HlyB-NBD with ATP and ATP-Mg^{2+} were obtained (Zaitseva *et al.*, 2004; Zaitseva *et al.*, 2005a). The SeMet-substituted H662A-HlyB-NBD with ATP-Mg^{2+} was also crystallized to solve the phase problem. Diffraction data were collected to 2.6 Å on the frozen ATP- and 2.5 Å on the frozen ATP-Mg^{2+} crystals of the protein. Since the initial MR approach was not successful for these crystals, the phase problem was solved by combination of single-

wavelength anomalous diffraction (SAD) and molecular replacement (MR) using the catalytic and the helical domains of the nucleotide-free structure of HlyB-NBD simultaneously.

The overall structures of ADP- and ATP-bound states of HlyB-NBD and its mutants are described (Chapters 5, 6). The implications of structural and functional results are discussed with relation to the mechanism of ABC transporters (Chapter 5-8).

Chapter 5

The ADP-bound structures of the wild type HlyB-NBD, HlyB-NBD H662A, and HlyB-NBD E631Q

5.1. General description of the ADP-bound structures of HlyB-NBD and its mutant forms

The N-terminally His-tagged nucleotide-binding domains of wild type HlyB, the H662A-, and E631Q-mutants were over-expressed in the soluble form in *E.coli* and purified as described in Chapter 2. The proteins were crystallized in the ADP-bound state and crystals diffracted to 1.6-1.9 Å (Chapters 2 and 4). Wild type HlyB-NBD and the H662A-mutant produced similarly shaped crystals-plates (Chapter 4, Figure 25), while the E631Q protein formed rod-shaped crystals (Chapter 4, Figure 32). Yet, all three crystals were of the same space group with one protein molecule and one ADP per asymmetric unit (Table 2). The structures were solved by molecular replacement using AmoRe (Navaza, 1994), with the nucleotide-free structure of HlyB-NBD (Schmitt *et al.*, 2003) as template. The initial solutions were refined using REFMAC5 (Murshudov *et al.*, 1997) employing TLS-grouped refinement (Winn *et al.*, 2001), followed by repetitive rounds of manual rebuilding into 2Fo-Fc and 1Fo-Fc maps using O (Jones *et al.*, 1991). ARP/wARP (Lamzin, 1993) was used to determine water molecules at a conservative threshold of 3σ in the structures. The final model of the wild type HlyB-NBD protein includes all 241 amino acids of the ABC-domain, which corresponds to residues 467-707 of full length HlyB, one histidine residue of the N-terminal affinity tag, one ADP molecule, and 176 solvent molecules. The final models for H662A- and E631Q-HlyB-NBD were very similar to the wild type, each of them containing one more histidine residue of the His-tag (total of two), and a total of 246 and 128 water molecules, respectively. Refinement statistics and model geometry are summarized in Table 2. Although the proteins were successfully crystallized both in the presence and absence of Mg^{2+}, neither of them incorporated a Mg-ion into the active site.

The observed monomeric organization of the ADP-bound HlyB-NBD is consistent with previously reported structures of isolated NBDs and ABC-transporters, which were crystallized with ADP or without nucleotides. Dimerization of the nucleotide-free NBDs was reported only for the "special" ABC-proteins, such as MalK, which harbor an additional C-terminal regulatory domains promoting dimer formation (Chen *et al.*, 2003). The crystal structures of the complete ABC transporters in the nucleotide-free state, BtuCD from *E.coli* and MsbA from *V. cholerae*, resemble a 'sandwich-like' dimeric arrangement of NBDs (Chang, 2003; Locher *et al.*, 2002; Reyes and Chang, 2005). Yet, the buried surface area between the two monomers is rather small in those crystal structures, 480 Å^2 in the case of BtuD, and considered insufficient for a specific protein dimer interface. Thus, the available crystal structures of the complete transporters also represent a monomeric organization of NBDs. Moreover, NBDs of the other complete ABC transporter, MsbA from *E.coli*, were crystallized as spatially separated domains. Investigations of the isolated NBDs in solution support the structural studies, detecting predominantly NBD-monomers in the absence of nucleotides or upon addition of ADP (Chapter 5; (Verdon *et al.*, 2003; Zaitseva *et al.*, 2005b)).

Comparison of the three crystal structures of HlyB-NBD (the wild type, E631Q, and H662A) in the ADP-bound state reveals an essentially identical fold. The rmsd values are 0.19 Å, 0.21 Å, and 0.26 Å for 241 Cα-atoms of wild type/H662A, wild type/E631Q, and H662A/E631Q proteins, respectively. Given significant impact of E631- and H662-mutations on ATPase activity of HlyB-NBD, such a high structural similarity between the wild type and two mutant ADP-bound forms implies that the functional relevance of those two conserved residues is likely restricted to the dimerized ATP-bound state and/or the fully assembled transporter.

Previously reported structures of isolated NBDs (Chen *et al.*, 2003; Diederichs *et al.*, 2000; Gaudet and Wiley, 2001; Hung *et al.*, 1998; Karcher *et al.*, 2005; Karpowich *et al.*, 2001; Lewis *et al.*, 2004; Scheffel *et al.*, 2005; Schmitt *et al.*, 2003; Verdon *et al.*, 2003; Yuan *et al.*, 2001) and full-length ABC-transporters (Chang, 2003; Locher *et al.*, 2002; Reyes and Chang, 2005) established the basic fold of an ATP-binding cassette. The nucleotide-binding domain of HlyB, similar to other ATP binding cassettes, forms an L-shaped molecule with two arms or domains, catalytic and helical (Figure 33). The larger catalytic domain, corresponding to residues 467-549 and 626-707 in HlyB, can be further subdivided into two subdomains, an ABC-β (Karpowich *et al.*, 2001) (residues 467- 494 and 522-535) and a F$_1$- or RecA-like subdomain (Story and Steitz, 1992) (residues 495- 521, 536- 549, and 626-707).
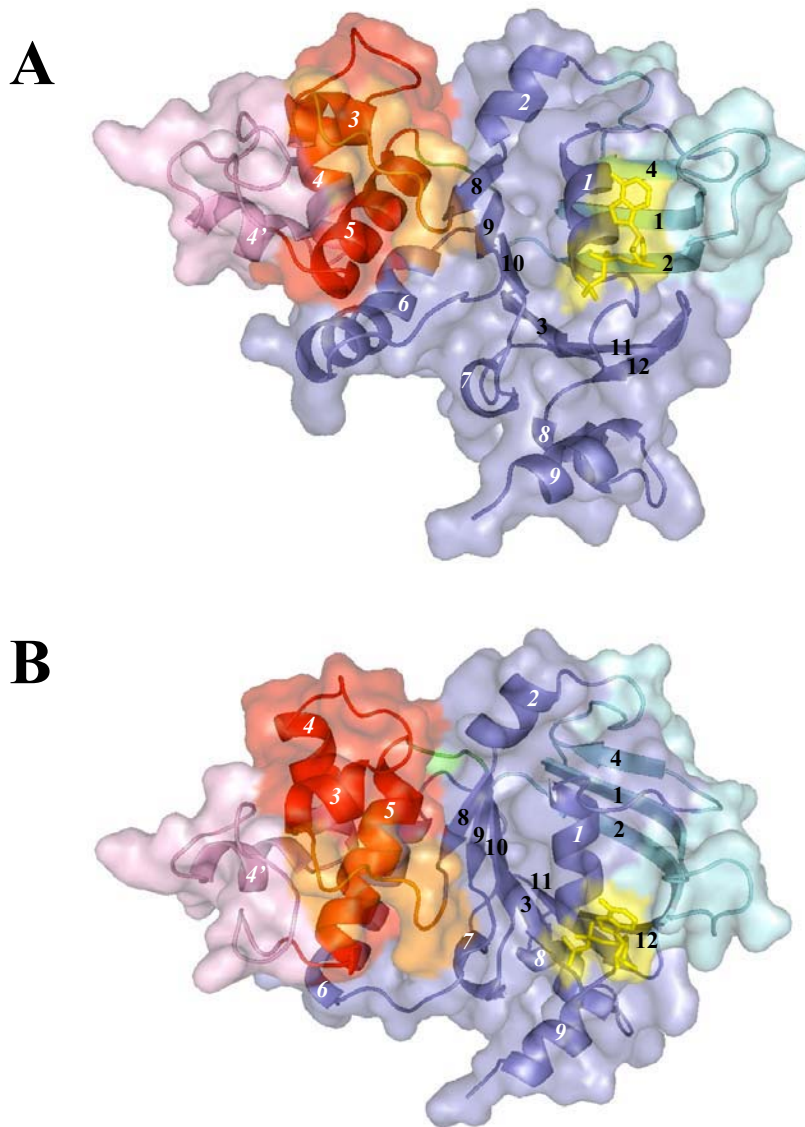
Figure 33. Domains organization of HlyB-NBD with bound ADP

A ribbon diagram with semi-transparent surface presentation of the protein.

   A. The top of the monomer is facing the TMDs of the transporter; the bottom part is facing the cytoplasm. The bound molecule of ADP is shown in stick presentation. The shades of blue color are used for the catalytic domain, while shades of red - for the helical domain of the protein. The large RecA-like subdomain is colored slate blue and the small ABC-β subdomain of the catalytic domain – cyan. The helical domain is colored red with the structurally diverse region (SDR) - pink. ADP is colored yellow; the Q-loop – orange; the Pro-loop – green. The surface reflects a color of the contacting atom/residue. The secondary structure elements are labeled according to HisP nomenclature (Hung *et al.*, 1998); the α-helices and the β-sheets are marked with white and black numbers, respectively.

   B. The HlyB-NBD monomer is facing the transmembrane domains (the bottom of the molecule represents the intersubunit interface).

The catalytic domain forms the nucleotide binding site and includes two β-sheets, six α-helices and several conserved motives (Figure 34), the Walker A (Walker *et al.*, 1982) (residues 502-510) and Walker B (residues 626-632) motifs, which are common to all P-loop NTPases (Vetter and Wittinghofer, 1999), the D-loop (residues 634-639), and the His-loop (residues 661-663). The smaller helical domain (residues 558-621), ABC-α (Karpowich *et al.*, 2001), formed by four α-helices, contains the C-loop or ABC-signature motif (residues 606-610) (Schmitt and Tampe, 2002). The Q-loop (residues 550-557) and Pro-loop (Schmitt *et al.*, 2003) (residues 622-625) link together both domains, catalytic and helical (Figures 33, 34). While all the aforementioned structural elements and general fold of the ADP-bound HlyB-NBD proteins emphasize the obvious conservation of ATP-binding cassette, it's noteworthy that the helical domain of HlyB-NBD includes a structurally diverse region (578–605) (Figure 33), which is unique to each individual NBD (Schmitt *et al.*, 2003). The helical domain is characteristic of ABC-transporters (Holland and Blight, 1999) and, therefore, may be important in signaling between soluble ATP-binding-cassettes and transmembrane domains of transporter, coupling ATP binding/hydrolysis of NBD to allocrite transport (Lebbink and Sixma, 2005; Locher *et al.*, 2002). The helical domain was also shown to be more flexible relative to the catalytic domain ((Diederichs *et al.*, 2000; Gaudet and Wiley, 2001; Karpowich *et al.*, 2001), and Chapter 8). In HlyB-NBD with bound ADP, the elevated B-factors of the helical domain relative to the catalytic domain also support the notion of higher flexibility of the helical domain (data not shown).

5.2. Architecture of the nucleotide-binding site

The protein-nucleotide interactions in the wild type HlyB-NBD and its two mutant proteins, H662A and E631Q, are basically the same. A closer look at the ADP-binding site is presented in Figures 35 and 36. The ADP molecule makes 27 direct and water-mediated contacts with the wild type HlyB-NBD protein, of which 9 are hydrogen bonds (< 3.2 Å) and 14 are van der Waals and hydrophobic interactions (< 4 Å).

The basic features of the nucleotide-binding site of HlyB-NBD are similar to other NBDs of ABC-transporters (Chen *et al.*, 2003; Gaudet and Wiley, 2001; Hung *et al.*, 1998; Karpowich *et al.*, 2001; Lewis *et al.*, 2004; Verdon *et al.*, 2003; Yuan *et al.*, 2001). Thus, a majority of the nucleotide-protein contacts in HlyB-NBD is provided by the residues of the Walker A motif, stabilizing the phosphate moiety of ADP via side and main chain interactions. The β-phosphate of ADP is involved in seven hydrogen bond interactions, while
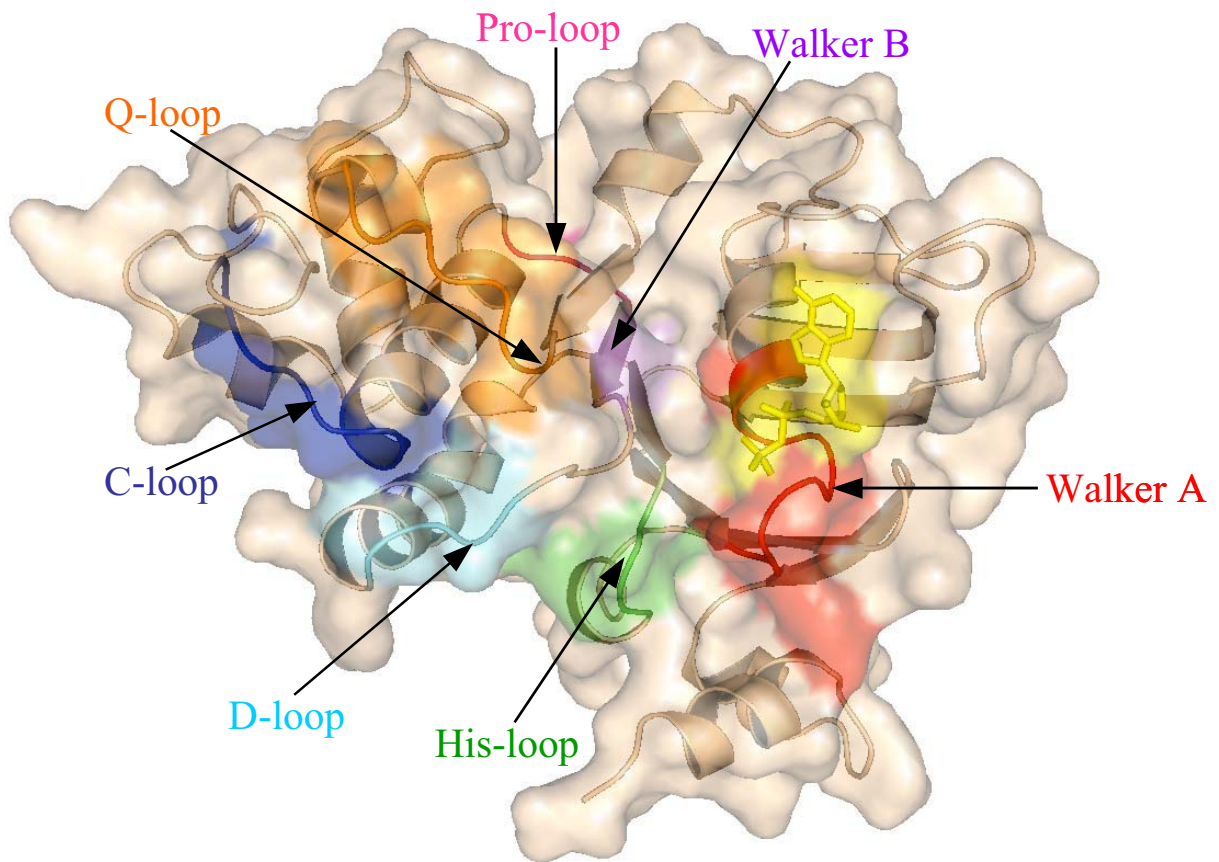
Figure 34. The conserved motifs of ABC transporters

A ribbon diagram with semi-transparent surface presentation of the HlyB-NBD with bound ADP. The top of the monomer is facing the TMDs of the transporter; the bottom part is facing the cytoplasm. The bound molecule of ADP is shown in stick presentation and colored yellow. The conservative motifs of ABC-transporters are indicated and colored; the Walker A motif – red; the Walker B motif – violet; the C-loop or ABC-motif – blue; the His-loop – green; the D-loop – cyan; the Q-loop – orange; the Pro-loop – hot-pink. The surface reflects a color of the contacting atom/residue.
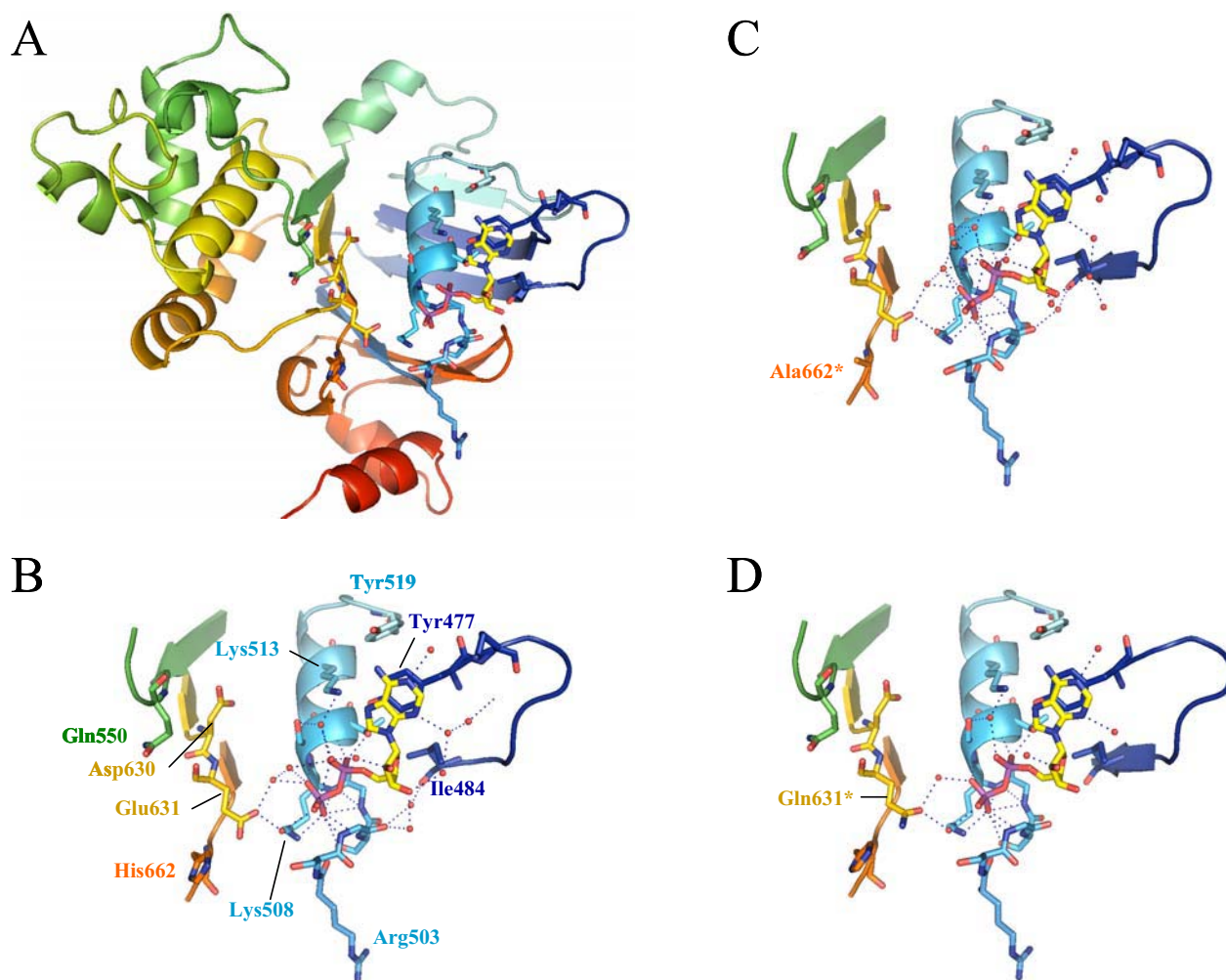
Figure 35. The active site of HlyB-NBD with bound ADP

    A. The ribbon diagram of the wild type HlyB-NBD with bound ADP. The secondary structure elements are rainbow-colored along the protein sequence starting with the dark blue of the N-terminus, followed by the gradually changing colors, such as light blue, green, yellow, orange, and red color of the C-terminal end. The top of the molecule is facing the TMDs of the transporter; the bottom part is facing the cytoplasm. The selected residues and bound molecule of ADP are shown in stick presentation. The carbon atoms of ADP are colored yellow, the phosphorus atoms – magenta, oxygen – red, and nitrogen – blue.

    B. Close-up view of the nucleotide-binding site of the wild type protein.

    C. Close-up view of the nucleotide-binding site of H662A mutant of HlyB-NBD.

    D. Close-up view of the nucleotide-binding site of E631Q mutant of HlyB-NBD.
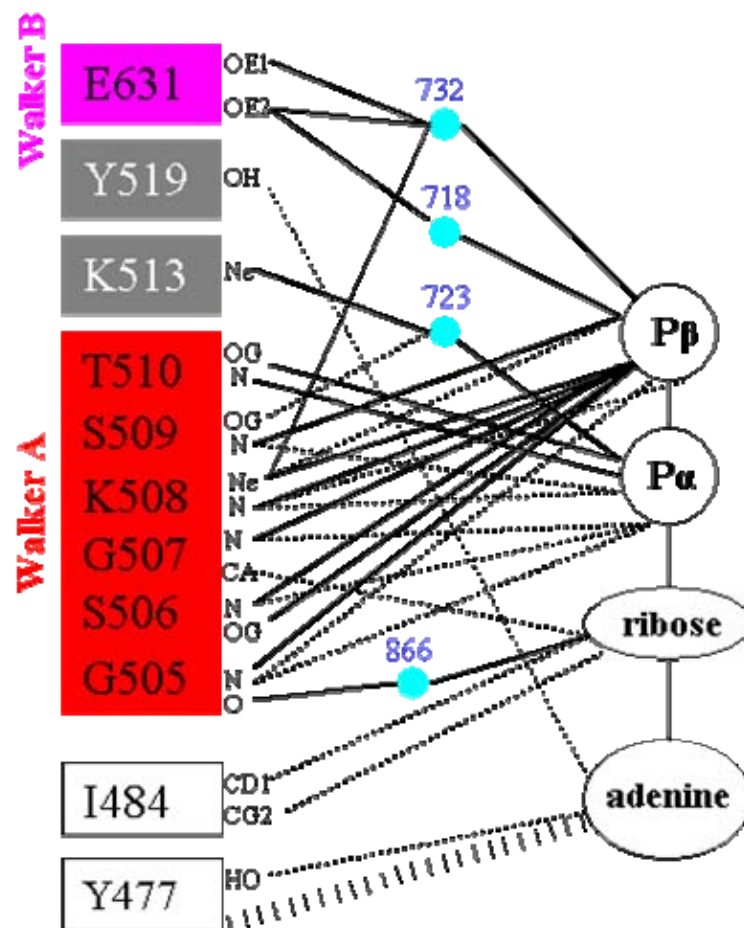
Figure 36. Schematic diagram of the main interactions between ADP and the wild type HlyB-NBD protein

The conserved motifs are colored in red (Walker A motif) and magenta (Walker B motif), and labeled accordingly. Turquoise spheres indicate water molecules. Hydrogen bonds and salt bridges are shown as solid lines (< 3.2 Å), while van der Waals and hydrophobic interactions are shown as dashed lines (< 4.0 Å). Letters next to amino acids represent the atoms involved in the interactions.

the α-phosphate makes 2 hydrogen bonds with the protein. Such a distribution of ligand-enzyme interactions may explain specific binding of ADP but not AMP to HlyB-NBD (Zaitseva *et al.*, 2004). The adenine ring of ADP interacts with an aromatic amino acid, Y477 in HlyB, via π-π stacking. This pattern has been observed in all other crystal structures of the nucleotide-bound NBDs with the only exception of NBD1 of mouse CFTR (Lewis *et al.*, 2004). While the ribose- and adenine-groups of ADP establish seven contacts with the protein, they belong either to van der Waals or hydrophobic interactions and one is a water-mediated link. The absence of hydrogen bonds with the adenine-group is a common feature of nucleotide-binding sites in various ABC-structures that explains the relatively broad nucleotide specificity of ABC subunits (Higgins, 1992). Thus, the phosphate groups of the nucleotide play a central role in ligand-enzyme binding.

5.3. *The conserved amino acid residues*

The position of the conserved glutamate of the Walker B motif, Glu631 in HlyB-NBD, differs in various ABC protein structures with bound nucleotides. In the wild type HlyB-NBD and both mutant structures, E631 (Q631 in the E631Q protein) creates multiple water-mediated contacts with the β-phosphate of ADP (Figures 35-36). In all three structures of HlyB-NBD, Glu631 also establishes a water-mediated contact with Lys508, the residue of the Walker A motif that is actively involved in the nucleotide binding. Thus, the functionally important glutamate in the HlyB-NBD structure makes very extensive contacts with the active site and bound ADP. Interestingly, in various ABC proteins the conserved glutamate does not follow a consistent pattern in its contacts with bound nucleotide. Thus, this residue of the Walker B is withdrawn from the active site of MJ0796 with bound ADP-Mg^{2+} (Yuan *et al.*, 2001), yet it establishes a water-mediated contact with the β-phosphate in the structure of the other ABC-subunit, MJ1267-ADP-Mg^{2+} (Karpowich *et al.*, 2001). Similarly, the conserved Glu was shown to interact with the γ-phosphate group in the ATP-bound structures of HisP (Hung *et al.*, 1998), MJ0796 (Smith *et al.*, 2002b), and HlyB-NBD (Chapter 6). Yet, the structure of another ATP-bound NBD, MalK, shows no contacts between the conserved glutamate and nucleotide (Chen *et al.*, 2003). Although the structural investigations of the different ATP-binding cassettes reveal an important functional positioning of the glutamate of the Walker B motif, which is adjacent to the protein nucleotide-binding site, additional biochemical and structural studies are required to clarify the exact function of this residue. A postulated role of the general base for the glutamate of the Walker B motif is currently under

debate (Moody *et al.*, 2002; Sauna *et al.*, 2002; Tombline *et al.*, 2004; Zaitseva *et al.*, 2005a). An alternative hypothesis of a substrate-assisted catalysis was introduced, where two conserved residues, the glutamate of the Walker B and the histidine of the His-loop, act together as a "catalytic dyad" (Zaitseva *et al.*, 2005a).

In the crystal structures of various ABC-domains, three other conserved residues of the ABC-transporters were shown to participate in the interaction with β-/γ-phosphate of nucleotide and/or Mg-ion (Chapter 6; (Chen *et al.*, 2003; Gaudet and Wiley, 2001; Hung *et al.*, 1998; Karpowich *et al.*, 2001; Lewis *et al.*, 2004; Verdon *et al.*, 2003; Yuan *et al.*, 2001). In the HlyB-NBD structure these conserved amino acids, His662 of the His-loop, D630 of the Walker B motif, and Q550 of the Q-loop, are located in the relative proximity to the active site (Figures 35 and 37), yet have no contact with ADP.

The conserved histidine-662 (alanine-662 in the H662A-mutant) has no connection with the nucleotide-binding site in all three structures of HlyB-NBD with bound ADP. Such a position of His (Karpowich *et al.*, 2001; Verdon *et al.*, 2003; Yuan *et al.*, 2001) or the corresponding non-canonical residue of the His-loop (Gaudet and Wiley, 2001; Lewis *et al.*, 2004) is consistent with all available structures of the ADP/ADP-Mg^{2+}-bound ABC-proteins, while the ATP-bound structures of various NBDs demonstrate direct or water-mediated link between the histidine and the γ-phosphate (Hung *et al.*, 1998).

Comparison of the previously reported structures of ABC subunits reveals a consistent pattern in the positioning of the conserved aspartate of the Walker B motif relative to the active site. In most of the Mg^{2+}-bound NBD structures this Asp-residue is bridged simultaneously with the Mg-ion and with the β- and/or γ-phosphate via a water molecule (Gaudet and Wiley, 2001; Karpowich *et al.*, 2001; Verdon *et al.*, 2003). The lack of Mg^{2+} in the active site usually does not obstruct the Asp-ligand contact. Thus, the Mg^{2+}-free structures of HisP-ATP (Hung *et al.*, 1998), MJ0796-ATP-Na$^+$ (Smith *et al.*, 2002b), HlyB-NBD-ATP (Chapter 6), and CFTR-ADP (Lewis *et al.*, 2004) still have their conserved aspartate residues being involved in the arrangement of the nucleotide-binding site. In some NBD structures no obvious connection is detected between the bound ligand and the conserved Asp (Chen *et al.*, 2003; Yuan *et al.*, 2001). Yet, in all reported nucleotide-bound NBD structures these Asp-residues of the Walker B motif are oriented toward the active sites and have potential opportunity to establish a contact with ADP/ATP or Mg-ion. Surprisingly, in the structures of the wild type, H662A-, and E631Q-mutant of HlyB-NBD, no interaction between the conserved D630 and ADP is observed (Figure 35). Moreover, the aspartate-630 and

Figure 37. Stereoview of the interactions between the Q-loop and the residues of the extended Walker B motif in HlyB-NBD H662A with bound ADP

The residues Val548, L549, and Gln550 of the Q-loop are colored green; the residues D630, E631, A632, and T633 of the extended Walker B motif are shown in yellow; the molecule of ADP is colored pink, the phosphorus atoms – magenta, oxygen – red, and nitrogen – blue. Water molecules are shown as red spheres. Protein-protein and protein-nucleotide interactions are colored and labeled blue. All residues and ADP are in stick presentation.

nucleotide are separated by more than 8 Å in the ADP-bound state of HlyB-NBD. A possible explanation for such a discrepancy in the positioning of the conserved Asp can be posthydrolysis conformational changes in the protein leading to the establishment of strong contacts between D630 and Q550, whereas Q550 is the conserved residue of the Q-loop that is unusually distantly located from the active site of the HlyB-NBD (see description below for Q550 in the ADP-HlyB-NBD structure as well as Chapter 6 for ATP/ATP-Mg^{2+}-HlyB-NBD structure). Thus, the main chain amide of Gln550 has a water-mediated connection with the side-chain carboxylate group of Asp630, which could be a primary reason for removing this conserved aspartate from the nucleotide-bound site (Figure 37). Besides, the side chain amide group of Gln550 is linked to both carboxyl and amide groups of the aspartate-630 main chain via the water-mediated contacts. In fact, the interactions between the Walker B motif and the Q-loop are not limited to the D-Q connection, but involve other residues of the aforementioned regions. Thus, the side-chain of Q550 directly interacts with the main chain

amide of Thr633, the residue of the extended D-loop, while the main chains of the Walker B motif and the Q-loop are firmly attached to each other via direct link between the amide group of Asp630 and the carboxyl group of Val548, respectively. Additional water-mediated contact between the main chain carboxyl groups of D630 and V548 further stabilize Walker B – Q-loop association. All described interactions hold the two protein motifs together in the ADP-bound structures of the wild type HlyB-NBD and its two mutant proteins, H662A and E631Q. It seems likely that withdrawal of the aspartate-630 from the active site weakens the affinity of the Mg-ion to the protein, resulting in the unexpected lack of Mg^{2+} in the ADP-HlyB-NBD nucleotide-binding site (see above).

Similar to the conserved glutamate of the Walker B motif, the position and interactions of the conserved glutamine of the Q-loop vary in different ABC structures. Some of NBDs have their invariant Q-residue positioned in the vicinity of the bound nucleotide (Lewis *et al.*, 2004; Verdon *et al.*, 2003). That especially is true for the ATP-bound proteins (Chen *et al.*, 2003; Hung *et al.*, 1998; Smith *et al.*, 2002b; Verdon *et al.*, 2003). For example, in the ADP-Mg^{2+}-bound structure of ABC transporter, GlcV, the conserved Gln of the Q-loop is connected with Mg-ion in the active site via a water-mediated link (Verdon *et al.*, 2003). The other NBDs have the conserved Gln being distantly located from the active site (Chapter 6; (Gaudet and Wiley, 2001; Karpowich *et al.*, 2001; Yuan *et al.*, 2001). It is also observed for the position of Gln550 of the Q-loop in the ADP-bound structures of HlyB-NBD. The Q550 residue is completely withdrawn from the nucleotide-binding site, pointing in the opposite direction and generating a distance of at least 11 Å between the residue and the bound ADP molecule (Figures 35 and 37). In the structure of other NBD, MJ1267 with bound ADP-Mg^{2+}, the position of the invariant Q89 is similar to that of Q550 relative to the active site, where the conserved Gln89 and ADP-Mg^{2+} are separated by more than 13 Å (Karpowich *et al.*, 2001).

Different positions of the conserved glutamine in various nucleotide-bound NBD structures could be explained by a specific role of the Q-loop. The Q-loop was proposed to interact with TMD domains (Locher *et al.*, 2002), which are specific to every ABC transporter. At the same time, the Q-loop connects the helical and catalytic domains and might provide a variable degree of flexibility between these two domains. Thus, it is possible that variable positions of the conserved Q-residue in the posthydrolysis NBD structures reflect variability between different ABC domains.

5.4. Conclusion

The overall ADP-bound structures of the wild type HlyB-NBD and its mutants are very similar to the previously reported NBD structures, including the monomeric organization, domain composition, and basic features of the active site. However, there is obvious dissimilarity between various ABC subunits. Importantly, the difference concerns not only the specific and variable regions in every ABC protein, but also the conserved motifs. Thus, the diverse structural positions of the conserved amino acids complicate direct comparison of the NBD domains from different systems. Therefore, crystallization and direct structural analysis of the various functional states of the same ABC subunit is of extreme importance. The detailed pictures of the active sites in every state of single ABC subunit will allow to understand the relationship between the function and structure and to propose the general mechanism of action in the ABC transporters.

Chapter 6

The structures of HlyB-NBD H662A dimers with bound ATP and ATP-Mg^{2+}

6.1. Overall structures of HlyB-NBD H662A dimers

The H662A mutant of HlyB-NBD, composed of the C-terminal residues 467-707 of full-length HlyB, was over-expressed and purified as described for the wild-type NBD (Chapter 2; (Zaitseva et al., 2004)). Crystals were obtained in the presence of ATP and ATP-Mg^{2+} and diffracted to 2.6 Å and 2.5 Å, respectively (Chapters 2 and 4). The structure of the H662A protein with ATP-Mg^{2+} was determined using a combination of SAD data set from a seleno-methionine substituted protein crystal and molecular replacement (Chapter 4). The refined structure has an R$_F$ value of 21.9 % and an R$_{free}$ of 26.4% without non-crystallographic symmetry (NCS) restraints. All amino acids except the N-terminal His-tag were visible in the electron density map. Both ATP- and ATP-Mg^{2+}-forms of HlyB-NDB H662A were crystallized as a dimer of dimers in an asymmetric unit (Figure 38). The final structure for the ATP-Mg^{2+} dimer contains 964 amino acids together with 4 ATP, 4 Mg^{2+}, and 172 water molecules that were located in 1F$_o$-F$_c$ difference maps at a conservative threshold of 3.5σ and manually checked for correct density. Further details of the refinement and the geometry of the structure are shown in Table 3 (Chapter 4). The structure of the ATP-bound protein was solved by molecular replacement using H662A-HlyB-NBD with ATP-Mg^{2+} as a model (Chapters 2 and 4) and resulted in 964 amino acids, 4 ATP, and 196 water molecules (Data collection and refinement statistics are shown in Table 3).

The dimer of dimers arrangement is likely not physiological as the buried surface area between each dimer pair is only 480 Å^2, which is not sufficient to be considered as specific protein-protein interactions. Besides, no biochemical evidence for the presence of such an architecture exists. Each monomer chain was designated A, B, C, and D with the corresponding dimer forms being AB and CD within an asymmetric unit. Two dimer
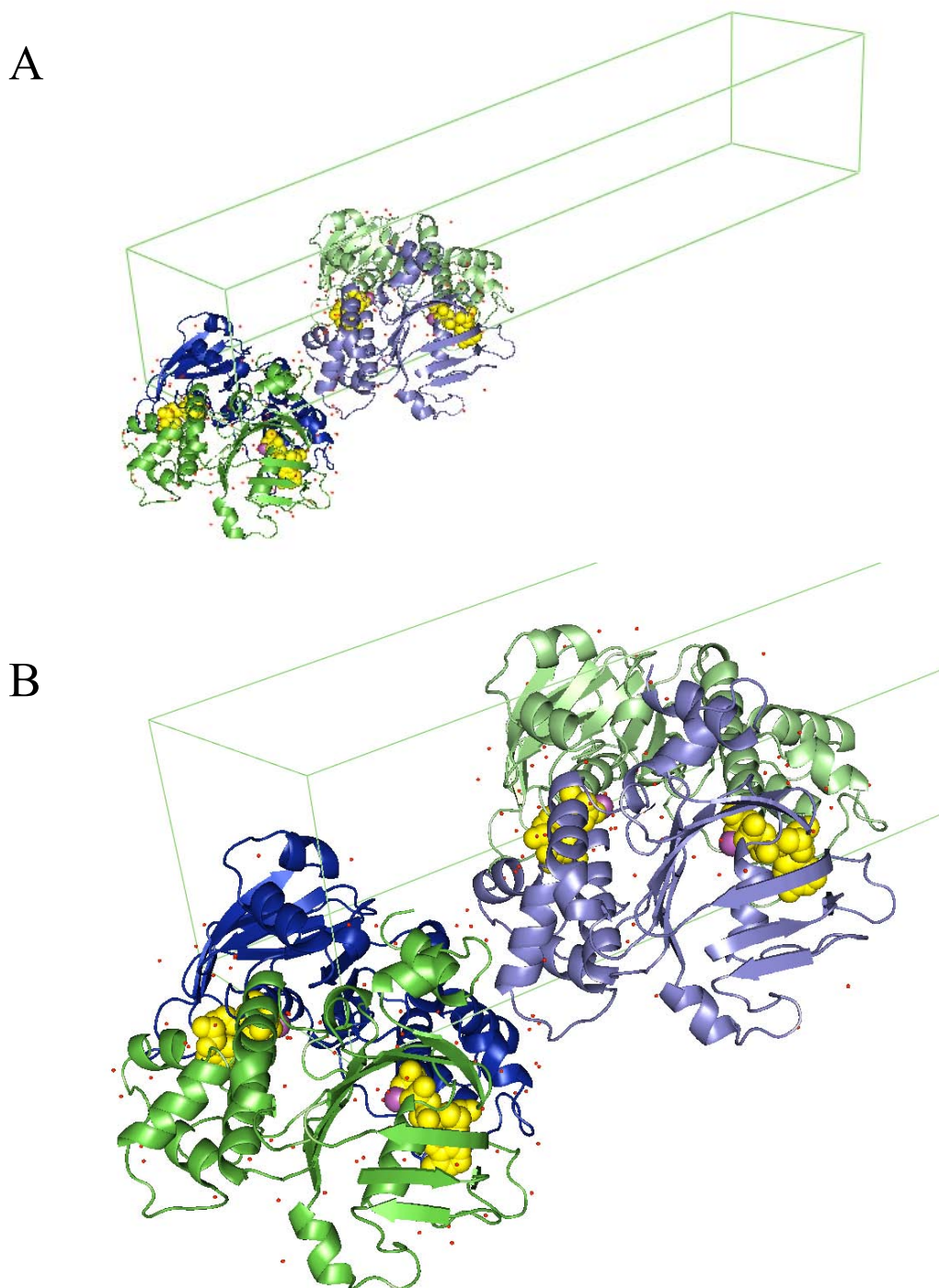
Figure 38. An asymmetric unit of the ATP-Mg^{2+}-HlyB-NBD H662A crystal

The cell unit is shown in the lime-colored lines. Each monomer is individually colored: A subunit green, B - blue, C - lime, and D - slate blue. The ATP-Mg^{2+} molecules are shown as surface-sphere presentation with ATP colored yellow and Mg-ion - magenta. Water molecules are shown as small red spheres.

A. A dimer of dimers arrangement of protein

B. Close-up view of Figure 38A

structures of the ATP-Mg^{2+}-bound protein within the asymmetric unit are essentially identical to each other with rmsd of 0.58 Å^2, when 482 Cα atoms of each dimer are aligned with each other. A comparable picture was observed for the ATP-bound HlyB-NBD H662A without Mg^{2+}, with rmsd of 0.71 Å for 472 Cα aligned atoms of each dimer. The residues excluded from the ATP-form alignment were P568, G600-A604, and D707 for the A- and C-subunits and D467, Q602-A604, and D707 for B- and D-subunits. This corresponds to the first N-terminal residue (D467), a peripheral loop of the helical domain (P568), two symmetrical loops at the likely TMD-NBD interface (600-604), and the last C-terminal amino acids (706, 707) of the subunits. The structural deviations between Cα atoms of AB- and CD-dimers for both ATP-Mg^{2+} and ATP-states of HlyB-NBD are not related to their conserved structural or functional elements and most likely reflect either slightly higher mobility of those regions identified by somewhat elevated B-factors or the crystallographic packing of the molecules in the asymmetric unit. Hereafter only one AB dimer composed of two H662A-HlyB-NBD monomers of either the ATP-Mg^{2+}- or the ATP-bound protein will be discussed, unless otherwise stated. When the AB dimer of the ATP-Mg^{2+}- and AB-dimer of the ATP-bound HlyB-NBD H662A were aligned, the Cα rmsd of 0.63 Å was calculated for 474 aligned atoms. The regions excluded from the analysis were the same as listed above for AB- versus CD-dimer alignment of ATP-bound protein, Q602-A604 and S706-D707 amino acids for A-subunits and G603, D707 amino acids for B-subunits, which are equivalent to two symmetrical loops at the likely TMD-NBD interface (602-604) and last one or two C-terminal residues (706, 707) of the subunits. Thus, the overall structures of the HlyB-NBD H662A dimers in the ATP-Mg^{2+}- and the ATP-forms are very similar. Nevertheless, the detailed structural analysis of the protein-protein and protein-nucleotide interactions revealed an asymmetry between two monomers of each type of dimer, ATP-Mg^{2+}- and ATP-loaded. Moreover, more prominent asymmetry was observed between two NBD-subunits and nucleotide-binding sites in the HlyB-NBD structure with bound ATP-Mg^{2+}, than in the Mg^{2+}-free structure.

The ribbon diagram of the overall structure of the ATP-Mg^{2+} loaded composite dimer of H662A mutant of HlyB-NBD is shown in Figure 39. All conserved motifs are primarily concentrated within the dimer interface and are highlighted with different colors. The His-loops, which normally contain His662 and are colored green in the figure, closely approach the γ-phosphates of the bound ATP. Two molecules of ATP are sandwiched between the monomers, forming two distinct ATP-binding sites. Each homodimer displays a symmetrical organization, since the rmsd values between the individual monomers are 0.62 Å for 240 Cα
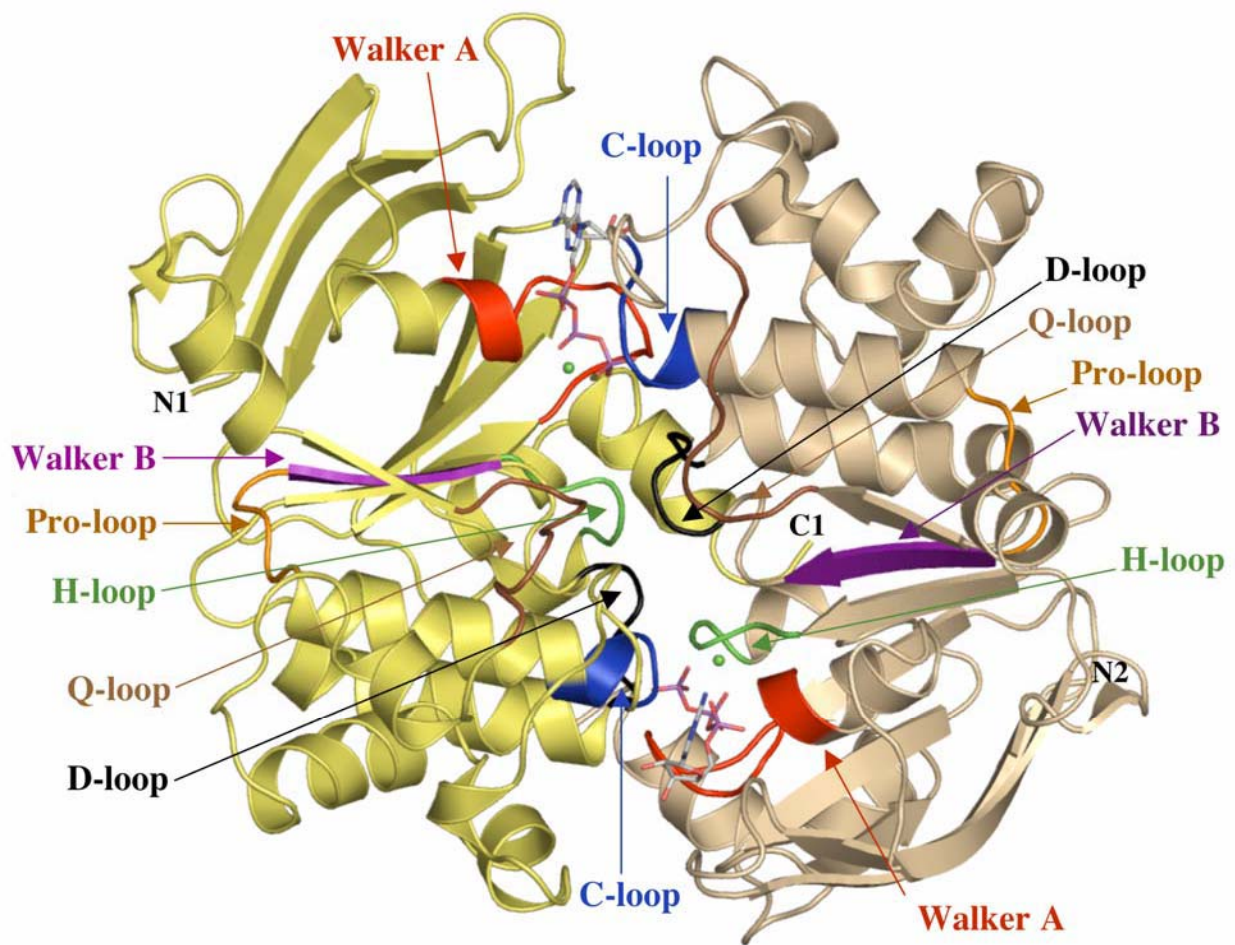
Figure 39. Crystal structure of the HlyB-NBD H662A dimer with bound ATP-Mg^{2+}

ATP in stick representation and Mg^{2+} (green spheres) are sandwiched at the interface of the two HlyB-NBD monomers (shown in light tan and light yellow). The N- and C-termini of the individual monomers are labeled. Conserved motifs are colored in red (Walker A motif), brown (Q-loop), blue (C-loop or ABC-signature motif), magenta (Walker B), black (D-loop), orange (Pro-loop), and green (H-loop) and labeled accordingly. The figure was prepared using PyMol (www.pymol.org).

atoms in the AB dimer and 0.72 Å for 239 Cα atoms in the CD dimer of protein with bound ATP-Mg^{2+}. The symmetry is also observed for HlyB-NBD-ATP subunits, with 0.77 Å for 235 aligned Cα atoms in the AB dimer and 0.52 Å for 238 Cα atoms in the CD dimer of the protein, suggesting the same overall structure of each subunit in the dimer.

A similar dimer organization was previously reported for two ABC-importers MJ0796 (Smith et al., 2002b) and MalK from *E.coli* (Chen et al., 2003), which were obtained in the presence of ATP-Na$^+$ and ATP alone, respectively. A comparison of the HlyB-NBD-ATP-Mg^{2+} dimer with MJ0796 (Smith et al., 2002b) and MalK (Chen et al., 2003) structures reveals rmsd of 1.57 Å for MJ0796 (327 Cα atoms) and 1.59 Å for MalK (347 Cα atoms). For HlyB-NBD-ATP, the above characteristics correspond to 1.60 Å (330 Cα atoms) and 1.60 Å (345 Cα atoms), respectively. The remarkable similarity of the structures of HlyB-NBD, MJ0796, and MalK demonstrates that such an arrangement of the ATP-bound NBD-dimer is most likely a universal feature not only of ABC-importers, but of ABC-exporters as well.

In contrast to the structures of MJ0796 (Smith et al., 2002b) and MalK (Chen et al., 2003), HlyB-NBD H662A was crystallized in the two ATP-bound forms, with and without Mg^{2+}. Notably, both ATP molecules are intact in the structure, containing Mg^{2+} in the active site (Figure 40). An omit map contoured at 4σ 1F$_o$-F$_c$ confirmed the presence of the unmodified β-γ phosphate bond in the structure of His662Ala mutant HlyB-NBD (Figure 40). Continuous density for the triphosphate moiety was still visible at a contour level of 8σ (not shown). Indeed, the H662A mutant displayed no detectable steady-state ATPase activity in solution (Chapter 7 Figure 70 and (Zaitseva et al., 2005b)). This implies that the conserved histidine H662 must play a crucial role in pre-hydrolysis events, rather than simply act as a 'γ-phosphate sensor' as suggested previously (Geourjon et al., 2001).

A comparison of the overall structures of the aforementioned proteins also reveals that the dimerization of HlyB-NBD-ATP-Mg^{2+} buries almost twice as much solvent accessible area as do the MJ0796 and MalK ATP-bound NBDs: 1890 Å^2 versus 1100 Å^2 and 1020 Å^2, respectively (Chen *et al.*, 2003; Smith *et al.*, 200b). The buried solvent-accessible area between the monomers of the HlyB-NBD-ATP dimer structure was calculated to be 1900 Å^2, which is very close to that of the ATP-Mg^{2+}-bound state of the protein. Such a difference between HlyB-NBD and two other ATP-bound dimers can be explained not only by more active involvement of the residues of the Walker A motif and the D-loop into the formation of the HlyB-NBD dimer interface (see below), but also by the presence of the extended C-terminus of HlyB-NBD (Figure 8: helix 9 and the following amino-acids). The C-terminal amino acid residues extensively participate in making intersubunit contacts with NBD in the
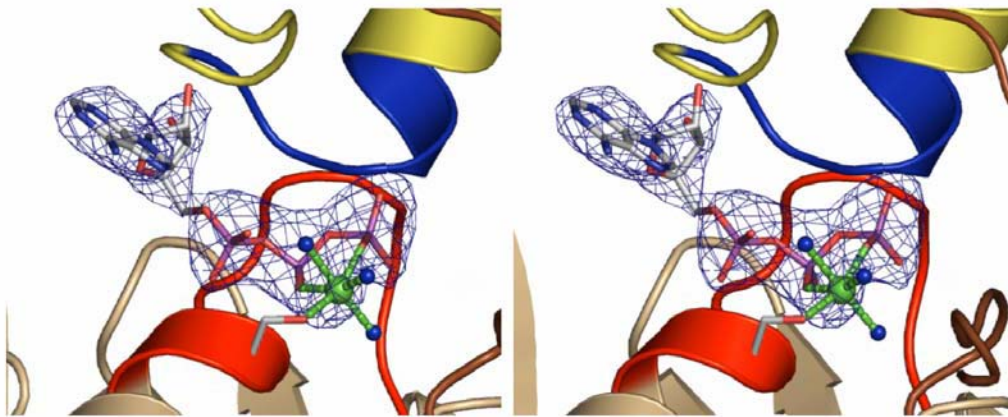
Figure 40. Stereoview of a 1Fo-Fc omit map contoured at 4σ of one of the ATP-Mg^{2+} complexes bound to the HlyB-NBD H662A homodimer

All refined ATP-Mg^{2+} complexes were omitted in structure factor calculation to clearly demonstrate the continuous electron density of the triphosphate moiety. Also shown are the three water molecules (blue spheres), which form, in combination with the β- and γ-phosphates and S509, the octahedral coordination sphere of the bound Mg^{2+} (green sphere). Color-coding is identical to Figure 39.

HlyB-NBD structure (see below), while no analog for such an elongated sequence exists in MJ0796. In the case of MalK, the structural elements corresponding to Y700-D707 of HlyB-NBD are not involved in the interactions with NBD. Instead, they participate in the formation of protein-protein contacts with C-terminal regulatory subunits of MalK (Chen et al., 2003).

Analysis of the van der Waals surface of HlyB-NBD dimer revealed two distinct tunnels in the proximity of the ATP-binding sites. The presence of tunnels clearly distinguishes the structures of HlyB-NBD dimers from the previously reported ATP-bound structures of the NBD components of ABC transporters. Dissimilarity in the intersubunit contacts and nucleotide-binding sites between the two analyzed structures of HlyB-NBD H662A (see below) is also extended to the structural difference of the tunnels. While in the ATP-Mg^{2+}-bound form of H662A dimer, each tunnel is open on the side facing TMDs and closed on the opposite side, both ends are closed in the ATP-bound state of protein without Mg^{2+}.

Importantly, the calculation of the solvent-accessible surface using a standard probe radius of 1.4 Å doesn't detect narrow water-accessible channels in the HlyB-NBD structure,

but rather results in two asymmetric cavities on the TMD-side of the protein dimer. One cavity reaches a solvent-accessible surface of the γ-phosphate of ATP in the first active site and the other cavity expands a bit further, separating ATP and catalytically active residues in the second active site. Thus, the observed structural asymmetry between the two active sites of the ATP-Mg^{2+}-bound dimer (see below) demonstrates a potential capability to produce a functional asymmetry, since only one of the cavities in the ATP-Mg^{2+}-bound HlyB-NBD dimer forms an apparent phosphate channel to release the γ-phosphate after ATP hydrolysis.

Two tube-shaped elongations of the cavities in HlyB-NBD-ATP-Mg^{2+} dimer structure can be detected with a program for calculation of the solvent-accessible surface employing extremely small probe size of 0.4 Å. Such a small size of the channels in the proximity of the ATP-binding sites emphasizes a transient nature of channels.

Thus, an overall assembly of the NBD-NBD complex and atomic details of the structural asymmetry in HlyB-NBD dimer could make a fundamental contribution to our understanding of a general mechanism of action of all ABC transporters.

6.2. Architecture of the ATP-binding site of HlyB-NBD H662A with ATP-Mg^{2+}

While the overall dimer interface for HlyB-NBD-ATP-Mg^{2+} is approximately 1890 Å^2, protein interaction with two ATP molecules buries a 450 Å^2 surface area directly involved in contact with the nucleotides. Thus, inter-subunit contacts can be divided into two groups: ATP-dependent interactions and direct monomer-monomer interactions.

Connections between HlyB-NBD and ATP are very extensive and originate from both monomers in the dimer. Each ATP molecule in the dimer structure is coordinated by the Walker A motif of one monomer (*cis*-site) and the C-loop (ABC-signature) of the other monomer (*trans*-site). Figure 41 shows the arrangement of the intra- and intermolecular interactions within the ATP-binding site of HlyB-NBD-ATP-Mg^{2+} that is similar to those in ATP-bound MJ0796 (Smith et al., 2002b) and MalK (Chen et al., 2003) structures. Both ATP and Mg^{2+}-ion are extensively involved into direct and solvent-mediated protein-nucleotide interactions, gluing the two monomers together. Two ATP molecules introduce at least **86** direct and water-mediated contacts at the dimer interface of which **26** are direct hydrogen bonds or salt links ($\leq$ 3.2 Å) with the protein, **12** are water mediated links, and the remaining **48** are attracted by van der Waals forces and by the hydrophobic interaction ($\leq$ 4.0 Å).

Additionally, the β- and γ-phosphates of ATP together with the side chain of S509 and three water molecules (turquoise spheres in Figure 41) interact with Mg^{2+} (the green sphere in Figure 41), completing the octahedral coordination sphere of Mg^{2+}. Such a powerful net of the substrate-protein connections explains the strong dependence of the NBD-dimer stability on the presence of ATP that was previously observed for the ATP-bound structure of MJ0796 (Smith et al., 2002b) and in the studies of pure HlyB-NBD in solution (Chapter 7).

6.2.1. Intramolecular (in cis) interactions in the ATP-binding site

As in all other P-loop ATPases (Vetter and Wittinghofer, 1999), the Walker A motif (G502-T510) wraps around the triphosphate moiety, providing the majority of the ligand-protein connections via main-chain and side-chain interactions. Thus, the side chain of the conserved lysine (**K508**) interacts with the β- and γ-phosphates, thereby fixing both groups in a defined orientation. The main chain amide of K508 further strengthens the above link forming an additional hydrogen bond with the β-phosphate and supplementary van der Waals contacts with the α- and β-phosphates of ATP. Another conserved residue of the Walker A motif, **Ser509**, is very intensively involved in direct and water-mediated contacts with all the three phosphates of ATP and directly binds to Mg^{2+}-ion in the active site. Both side- and main chains of **Thr510** also contribute to the stability of the ATP-protein complex by forming two strong hydrogen bonds (2.6-3.0 Å)[1] with the α-phosphate of ATP and one van der Waals contact with the O-5'-ribose group of ATP. The other residues of the Walker A motif, **S504-G507**, further strengthen substrate-protein interaction providing two more hydrogen bonds and eight van der Waals connections with the α-, β-, and γ-phosphates, and one hydrophobic contact with the ribose ring of ATP.

As observed in all nucleotide-bound crystal structures of ABC-NBDs, the adenine ring of ATP interacts with a corresponding aromatic amino acid (**Y477** in HlyB-NBD) via π-π stacking. This link is supported by the interaction between the polar OH-group of Y477 and the adenine. The side chain of **I484** makes the hydrophobic contacts with ribose. The active site Mg-ion binds to the β- and γ-phosphates and to the side-chain OH-group of Ser509. Three water molecules complete the coordination sphere of the co-substrate metal ion. These additional water molecules act as points connecting residues within the ATP-binding site and, as a result, participate in the formation of a complex network of interactions. One of these

---

[1] The numbers in parentheses reflect the range of the distances between the reactive groups in all four ATP-binding sites of the two HlyB-NBD H662A dimers in the asymmetric unit.
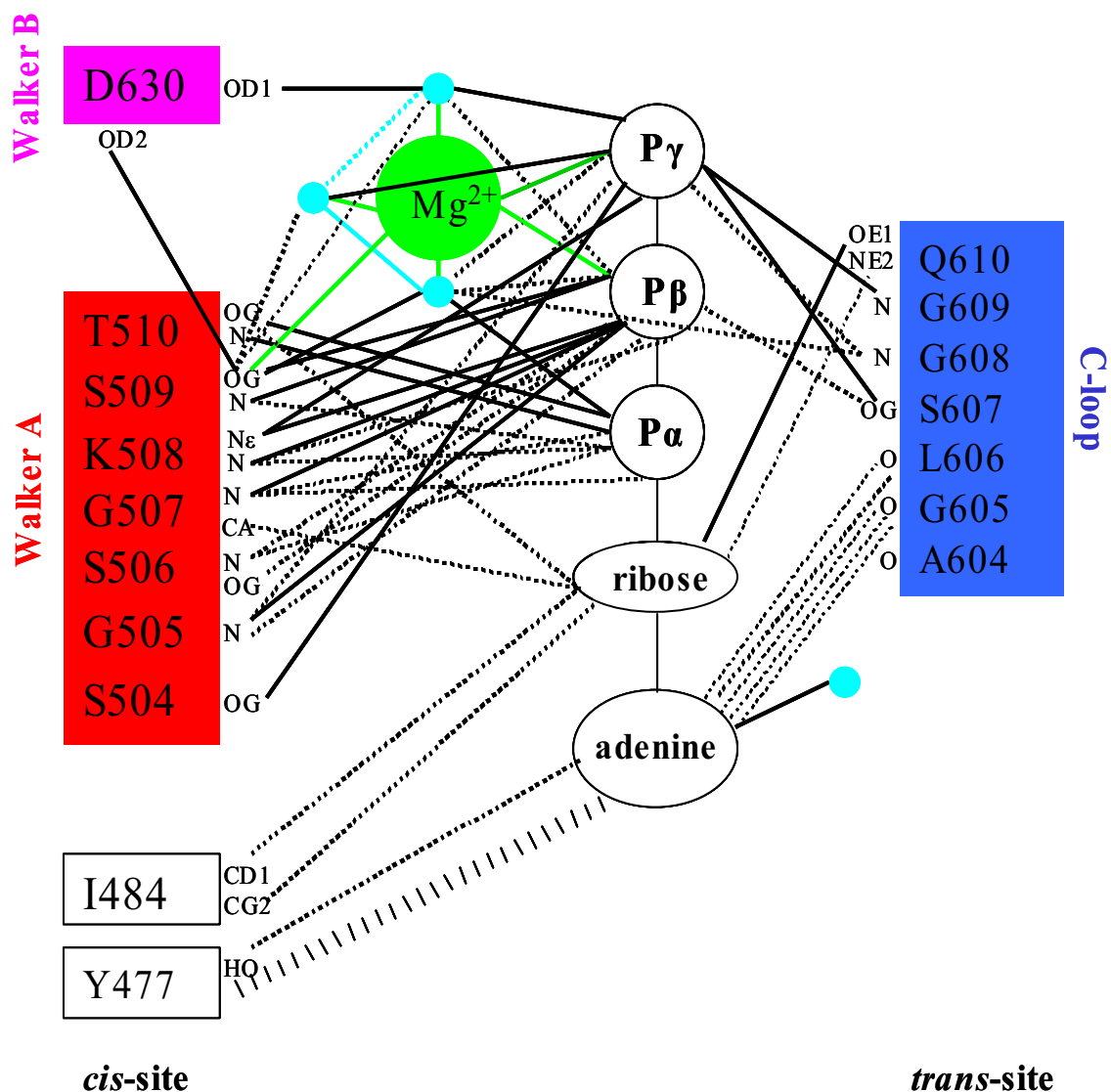
Figure 41. Schematic diagram of the main interactions between ATP-Mg^{2+} and HlyB-NBD H662A protein

Color-coding is identical to Figure 39. Turquoise spheres indicate water molecules. Hydrogen bonds and salt bridges are shown as solid lines, while van der Waals and hydrophobic interactions are shown as dashed lines. Letters next to amino acids represent the atoms involved in the interactions.

solvent molecules is hydrogen-bonded to D630 of the Walker B motif, a well-known arrangement in ATP- and GTP-utilizing enzymes (Vetter and Wittinghofer, 1999). This entire area is further stabilized by the interactions of D630 with S509 and by a hydrogen bond between T510 and Y477 connecting the adenine binding region with the Walker A motif.

6.2.2. Intermolecular (in trans) interactions in the ATP-binding site

Further interactions with ATP arise from the C-loop (ABC-signature) of the *trans*-monomer with all the residues of the C-loop actively contributing to the stability of the ATP-dimer. However, the key residues in ATP-binding and, thus, in ATP-induced dimerization of HlyB-NBD are **S607** and **G609**, which are highly conserved in ABC-transporters. Both amino acids provide a very high discrimination for ATP versus ADP by forming strong connections with the γ-phosphate. While the main chain amide group of **Gly609** creates a hydrogen bond with the γ-phosphate (2.7-2.8 Å), the side chain OH-group of **S607** establishes another strong connection to the γ-phosphate (2.8-3.2 Å). Further direct and water mediated interactions of **G608** with the γ-phosphate reinforce the ATP-protein linkage. A significant contribution to the nucleotide binding is provided by the side chain carbonyl oxygen of **Gln610**, which creates a strong hydrogen bond (2.80Å) with the ribose OH-group located at the 2' positions of the pentose ring. This link is further supported by van der Waals attraction between the side chain amide group of Q610 and 3'-OH of ribose. The other residues of the ABC-signature motif of HlyB-NBD, such as **G605** and **L606**, participate in van der Waals interactions via their main chain carbonyl groups and are also involved in the hydrophobic contacts with adenine of ATP. Ala604 also contributes to the ligand-protein stability in 3 out of 4 ATP-binding sites observed in the HlyB-NBD structure by a supplemental direct or water-mediated van der Waals connection to the adenine ring of the nucleotide (see below).

Overall, one ATP molecule makes at least 37 direct contacts with the homodimer, of which 13 are hydrogen bonds (<3.2 Å) and 24 are van der Waals and hydrophobic interactions (< 4 Å). As shown in Figure 41, 26 contacts are made with residues in the *cis*-monomer and the remaining 11 with the *trans*-monomer C-loop. The γ-phosphate of ATP is involved in 10 interactions: 1 with Mg-ion, 6 direct connections with the protein (4 hydrogen and 2 van der Walls links; 3 bonds from the *cis*- and 3 from the *trans*-site), and 3 water-mediated contacts that coordinate Mg^{2+} and set up a complex network of interactions.

6.2.3. Structural asymmetry of the ATP-binding sites in the HlyB-NBD dimer

Two ATP-binding sites of the HlyB-NBD-H662A dimer are very similar and have the same basic features as described above (Figure 41). However, slight variations in a position of the protein backbone and/or side chains and, particularly, a different distribution of solvent molecules in each ligand-binding site introduce asymmetry by means of water-mediated ATP-protein contacts. Thus, the positioning of water 22 in A-site[2] allows to generate additional water-mediated contacts between the adenine group of the nucleotide and two residues of the ABC-signature, A604 and L606, thus stabilizing the binding of ATP (see Figure 42A with new links shown in blue).

When compared to the aforementioned extra links in the active A site, the neighboring site B[3] of the same HlyB-NBD-H662A dimer includes a few more contacts (Figure 42B – new contacts are highlighted in blue). In addition to the direct van der Waals contact of Ala604 and adenine, new functionally significant connections appear in the vicinity of the γ-phosphate. Next to the three waters that participate in Mg^{2+} coordination, two more water molecules, 90 and 109, were unambiguously identified in the binding site. Water 109 connects the γ-phosphate of ATP to **Q550** of the Q-loop. This water-mediated interaction is also present in the ATP-bound structures of MJ0796 (Smith et al., 2002b) and HisP (Hung et al., 1998). In the AMP-PNP-Mg^{2+}-bound form of GlcV (Verdon et al., 2003a), this interaction occurs without water mediation. In contrast, the corresponding side-chain amide groups of Q82 and the γ-phosphate are spatially separated (6.3-8.6 Å) in the MalK-ATP structure (Chen et al., 2003). A possible explanation for lack of the interaction between the conserved Gln and ATP could be the absence of a suitable solvent molecule-mediator. Indeed, only 10 solvent molecules were detected in the MalK-ATP structure at 2.6 Å resolution. Yet, the existence of such a solvent molecule would facilitate a contact only in one of the two active sites of MalK-dimer.

The second water molecule, water 90, bridges the γ-phosphate group with **E631** and connects E631 to the bound Mg^{2+} via water 36, which is part of the Mg^{2+}-coordination sphere (Figure 42B). In the AMP-PNP-Mg^{2+}-bound structures of Rad50 (Hopfner et al., 2000) and GlcV (Verdon et al., 2003a), the corresponding Glu residue interacts with bound Mg^{2+} via one water molecule. In the HisP-ATP structure the Walker B glutamate, E179, forms one

---

[2] The A-ATP-binding site is composed of the Walker A motif of the A chain (*cis*-chain) and the C-loop of the B chain (*trans*-chain) of the AB HlyB-NBD H662A dimer with ATP-Mg^{2+} bound at the AB interface.

[3] The B-ATP-binding site is composed of the Walker A motif of the B chain (*cis*-chain) and the C-loop of the A chain (*trans*-chain) of the AB HlyB-NBD HlyB-NBD H662A dimer with ATP- Mg^{2+} bound at the AB interface.
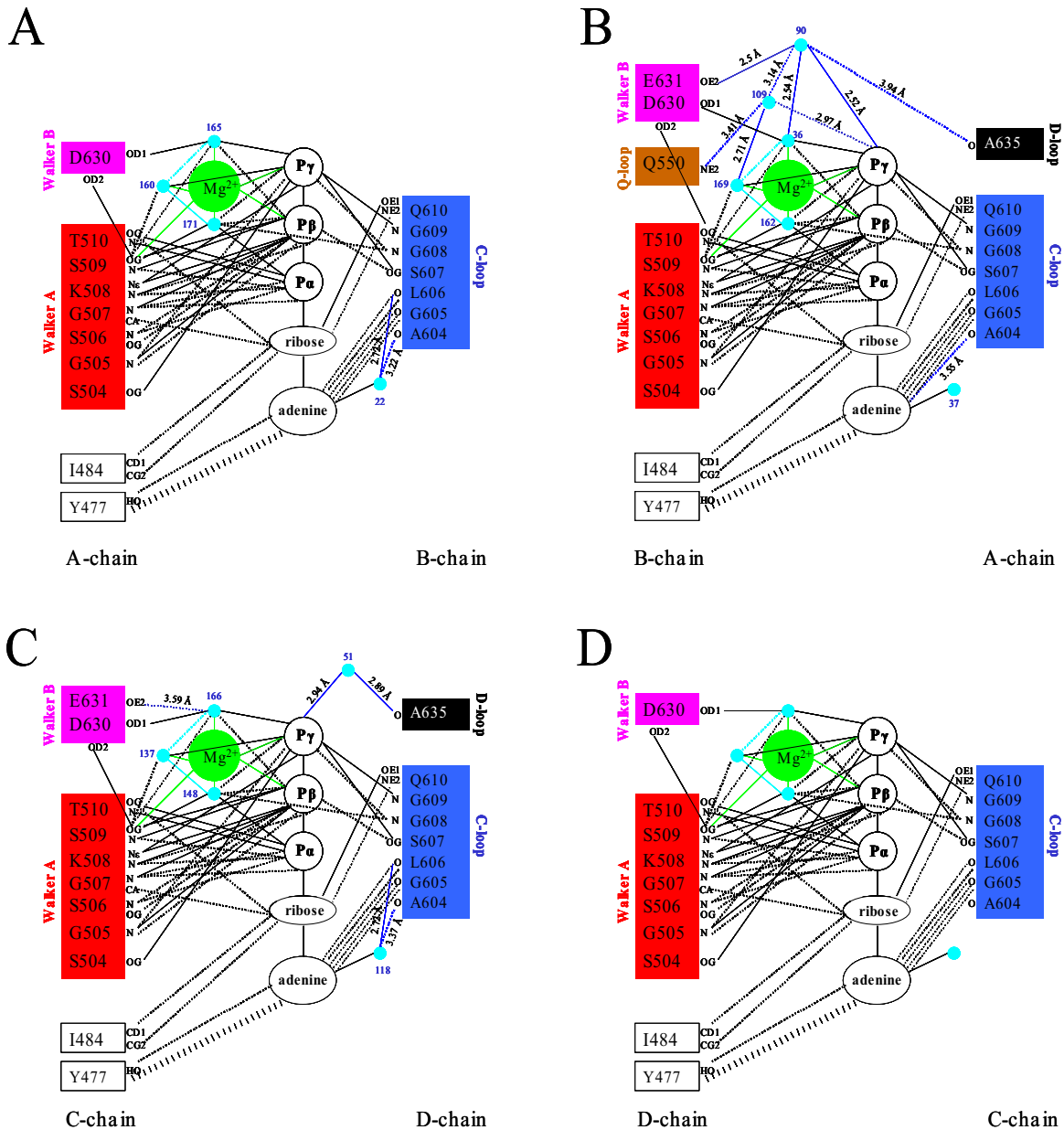
Figure 42. Schematic diagram of the interactions between ATP-Mg^{2+} and HlyB-NBD H662A in all four sites of two dimers of an asymmetric unit

Color-coding is identical to Figure 39. Turquoise spheres indicate water molecules. Hydrogen bonds and salt bridges are shown as solid lines, while van der Waals and hydrophobic interactions are shown as dashed lines. Letters next to amino acids represent the atoms involved in the interactions.

A. The A-ATP-binding site composed of the Walker A motif of A chain (*cis*-chain) and the C-loop of B chain (*trans*-chain) of the AB-dimer.
B. The B-ATP-binding site composed of the Walker A motif of B chain (*cis*-chain) and the C-loop of A chain (*trans*-chain) of the AB-dimer.
C. The C-ATP-binding site composed of the Walker A motif of C chain (*cis*-chain) and the C-loop of D chain (*trans*-chain) of the CD-dimer.
D. The D-ATP-binding site composed of the Walker A motif of D chain (*cis*-chain) and the C-loop of C chain (*trans*-chain) of the CD-dimer.

water-mediated contact with the γ-phosphate (Hung et al., 1998), while no interaction between E159 and ATP is detected in the MalK-ATP dimer structure (Chen et al., 2003). Water 90 also mediates the connection of the γ-phosphate group to **Ala 635**, the *trans*-monomer residue of the D-loop. A direct van der Waals interaction of the γ-phosphate with the corresponding amino acid of the D-loop is also observed for MalK (Chen et al., 2003) and MJ0796 (Smith et al., 2002b) in ATP-bound structures.

Thus, a comparison of two ATP-binding sites of the HlyB-NBD-H662A AB dimer with bound ATP-Mg^{2+} clearly demonstrates structural asymmetry, which might lead to functional asymmetry as well. While both active sites effectively bind ATP and Mg-ion along the dimer interface, only one B site attracts additional amino acid residues. As a result of these interactions, all conserved motifs of the ABC-transporters (except for the His-loop with a modified conserved histidine residue), the Walker A and B motifs and the Q-loop from *cis* monomer together with the ABC-signature and the D-loop of the *trans* monomer, are connected together via the single γ-phosphate of ATP (Figure 42B). The distant positioning of those supplementary amino acids from the ATP γ-phosphate reduces the significance of those residues in ATP-binding, and instead suggests their role in post-binding events such as the activation of ATP hydrolysis, the initiation of the transition state, and the ATP hydrolysis itself.

In agreement with the summarized differences between the two active centers of the AB protein dimer, the CD HlyB-NBD-H662A dimer demonstrates a similar asymmetry pattern. Here, the active D site is an exact replica of the basic ATP-protein interactions (Figure 42D) in HlyB-NBD H662A with bound ATP-Mg^{2+}, while the site C of the CD dimer differs from that fundamental model by the presence of additional ligand-protein contacts (Figure 42C). These contacts include three water-mediated interactions between ATP and the residues of the HlyB-NBD dimer. Thus, the side chain carbonyl of *cis*-chain E631 and the main chain carbonyl of trans-chain A635 are linked to the γ-phosphate, while water 118 provides a connection between the adenine group of ATP and the two ABC-signature residues, L606 and A604. No suitable solvent molecule was identified in the vicinity of the C/ATP-binding pocket to mediate interactions between Q550 and the γ-phosphate.

Thus, the structure of HlyB-NBD-H662A with bound ATP-Mg^{2+} revealed asymmetry between two nominally equivalent active sites of this dimeric enzyme. The direct association of the active sites with the dimer interface might also result in functional asymmetry. Such asymmetry adds a note of support to the hypothesis of the sequential or alternating

mechanism of ATP hydrolysis in HlyB (Zaitseva et al., 2005a) and other ABC transporters (Janas et al., 2003; Senior et al., 1995).

6.3. Monomer-monomer interactions in the HlyB-NBD-H662A dimer with bound ATP-Mg^{2+}

While ATP undoubtedly plays a leading role in the formation of HlyB-NBD H662A homodimer by introducing strong intersubunits contacts, protein-protein interactions also significantly contribute to dimer stability. Such connections comprise the total of **69** links, of which 20 are water mediated (Figure 43). All intersubunit protein-protein interactions can be divided into two groups, symmetric and asymmetric, that are schematically illustrated in Figure 44.

The symmetric interactions involve 17 amino acid residues from each protein chain that belong mostly to the conservative regions of ABC transporters (Walker A and B- motifs, Q-, C-, D-, and His-loops). The HlyB-NBD H66A subunits introduce **42** symmetric contacts to the dimer interface, of which **30** are direct NBD-to-NBD connections. Thus, this type of interactions composes the main core of the protein-protein intersubunit contacts, which include **7** direct hydrogen bonds or salt bonds (< 3.2 Å), **23** van der Waals and hydrophobic links (< 4.0 Å) and **12** water-mediated contacts (Figure 44A, C).

While the majority of the symmetric contacts originate from the conservative motifs, the asymmetric interactions between subunits extensively involve the C-terminal end of the A-protein chain (amino acids 700 –707) and the extended D-loop region (residues 637- 642) of the B-chain of HlyB-NBD H662A. The total of **27** asymmetric connections are made to stabilize the dimer interface. They include **19** direct protein-protein contacts, of which **2** are hydrogen bonds and **14** are hydrophobic interactions (Figure 44B). Note that hydrophobic bonds are very important because the main driving force for protein folding is minimization of the solvent-exposed non-polar surface area. Since hydrophobic bonds obtain energy from van der Waals interactions and from the exclusion of water from the site of interaction, they are often much stronger than what would be predicted by the energetic contribution of van der Waals forces alone. The strength of hydrophobic interactions is comparable to the strength of hydrogen bonds; it varies with side chain from a maximum of approximately 3 kcal/mol for Trp side chain to 0 for non-hydrophobic residues. Van der Waals attractions are very weak,
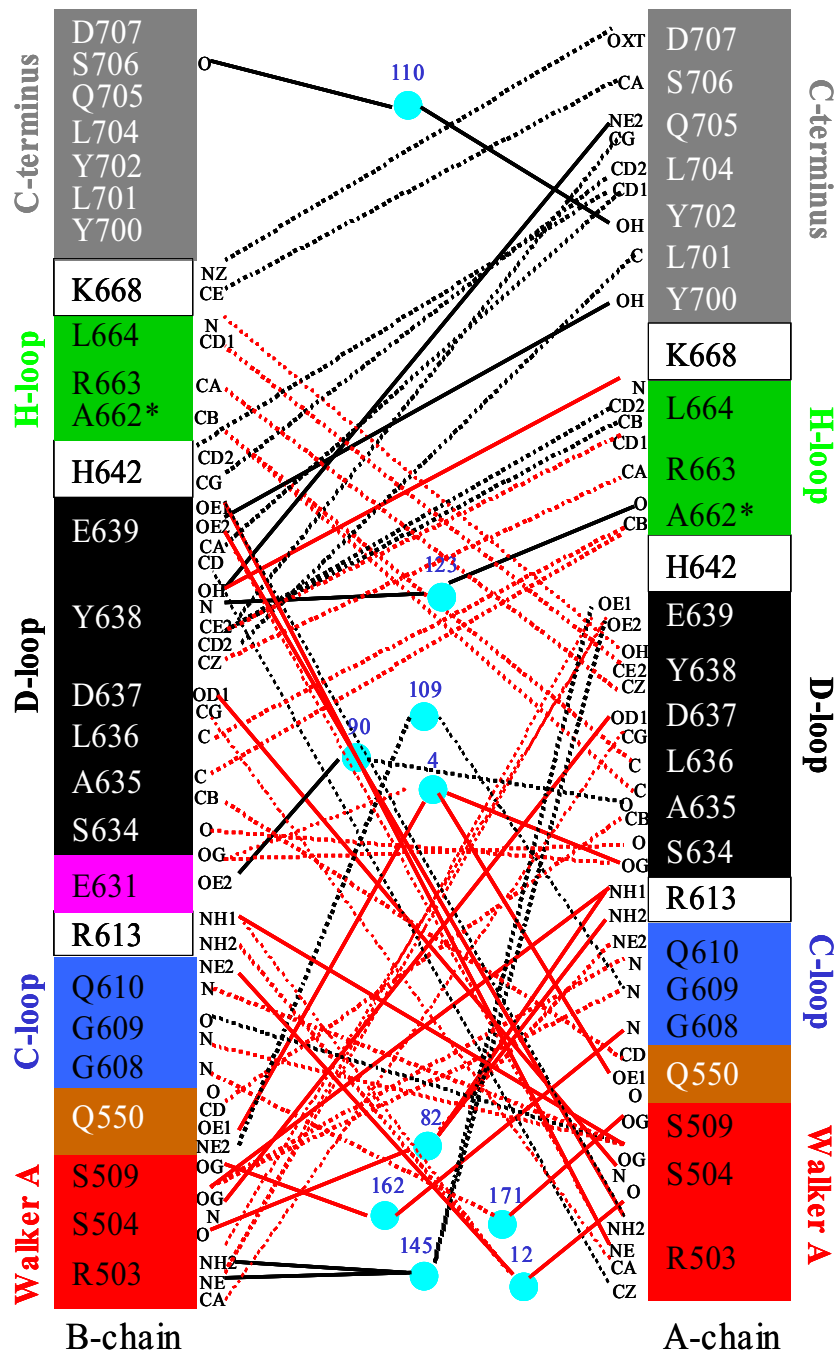
Figure 43. Schematic diagram of protein-protein interactions across the AB-dimer interface of HlyB-NBD H662A with bound ATP-Mg^{2+}

Color-coding is identical to Figure 39. Turquoise spheres indicate water molecules. The numbers in blue identify the numbers of water molecules in the structure. The residues of the C-terminal extension are colored gray. Hydrogen bonds and salt bridges are shown as solid lines, while van der Waals and hydrophobic interactions are shown as dashed lines. The lines in red designate symmetric contacts, the lines in black – asymmetric. Letters next to amino acids represent the atoms involved in the interactions.
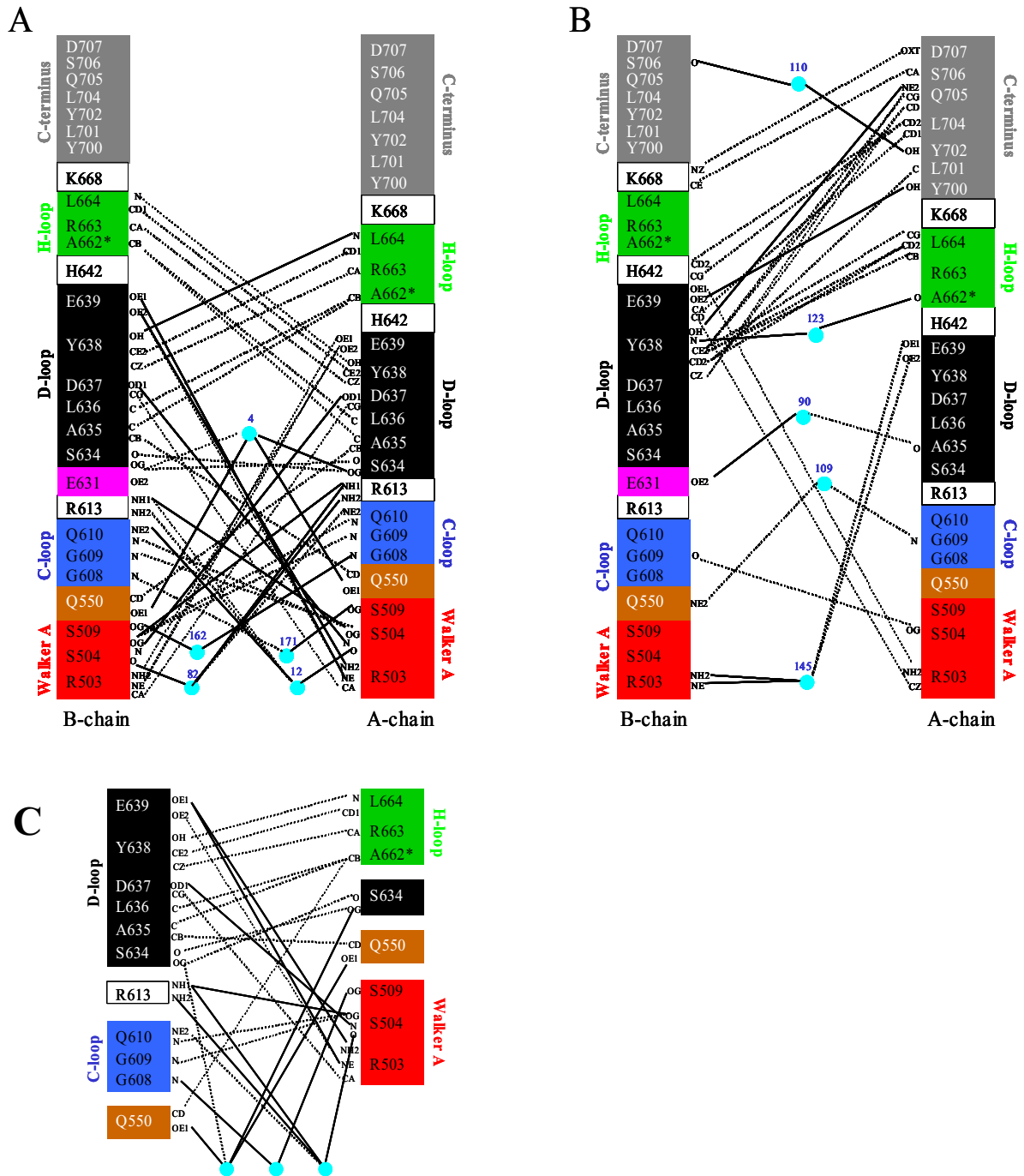
Figure 44. Schematic diagrams of the symmetric and asymmetric protein-protein interactions across the AB-dimer interface in HlyB-NBD H662A with bound ATP-Mg^{2+}

A. Symmetric contacts

B. Asymmetric contacts

C. Simplified presentation of the symmetric interactions

Color-coding is identical to Figure 39. Turquoise spheres indicate water molecules. The numbers in blue identify the numbers of water molecules in the structure. The residues of the C-terminal extension are colored gray. Hydrogen bonds and salt bridges are shown as solid lines, while van-der-Waals and hydrophobic interactions are shown as dashed lines. Letters next to amino acids represent the atoms involved in the interactions.

approximately 0.01 to 1 kcal/mol per atom pair, which is just slightly greater than the average thermal energy of molecules at room temperature, while hydrogen bonds are on the order of 3 to 7 kcal/mol.

Altogether, 21 amino acid residues from the B-monomer and 24 from the A-monomer participate in the protein-protein interactions between the two HlyB-NBD H662A subunits. Six (S504, G609, Q610) of 38 amino-acid residues making direct intersubunit contacts in the dimer also directly interact with ATP.

The detailed analysis of the HlyB-NBD-H662A dimer with bound ATP-Mg^{2+} revealed structural asymmetry between two subunits and an extensive intercommunication between them (see also below). Along with the structural difference of the ATP-binding sites, the intersubunit asymmetry further supports an idea of the functional asymmetry in the NBD-dimer and, hence, the hypothesis of either sequential or alternating ATPase cycles in ABC-transporters (Janas et al., 2003; Senior et al., 1995; Zaitseva et al., 2005a).

6.4. Characteristic features of the ATP-Mg^{2+} bound HlyB-NBD H662A dimer

6.4.1. His-loop

A sequence alignment of various NBDs (Chapter 1, Figure 8) emphasizes the conservation and importance of His662, located in the H-loop or the switch II region preceding helix 7 (colored green in Figure 39). A mutation of the conserved histidine in HisP (H211) (Shyamala et al., 1991) and MalK (H192) (Davidson and Sharma, 1997) resulted in background steady-state ATPase activity (< 2%), and completely abrogated transport (Davidson and Sharma, 1997; Nikaido and Ames, 1999). The reported high residual activity for the MalK mutant lacking the histidine (Walter et al., 1992) has not been confirmed (personal communication, E. Schneider). In the case of the HlyB-NBD (Chapter 7, (Zaitseva et al., 2005b)), substitution of His662 for alanine reduced the steady state ATPase activity to the background levels (< 0.1%).

The importance of the conserved His is also supported by the structural alignment (data not shown) of HlyB-NBD H662 with other ATPases and GTPases containing the Walker A motif. The alignment shows that position 662 in HlyB coincides with the residues of the proteins, which have been suggested to be essential for catalysis: H885 (Rad50)

(Hopfner et al., 2000), Y311 (α-chain of F_1-ATPase) and E328 (β-chain of F_1-ATPase) (Abrahams et al., 1994), Q194 (RecA) (Datta et al., 2003; Story and Steitz, 1992), Q61 (p21^{ras}) (Pai et al., 1990), H85 (EF-Tu) (Berchtold et al., 1993), and H465 (T7-helicase) (Sawaya et al., 1999).

Structural studies of the ABC-ATP-dimers further demonstrate the significance of the conserved His in the intermolecular interaction between two NBD-monomers of various transporters. Thus, in the MalK (Chen et al., 2003) and the EQ-MJ0796 dimer structures (Smith et al., 2002b), the side chain of His directly interacts with the γ-phosphate of ATP. In the HisP structure the same contact is mediated via a water molecule (Hung et al., 1998), albeit the HisP crystallographic dimer does not correspond to a functionally relevant NBD dimer structure. The conserved histidine of the His-loop is also intensively involved into contacts with the D-loop of the opposing NBD-subunit in all ABC-ATP-dimer structures. In MalK-ATP (Chen et al., 2003) the conserved His of the *cis*-monomer simultaneously interacts with the *trans*-D-loop (N163, L164, and D165 amino acids) and with the ATP γ-phosphate, serving as a mediator between the two protein subunits and connecting an active center of one monomer and the conserved motif of the other monomer. A similar picture is observed in the EQ-MJ0796-ATP-Na structure, where the D-loop (A175, L176, and D177) also interacts with the ATP molecule of the opposing subunit via the conserved histidine (Smith et al., 2002b). Additionally, the same D-loop sets up a water-mediated contact with the ATP γ-phosphate in *trans* via Ala175. In the DNA repair dimer enzyme Rad50 with bound AMP-PNP-Mg^{2+} (Hopfner et al., 2000) the conserved histidine of one monomer interacts with the D-loop of the other monomer via a water molecule. The same water molecule also contacts the γ-phosphate of ATP and the Q-loop, providing contacts between the D-loop of one monomer and the two conservative motifs, H- and Q-, of the other monomer.

While the HlyB-NBD-H662A-ATP-Mg^{2+} dimer intersubunit contacts involve extensive protein-protein interactions resulting in the total buried surface between the monomers twice as large as in the MalK-ATP (Chen et al., 2003) and the EQ-MJ0796-ATP-Na dimers (Smith et al., 2002b), the lack of the conserved histidine in the crystal structure of HlyB-NBD seems to disrupt very important protein-nucleotide and protein-protein interactions in the vicinity of the active center. Thus, in contrast to the MJ0796-ATP-Na (Smith et al., 2002b) and Rad50-AMP-PNP-Mg^{2+} dimers (Hopfner et al., 2000), no direct contact of the γ-phosphate ATP with either the His- or D-loop was observed upon replacing histidine-662 with alanine in the HlyB-NBD-H662A-ATP-Mg^{2+} structure. However, similarly to other NBD-dimer structures, the corresponding residues of the HlyB D-loop,

A635 and L636, maintain their interactions with H662A* of the His-loop in *trans*. Tyrosine-638 reinforces the H-D-loops' connection by multiple links with R663 and L664, which immediately follow alanine-662 in the HlyB-NBD-H662A sequence.

The lack of His doesn't seem to interfere with dimerization of NBD. Moreover, the replacement of the conserved histidine with alanine contributes to the higher dimer stability. In contrast to the wild type protein, dimers of the mutant HlyB-NBD H662A with bound ATP or ATP-Mg^{2+} were detected by means of gel-filtration (Chapter 7) and were also obtained as a result of protein crystallization (Chapter 4).

6.4.2. D-loop

The structure of the ATP composite dimer of HlyB-NBD H662A explains the conservation of the D-loop region in ABC transporters. All residues of the D-loop in both subunits, S634-E639, are extensively involved in direct intermolecular connections. The multiple contacts throughout the *trans*-monomer, which are shown schematically in Figure 45, demonstrate that each D-loop makes connections with the Walker A motif, Q-, H-, and D-loops of the opposite subunit. Moreover, the D-loop of the A-subunit has a weak asymmetric water-mediated contact with E631 of the Walker B motif of the B-monomer, while the D-loop of the B-subunit extensively interacts with the C-terminal end of the A-monomer (Figure 44B). Besides, the D-loops in the ATP-Mg^{2+}-HlyB-NBD H662A structure form protein-mediated contacts with both ATP molecules via a Walker A residue. Thus, the D637 residues located in the ABC-hallmark D-loop form the symmetric hydrogen bond (2.7-2.9 Å) with the amide backbone of S504 of the Walker A in the opposite monomer (Figure 44A, C). An identical intermolecular contact between the conserved serine of the Walker A motif, S38 and S40, and the conserved aspartate of the D-loop, D165 and D177, is detected for the MalK (Chen et al., 2003) and MJ0796 dimers (Smith et al., 2002b), respectively. Such a link connects the γ-phosphate of ATP with the D-loop of the *trans*-monomer in all three structures. Besides, the D-loop of the EQ-MJ0796-ATP-Na$^+$ dimer establishes an additional water-mediated link with the γ-phosphate of ATP and contacts the Na-ion in the ATP-binding site via the Q-loop (Q90).

Thus, an arrangement of the two D-loops represents a "brain" center of the HlyB-NBD-ATP-Mg^{2+} composite dimer. This center senses and transmits signals from different regions of one protein subunit to the other, thus linking together both monomers.
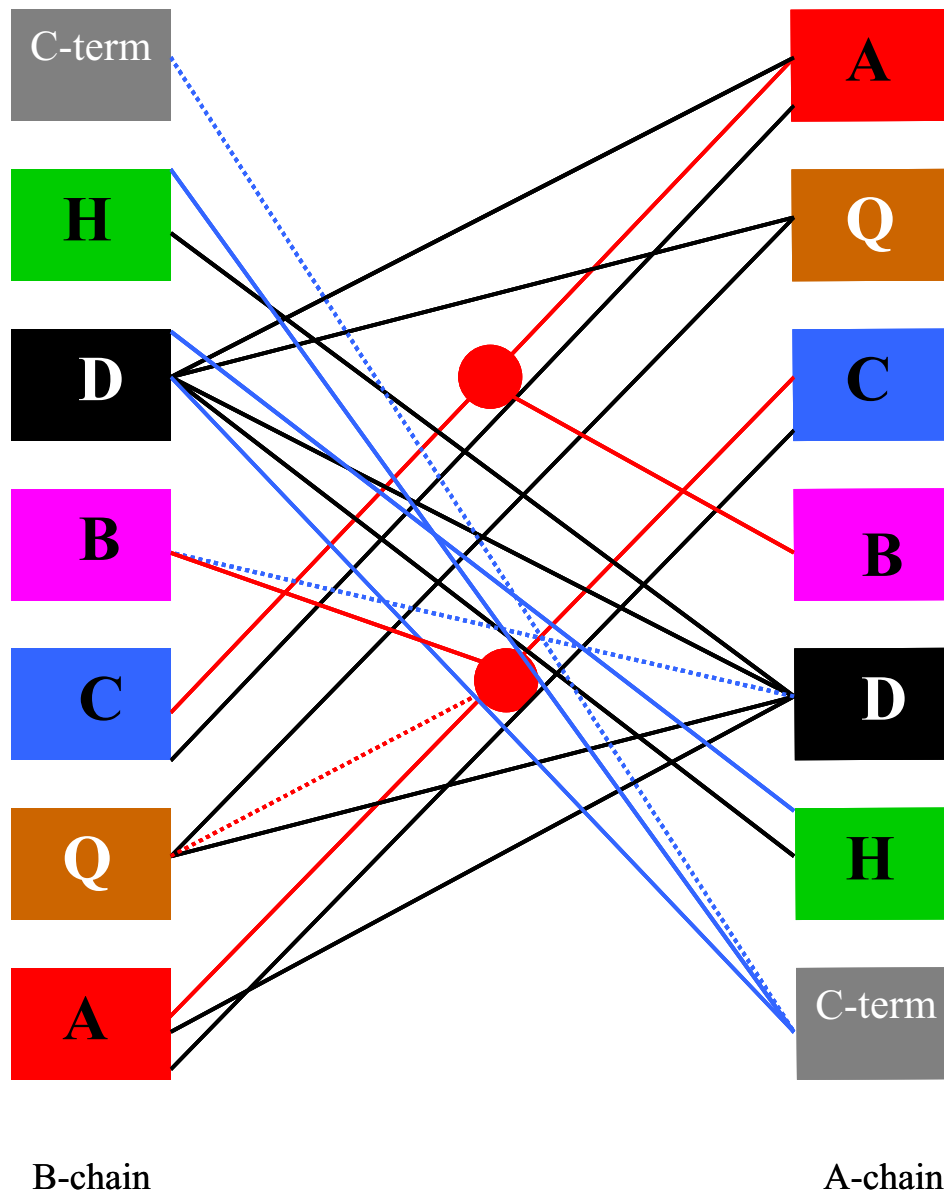
Figure 45. Summarized scheme of protein-protein and nucleotide-protein interactions across the AB-dimer interface in HlyB-NBD H662A with bound ATP-Mg^{2+}

Color-coding is identical to Figure 39: A stands for the Walker A motif, Q – the Q-loop, C – the C-loop or ABC-signature, B – the Walker B motif, D – the D-loop, H – the H-loop, C-term – the C-terminus. The residues of the C-terminal extension are colored gray. Red spheres indicate two ATP molecules. Red lines designate nucleotide-protein interactions; black lines – symmetric protein-protein interactions; blue lines – asymmetric protein-protein connections. The solid lines indicate direct contacts, dashed lines – single water-mediated interactions.

6.4.3. Q-loop

In the MalK and EQ-MJ0796 ATP-bound structures the conserved glutamine residue of the Q-loop is located in the vicinity of the ATP-binding site, which is also true for the Rad50 dimer, a DNA repair enzyme. In the EQ-MJ0796 dimer the side-chain amide of the corresponding Q90 is connected with the γ-phosphate of the ligand through one water molecule. While the Q82-residue in MalK-ATP has no contact with ATP, the calculations resulted in the shortest distance of 5.2 Å from Q82 to ATP, measured from the carbonyl group of Gln to the γ-phosphate. In contrast, Q550 is located 6.3-6.8 Å away from the nearest ATP-site HlyB-NBD H662 dimer. Such a position of the conserved residue and the specific distribution of the solvent molecules allow a single water-mediated connection of the glutamine-550 with the γ-phosphate only in the B-site, one of the four active sites in two dimers observed for ATP-Mg^{2+}-protein structure (Figure 42B).

The aforementioned locations result in the close proximity of the two Q550 residues, permitting a water-mediated contact between the side chain carbonyls of the glutamines (Figure 44A, C). Interestingly, the same water molecule provides a connection for two other residues, serines-634, of the opposite D-loops in the HlyB-NBD dimer (Figure 44A, C). Thus, a unique intermolecular contact between two Q-loops and two D-loops is established in HlyB-NBD structure. This water-mediated type of Q-D-loop intercommunication is identical to that of the CD-dimer of HlyB-NBD.

Another interesting feature of the HlyB-NBD H662A structure is a strong connection between the main chains of two conserved residues, Q550 of the Q-loop and D630 of the Walker B motif, in the same subunit. While they set up a hydrogen bond (3.2-3.3 Å) in HlyB-NBD-ATP-Mg^{2+}, the distances between the corresponding amid and carbonyl groups in EQ-MJ0796-ATP-Na^+ and MalK-ATP-bound structures are 3.7-3.8 Å and 4.1-5.2 Å, respectively. Thus, the Asp-Gln bond mediates a contact for Q550 with the ATP-binding site in HlyB-NBD. It seems likely that an interaction of the original conserved histidine-662 of the H-loop with ATP enhances communication of the conserved Gln550 with the active center. Assuming that the Q-loop also connects the transmembrane- and NBD-components of an ABC transporter (Locher et al., 2002), a network transmitting signals between two NBD monomers with bound ATP-Mg^{2+} and two membrane subunits can be of a great importance in the coupling of ATP hydrolysis and allocrite transport.

Thus, while the D-loops have a potential to participate in the inter-NBD signaling system, the Q-Q-loop-contacts could be the likely mediators transmitting the ATP-binding/hydrolysis signals from the NBD-components to the TMD-domains and ensuring that all four domains (2TMD and 2NBD) are capable to sense an ATP-binding/hydrolysis event in one single active site.

6.4.4. Walker B glutamate

In the H662A crystal structure, the OE1 carbonyl group of E631 forms a hydrogen bond with the backbone amide of A662 (2.9-3.1 Å) in the same monomer. Another carbonyl of E631, OE2, contacts the γ-phosphate of ATP via a water molecule in one of the two active sites of the HlyB-NBD dimer. In the MalK-ATP structure (Chen et al., 2003), the same E159–His192 hydrogen bond of 3.0 Å long is also present, yet no connection between the glutamate and ATP is observed. In the case of the MJ0796 E171Q-ATP-Na$^+$ (Smith et al., 2002b), however, the distance between the side chain of Q171 and the backbone amide of H204 is 4.4 Å, while the NE2-group of Q171 EQ-MJ0796 is linked to the γ-phosphate through the solvent molecule.

When the two dimer structures, HlyB H662A and MJ0796 E171Q (Smith et al., 2002b), were aligned using the Walker A and B motifs as the anchor points with rmsd of 12 Cα atoms below 0.5 Å, a nearly 90° displacement of the side chain of Q171 in the MJ0796-E171Q structure relative to the side chain of E631 (HlyB-NBD) was revealed (Figure 46). This flip-out could be explained by the NE2-group repulsion of the glutamine-171 from the backbone and the side chain of H204. As part of this process, the amide group of Q171 establishes a link with ATP but not with the histidine. Thus, E/Q mutation in MJ0796 is likely to disrupt the interaction between the backbone of H204 and the glutamate.

To test the hypothesis that H662 and E631 could form a link, H662 was re-introduced 'in silico' into the HlyB-NBD structure and the model was energy minimized. The hypothetical structure obtained after this procedure is shown in Figure 47. The most important conclusion from this model is that E631 in HlyB can form intramolecular hydrogen bonds with the backbone and the side chain of H662 simultaneously. Furthermore, one nitrogen atom of the imidazole side chain of the re-introduced H662 interacts with the side chain of E631, while the other nitrogen atom interacts with the γ-phosphate of ATP and water 90. This organization postulates a bifurcated interaction between H662 and E631, which reinforces the importance of H662 in the catalytically active protein.
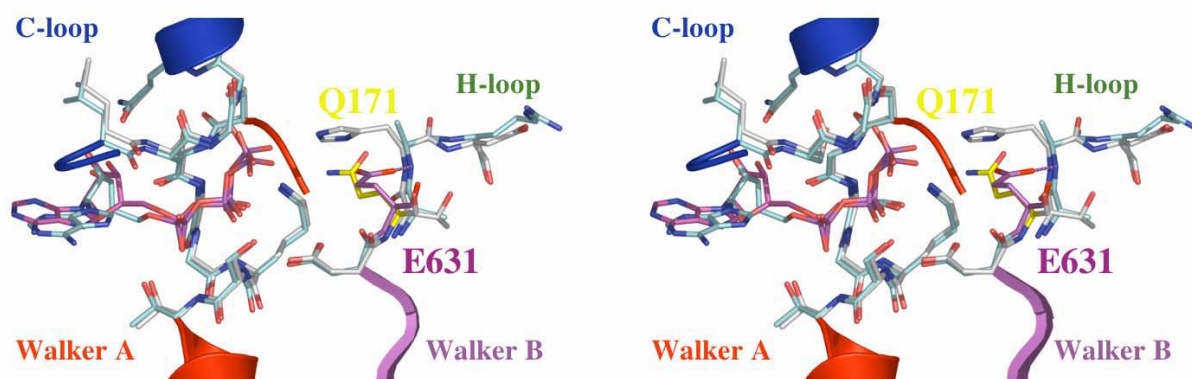
Figure 46. Stereoview of superposition of HlyB-NBD H662A in complex with ATP-Mg^{2+} and the ATP sandwich dimer of MJ0796 (Smith et al., 2002)

The backbone of the Walker A and B motifs, C-loop, and H-loop of HlyB-NBD H662A are shown in cyan and the corresponding backbone of MJ0796 E171Q in gray. ATP molecules are shown in cyan (HlyB-NBD H662A) and magenta (MJ0796 E171Q). The interaction between side chain of E631 (magenta) and the backbone amide of A662 is highlighted. As shown, the flip-out of Q171 (yellow) destroys this interaction in the MJ0796 E171Q structure.

Based on the model proposed in Figure 47, one can envision two extreme scenarios for the function of E631 and H662. In the first one, E631 serves as a platform to position H662 in the proper orientation to catalyze ATP hydrolysis, whilst H662 is acting as a 'linchpin' (Zaitseva *et al.*, 2005b). In the other one, their roles are reversed. In contrast to the apparently essential nature of the H-loop histidine, some ABC-proteins with glutamate to glutamine substitutions still display a significant residual level of ATPase activity (Verdon *et al.*, 2003b; Tombline *et al.*, 2004) This suggests a leading role of the H662 residue and a chaperone or platform function for E631. In this case, the defective activity in E/Q mutant ABC proteins could be explained by the inability of the glutamine to form the proposed bifurcated interaction with the backbone and the side chain of the histidine. As a result, the histidine side chain would be no longer fixed in one place and may adopt multiple, mainly non-productive conformations. Nevertheless, in various NBDs containing E/Q exchange such plasticity may be more or less tolerated.
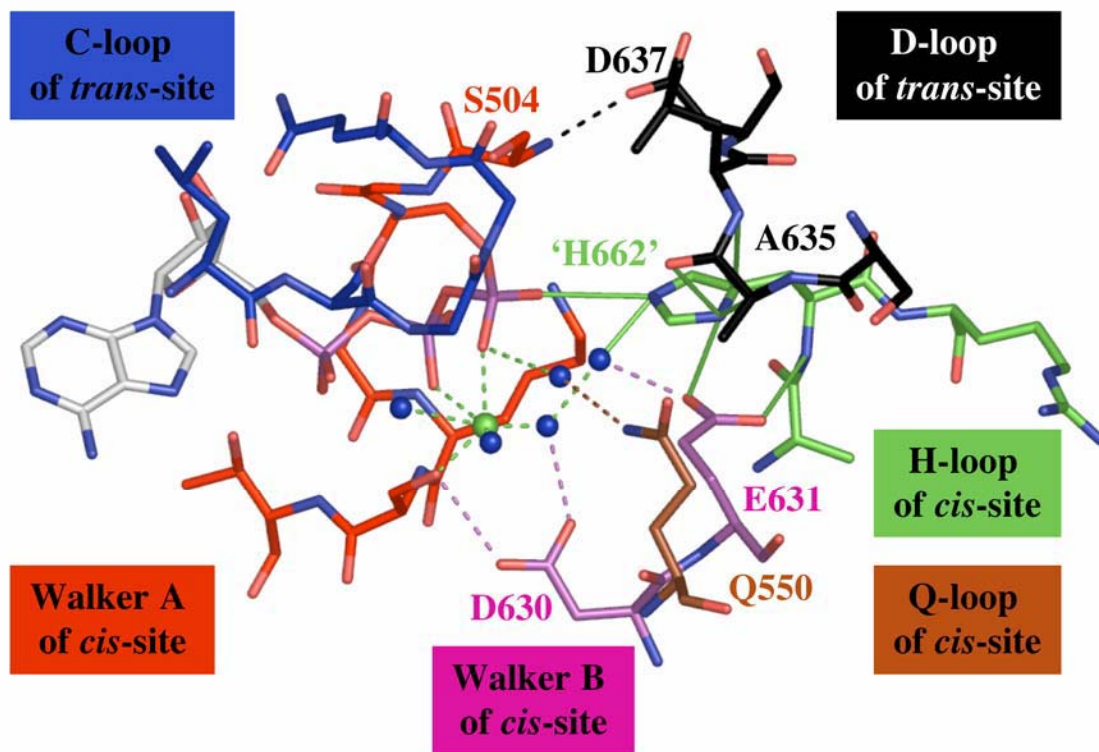
Figure 47. Simulated model of the pre-hydrolysis state of the HlyB-NBD after restoring H662

The figure demonstrates the key role of H662 through interactions with the γ-phosphate, E631, and the D-loop. Color-coding is identical to Figure 39. Blue spheres indicate water molecules. B-ATP binding site was chosen for the model. For further details please see text.

6.4.5. The C-terminal end

The importance of the C-terminal regions was investigated for Multidrug Resistance Protein 1, MRP1 (Westlake et al., 2004), a member of the ABC-transporter family. These studies showed that the truncation of a C-end in MRP1, which corresponds to sheet 12 and helices 8 and 9 in HlyB-NBD, eliminated transport activity, but didn't affect allocrite binding. Furthermore, those studies suggested that the loss of activity appears to be a result of reduced ATP-binding and hydrolysis in one of the nucleotide binding domains of MRP1. The

available monomer structures of the ABC-exporters, HlyB-NBD (Schmitt et al., 2003), LmrA (Protein Data Bank number 1MV5), and TAP1 (Gaudet and Wiley, 2001) show no evidence of the direct influence of the C-terminal region on the ATP-binding site of NBD. The dimer structures of two ATP-bound ABC-importers, MJ0796 and MalK, also provide no information about that specific issue. As was mentioned in Section 6.1, the C-terminal regions in HlyB-NBD, MJ0796, and MalK ATP-bound dimer NBD complexes are quite dissimilar. The last 14 C-terminal amino acids of HlyB (the region following helix 8, which includes helix 9) have no counterpart in MJ0796 (Chapter 1, Figure 8), while MalK has its own unique 15-kDa regulatory domain as a C-terminal extension that plays important role in the protein dimerization (Chen et al., 2003). HlyB-NBD H662A, the first representative of the ATP-bound dimer structure of an ABC exporter, sheds light on the potential role of the C-terminal region. Both the Mg^{2+}-bound and Mg^{2+}-free forms of HlyB-NBD H662A reveal an active contribution of the C-terminus to the intersubunit connections, suggesting a possible explanation for the truncation effect in the MRP1 protein.

The structural studies of HlyB-NBD dimer with ATP-Mg^{2+} showed that the five C-terminal amino acids of the A subunit of the HlyB-NBD dimer, Y700-D705, extensively participate in the asymmetric intersubunit interaction, making many hydrophobic and polar contacts with the D-loop (Y638 and E639) and the neighboring H642 of the B-monomer (Chapter 6.3 and Figure 44B). The other C-terminal links of the A-subunit include contacts between the last two amino acids (S706, D707) and Lys668 of the opposite subunit and a single water-mediated bond with the C-terminus of the B-protein, connecting the side chain of A/Y702 and main chain carbonyl of B/S706 (Figure 44B).

Given the significant contribution of the C-terminal amino acids to the formation of the dimer interface and its potential stabilization, the simplest rationalization of the reduced ATP-binding/hydrolysis in the truncated ABC-exporters would be the impaired NBD-dimerization upon removal of the C-terminus (Westlake et al., 2004). However, an alternative explanation could be either the decreased binding of the allocrite to NBD of the exporter or the obstructed transmission of signal from the bound allocrite to the ATP-binding site, or all of the three suggestions above. The importance of the C-terminal region is also discussed below in the light of the potential allocrite-conducting tunnels discovered in the HlyB-NBD dimer structure.

6.5. Molecular tunnels in the interior of the HlyB-NBD-H662A dimer with ATP-Mg^{2+}

The detailed analysis of the van der Waals surface of the ATP-Mg^{2+}-HlyB-NBD dimer revealed the presence of two parallel narrow tunnels, of approximately 20 Å in length, located proximally to the ATP-binding sites (Figures 48, 49). The tunnels are formed at the dimer interface (Figures 48-53) so that both subunits contribute to the construction of the tunnel walls. Every tunnel spans the dimer from the side exposed to the cytoplasm to the side interacting with transmembrane domains of the transporter (Figures 51, 52). Each tunnel entrance on the cytoplasmic side is covered with its own lid, formed by the helix-9 and the following C-terminal amino acids of the monomer (Figures 50-52, 54). Helix-9 is attached to the main body of the NBD via a flexible hinge (Figure 52B), which may allow access to the translocation channel from the cytoplasm by the moving the lid aside. The narrow opening of the tunnel entrance is completely obscured by Leu701, which is located in the middle of the helix-9 and entirely buried in the protein interior (Figure 54).

The surface of each tunnel is lined mostly with amino acid residues that are conserved in ABC-transporters (Figure 55). The tunnel entrance on the cytoplasmic side is created by residues of the Walker A motif (V501, G502, and R503), the D-loop (D637 and Y638), and L664, an amino acid of the extended His-loop region. In fact, Leu501, Arg503, and particularly D637 also contribute to the main part of the channel as well. The other residues participating in the formation of the tunnel body are S504 and K508 of the Walker A motif, L636 and D637 of the D-loop, and A661 and H/A662* of the His-loop. All the aforementioned amino acids donate to the lining only the backbone atoms and/or the non-polar side-chain moieties. Each tunnel ends with a clover-leaf shaped cavity on the NBD surface facing the transmembrane domains. Three conserved amino acids, Glu631 of the Walker B motif, Ala635 of the D-loop, and Gly609 of the C-loop, and the γ-phosphate of ATP surround a junction between the tunnel and the cavity. The side chain of Glu631, the main chain of Ala635, and ATP seem to play role of the circular muscles (Figure 56), being capable to contract and close the opening (see below). The cavity at the end of each tunnel is built of Q550 of the Q-loop, S607 and G608 of the C-loop, Q612 of the extended C-loop, D630 and E631 of the Walker B motif, A632, T633, S634, A635, and L636 of the extended D-loop, and I660 of the extended H-loop (Figure 57). The majority of the residues lining the channel and the cavity participate in either ATP-binding or formation of the NBD-dimer interface or both. In particular, all the amino acids in direct contact with the γ-phosphate of
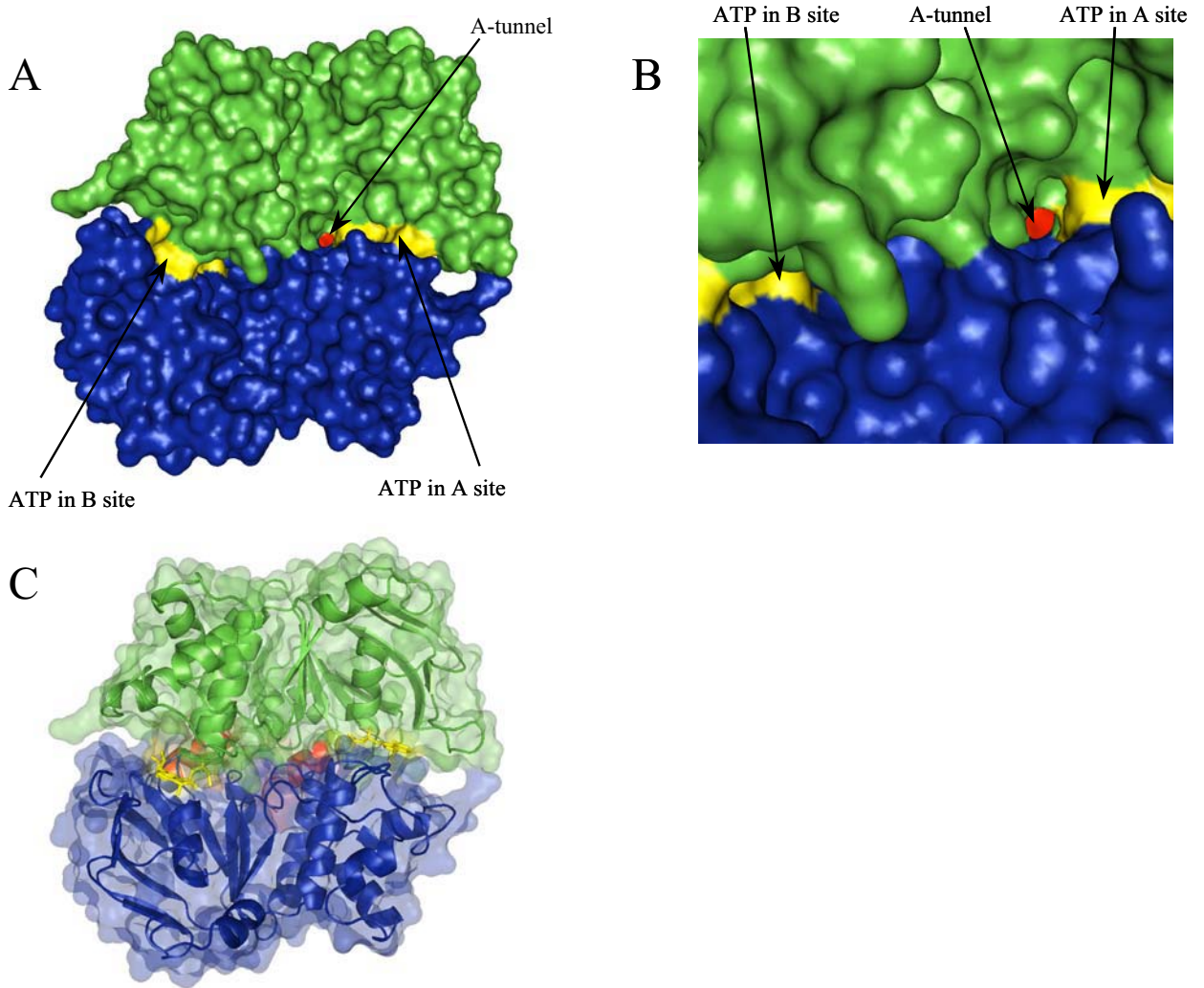
Figure 48. Molecular surface of the HlyB-NBD H662A dimer with bound ATP-Mg^{2+}, facing the TMDs

The figure was prepared using PyMol (www.pymol.org).

A. Monomer A is colored green and B monomer – blue. Two ATP-Mg^{2+}-complexes bound at the dimer interface are shown in yellow. A-tunnel is indicated by an arrow. The C-terminus (colored red S699-D707), located on the opposite side of the dimer, can be seen through the tunnel.

B. The same as A. Close-up view.

C. The same as A. The ribbon diagram with semi-transparent molecular surface presentation of the dimer.
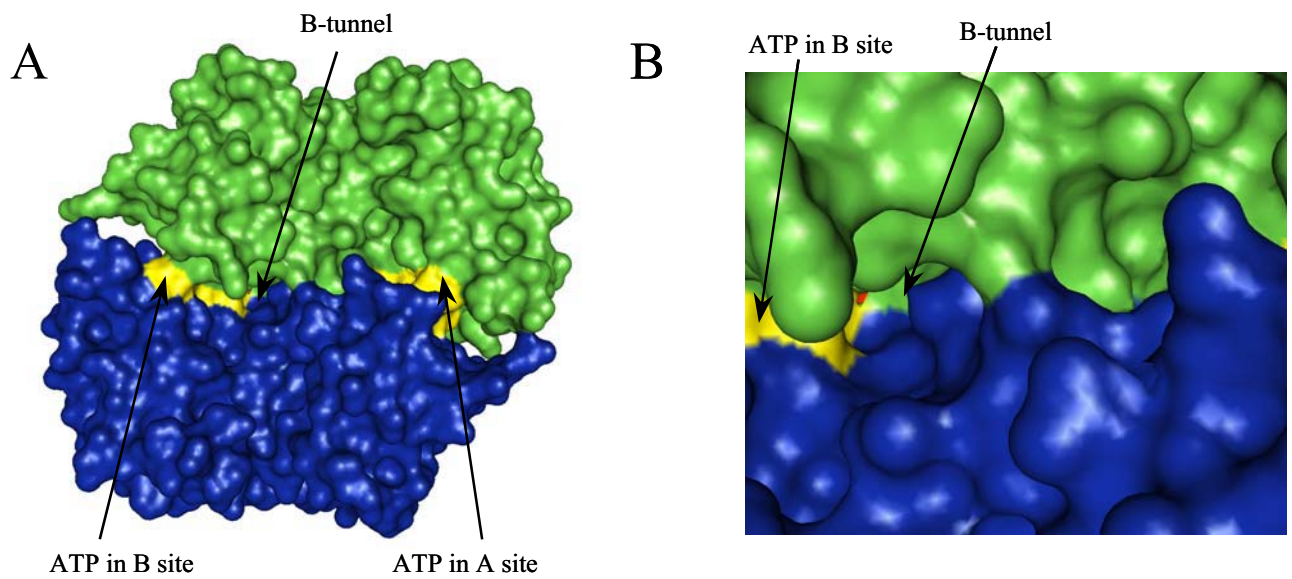
Figure 49. Another view of the HlyB-NBD H662A dimer with bound ATP-Mg^{2+} from the side facing the TMDs, which is slightly tilted relatively to the one shown in Figure 48 to demonstrate B-tunnel

The color scheme is the same as in Figure 48.

    A. The molecular surface of the dimer. B-tunnel is indicated by an arrow.

    B. Close-up view of A.

A

B

Groove of A-tunnel

Groove of A-tunnel
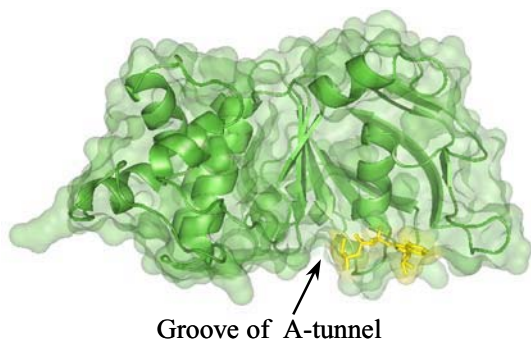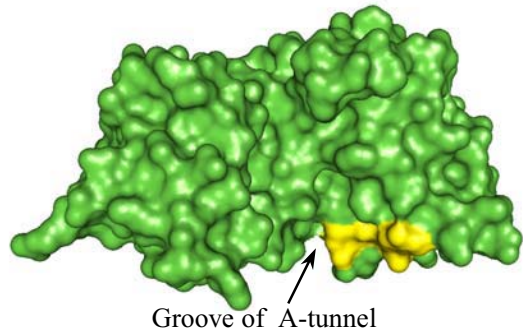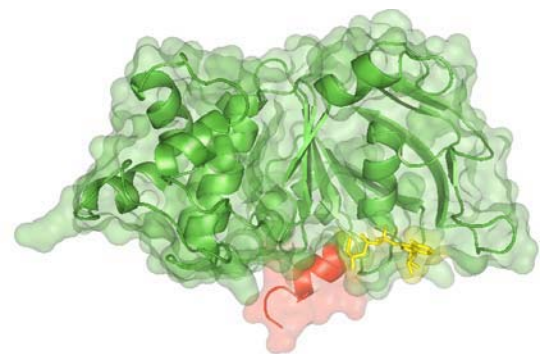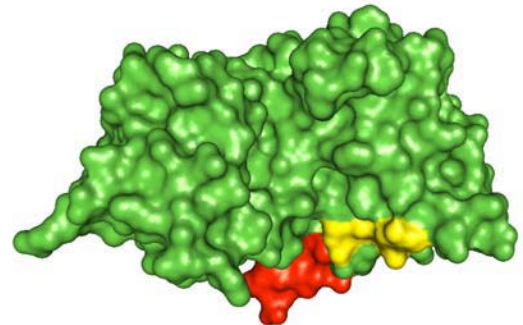
Figure 50. The A monomer of HlyB-NBD H662A with bound ATP-Mg^{2+} facing the TMDs

The color scheme is the same as in Figure 48. The bottom of the molecule represents the intersubunit interface

    A. The monomer is shown without the C-terminus (S699-D707) to demonstrate the groove of the tunnel. The molecular surface presentation (top figure) and ribbon diagram with semi-transparent surface presentation of the dimer (bottom figure).

    B. The entire A monomer is shown with the C-terminus (S699-D707) colored red. The molecular surface presentation (top figure) and ribbon diagram with semi-transparent surface presentation of the dimer (bottom figure).
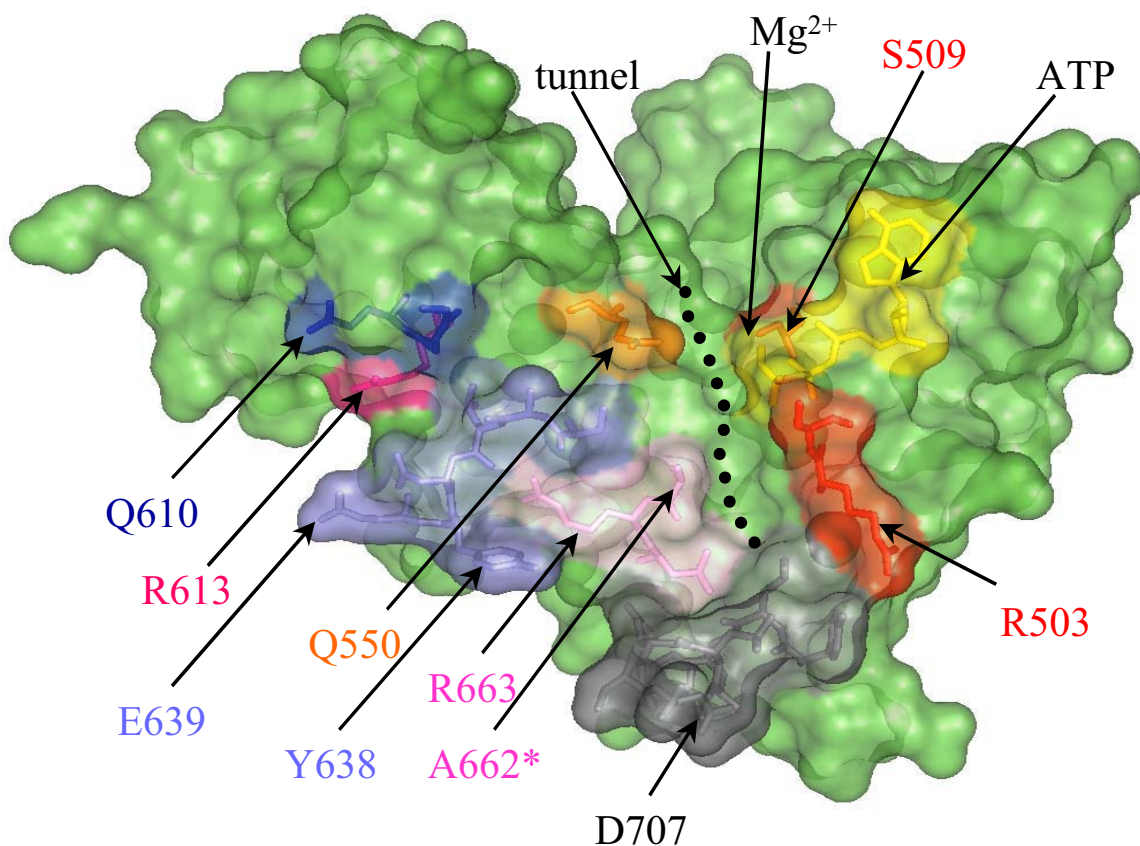
Figure 51. Amino acid residues involved in the intersubunit protein-protein interactions in the HlyB-NBD H662A dimer with bound ATP-Mg^{2+}

The A monomer of HlyB-NBD H662A with bound ATP-Mg^{2+} facing the dimer interface (the top of the molecule is facing the TMDs of the HlyB transporter). The semi-transparent surface presentation of the dimer. All amino acid residues involved in the intersubunit protein-protein interactions and ATP are shown in sticks and colored differently. The surface reflects a color of the contacting residue.

The major part of the monomer is colored green. ATP is shown in yellow. The groove of the tunnel is indicated by arrow and black dotted line. The C-terminus (Y700-D707) is colored gray. R503, S504, S509 (Walker A motif) is red; Q550 (Q-loop) – orange; G608, G609 and Q610 (C-loop) – blue; R613 – hot pink; S634, A635, L636, D637, Y638 and E639 (D-loop) – slate blue; A662*, R663, and L664 (H-loop) – pink.
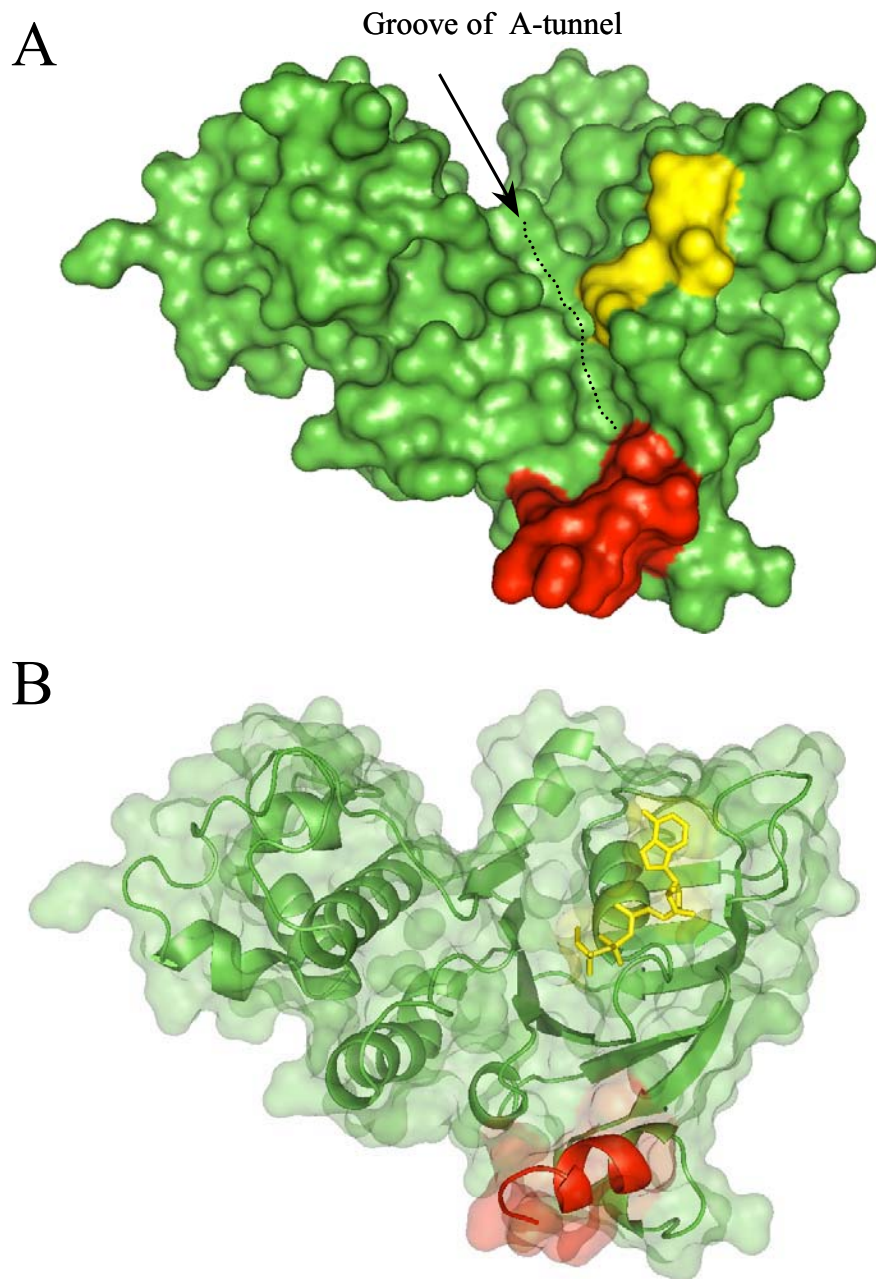
Figure 52. The A monomer of HlyB-NBD H662A with bound ATP-Mg^{2+} facing the intersubunit interface (the top of the molecule is facing the TMDs).

The color scheme is the same as in Figure 48.

A. The molecular surface presentation. The groove of the tunnel is indicated by arrow and black dotted line.

B. The ribbon diagram with semi-transparent surface presentation of the dimer.
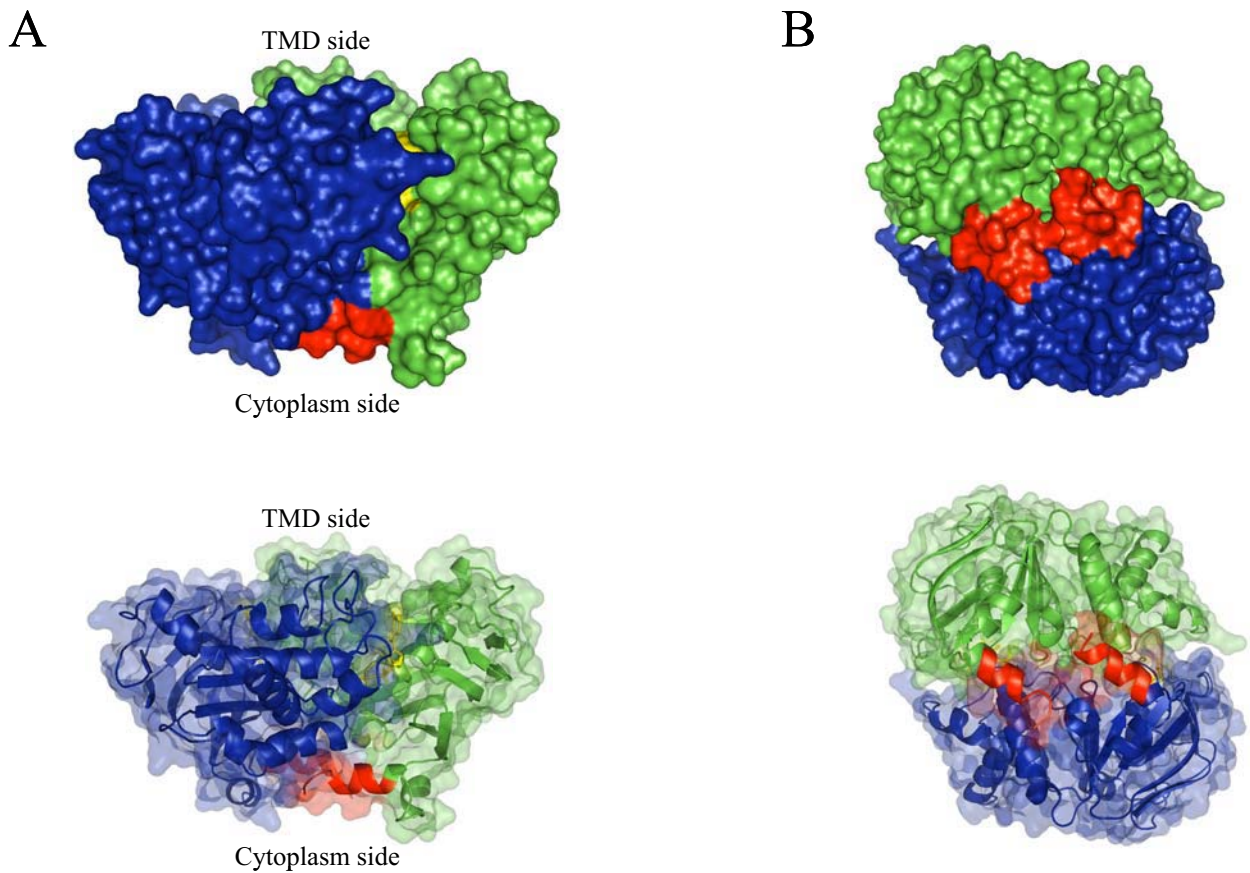
Figure 53. The HlyB-NBD H662A dimer with bound ATP-Mg^{2+}

The color scheme is the same as in Figure 48.

A. The side view of the dimer. The top of the dimer is facing the TMDs of the transporter. The bottom part is facing the cytoplasm. The molecular surface presentation (top figure) and stereo ribbon diagram with semi-transparent surface presentation of the dimer (bottom figure).

B. The dimer facing the cytoplasm (the opposite side of the dimer is facing the TMDs). The molecular surface presentation (top figure) and stereo ribbon diagram with semi-transparent surface presentation of the dimer (bottom figure).
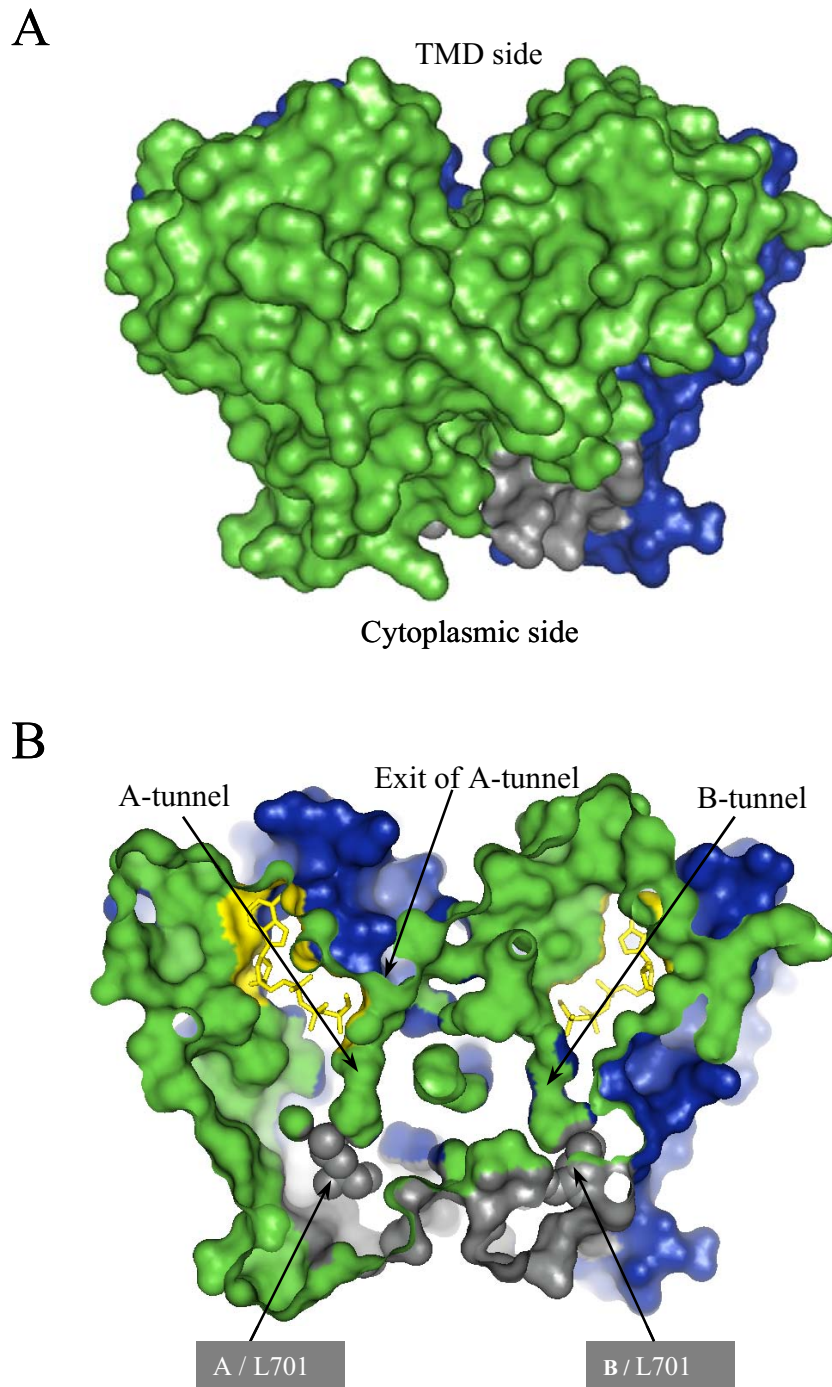
Figure 54. The side view of the HlyB-NBD H662A dimer with ATP-Mg^{2+}

The monomer A is colored green and monomer B is blue. Two ATP-Mg^{2+} complexes bound at the dimer interface are shown in yellow. The surface of the C-termini (S699-D707) is colored gray. The top of the dimer is facing the TMDs of the transporter. The bottom part is facing the cytoplasm.

A. Molecular surface presentation.

B. Cut through the molecular surface presentation of the dimer. The ATP-Mg^{2+} complex is shown in stick presentation with the surface reflecting a color of the contacting molecule/atom. Both A- and B-tunnels are indicated by the arrows. The exit of A-tunnel facing the TMD-side is also shown. The C-terminal amino acids Leu701 from each subunit, A and B, are shown in gray spheres.
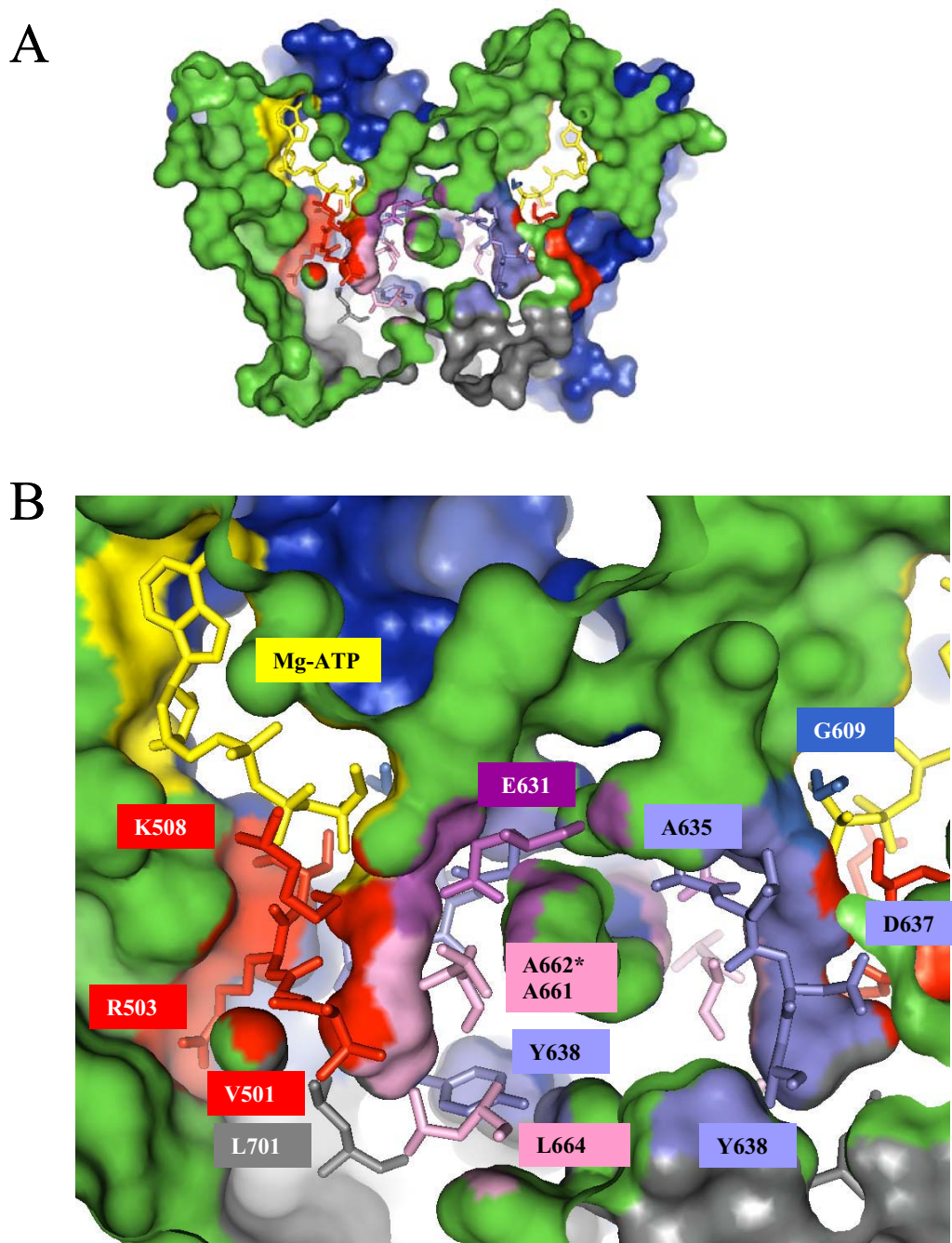
Figure 55. Cut through the molecular surface presentation of the HlyB-NBD H662A dimer with ATP-Mg^{2+} - I

The color scheme is the same as in Figure 54. The ATP-Mg^{2+}complex (yellow) and the amino acids lining the tunnels are shown in stick presentation with the surface reflecting a color of the contacting residue/atom. Additionally the residues of the Walker A motif are colored red; the C-terminal L701 – gray; the H-loop – pink; the D-loop – slate blue; the Walker B E631 – magenta; the C-loop G609 – cyan blue. Please see text for more detailed description.

A. Side view of the dimer. The top of the dimer is facing TMDs of the transporter. The bottom part is facing the cytoplasm.

B. Close-up view of A.

Figure 56. Cut through the molecular surface presentation of the HlyB-NBD H662A dimer with ATP-Mg^{2+} - II

Close-up views of the dimer from the side. The color scheme is the same as in Figure 54. The triphosphate moiety of ATP, Mg-ion, and amino acids lining the exit of the tunnels are shown in stick presentation with surface reflecting a color of the contacting atom. Phosphorus and Mg atoms are colored magenta, oxygen – red, nitrogen – blue. The Glu631 residues of the Walker B motif are colored pink; Ala635 of the D-loop – green. Please see text for more detailed description.

A. A-tunnel. Side view of the dimer, the same as in Figures 54-55.

B. B-tunnel. Side view of the dimer, the opposite side from Figure 56A view with B subunit in front.
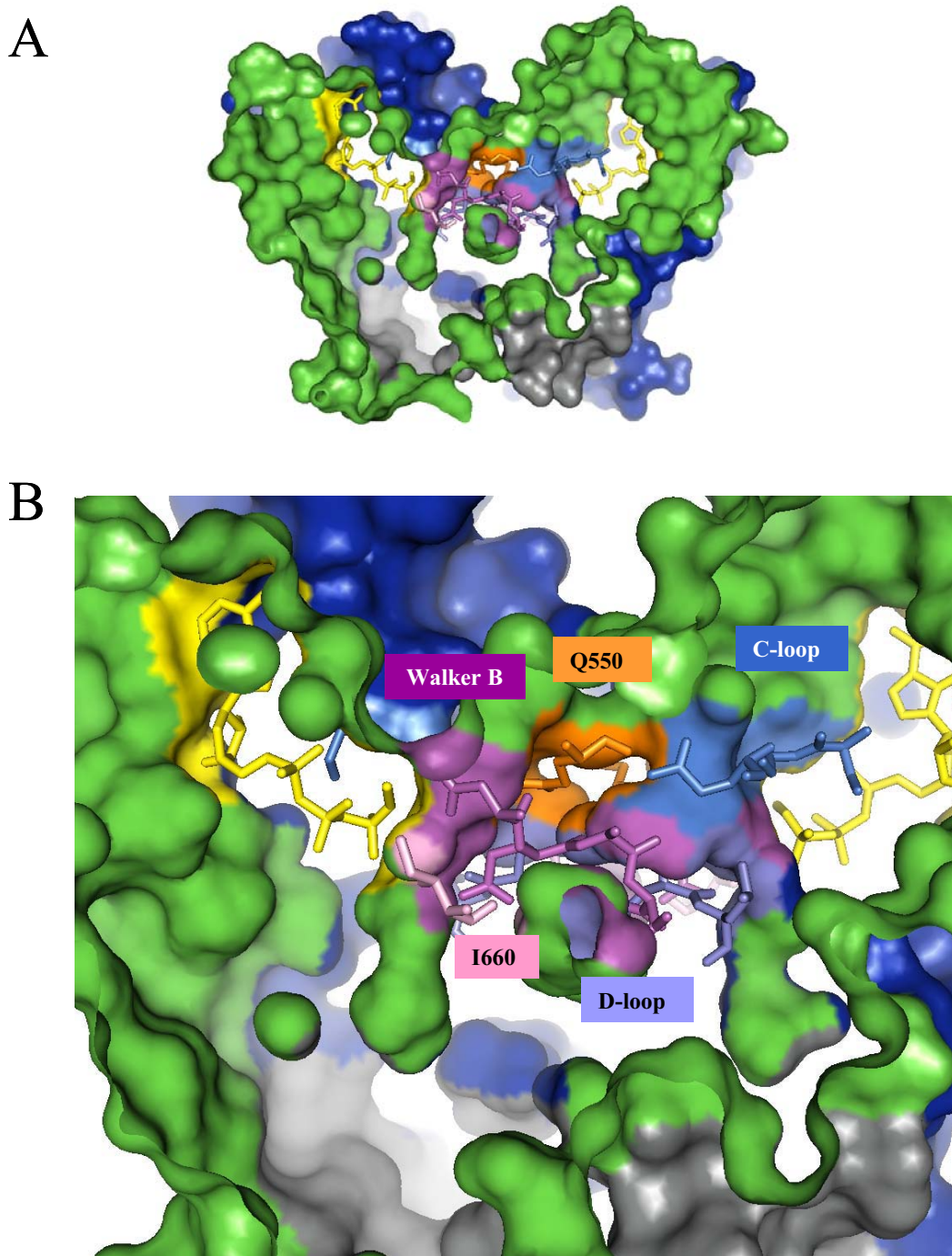
Figure 57. Cut through the molecular surface presentation of the HlyB-NBD H662A dimer with ATP-Mg^{2+} - III

The color scheme and view are the same as in Figure 54. The ATP-Mg^{2+} complexes (yellow) and amino acids lining exits and cavities of the tunnels are shown in stick presentation with surface reflecting a color of the contacting residue/atom. The I660 residues of the H-loops are colored pink; the residues of the D-loops – slate blue; of the Walker B – magenta; of the C-loops – cyan blue; two Q550 residues of the Q-loops – orange. Please see text for more detailed description.

A. Side view of the dimer. The top of the dimer is facing the TMDs of the transporter. The bottom part is facing the cytoplasm.

B. Close-up view of A.

ATP (S504, K508 of the *cis*-monomer and S607, G608, G609 of the *trans*-monomer) also compose the walls of the tunnel and the cavity. The only exception is G505 exposed to the external dimer surface, which makes a van der Waals connection (3.5 Å) with the γ-phosphate and a strong hydrogen bond (2.7 Å) with the β-phosphate of ATP.

According to the analysis of the van der Waals surfaces, the diameter of the each tunnel is approximately 2.5-3 Å with the groove of the tunnel being more prominent in the *cis*-subunit (Figures 50, 52). Such a duct is too narrow to permit even a fully unfolded HlyA protein as a substrate to pass through. However, the channel could be expanded in the reaction cycle of ABC-transporters (see below).

While both tunnels are open on the side of the dimer that faces the TMDs, the aforementioned asymmetry in the assembled ATP-Mg^{2+}-bound dimer leads to the partial blocking of the outlet of the B-channel[4] (Figure 56B). The two conserved residues, glutamate-631 of the Walker B motif (the B-subunit) and alanine-635 of the D-loop (the A-subunit), located at the end of the B-tunnel of the HlyB-NBD H662A dimer, seem to be mainly responsible for the channel obstruction by forming links to the γ-phosphate of ATP. The comparison of the HlyB-NBD-ATP-Mg^{2+} with the MalK (Chen et al., 2003) and the MJ0796 E171Q (Smith et al., 2002b) structures with bound ATP suggests that another conserved residue, the histidine of the His-loop, entirely plugs the potential tunnels in these dimers by the same mechanism, i.e. by making the connections to ATP in the active site. As a result, the tunnels are indistinguishable in the MalK and MJ0796 dimers.

The other two amino acids, glutamine-550 of the Q-loop (the B-subunit) and glycine-608 of the C-loop (the A-subunit), also tend to constrict the opening of the B-tunnel of the HlyB-NBD dimer while making their connections with the γ-phosphate (Figure 58). However, in contrast to E631 and A635, Q550 and G608 are positioned in the midst of the cavity at some distance from the tunnel exit, so their interference might be not that critical for the tunnel blocking.

---

[4] The B-ATP-binding site is composed of the Walker A motif of the B chain and the C-loop of the A chain of the AB HlyB-NBD dimer with ATP bound at the AB interface; the B channel is located proximal to the B-site of the dimer
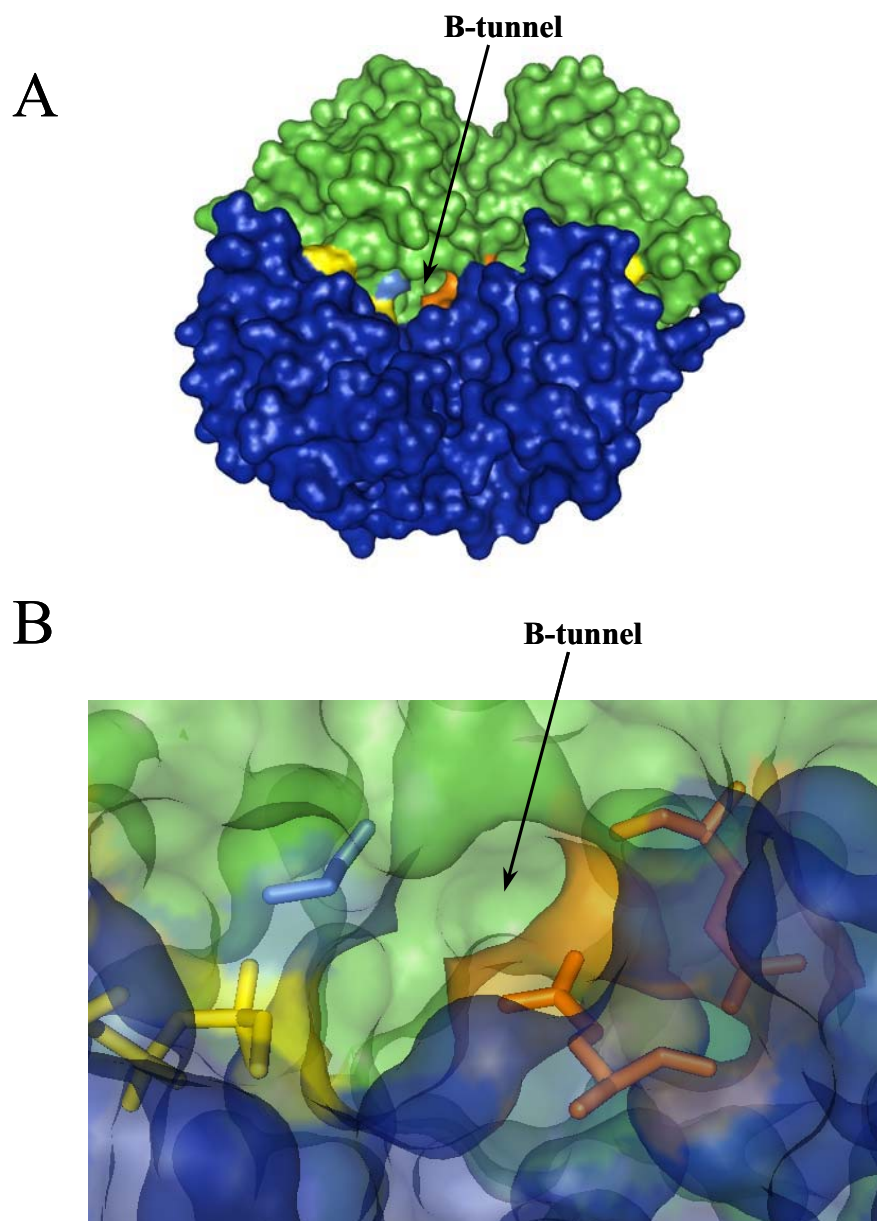
Figure 58. Molecular surface of the HlyB-NBD H662A dimer with bound ATP-Mg^{2+}, facing the TMDs

A. Monomer A is colored green and monomer B – blue. Two ATP-Mg^{2+} complexes bound at the dimer interface are shown in yellow. An arrow indicates the slightly constricted cavity of B-tunnel. The surfaces corresponding to Q550 residues of the Q-loop are colored orange and G608 of the C-loop - cyan blue.

B. The same as A. Close-up view with the semi-transparent molecular surface presentation of the dimer. Q550, triphosphate of ATP, Mg^{2+}, and G608 are shown in stick presentation with surface reflecting a color of the contacting residue/atom.

6.6. Structural details of HlyB-NBD H662A with bound ATP

The overall conformations of the two forms of HlyB-NBD H662A, with bound ATP and with ATP-Mg^{2+}, are very similar as is evident from rmsd of 0.63 Å for 474 Cα aligned atoms of each dimer (see Section 6.1). Still there are several very important differences. The most obvious dissimilarity between the two dimers is the packing of the C-terminal ends of their subunits (Figure 59). In the ATP-Mg^{2+}-structure the C-terminus of each monomer packs separately from each other, whereas in the ATP-bound dimer they are merged into a single moiety.

An even more important distinction between the two protein complexes is the complete sealing of both tunnels in the ATP-bound HlyB-NBD (Figure 60). The 'reshaped' C-terminal lid close each tunnel on the side facing the cytoplasm, whereas the two conserved residues from the opposite subunits of the dimer, Ala635 and E631, and the γ-phosphate of ATP completely block each opening on the side facing transmembrane domains (Figure 61). The alanine and the glutamate practically fill the entire floor of each cavity on the upper membrane-facing surface of the NBD-dimer.

Similar to the site B of the HlyB-NBD dimer with bound ATP-Mg^{2+}, two amino acids of site B of ATP-dimer, Gln550 of the Q-loop and Gly608 of the C-loop, partially fill the interior of the cavity (Figure 62). Glycine-608 exposes its Cα group into the cavity while contacting the γ-phosphate via the main chain amide group, whereas the amide side chain of glutamine-550 points towards the γ-phosphate of ATP yet is positioned too far to make a connection with the nucleotide. In other crystal structures of ABC transporters with bound ATP, the corresponding glutamate residue of the Q-loop normally establishes a water-mediated contact with the γ-phosphate, such as Q90 in MJ0796 (Smith et al., 2002b) or Q100 in HisP (Hung et al., 1998). In fact, a water-mediated contact of Q550 with ATP is detected in the B-site of ATP-Mg^{2+}-bound HlyB-NBD H662A (Figure 42B). Thus, it's possible that the Q-loop interacting with ATP can also contribute to the blocking of the molecular tunnel at some point of the ATP-hydrolytic cycle.

It is tempting to suggest that the observed tunnels in the proximity of the nucleotide-binding sites may take part in the allocrite translocation of the ABC-transporters. Then in the fully assembled transporter, the cavities adjacent to the ATP-binding sites and to the NBD-channels may serve as the docking sites for the regions of TMDs directly involved in the allocrite translocation. In that case, the Q-loop and its surface-exposed conserved glutamine would play a significant role in the transport of substrate across the membrane.
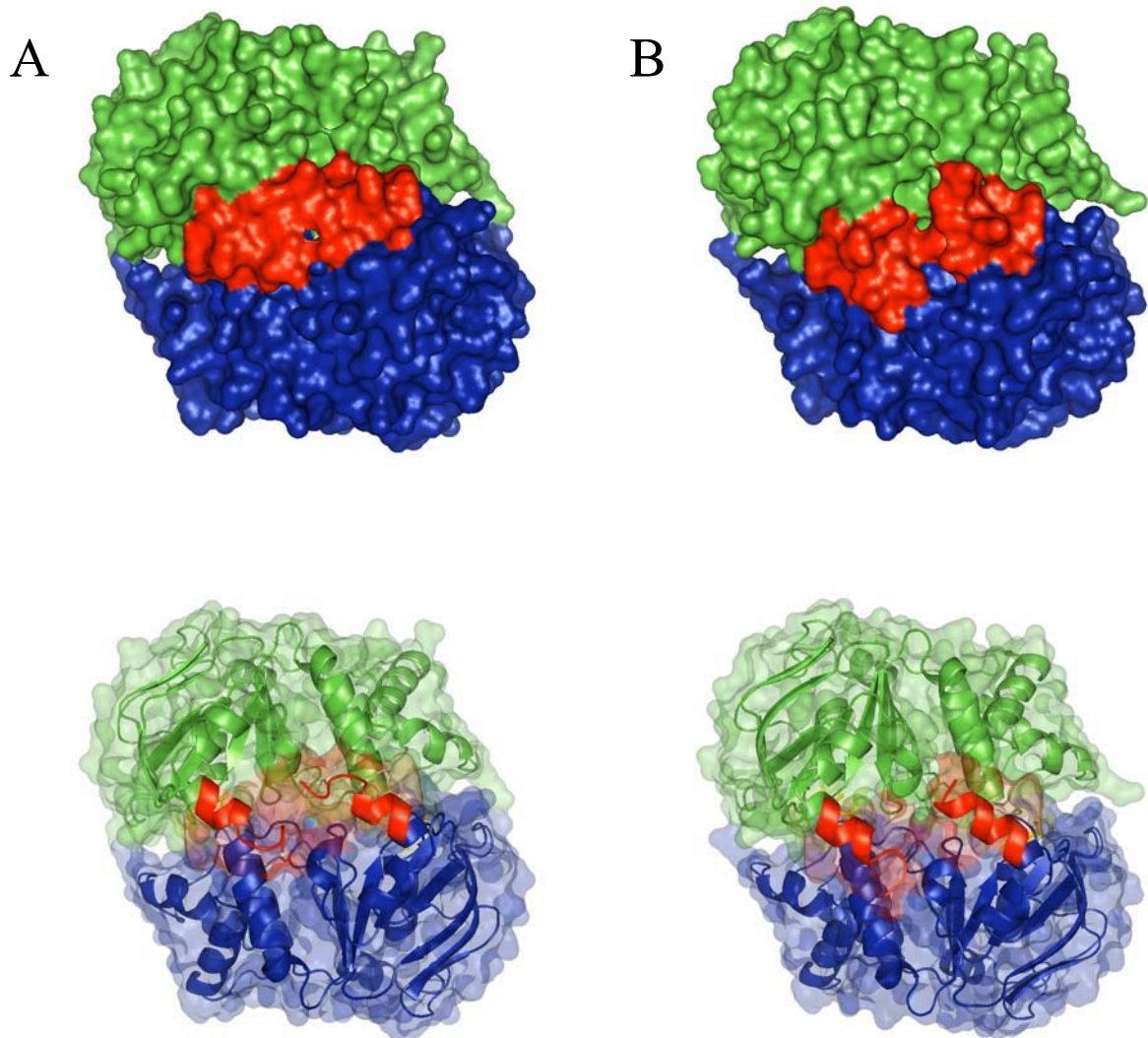
Figure 59. Different packing of the C-termini (colored red) of the ATP-bound HlyB-NBD H662A dimers in the absence and presence of Mg-ion in the active sites

The color scheme is the same as in Figure 48. Overall view of the two ATP-dimers from the side facing the cytoplasm (the opposite side of the dimers is facing the TMDs).

A. Dimer with bound ATP without Mg^{2+}. The molecular surface presentation (top figure) and ribbon diagram with semi-transparent surface presentation of the dimer (bottom figure).

B. Dimer with bound ATP-Mg^{2+}. The molecular surface presentation (top figure) and ribbon diagram with semi-transparent surface presentation of the dimer (bottom figure).
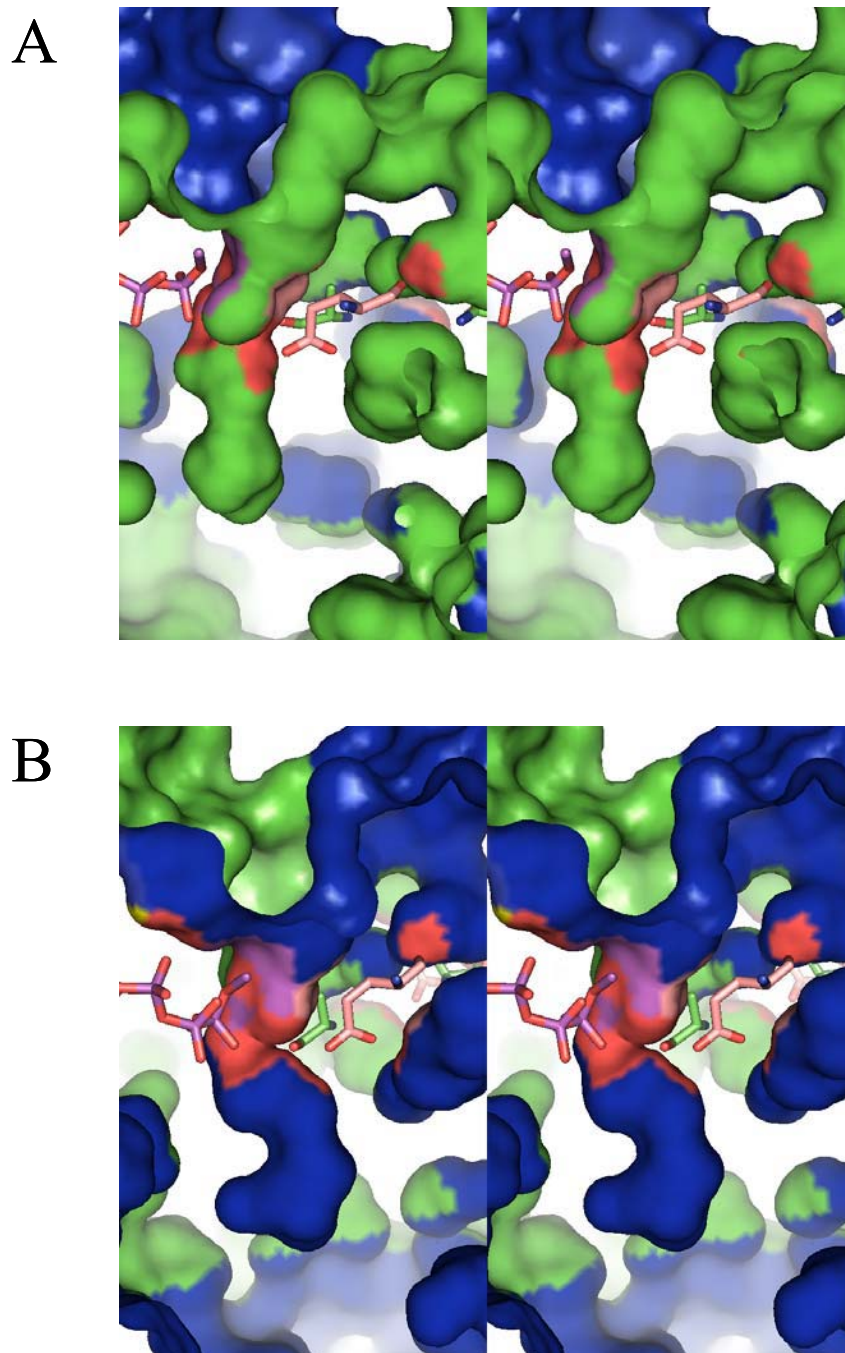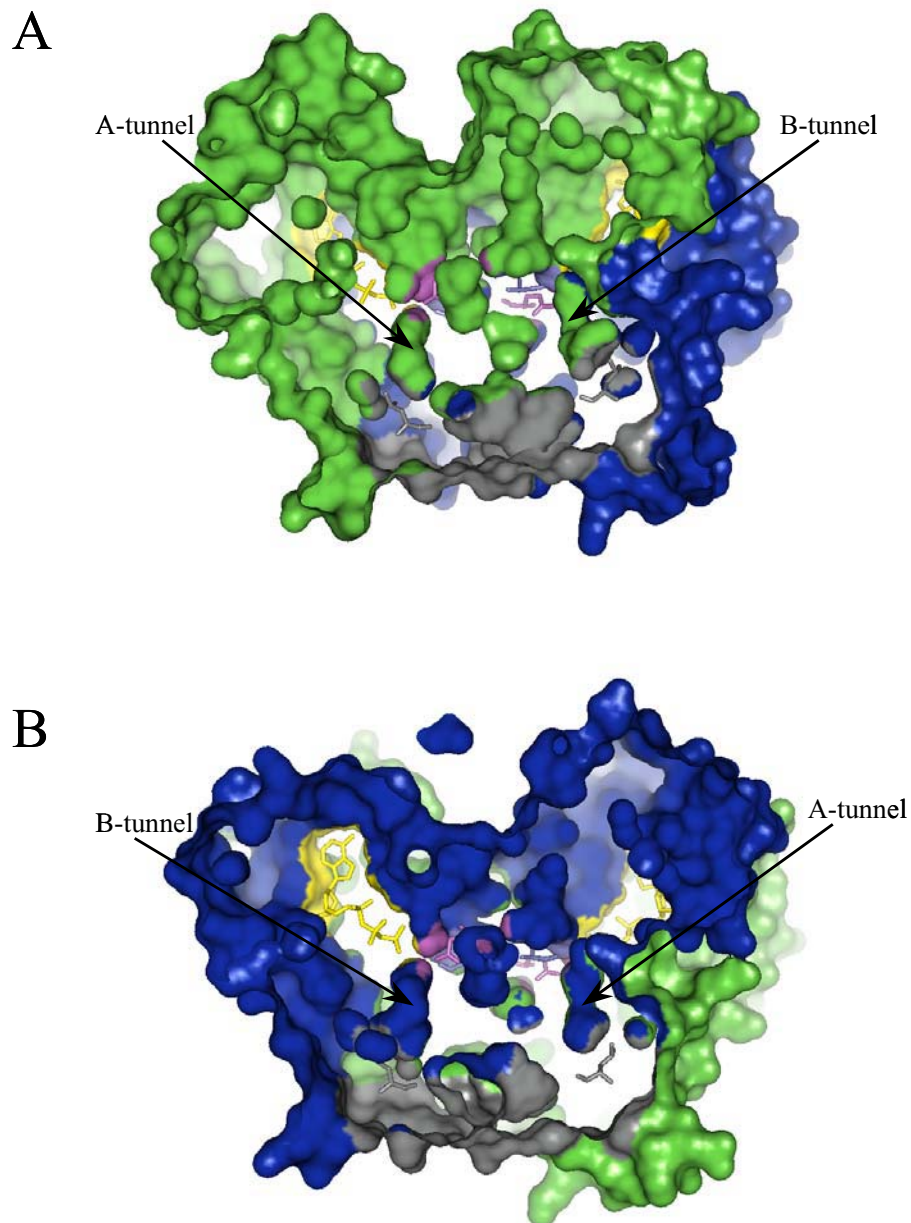
Figure 60. Cut through the molecular surface presentation of the HlyB-NBD H662A dimer with bound ATP without Mg^{2+}

The color scheme is the same as in Figure 54: monomer A is colored green and B monomer – blue. The surface of the C-termini (S699-D707) is colored gray. Two bound molecules of ATP and residues, E631, A635, and L701, are shown in stick presentation with surface reflecting a color of the contacting residue/atom. ATP is colored yellow; E631 – magenta; A635 – slate blue; L701 - gray. The top of the dimer is facing the TMDs of the transporter. The bottom part is facing the cytoplasm. The tunnels are indicated, which are sealed from both ends.

A. Side view of the dimer, the same as in Figures 54-55.

B. Side view of the dimer, the opposite side from Figure 60A with B subunit in front.
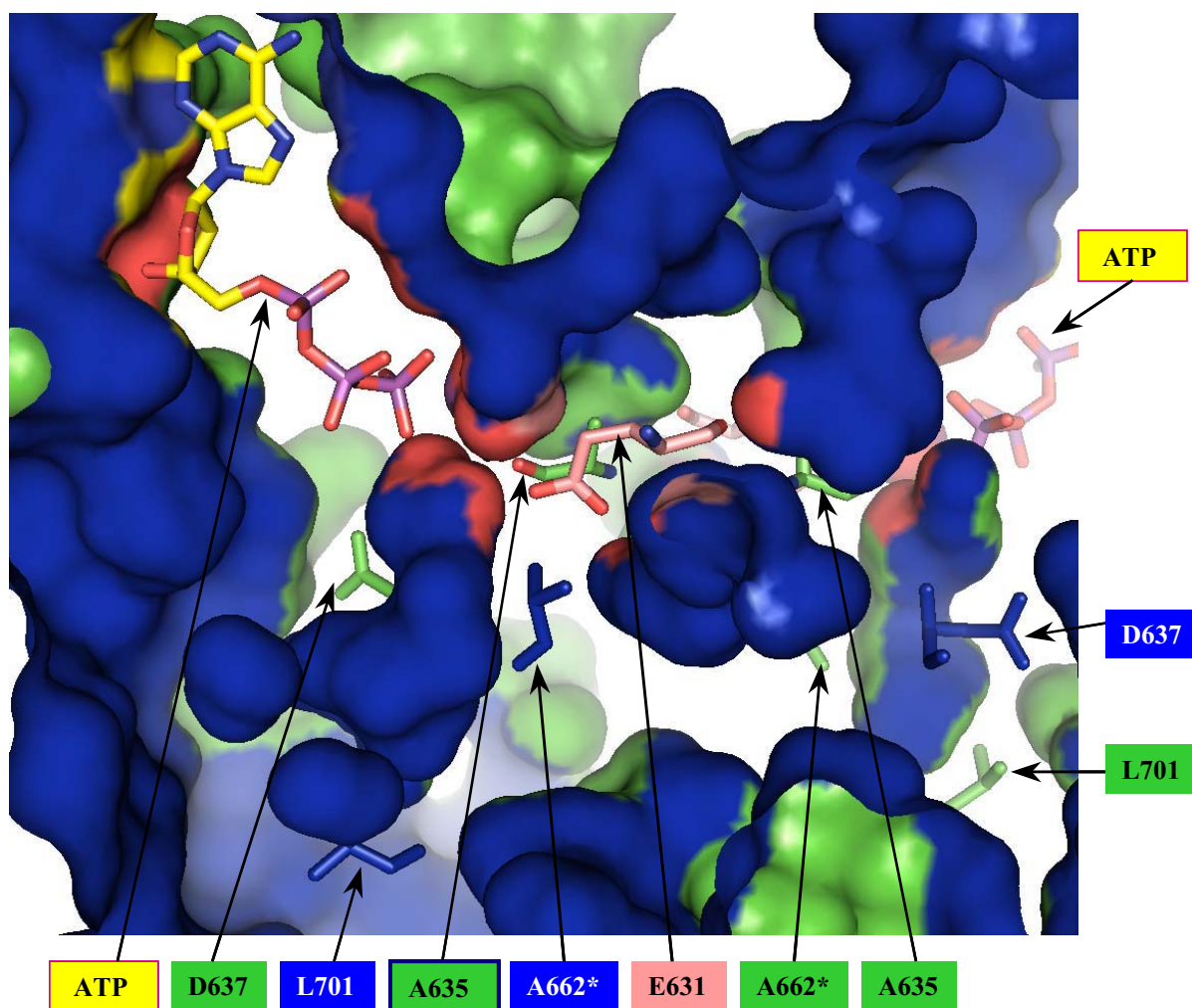
Figure 61. A close-up view of the cut through the molecular surface presentation of the HlyB-NBD H662A dimer with bound ATP without Mg^{2+}

The same side view as in Figure 60B, a close-up view of the sealed tunnels. The color scheme is the same as in Figure 54. ATP, amino acids sealing the tunnel exits, and some residues outlining the tunnels are shown in stick presentation with surface reflecting color of the contacting residue/atom. Carbon atoms of ATP are colored yellow, Glu631 of the Walker B motif – pink; Ala635 of the D-loop – green; phosphorus – magenta, oxygen – red, nitrogen – blue. All other amino acids replicate the color of the corresponding monomer. The top of the dimer is facing the TMDs of the transporter. The bottom part is facing the cytoplasm.
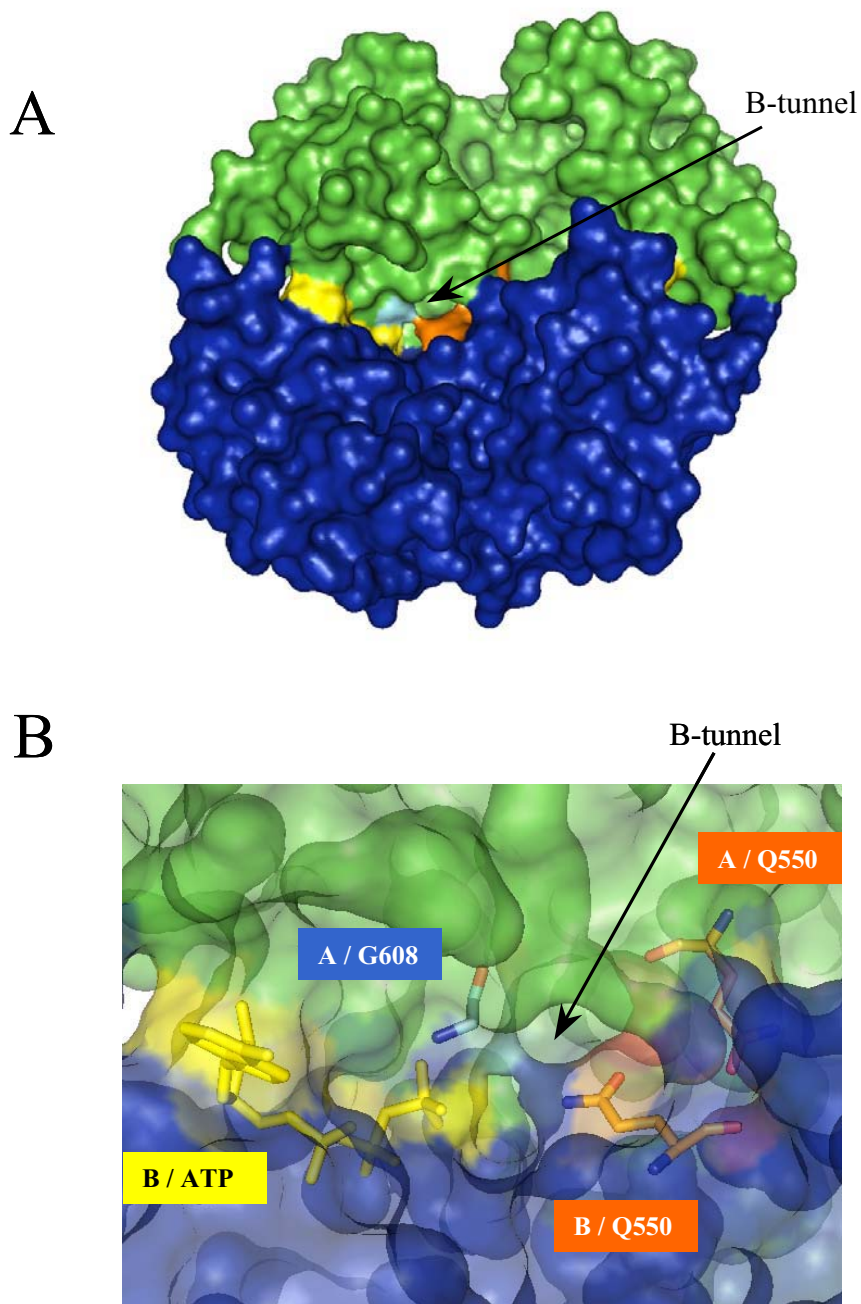
Figure 62. Molecular surface of the HlyB-NBD H662A dimer with bound ATP, facing the TMDs

- A. Monomer A is colored green and B monomer – blue. Two ATP molecules bound at the dimer interface are shown in yellow. An arrow indicates constricted cavity of the tunnel B. The surfaces corresponding to Q550 residues of the Q-loop are colored orange and G608 of the C-loop - cyan blue.

- B. The same as A. Close-up view with semi-transparent molecular surface presentation of the dimer. Q550, ATP, and G608 are shown in stick presentation with surface reflecting a color of the contacting residue/atom. Nitrogen and oxygen atoms of Q550 and G608 are colored blue and red, respectively.

6.6.1. ATP-protein interactions

The details of various ATP interactions with the HlyB-NBD dimer in the absence of Mg-ions are schematically shown in Figure 63. Four active centers of the two ATP-dimers within the asymmetric unit were examined to detect protein-nucleotide interactions and to evaluate the difference in the interaction patterns of the ATP- and ATP-Mg^{2+}-loaded dimers of HlyB-NBD H662A. Here, the direct nucleotide-protein interactions are almost identical to those observed in HlyB-NBD with Mg^{2+} in the active site. The ATP is sandwiched between two conservative motifs, the Walker A and C-loop, which establish all direct contacts between ATP and both subunits. Despite the absence of a Mg-ion, which coordinates three water molecules in the active site of the ATP-Mg^{2+}-bound structure, between three and five solvent molecules are located in the vicinity of the γ-phosphate of ATP in the ATP-bound HlyB-NBD structure. These solvent molecules provide a replacement for some connections observed in the ATP-Mg^{2+} structure due to the presence of Mg^{2+}-coordinated water, and take part in setting new connections. Thus, even in the absence of a Mg-ion, the OD1-carbonyl of the aspartate-630 is linked to the γ-phosphate via a water molecule, while its other carbonyl, OD2, is connected with the side chain of S509 of the Walker A motif via a hydrogen bond.

A very important difference between the active sites in the ATP- and ATP-Mg^{2+}-bound proteins is that Glu631 of the Walker B motif is bridged via a water molecule to the γ-phosphate of ATP in *all* active sites of the Mg-free dimer structure. In addition, two conserved residues of the opposite subunit's D-loop, A635 and D637, establish water-mediated contacts with the γ-phosphate in three out of four ATP-binding sites in two protein dimers of the asymmetric unit. In the B site, alanine-635 is located at the same distance from the corresponding ATP, as in all other sites, approximately 4.75 Å, and yet lacks a solvent molecule to mediate a link with the γ-phosphate. Thus, in contrast to the HlyB-NBD-ATP-Mg^{2+} structure and similarly to the MJ0796-ATP dimer structure (Smith et al., 2002b), the D-loop of Mg^{2+}-free HlyB-NBD is connected to the opposite nucleotide-binding site via a solvent molecule. Besides, an additional amino acid of the Walker A motif, G502, is included into the network of the nucleotide-protein interactions by means of a water mediated connection with the γ-phosphate.

The slight asymmetry between four ATP-binding sites is mainly due to a specific distribution of water molecules. Thus, one of the two active sites of each HlyB-NBD-ATP dimer involves amino acids of the His-loop into distant water-mediated interactions with ATP, linking both H662A* and A661 to the γ-phosphate via two solvent molecules.
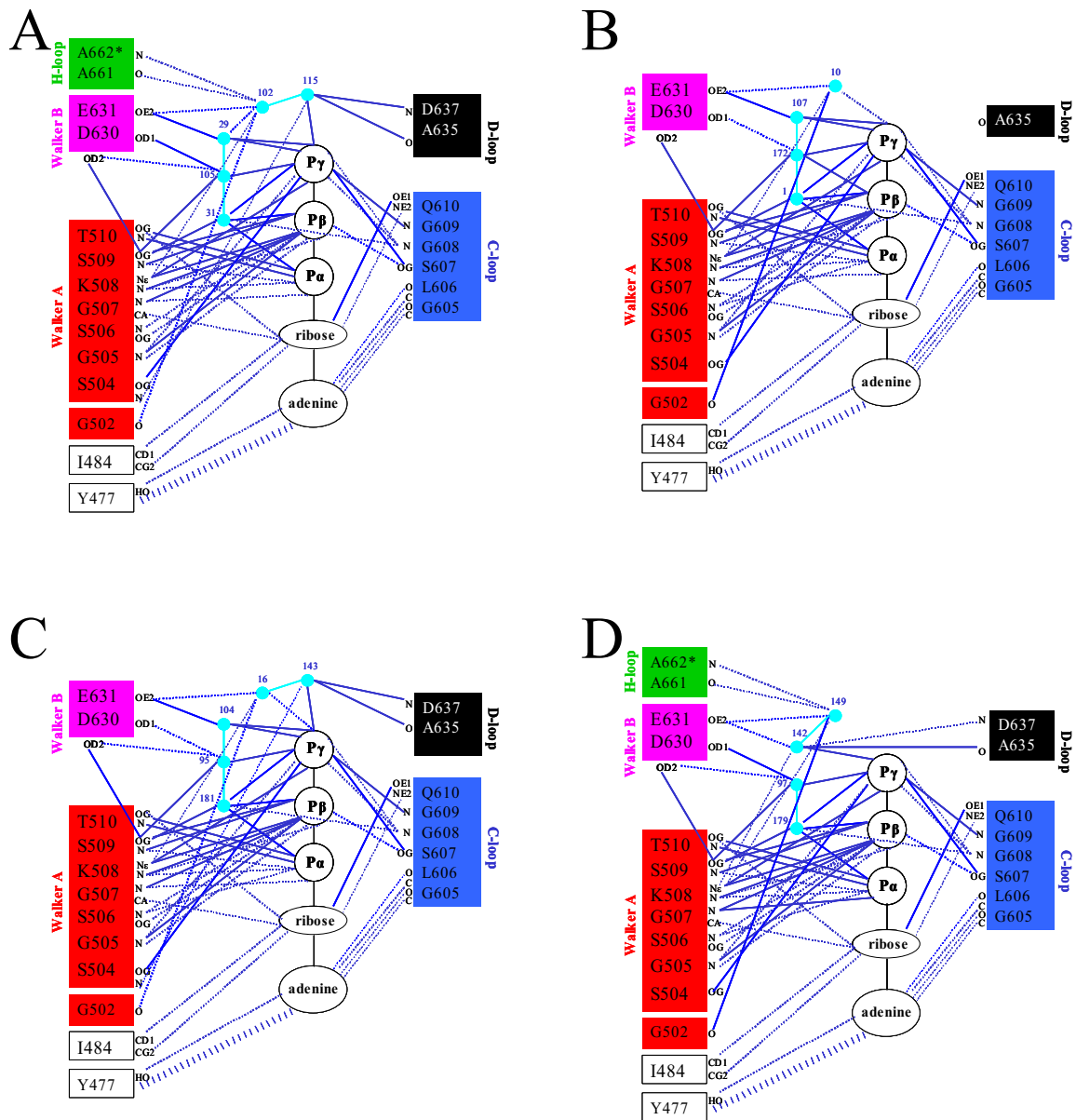
Figure 63. Schematic diagram of the interactions between ATP and HlyB-NBD H662A in all four sites of two dimers of the asymmetric unit

Color-coding is identical to Figure 39. Turquoise spheres indicate water molecules. Hydrogen bonds and salt bridges are shown as solid lines, while van der Waals and hydrophobic interactions are shown as dashed lines. Letters next to amino acids represent the atoms involved in the interactions.

A. A-ATP-binding site composed of the Walker A motif of A chain (*cis*-chain) and the C-loop of B chain (*trans*-chain) of AB-dimer.

B. B-ATP-binding site composed of the Walker A motif of B chain (*cis*-chain) and the C-loop of A chain (*trans*-chain) of the AB-dimer.

C. C-ATP-binding site composed of the Walker A motif of C chain (*cis*-chain) and the C-loop of D chain (*trans*-chain) of CD-dimer.

D. D-ATP-binding site composed of the Walker A motif of D chain (*cis*-chain) and the C-loop of C chain (*trans*-chain) of CD-dimer.

131

Overall, the two ATP molecules of the AB-HlyB-NBD dimer in the absence of Mg^{2+} participate in **93** nucleotide-protein interactions, **26** of which are hydrogen bonds or salt links (< 3.2 Å), **22** are water-mediated, and **45** are van der Waals or hydrophobic connections (< 4.0 Å). In other words, the ATP-bound structure has approximately the same number of direct ATP-protein links and twice as many water-mediated contacts in the active site as the ATP-Mg^{2+}-bound structure. The difference includes all additional water-mediated links connecting the γ-phosphate with the conserved ABC-residues, including E631 of the Walker B motif, A635 and D637 of the D-loop, G502 of the Walker A motif, and A661 and A662* of the His-loop. The evidence of the more extensive involvement of ATP in protein-ligand interactions is consistent with the calculated areas of the buried surfaces between two ligand molecules and the HlyB-NBD dimer, equal to 560 Å^2 and 450 Å^2 in the ATP- and ATP-Mg^{2+}-structures, respectively.

6.6.2. Protein-protein interactions

The total buried solvent-accessible area between the monomers in the ATP- and ATP-Mg^{2+} dimers is about the same, suggesting that the stability of the two dimer forms is similar. This agrees well with studies of the HlyB-NBD H662A behavior in solution (Chapter 7), which detect protein dimerization upon ATP addition, yet show no Mg^{2+}-effect on the formation of protein dimers in the presence of ATP. Nevertheless, the buried surface between two subunits in the ATP-bound HlyB-NBD, excluding ATP-protein contacts, is slightly lower then that in the ATP-Mg^{2+} form of the dimer, approximately 1340 Å^2 and 1440 Å^2, respectively. According to these data, the ATP-bound form of the dimer seems to have weaker protein-protein contacts, compared to the ATP-Mg^{2+}-structure.

On the other side, the basic intermolecular protein-protein interactions are preserved in both dimers, whereas some of the connections are missing and some new ones appear in the dimer interface of the ATP-bound HlyB-NBD (Figure 64) comparatively to the ATP-Mg^{2+}-protein. Indeed, the specific folding of the C-terminal extensions in each ATP-dimer of HlyB-NBD H662A (Figure 59), with and without Mg-ions in the active sites, exemplifies the difference in intersubunit interactions between the two structures.

The total of **50** intersubunit contacts are detected in the HlyB-NBD sandwich with bound ATP, which are 19 fewer than in the ATP-Mg^{2+}-bound dimer. The A- and B-monomers contribute 22 and 24 amino acids, respectively, to establish connections between the two subunits, in which 20 residues from A and 22 from B directly contact each other
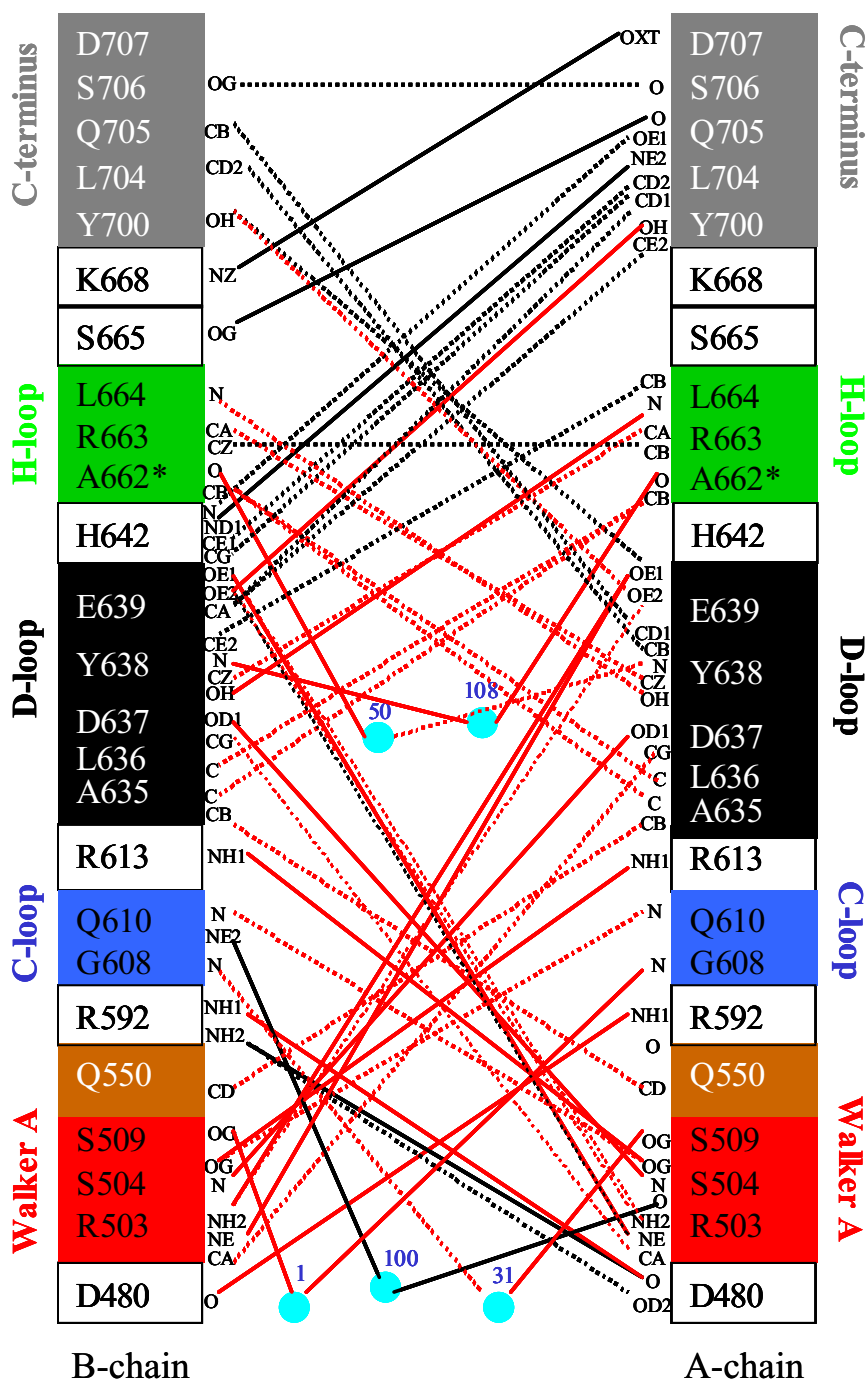
Figure 64. Schematic diagram of the protein-protein interactions across the AB-dimer interface of HlyB-NBD H662A with bound ATP

Color-coding is identical to Figure 39. Turquoise spheres indicate water molecules. The numbers in blue identify water molecules in the structure. The residues of the C-terminal extension are colored gray. Hydrogen bonds and salt bridges are shown as solid lines, while van der Waals and hydrophobic interactions are shown as dashed lines. The lines in red designate symmetric contacts, the lines in black – asymmetric. Letters next to amino acids represent the atoms involved in the interactions.

(Figure 64). Thus, the ATP-bound dimer involves four more residues for the direct protein-protein contacts then the ATP-Mg^{2+} dimer. The same set of amino acids from each subunit, Ser504, Ser509, and Q610, participates in both direct NBD-NBD and nucleotide-protein contacts simultaneously, reproducing the pattern observed in the ATP-Mg^{2+}-bound dimer.

All of the above interactions can also be divided into symmetric and asymmetric ones (Figure 65). Symmetric interactions involve 16 amino acids from each side of the dimer to set up direct protein-protein contacts. Both A and B subunits participate in **32** symmetric connections, including **11** hydrogen bonds (< 3.2 Å), **4** water-mediated contacts, **10** hydrophobic (< 4.0 Å), and **7** van der Waals interactions (< 4.0 Å) (Figure 65A). Although the ATP-Mg^{2+}-HlyB-NBD H662A dimer has 10 more symmetric contacts and additionally engages one extra residue from each monomer for the direct contacts, their total contribution into the dimer stability is approximately the same as for the ATP-bound dimer, since all symmetrical interactions in the former dimer comprise 7 hydrogen bonds, 12 hydrophobic, 11 van der Waals, and 12 water-mediated connections (Figure 44A).

Apart from the dimer stability, some of the connections in the Mg^{2+}-ATP-bound protein may be important in signaling between subunits. Thus, the symmetric interaction between Q550 of one monomer and Q550 of the other, detected in the Mg^{2+}-ATP dimer, does not exist in ATP-bound HlyB-NBD without Mg-ions (Figures 64-65). The same is true for the water-mediated link between two equivalent serine-634 residues of the opposite D-loops. Due to more distant positioning between the aforementioned serine residues, no intersubunit connection between either Q-loops or D-loops exists in the ATP-bound form of dimer, in contrast to the ATP-Mg^{2+} dimer.

The asymmetric protein-protein intersubunit contacts in the ATP-complex include the total of **18** links, **4** of which are hydrogen bonds, **8** hydrophobic, **5** van der Walls, and **1** water mediated interactions (Figure 65B). Direct protein-protein contacts involve 11 residues from each monomer of the ATP-dimer. For the comparison, the asymmetric intersubunit interactions in the Mg^{2+}-ATP protein comprise total of 27 contacts - 2 hydrogen bonds, 14 hydrophobic, 3 van der Waals, and 8 water-mediated connections. However, only 9 amino acids from the A monomer and 4 from the B monomer make direct contacts with each other (Figure 44B). Nevertheless, given the high strength of the asymmetric connections in the ATP-Mg^{2+} HlyB-NBD dimer, those contacts seem to significantly contribute to the dimer stability.

The overall patterns of the asymmetric connections in the two dimers are quite different (Figures 44B, 65B). In the ATP-Mg^{2+} HlyB-NBD dimer, the C-terminus of the A
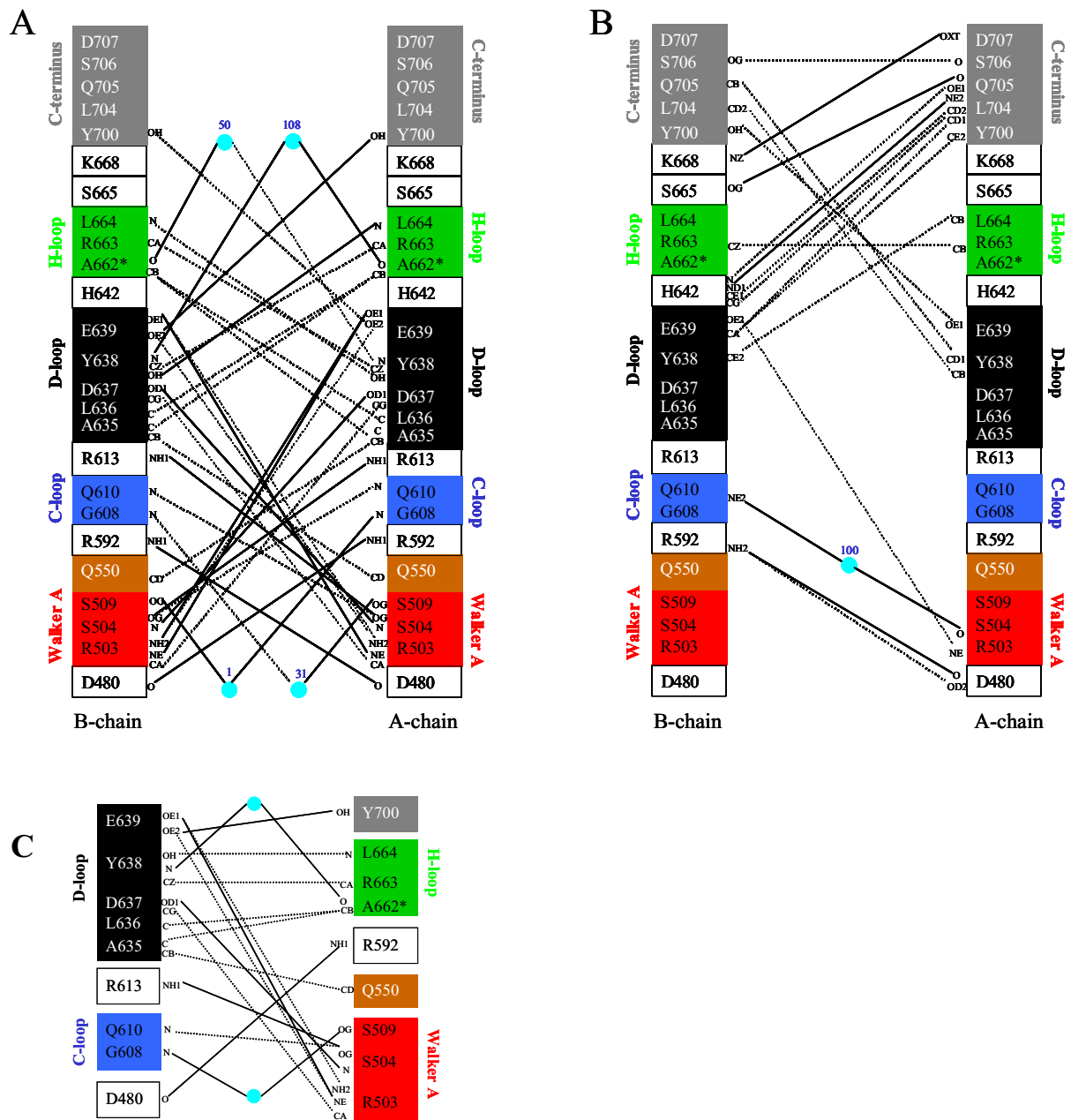
Figure 65. Schematic diagrams of the symmetric and asymmetric protein-protein interactions across the AB-dimer interface in HlyB-NBD H662A with bound ATP

- A. Symmetric contacts
- B. Asymmetric contacts
- C. Simplified presentation of the symmetric interactions

Color-coding is identical to Figure 39. Turquoise spheres indicate water molecules. The numbers in blue identify the water molecules in the structure. The residues of the C-terminal extension are colored gray. Hydrogen bonds and salt bridges are shown as solid lines, van-der-Waals and hydrophobic interactions are shown as dashed lines. Letters next to amino acids represent the atoms involved in the interactions.

subunit is involved in contacts with the opposite NBD monomer, supplying 9 direct links, while the corresponding region of the B subunit seems to be excluded from the NBD-NBD interface, providing only one water-mediated connection from S706 of the B-monomer to Y702 of the A-monomer. In contrast, both C-terminal extensions contribute to the dimer interface of the Mg^{2+}-free ATP-HlyB-NBD. Altogether, the B-monomer of the ATP-bound HlyB-NBD dimer provides 5 links to the opposite subunit and the A-monomer supplies 10 more; all of them are direct protein-protein interactions, including one contact between two C-termini. Moreover, asymmetry of the C-terminal connections in the ATP-bound structure is less pronounced than in the ATP-Mg^{2+} HlyB-NBD dimer. Thus, tyrosine-700 sets up a symmetric hydrogen bond with glutamate-639 of the D-loop of the opposite subunit (Figure 65A). The other contact between C-terminal residues is asymmetric, yet involves the same amino acids in the two monomers. In this case, the side chain of serine-706 of the B-monomer interacts with the main chain carbonyl of serine-706 of the A-monomer (Figure 65B). Similarly, two arginine-663 residues of the two H-loops contact each other.

In agreement with the ATP-Mg^{2+} structure of HlyB-NBD, the C-terminal amino acids of the Mg-free dimer tend to set up a majority of the connections with the opposite D-loop and the extended D-loop sequence, which includes H642 residue of the B subunit.

In addition to the C-terminus' participation, the group of the asymmetric interactions in the ATP-dimer also includes other connections, such as those between the extended H-loop of the A-monomer and the opposite D-loop, the C-loop of the B-subunit and the Walker A motif of the A subunit, the D-loop of the B subunit and the Walker A of A subunit, the aforementioned contact between the opposite H-loops, and a few other contacts. However, no interaction between the E631 of the Walker B and A635 of the D-loop of the other subunit is observed in the ATP-bound dimer of HlyB-NBD H662A.

Overall, the ATP-dimer of HlyB-NBD has significantly lower number of total water-mediated connections between the subunits, 5 versus 20 in the ATP-Mg^{2+}-bound dimer. In contrast to the Mg^{2+}-ATP structure of HlyB-NBD H662A, the Mg^{2+}-free ATP-dimer lacks connections between the D-loops of the opposite subunits. The Q-loops have no contacts with each other either. Besides, the Walker B motif has no connection with the opposite D-loop, as well as neither of the active centers has contact with the Q-loop. On the other hand, in the ATP-bound dimer the two H-loops set up a link between the monomers that is not observed in the Mg^{2+}-ATP structure (Figure 66).

Thus, the specific patterns of the intersubunit contacts in the ATP- and ATP-Mg^{2+}-bound dimers of HlyB-NBD H662A suggest that Mg^{2+} binding at the active NBD centers
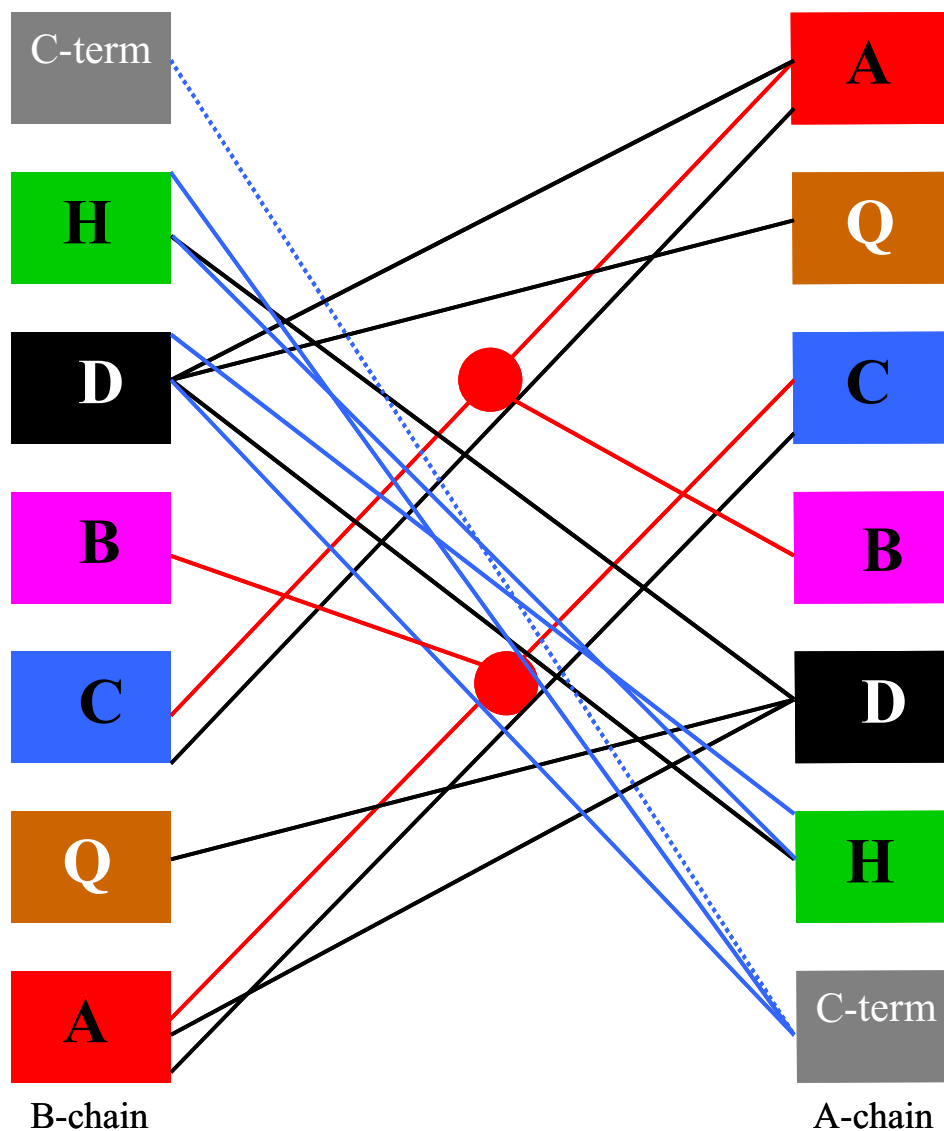
Figure 66. Summarized scheme of protein-protein and nucleotide-protein interactions across the AB-dimer interface in HlyB-NBD H662A with bound ATP

Color-coding is identical to Figure 39: A stands for the Walker A motif, Q – the Q-loop, C – the C-loop or ABC-signature, B – the Walker B motif, D – the D-loop, H – the H-loop, C-term – the C-terminus. The residues of the C-terminal extension are colored gray. Red spheres indicate two ATP molecules. Red lines designate nucleotide-protein interactions; black lines – symmetric protein-protein interactions; blue lines – asymmetric protein-protein connections. The solid lines indicate direct contacts, dashed lines – single water-mediated interactions.

changes not only the local environment but influences more distant protein-protein interactions, inducing conformational changes throughout the entire dimer. This statement is further supported by the observation of the different functional states of the potential tunnels for allocrite translocation in the crystals structures of the ATP- and ATP-Mg^{2+}-bound dimers. Moreover, Mg^{2+} binding seems to initiate a more pronounced asymmetry between two nucleotide-binding sites and two protein subunits in the HlyB-NBD dimer.

6.7. Phosphate channel of the ATP-Mg2+-HlyB-NBD dimer

The surface of a protein can be evaluated as van der Waals, Connolly, or solvent accessible surface. The van der Waals surface of the protein is limited by van der Waals spheres of its atoms. The solvent accessible surface (SAS) is obtained by adding the radius value of a probe sphere to the van der Waals surface of the protein. The Connolly surface, which is also called molecular, is composed of the underlying surface of a spherical probe rolling on the van der Waals surface of a protein.

While analysis of the van der Waals surface of the HlyB-NBD ATP-Mg^{2+} bound dimer demonstrates two open tunnels proximal to the ATP-binding sites (Figures 48-52, 54), the SAS representation of both ATP- and ATP-Mg^{2+}-dimers using a probe radius of water (1.4 Å) shows no evidence of channels. Yet, SAS reveals two cavities on the membrane-facing side of each protein dimer (Figure 67). While both cavities are formed at the dimer interface of the two identical protein subunits, the cavities of the ATP-Mg^{2+}-dimer of HlyB-NBD differ significantly in shape. One cavity of the dimer, adjacent to the A channel and to the A binding site (Figure 67), extends into the interior of the protein along the dimer interface reaching the γ-phosphate of ATP. In contrast, the cavity on the other side of the dimer, adjacent to the B-binding site, is more shallow and has no contact with the neighboring ATP molecule. In the ATP-bound dimer of HlyB-NBD, the two water accessible cavities on the membrane-facing surface look similar to each other and to the B-cavity of the ATP-Mg^{2+}-dimer. Therefore, in the ATP-bound HlyB-NBD dimer, the phosphate moieties of both nucleotides are completely buried within the protein (Figure 67).

Thus, comparison of the water-accessible cavities of the two nucleotide-bound dimers of HlyB-NBD shows that binding of ATP-Mg^{2+}is required to promote asymmetry between the active sites. Such asymmetry results in a channel within one of the active sites, the possible function of which is to release the cleaved γ-phosphate group upon ATP hydrolysis.
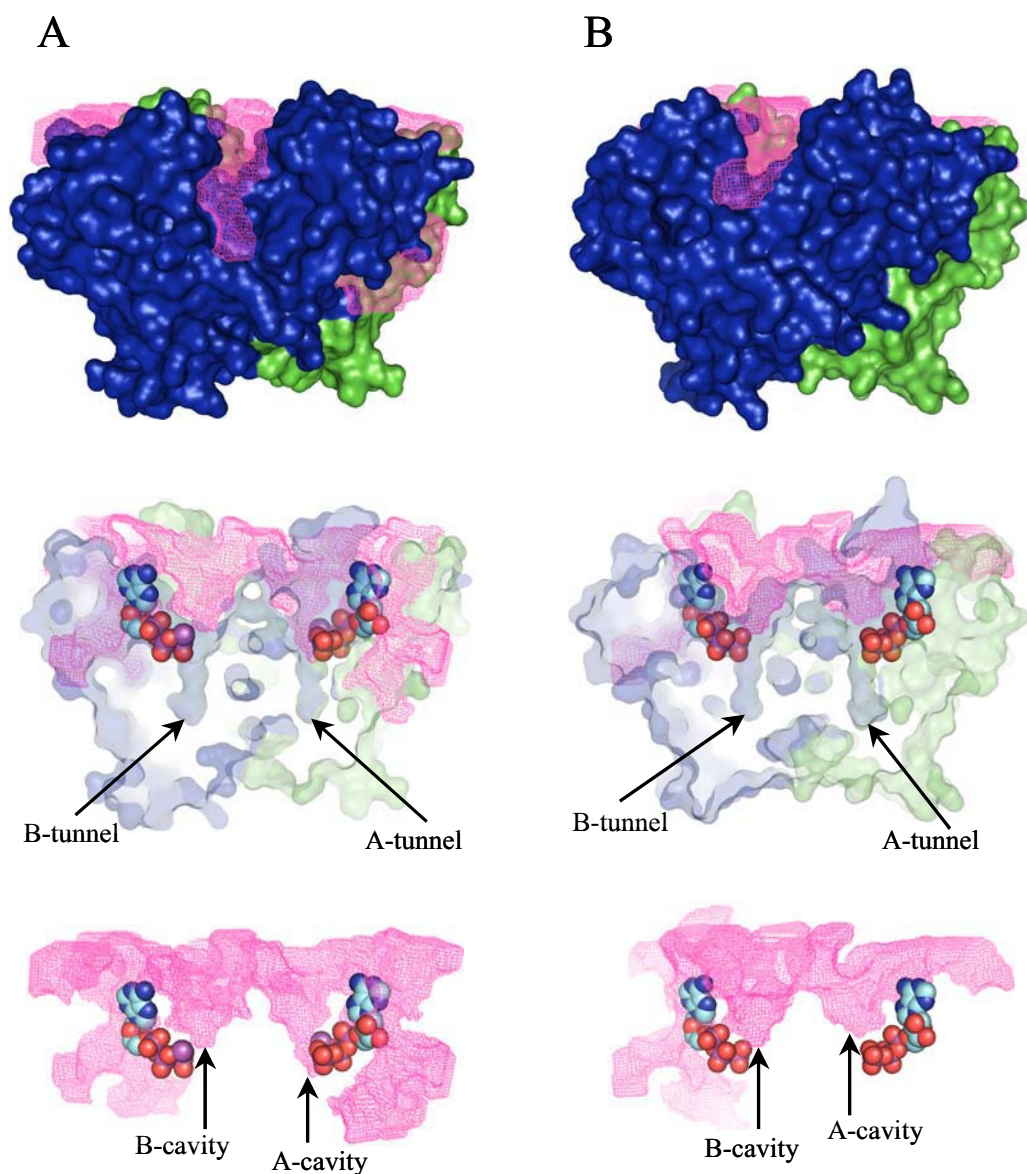
Figure 67. Solvent accessible surface for the HlyB H662A dimers in two states, with bound ATP-Mg^{2+} and with bound ATP

The monomer A is colored green and the B-monomer – blue. The water accessible surface is shown as pink net with an emphasis on the cavities adjacent to the nucleotide-binding sites. The solvent accessible surface for each dimer was generated and visualized using the programs VOIDOO and MAMA (Uppsala Software Factory).

The side view of the HlyB-NBD H662A dimers. The top of the dimer is facing TMDs of the transporter. The bottom part is facing the cytoplasm. The van der Waals surface presentation of the dimers (top figures), the semi-transparent van der Waals surface presentation of the dimers with the nucleotide molecules depicted in sphere representation (middle pictures), and the water accessible surface presentation of the dimers with the nucleotides in the active sites (bottom figures).

A. The HlyB-NBD H662A dimer with bound ATP-Mg^{2+}

B. The HlyB-NBD H662A dimer with bound ATP

Importantly, the presence of the phosphate channel in the protein structure may allow release of the γ-phosphate even in the assembled protein dimer. Removal of the γ-phosphate from one single active site may trigger dissociation of the protein dimer and release of ADP.

6.8. Suggested mechanism of allocrite transport in ABC-transporters

The crystal structures of the ligand-bound NBDs of the HlyA transporter revealed the key architectural features that are essential for our understanding of the transport mechanism of ABC-proteins. Thus, the HlyB-NBD dimer in complex with ATP-Mg^{2+} displays a pronounced asymmetry, which results in a solvent accessible channel for the γ-phosphate release. Moreover, transient tunnels proximal to the ATP-binding sites were discovered, which are created at the dimer interface of HlyB-NBD. Such structural findings combined with previous genetic, biochemical, and structural knowledge of ABC-transporters, suggest a novel transport mechanism that can be generalized for all members of this protein superfamily.

The current model of ABC transporters suggests the existence of a channel or tunnel to transport allocrite across the membrane. However, the exact location of such a channel in the protein complex is unknown. Detection of the transient tunnels within the HlyB-NBD dimer structure makes it tempting to suggest that function of these tunnels is to transport the allocrite. In that case one can envision the following picture of HlyA transfer across the membrane. In ABC-exporters, such as the haemolysin A transporter, the allocrite approaches the pre-assembled NBD-ATP-Mg^{2+} dimer from the cytoplasmic side (Figures 53, 54) and binds to it. The previous studies of HlyB confirm the existence of an allocrite recognition site in the NBD-portion of HlyB (Benabdelhak *et al.*, 2003). As an alternative version, the allocrite may bind to one of the NBD-monomers and induce functional NBD dimerization in the presence of ATP; yet, this version seems less likely. The substrate binding would cause conformational changes in the protein that promote significant NBD-dimer asymmetry, forming one fully open tunnel and unlocking this tunnel from the cytoplasmic side (see further details below). Opening of the tunnel cytoplasmic entrance could be accomplished by a conformational change of the C-terminus of HlyB-NBD. The notion of the enhanced conformational flexibility of the C-terminal end is supported by structural plasticity of this region detected by comparison of the different functional states of HlyB-NBD (Chapters 6 and 8). Passing the tunnel, the allocrite has to be released on the other side of NBD dimer at the junction with TMDs, where it likely enters another tunnel in the membrane part of the

transporter. It's possible that the membrane channel and the NBD channel form a continuous conduit to provide unidirectional transport of the substrate out of cell. Therefore, the cavity located at the exit of the NBD-tunnel may serve as a docking site for TMD to extend the translocation tunnel across the membrane. The TMD regions contributing to the construction of the continuous tunnel would also interact with a neighboring ATP molecule that is exposed to the NBD surface facing the transmembrane domain (Figure 48). Thus, the TMDs of HlyB and possibly of other ABC-transporters seem to have an opportunity to directly participate in the ATP-binding/hydrolysis events. Such an idea may be supported by the photoaffinity labeling studies, which demonstrate direct interaction of nucleotide with the NBD and one of the TMD subunits of the histidine transporter (Hobson *et al.*, 1984).

The fact that the NBD-tunnel is predominantly built of the amino acids of the conservative motifs suggests that such an architecture could be a universal feature of the exporters of hydrophilic allocrites or of even all ABC transporters. On the other side, in case if the tunnel participates in a transport event, it implies that either NBD tunnel has low specificity for the allocrite or it undergoes some transformation upon substrate binding to provide some specificity for the transported substrate, or both. It is possible that the C-terminal part and/or another substrate-binding region of the NBD-exporters serve as a specificity selector for the transported substrate. The low specificity of the NBD translocation tunnel might also explain a necessity of the additional accessory proteins/domains in the ABC-exporting systems; they would be required to enhance the specificity of transporter.

According to the HlyB-NBD H662A structure with bound ATP-Mg^{2+}, the tunnel may remain open when intact ATP molecule is bound to the active site, which is adjacent to the transport pore (Figure 40). The presence of the γ-phosphate of ATP seems to not constrict the tunnel (see A-tunnel in the HlyB-NBD ATP-Mg^{2+}-structure, Figures 54-57), suggesting that ATP-hydrolysis in the 'translocation site' of NBD is not required for the substrate translocation through that pore. Interestingly, the structural picture implies that an allocrite may directly pass the intact ATP molecule on the way out of or into the cell, since the nucleotide is one of the constituents of the tunnel wall (Figures 51, 54-57). In the structure of the H662A mutant protein with bound ATP-Mg^{2+}, the TMD-exit of the tunnel is unlocked by the His662Ala substitution, which disrupts the connection between the conserved histidine-662 and ATP. In the wild type ABC proteins, the pore opening and disruption of the connections between the hydrolytically active residues and ATP may be provided by the pronounced asymmetry within the NBD-dimer. The notion of a progressing asymmetry is supported by the slightly asymmetric architecture observed in the structure of the HlyB-NBD

H662A dimer with bound ATP, which is further enhanced upon binding of Mg^{2+} to the active site. An even more prominent asymmetry could result from the allocrite binding and following conformational changes in the protein transmembrane complex. In that case, one of the tunnels would permit the substrate to pass through the 'disassembled ATPase site', while the other tunnel would stay locked by the fully functional ATP-binding site. ATP hydrolysis would also occur asymmetrically in the latter active ATP-binding site and, most likely, simultaneously with or immediately after the translocation of the allocrite via the tunnel on the opposite side of the NBD dimer. The other ATP-molecule bound next to the open translocation tunnel would stay intact. In the proposed model only one ATP molecule is hydrolyzed per one translocation step, yet, binding of two ATP-molecules would ensure stability of NBD dimer, which is necessary to maintain fully functional integral tunnel for the allocrite transport.

Thus, our model of coupling of ATP-binding/hydrolysis to the allocrite transport requires ATP binding to both composite sites and postulates an active cycle as an alternation of the activity not only for the ATP-binding/hydrolytic sites, but also for the allocrite tunnels (for the canonical NBDs). Moreover, the fully assembled active ATP-site on one side of the NBD dimer always locks its own allocrite tunnel, while simultaneous opening of the allocrite tunnel on the opposite site of the protein dimer disrupts its neighboring ATPase site. Thus, each active site of the NBD dimer participates either in ATPase or transport activity at a time.

The studies of the human cystic fibrosis transmembrane conductance regulator (CFTR) showed that the hydrolytically deficient EQ-mutation prevent normal rapid closing of the CFTR channel (Vergani *et al.*, 2005). Thus, ATP hydrolysis seems to be required to lock an active allocrite channel of CFTR. In the light of the proposed model, the energy of ATP hydrolysis, produced in one active site of NBD dimer, may be employed to develop conformational changes that lead to closing the transport tunnel in the other site of the dimer. The same energy could be concurrently utilized to form 'a post-hydrolysis phosphate channel' to eject the free γ-phosphate from the active ATPase site. The TMDs seem to not obstruct the Pi-release, since only the opposite site of NBD is fully involved in the interaction with the TMD to assemble the transport tunnel. However, the catalytically active amino-acid residues most likely limit mobility of the γ-phosphate in the active site immediately after ATP hydrolysis (similar to that observed in the B-site of the HlyB-NBD dimer with intact ATP-Mg^{2+} or in either site of the ATP-bound dimer). Thus, small conformational changes in the active site would form an asymmetric cavity wide enough to release the free phosphate, yet the allocrite channel could still be inaccessible for the solvent (similar to the tunnel A in the

ATP-Mg^{2+}-bound structure of HlyB-NBD). Such structural alterations would create a transitional state of the ABC-transporter, which could be trapped in the presence of vanadate. At this particular time point, the translocation through one of the channels is already completed and both channels are likely closed. The notion of such transition state is supported by the studies of the maltose transporter from *E.coli* (Sharma and Davidson, 2000).

Removal of Pi from the active site possibly leads to the irreversible re-arrangement of the intra- and intersubunit connections in the NBD dimer that result in the conformational changes in the entire transporter, completing the ATPase-translocation cycle. All those structural alterations split the NBD-dimer into the monomers or spatially separated subunits/domains. It is possible that the NBD dimer can be partially opened, just enough to release ADP from the catalytic site, while the ATP molecule in the other NBD site remains bound without being hydrolyzed. Such alternative seems more likely for the single polypeptide ABC-transporters, such as CFTR, where all subunits of the transporter are pre-assembled (Vergani *et al.*, 2005). Semi-open NBD-dimers with one bound ATP-molecule could also be anticipated for the ABC-transporters, whose subunits can be pre-assembled in the absence of ATP or have high affinity to ATP. In that case, rebinding of ATP to the hydrolytically silent ATP-binding site is not required for the next catalytic cycle.

In HlyB-NBD, the C-terminus seems to play the role of a lid (Figures 50-53) sealing the channel from the cytoplasmic side of the transporter. Since the C-terminal extension of NBD is a common feature of all ABC-exporters, similar closure constructs may exist in all other exporters as well. In ABC-exporters, the binding of the specific substrate to NBD and to an accessory protein/domain may serve as a signal to move the lid and open the tunnel. Such an extension is not a universal attribute of ABC-importers (Smith *et al.*, 2002b). However, whenever present, the C-terminal end can also act as a lid. In ABC-importers, the function of a key unlocking the tunnel can be performed by an accessory substrate-binding protein, located in the periplasm or attached to the outer surface of cell. It seems likely that specific interaction of the substrate-binding protein with bound allocrite and the transmembrane transporter induces conformational changes, leading to the asymmetric opening of one of the transport tunnels.

However, an extreme caution is required to evaluate and interpret the reported structural findings in the HlyB-NBD structure. Further structural and biochemical studies of the allocrite-bound HlyB-NBD and particularly of the full-length HlyB transporter are desired to elucidate the mechanism of action of ABC proteins.

6.9. Conclusions

The two crystal structures of the HlyB-NBD H662A dimer are reported here, in the ATP- and ATP-Mg^{2+}-bound forms. Due to the H662A exchange, both structures represent the protein trapped in a pre-hydrolysis form.

This is the first time that the ATP-Mg^{2+} bound form of an NBD of ABC-transporter has been described. Moreover, these are the first crystal structures of an ABC-NBD performing export function, which shows the canonical C-loop-ATP-Walker A architecture with two molecules of ATP bound at the dimer interface and gluing together both monomers. Thus, the HlyB-NBD H662A structures confirm that the composite arrangement is the universal form of the NBD dimers in all ABC-transporters. While similar organization of the intersubunit interface was already described for two other ATP-bound dimeric structures (Chen *et al.*, 2003; Smith *et al.*, 2002b), the structural and potential functional role of the C-terminus in ABC-transporters is a novel finding.

The observed structural asymmetry between two protein subunits and between two active centers of the same NBD-dimer, combined with the structural differences between the ATP- and ATP-Mg^{2+} bound forms of HlyB-NBD and with the detection of the transient tunnels in the HlyB-NBD dimer, provide a hint to reconstruct the detailed picture of the molecular mechanism, which couples transport of allocrite and ATP hydrolysis in ABC transporters.

Chapter 7

Functional characterization and ATP-induced dimerization of the isolated HlyB-NBD

7.1. ATPase activity of HlyB-NBD in different buffers at various pH

Extensive search for conditions providing NBD-HlyB stability in the solution showed that 100 mM CAPS, pH 10.4, 20% glycerol is the best storage buffer (Zaitseva *et al.*, 2004). Although the protein was found to be functionally inactive in that buffer, the enzyme capability to cleave ATP was readily restored upon dilution of the concentrated protein from storage buffer into various assay buffers. To obtain information on the pH-dependence of ATPase activity, a broad spectrum of pH values and buffers were tested. Therefore, a series of buffers with overlapping pH-ranges were chosen: Malonate (pH 4.2-7.0), ADA (pH 6.0-7.0), HEPES (pH 6.2-8.0), Tris (pH 7.1-9.0), CHES (pH 9.3-10.0) and CAPS (pH 10.4-11.0) (Figure 68). Hydrolysis of ATP by HlyB-NBD was tested in 100 mM buffer in the presence of 20% glycerol. High buffer concentration was chosen to retain constant pH in all buffers upon generation of free phosphate during the assay. Glycerol was used for protein stabilization in assay solutions.

Normally, pre-dilution of HlyB-NBD was necessary because of the high protein concentration and presence of CAPS in the storage solution. However, some buffers, such as HEPES, for example, were found to promote protein aggregation/or denaturation. So efforts were taken to limit the length of the protein exposure to buffers being assayed. Consequently HlyB-NBD was pre-diluted into buffer-free solution of glycerol and ATP; usually 20% glycerol and 1 mM ATP were used. Glycerol and ATP temporarily protected the diluted protein from precipitation in the absence of CAPS. The buffering components were added to the assay immediately before starting the reaction with $MgCl_2$.

Interestingly, the level of ATP hydrolysis was found to be significantly dependent not only upon pH, but also upon the buffer tested indicating the importance not only of pH but

A
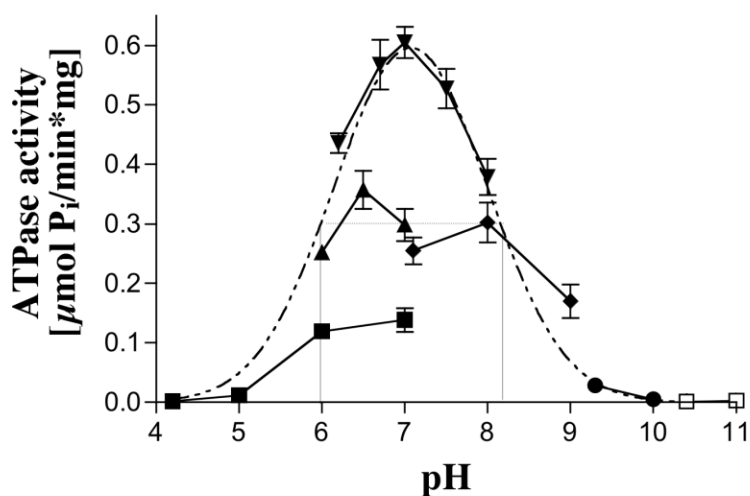
B
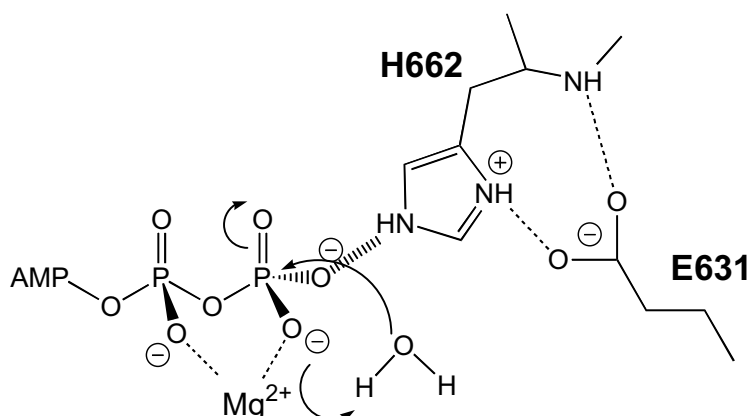
Figure 68. Effect of buffer and pH on the ATPase activity of HlyB-NBD

A. Buffers used were: malonate pH 4.2-7.0 (closed squares), ADA pH 6.0-7.0 (closed triangles), HEPES pH 6.2-8.0 (inverted closed triangles), Tris pH 7.1-9.0 (closed diamonds), CHES pH 9.3-10.0 (closed circles), and CAPS pH 10.4-11.0 (open squares). ATPase activity at 22 °C was determined from the average of at least three independent experiments with deviations of data points from the mean given as errors. The dashed line shows the fit of the experimental data using a Gaussian function. Vertical lines indicate the two $v_{max, 50\%}$ points around pH 6.1 and 8.2.

B. Structural model explaining the observed pH-dependence. The model was derived from the crystal structure of HlyB-NBD H662A in complex with ATP-Mg^{2+} (Zaitseva *et al.*, 2005a). Arrows indicate the molecular steps of the proposed ATP-Mg^{2+}-driven proton abstraction and the nucleophilic attack of the catalytic water.

buffer itself. Thus, at pH 7.0 the highest ATPase activity for HlyB-NBD was observed in 100 mM HEPES, 20% glycerol (v_{max}=0.6 μmol ATP/min*mg HlyB-NBD); twice lower level of activity was detected in 100 mM ADA, 20% glycerol or 100 mM Tris, 20% glycerol (v_{max} around 0.3 μmol ATP/min*mg HlyB-NBD); and the lowest protein activity was determined in 100 mM malonate, 20% glycerol (v_{max}= 0.14 μmol ATP/min*mg HlyB-NBD).

Despite the specific effect of each buffer on the functional activity of the protein, the pH optimum for ATP hydrolysis stayed close to neutral, regardless of the buffer. ATPase activity sharply declined to undetectable level at pH below 5 and at pH above 10. Using a Gaussian peak distribution, the $v_{max\,50\%}$ values were determined to be 6.1 and 8.2 (shown by the vertical lines in Figure 68A).

Knowledge of the crystal structure of the HlyB-NBD H662A in complex with ATP-Mg^{2+} (Zaitseva *et al.*, 2005a) and the derived 'linchpin' model can be used to explain the $v_{max\,50\%}$ values. This model is summarized schematically in Figure 68B, with H662 playing a key role in catalysis. A pH of 6.2 might correspond to the pKa values of the side chain of glutamate or aspartate or the γ-phosphate group of ATP, whilst the pH of 8.2 might reflect the pKa value of a histidine fixed in a salt bridge (Yang *et al.*, 1997). In the scheme presented in Figure 68B, arrows show the potential pathway of ATP hydrolysis. According to the proposed model, the side chain of His662 forms a salt bridge with the γ-phosphate group of ATP and stabilizes the transition state of enzyme. ATP, following the principle of substrate-assisted catalysis (Dall'Acqua and Carter, 2000), abstracts a proton from the attacking water molecule, which cleaves ATP after nucleophilic attack. Direct interaction of His with the substrate or E631 might explain the elevated pKa value of 8.2 over the intrinsic pKa of 6.0.

7.2 Kinetic analysis of ATP hydrolysis

As shown in the inset of Figure 69, HlyB-NBD demonstrated a non-linear dependence of ATPase activity on enzyme concentration over the range of 0.07-1 μM. However, at protein concentrations above 2 μM, ATPase activity showed a linear dependence on the enzyme concentration, resulting in a constant rate of the specific ATP hydrolysis (Figure 69). The relationship between *specific ATPase activity versus protein concentration* can be described with the Hill equation (equation (2), see Chapter 7.2 below for the Michaelis-Menton and Hill equations), which is normally used for substrate dependent activity. According to Hill equation that describes protein behavior in a statistically relevant
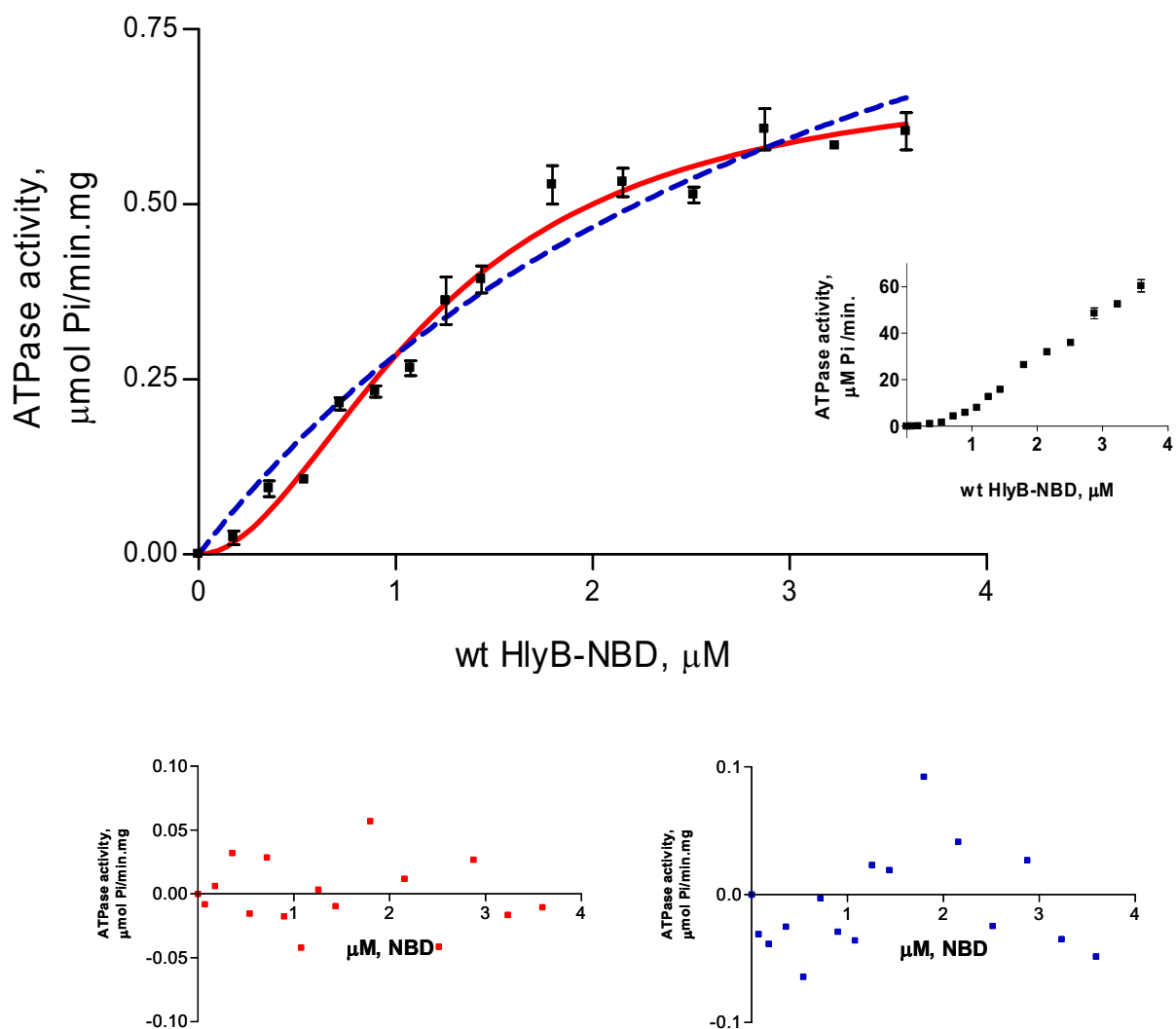
Figure 69. ATPase activity of wt HlyB-NBD as a function of enzyme concentration

The assay was performed in a buffer containing 100 mM HEPES pH 7.0, 20% glycerol, 10 mM $MgCl_2$, and 1 mM ATP. Data were fitted according to the Michaelis-Menten equation (1), blue dashed line, or the Hill equation (2), red solid line. The residuals are presented in the bottom panel. The residuals, i.e. the difference between the experimental data and fitted line, are plotted for the equation (1), blue squares, and for the equation (2), red squares. ATPase activity was determined from the average of at least two independent experiments with the average of the absolute deviations of data points from their mean given as errors.

manner, the maximal velocity of the reaction, V_{max}, was calculated to be 692 ± 38 nmol/min*mg, the Hill coefficient $h = 1.9 \pm 0.2$, and the kinetic constant $K_{0.5} = 1.2 \pm 0.1$ µM HlyB-NBD. Although these parameters have different meanings compared to the standard definition of the Hill equation, we found them very convenient for the description of the functional activity of HlyB-NBD at various protein concentrations. Thus, the Hill coefficient reflects a measure for the degree of cooperativity between monomeric protein subunits and $K_{0.5}$ indicates the concentration of the monomeric HlyB-NBD required to reach 50% of the saturating reaction activity.

The greater than the first order dependence of ATPase reaction on enzyme concentration over 0.07-1 µM range of HlyB-NBD (Figure 69) suggests that the active form of enzyme is an oligomer and that the monomer is most likely the predominant species within this protein range. Since formation of the active oligomeric species might be the rate-limiting step in the hydrolytic reaction at low enzyme concentrations (<1 µM), the rate of reaction increases with increasing protein concentration, resulting in a non-linear dependence of ATPase activity on enzyme concentration. The same dependence of ATPase reaction on protein concentration has been detected for all tested enzyme concentrations of HisP (up to 40 µM) (Nikaido *et al.*, 1997) and Mdl1p-NBD (up to 150 µM) (Janas *et al.*, 2003), the isolated ABC components of a histidine importer and a peptide exporter from yeast, respectively. In contrast to the aforementioned ABC-ATPases, HlyB-NBD demonstrated a non-linear dependence only at low concentrations of enzyme, switching to the constant activity rate at protein concentrations above 2 µM. Apparently, at higher HlyB-NBD concentrations in ATP-containing solution the monomer/oligomer equilibrium is shifted to the active oligomeric state. Within this range of enzyme concentrations, the product release or ATP hydrolysis becomes rate limiting, resulting in a linear relationship between ATPase activity and protein concentration. The analysis of ATP hydrolysis of various ABC transporters and isolated NBD components revealed that only "pre-formed" ABC-dimers, such as MalK (Chen *et al.*, 2003) and OpuAA (Horn *et al.*, 2003), or full-length transporters, such as MRP, show a linear dependence of activity on the concentration of enzyme. MalK, an isolated ABC component of the *E.coli* maltose transporter (Ehrmann *et al.*, 1998), forms a homodimer via interaction of its C-terminal regulatory domains even in the absence of nucleotides in solution (Chen *et al.*, 2003). The same stabilization very likely occurs also in OpuAA (Horn *et al.*, 2003), the isolated NBD of the osmo-regulated ABC-transporter OpuA from *Bacillus subtilis*. MRP, human multidrug resistance protein, is a complete transporter representing a fusion of two nucleotide-binding domains and two transmembrane domains

(Chang *et al.*, 1997). The linear relationship between ATPase activity and enzyme concentration exhibited by the "pre-formed" dimeric proteins may serve as an indication that ATPase activity of HlyB-NBD and other isolated ABC-ATPases is also mainly attributed to the dimeric form of the enzyme. Thus, we assume that the oligomeric form of HlyB-NBD responsible for ATPase activity is a dimer. To the best of our knowledge, this is the first time that a complete functional dimerization of isolated monomeric ABC subunits was observed in the course of an ATPase reaction. Several hypotheses can account for the sigmoidal shape of velocity against protein concentration (Figure 69). One interpretation is that such form of the relationship reflects an existence of more than one spatially distinct sites involved in enzyme dimerization. This theory is supported by our crystallization studies (Chapter 6) and data collected for other ABC-subunits, demonstrating ATP-induced protein dimerization (Smith *et al.*, 2002b; Chen *et al.*, 2003). Another explanation for the non-hyperbolic shape of curve can be the oligomerization of more than two protein monomers in the process of ATP hydrolysis. However, no evidence of such multimeric species was obtained in our work and in the intensive studies of other ABC-transporters. It is also possible that the sigmoidal dependence of reaction velocity on the enzyme concentration represents kinetics of many coinciding processes, which may include enzyme dimerization, ATP-binding and hydrolysis, and even protein aggregation or denaturation. We cannot rule out different rates of protein denaturation at varying concentrations of HlyB-NBD, yet in order to explain the observed shape of the curve, the precipitation rate of protein has to be *inversely* related to the enzyme concentration, which contradicts the results of the detailed studies we conducted. Neither did we detect the evidence of obvious enzyme precipitation within the reaction duration, since the reaction conditions were chosen the way that the rate of product formation remained constant over experimental time.

Favoring the existence of spatially distinct sites involved in the enzyme dimerization together with a possible interdependence between ATP-binding and dimerization on the function of *activity rate versus enzyme concentration*, we set the apparent dimerization constant, K_D, equal to $K_{0.5}$= 1.2 µM, which was calculated from the experimental data. However, one has to keep in mind that this number reflects the rate of monomer-monomer interaction for the isolated domains of HlyB-NBD under the assayed conditions. One should expect K_D to be much lower for the fully assembled functional HlyA transporter, where strong intermolecular interactions between full-length HlyB, HlyD, TolC and substrate are observed (Holland *et al.*, 2003; Schlor *et al.*, 1997; Thanabalu *et al.*, 1998; Benabdelhak *et al.*, 2003). Still, the protein dimerization constant obtained for HlyB-NBD in our experimental studies is

about two orders of magnitude lower than those theoretically calculated for other isolated NBDs, such as HisP and Mdl1p-NBD (Nikaido *et al.*, 1997; Janas *et al.*, 2003) and one order of magnitude lower than the experimentally determined K_D value for OpuAA (Horn *et al.*, 2003). In our opinion, a K_D of 1.2 µM is a result of both, the optimized conditions for ATPAse assay and the particular storage buffer for the enzyme, designed to restrain denaturation before functional analysis. We believe that substantially higher values of K_D obtained in the aforementioned theoretical calculations (Nikaido *et al.*, 1997; Janas *et al.*, 2003) as well as in the initial studies of ours were caused by the exceeding protein instability in the conditions preceding functional assay.

At constant enzyme concentrations, 1.1 µM or 3.6 µM, data for ATPase activity as a function of ATP concentration can be fitted either according to Michaelis-Menten equation (1) or Hill equation (2) (Figure 70).

$$v = \frac{v_{max}[S]}{K_M + [S]}$$ Michaelis-Menten equation (1)

$$v = \frac{v_{max}[S]^h}{K_{0.5}^h + [S]^h}$$ Hill equation (2)

Using equation (2), which fits experimental data better according to statistical analysis (GraphPad Prism), the maximum velocity of the reaction (v_{max}) for 1.1 µM and 3.6 µM HlyB-NBD were determined as summarized in Table 4.

	$K_{0.5}$ [mM]	v_{max} [nmol/mg*min]	k_{cat} [min^{-1}]	h
wt (1.1 µM)	0.36 ± 0.05	202 ± 16	5.6 ± 0.7	1.31 ± 0.13
wt (3.6 µM)	0.26 ± 0.03	600 ± 34	17 ± 1	1.35 ± 0.14
H662A (3.6 µM)	N. M.	N. M.	N. M.	N. M.

Table 4. Kinetic parameters of the wild type HlyB-NBD and HlyB-NBD H662A proteins

Parameters were determined according to Hill equation (2). N.M. – no measurable ATPase activity; wt – the wild type protein; H662A – H662A HlyB-NBD. Parameters are the average of at least two independent experiments with standard deviations given as errors.
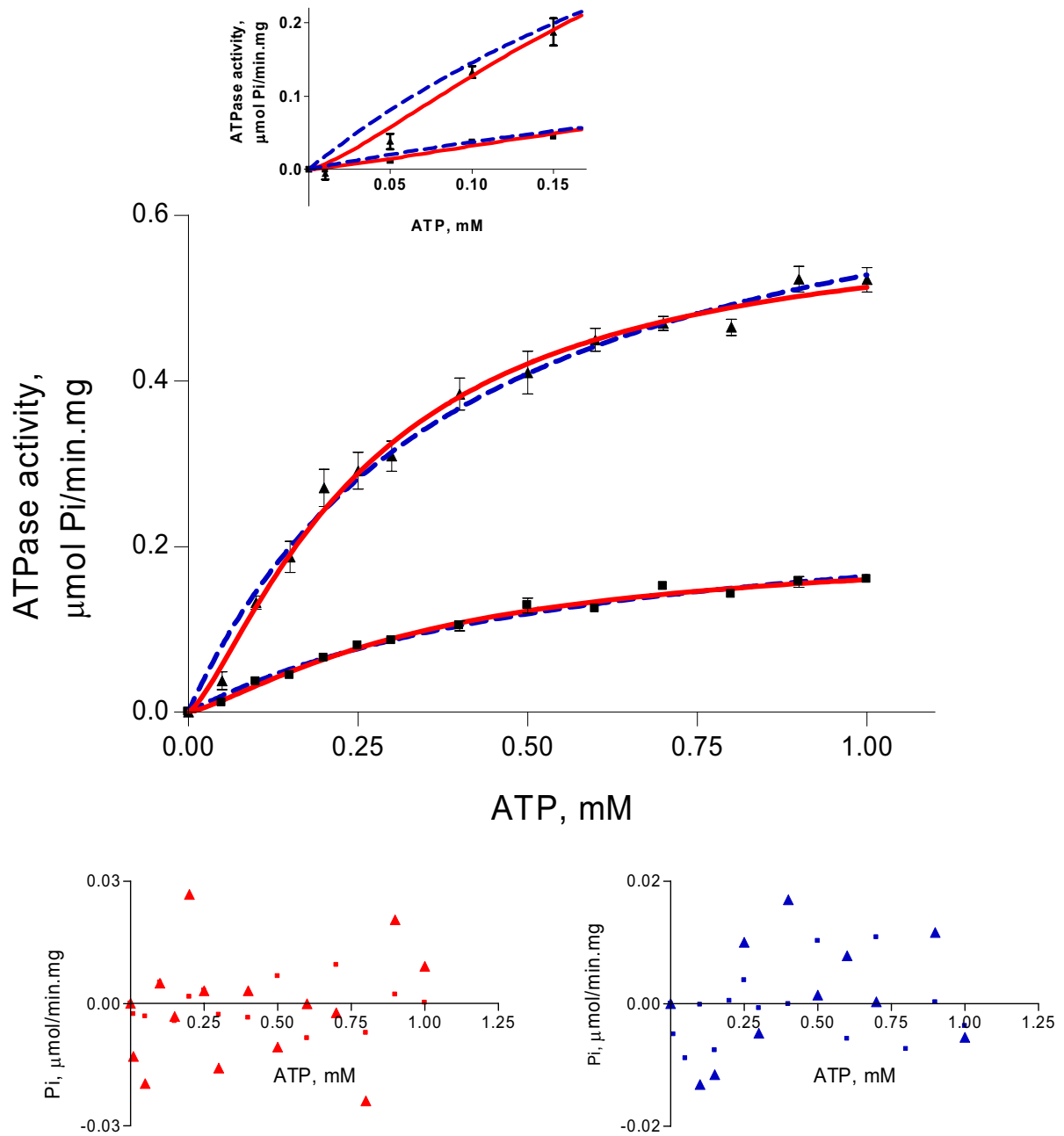
Figure 70. ATPase activity of wt HlyB-NBD as s a function of ATP concentration

Assay was performed at 1.1 μM and 3.6 μM enzyme concentrations in 100 mM HEPES pH 7.0, 20% glycerol, 10 mM MgCl$_2$ and varying ATP concentrations. Data were fitted according to the Michaelis-Menten equation (1), blue dashed line, or the Hill equation (2), red solid line. The residuals are presented in the bottom panel. The residuals are plotted for the equation (1), blue squares (1.1 μM enzyme) and blue triangles (3.6 μM enzyme), and for the equation (2), red squares (1.1 μM enzyme) and red triangles (3.6 μM enzyme). ATPase activity was determined from the average of at least two independent experiments with average of the absolute deviations of data points from their mean given as errors.

At a fixed enzyme concentration, the kinetic parameters of ATPase activity strongly depended on the oligomeric state of the protein. Note that at the aforementioned protein concentrations HlyB-NBD is expected to be in different functional and/or oligomeric states (Figure 69). The apparent affinity of the substrate, Mg^{2+}-ATP, to HlyB-NBD increased by 100 µM (Table 4) as a result of an increase in protein concentration and, accordingly, of the shift of the monomer-dimer equilibrium to the predominantly active dimeric state. This change in functional protein state also affected the ATPase reaction rate, which increased threefold attaining a k_{cat} 17 ± 1 min^{-1}. The Hill coefficient for ATP hydrolysis, however, does not vary much between the two tested protein concentrations, suggesting that ATP binding yields the same degree of cooperativity between two active sites of dimer at various enzyme concentrations.

Thus, the sigmoidal shape of the activity plots of the *reaction velocity versus substrate concentration* as well as *versus enzyme concentration* indicates that ATP hydrolysis does not follow Michaelis-Menten kinetics and suggest positive cooperativity between two HlyB-NBD subunits. Positive cooperativity of ATPase activity reported for HlyB-NBD (Benabdelhak *et al.*, 2005) and also observed in our work supports the notion of ATP-induced protein dimerization for the isolated ABC-components (Moody *et al.*, 2002; Smith *et al.*, 2002b; Verdon *et al.*, 2003). The value of v_{max} obtained in our studies for HlyB-NBD (0.6-0.7 µmol/mg*min) is very close to that previously reported for HlyB-NBD (Benabdelhak *et al.*, 2005) and a HlyB-NBD fused to glutathione S-transferase (Koronakis *et al.*, 1993) and is among the highest ones reported not only for isolated ABC domains, but also for full-length ABC-transporters.

7.3. *Dimerization, activity, and stability: Behavior of HlyB-NBD and its H662A mutant in the absence of nucleotides in various buffers*

Despite the indication of the possible interaction of the HlyB-NBD subunits in the course of ATP hydrolysis, SEC experiments showed that HlyB-NBD exists predominantly as a monomer in solution (see below). The lack of evidence of HlyB-NBD oligomerization in the performed SEC experiments is consistent with SEC studies of the other isolated wild type ABC-components, such as MJ0796 ABC from *Methanococcus jannaschii* (Moody *et al.*, 2002) and GlcV from *Sulfolobus solfataricus* (Verdon *et al.*, 2003). However, the notion of NBD-dimerization was supported by studies of many ABC-ATPases and fully assembled ABC

transporters. Thus, the nucleotide-binding subunits, HisP from *Salmonella typhimurium* (Hung *et al.*, 1998), MalK from *E.coli* (Chen *et al.*, 2003), MalK from *Thermococcus litoralis* (Diederichs *et al.*, 2000), the E171Q mutant of the MJ0796 ABC from *Methanococcus jannaschii*, which is defective in ATP hydrolysis (Smith *et al.*, 2002b), and also the complete transporters, BtuCD from *E.coli* (Locher *et al.*, 2002) and MsbA from three different organisms, *E.coli*, *Vibrio cholera*, and *Salmonella typhimurium* (Chang, 2003; Chang and Roth, 2001; Reyes and Chang, 2005) were crystallized as dimers. While the nature of the obtained dimers was questionable in some cases, dimerization of various isolated ABC subunits with single amino-acid mutation within the conservative Walker B or ABC-signature motives was detected by fluorescence binding experiments (Smith *et al.*, 2002b), gel-filtration (Janas *et al.*, 2003; Moody *et al.*, 2002; Verdon *et al.*, 2003), and analytical ultracentrifugation (Moody *et al.*, 2002). Functional studies of various ABC transporters also support the idea of protein oligomerization in the process of ATP hydrolysis. Analysis of reconstituted and detergent-solubilized complete transporters for maltose and histidine demonstrated non-Michaelis-Menten kinetics of ATPase activity at various ATP concentrations (Davidson *et al.*, 1996; Liu *et al.*, 1997). Isolated nucleotide-binding subunits of a histidine importer and a peptide exporter, HisP and Mdl1p-NBD, respectively, showed non-linear dependence of ATP hydrolysis on enzyme concentration, suggesting oligomerization of the monomers in the course of reaction (Janas *et al.*, 2003; Nikaido *et al.*, 1997). Functional interaction of two MalK monomers was also detected with vanadate-catalyzed photocleavage experiments following ATP-hydrolysis (Fetsch and Davidson, 2002). Yet, with the only exception of MalK from *E.coli* (Chen *et al.*, 2003) and OpuAA from *Bacillus subtilis* (Horn *et al.*, 2003), which both contain an additional 15 kDa C-terminal domain, the wild type ABC subunits were unable to form stable dimers in solution upon isolation from their cognate transmembrane components.

In order to demonstrate ATP-induced dimerization of the ABC components we employed a HlyB-NBD mutant with alanine in place of the invariable histidine (H662 in HlyB). The replacement of the highly conserved histidine residue in the H-motif of various ABC subunits completely abolish transport of the allocrite across the membrane by the corresponding transporter (Davidson and Sharma, 1997; Nikaido and Ames, 1999; Shyamala *et al.*, 1991; Walter *et al.*, 1992). While all reported His-mutant ABC-ATPases were capable to bind ATP, none of them demonstrated ATP hydrolysis in the isolated state (Nikaido and Ames, 1999) and upon reconstitution into the liposomes (Davidson and Sharma, 1997) or in the membranes (Shyamala *et al.*, 1991). The only reported case of a detected uncoupled

ATPase activity for a His-modified NBD of the maltose transporter from *Salmonella typhimurium* (Walter *et al.*, 1992) was not confirmed in the later studies (Schneider E., personal communication). The ABC-subunit of the histidine transporter with the conserved histidine replaced, H211R-HisP from *Salmonella typhimurium,* was also found to be defective in ATP hydrolysis (Nikaido and Ames, 1999). However, H211R/wild type heterodimers of HisP split ATP in solution as well as upon reconstitution into complete membrane-bound transporter. Interestingly, while H211**R**-HisP supported activity of the wild type protein, H211**D**-HisP did not, suggesting an importance of the replacing residue for the activity.

Recent structural studies revealed the functionally significant position of the conserved histidine in an ATP binding cassette. In the HisP-ATP structure, His-211 interacts with the γ-phosphate of ATP via a water molecule (Hung *et al.*, 1998). The dimer structures of the isolated E171Q-MJ0796 ABC-subunit (Smith *et al.*, 2002b) and MalK (Chen *et al.*, 2003) with bound ATP also demonstrated that the conserved histidine residue was located next to the ATP-biding pocket, directly contacting the γ-phosphate of the substrate. The last two examples represent the most relevant dimeric structure according to the majority of the collected biochemical data for ABC-components. All this factual information motivated a detailed study of HlyB-NBD with the substituted conserved histidine.

It was found that replacement of the conserved histidine (His 662) by alanine in HlyB-NBD completely eliminated hydrolysis of ATP under the same conditions as those tested for the wild type protein (Table 4 and Figure 71). Yet, analytical SEC experiments demonstrated essentially the same behavior of HlyB-NBD H662A as for the wt protein in various nucleotide-free buffers. After dilution from storage buffer and short-term incubation in the tested nucleotide-free buffers, both proteins were eluted as single monomeric peaks in all buffers, with the exception of HEPES (100 mM HEPES pH 7.0, 20% glycerol). When pre-incubated in HEPES buffer prior to SEC, wt and H662A were eluted through many fractions with no real peak formed (Figure 72A). Addition of 1 mM $MgCl_2$, for example, to the SEC buffer partially restored the H662A mutant protein mobility, forming a somewhat delayed wide peak with a shoulder of 'tailing' material in the elution buffer (Figure 72A). Addition of 100 mM NaCl to HEPES buffer seemed to completely prevent interaction of the proteins with the column. A symmetric protein peak was eluted at the position expected for the monomer, 28 kDa (Figure 72A). However, the ATPase activity of HlyB-NBD in the above solution was only 10% of the one in HEPES buffer without salt (data not shown). Increasing NaCl concentration from 100 mM up to 1 M in the running buffer did not alter protein mobility on the column. The sample was eluted as a single peak corresponding to the monomeric species
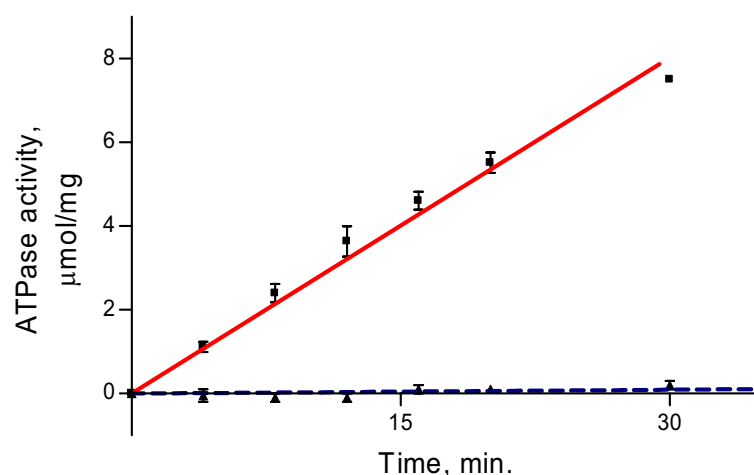
Figure 71. ATPase activity of the wt HlyB-NBD (squares, red solid line) and HlyB-NBD H662A (triangles, blue dashed line)

The assay was performed at 3.6 µM enzyme concentration in 100 mM Tris, pH 8.0, 20% glycerol, 10 mM $MgCl_2$, and 1 mM ATP. Values for the activity were determined from the average of at least two independent experiments with average of the absolute deviations of data points from their mean given as errors.

of HlyB-NBD, although no ATP hydrolysis was detected at such high salt concentration (data not shown).

To find out whether pH or the nature of buffer is responsible for protein instability, HlyB-NBD was subjected to SEC under the same conditions, particularly the same pH, but with ADA replacing HEPES. A sharp peak corresponding to the monomer protein was eluted in 100 mM ADA pH 7.0, 20% glycerol (Figure 72B). The elution volume of the protein was identical to the one eluted in HEPES buffer supplemented with 100 mM NaCl. Note that the ATPase activity of HlyB-NBD in ADA buffer at pH 7.0 was half of that observed in HEPES buffer at the same pH (Figure 68). Other buffers and pH's used for SEC included CAPS buffer (100 mM CAPS pH 10.4, 20% glycerol), in which no ATPase activity was detected, and malonate pH 5.8 (50 mM malonate pH 5.8, 100 mM sodium acetate, 20% glycerol), where protein activity was 4- 5 times lower than in a salt-free HEPES buffer. In both buffers HlyB-NBD was eluted as a symmetrical peak at the 28 kDa position, demonstrating relatively stable character of the enzyme (Figure 72B).
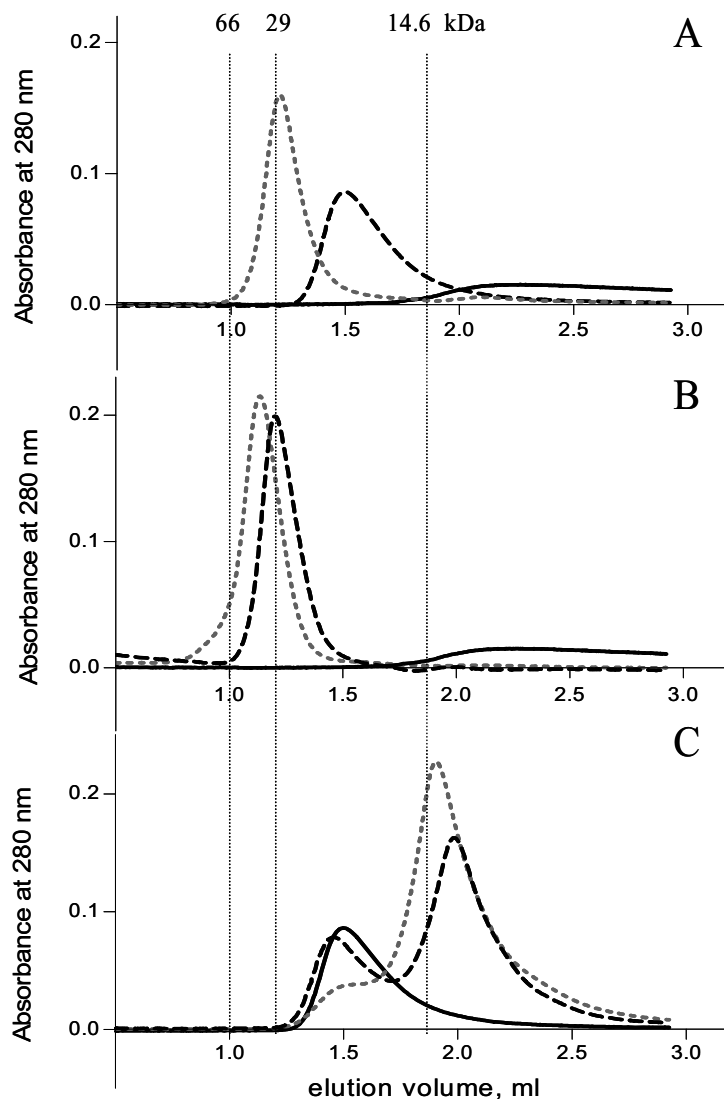
Figure 72. Analytical size-exclusion chromatography of wt HlyB-NBD or H662A-HlyB-NBD without nucleotides in the running buffers

The elution profiles of the proteins were recorded at 280 nm.

- **A.** Mobility of HlyB-NBD in 100 mM HEPES pH 7.0, 20% glycerol: without salt (black solid line), with 1 mM $MgCl_2$ (black dashed line), and with 100 mM NaCl (gray dotted line).

- **B.** Mobility of HlyB-NBD in various buffers in the presence of 20% glycerol: 100 mM HEPES pH 7.0 (black solid line); 100 mM ADA pH 7.0 or 50 mM malonate pH 5.8, 100 mM sodium acetate (black dashed line); CAPS pH 10.4 (gray dotted line). Note that the monomer peak of the protein was eluted earlier in CAPS buffer, compared to ADA or malonate buffer. The reason for that is a non-ideal behavior of the gel-filtration matrix at pH 10.4 of CAPS, which resulted in an altered mobility of all tested proteins. In CAPS pH 10.4 like in ADA pH 7.0 or malonate pH 5.8 buffers HlyB-NBD was eluted at the same position as carbonic anhydrase (29 kDa) used for column calibration.

- **C.** Mobility of HlyB-NBD H662A in HEPES pH 7.0, 20% glycerol, 1 mM $MgCl_2$: pre-incubated with 1 mM ATP, (gray dotted line); pre-incubated with 1 mM ADP (black dashed line); without pre-incubation (black solid line). The first peak at 1.5 ml corresponds to the eluted protein. Free nucleotides from the injected sample were eluted with the second peak at around 1.9-2.0 ml.

157

Thus, HlyB-NBD was typically eluted from the column as a monomer at the position corresponding to the 29 kDa standard protein (carbonic anhydrase) in all tested nucleotide-free buffers with the only exception of HEPES. A change of pH, buffers, and elevation of protein concentrations up to 70 μM did not induce formation of the dimeric HlyB-NBD species detectable by SEC (data not shown). Protein incubation in the buffer optimal for ATPase activity, HEPES pH 7.0, tended to destabilize the enzyme in the absence of nucleotides. Variation of salt concentration in HEPES buffer demonstrated the inverse correlation between HlyB-NBD stability and activity.

7.4. Dimerization, activity, and stability: Effect of ATP/ADP on protein behavior in various buffers

In all tested buffers, addition of ADP didn't alter HlyB-NBD/HA-mutant mobility neither upon short-term pre-incubation of enzyme with the nucleotide nor in the continuous presence of the nucleotide. In other words, the resulted protein sample was always eluted from the Superdex 75 column at the same position as in the absence of nucleotides in various buffers. However, a variety of ATP effects on the enzyme was observed, depending on the protein tested (wild type or mutant), the buffer used, ATP concentration, and the presence/absence of ATP in the column buffer.

HEPES buffer was again very different from all the other tested buffers. Both HlyB-NBD and H662A mutant were found to be extremely unstable in a salt-free HEPES-buffer in the absence of nucleotides, and ATP addition induced an even greater protein instability. HlyB-NBD precipitation was not detectable in solution at low protein concentrations, used for ATPase assay in HEPES buffer pH 7.0. However, it was apparent at concentrations of 2 mg/ml and higher, especially upon the addition of ATP. Visible precipitation of 2 mg/ml HlyB-NBD was observed immediately upon protein dilution into HEPES-Na pH 7.0, 20% glycerol, 1 mM ATP, and 0.1 mM EDTA. In the same buffer without nucleotide the turbidity of 2 mg/ml HlyB-NBD was detectable within few hours of protein incubation on ice. Destabilizing effect of ATP on the wild type HlyB-NBD protein in HEPES pH 7.0 was also observed with size-exclusion chromatography at lower protein concentrations (not shown). To compare individual effects of ATP and ADP on the enzyme under conditions optimal for ATPase reaction and to avoid ATP hydrolysis in the presence of Mg^{2+}, H662A-HlyB-NBD,

which displayed no ATPase activity above background (Table 4 and Figure 71), was analyzed by gel-filtration in HEPES-Na pH 7.0, 20% glycerol, 1 mM $MgCl_2$ (HEPES buffer with $MgCl_2$).

When using nucleotide-free Mg-containing HEPES running buffer for gel-filtration, protein pre-incubation with 1 mM ADP didn't change the elution characteristics of HlyB-NBD H662A, while pre-incubation of the sample with 1 mM ATP caused a pronounced tailing of the elution peak, suggesting an increasing tendency of the protein to precipitate after short-term interaction with ATP (Figure 72C). The effect of 1-hr-incubation of ATP and H662A-HlyB-NBD in other buffers, used in prior experiments, was also tested by gel-filtration. After pre-incubation of the H662A-mutant with ATP, the protein was always eluted as a single monomeric peak in all buffers tested, including HEPES pH 7.0 supplemented with 100 mM or 1 M NaCl, CAPS pH 10.4, ADA pH 7.0, and malonate pH 5.8 buffers (data not shown). Thus, the most optimal buffer for ATPase activity, HEPES pH 7.0 without NaCl, was the only one, which changed the gel-filtration pattern upon incubation of HlyB-NBD or its H662A-mutant with ATP for a short period of time. Since ATP promoted protein instability in HEPES pH 7.0, it made it impossible to use SEC to monitor enzyme characteristics in the continuous presence of ATP in the buffer.

However, ATP-containing buffers where the wild type HlyB-NBD demonstrated significantly lower or no ATPase activity were found to be more informative, demonstrating detectable and reproducible differences between the wild type protein and the H662A mutant by SEC. Figure 73 shows SEC chromatograms of H662A in two different buffers: malonate buffer pH 5.8, where the wild type protein demonstrated an ATPase activity of 20% compared with the maximum level (Figure 73A), and storage CAPS buffer pH 10.4, where no activity was detected (Figure 73B). In both buffers a shift of the monomeric peak of H662A mutant towards a higher molecular weight was observed upon ATP addition. For malonate buffer pH 5.8, at least 1mM ATP was required to observe that shift. The higher the ATP concentration added, the more significant was the shift from a monomeric, 28 kDa species (Figure 73A), to a dimeric form, approaching an apparent molecular weight of roughly 50 kDa at 5 mM ATP. While the H662A mutant protein exhibited a steady change in the peak position throughout the entire range of ATP concentrations tested, the eluted position of the wild type HlyB-NBD was only slightly moved to the higher molecular weight area at the highest ATP concentration (5 mM) in malonate buffer pH 5.8. Since a shift in the position of the eluted protein was detected for both proteins in the presence of ATP, this eliminates the possibility that either of the tested proteins is a single homogenous species and is consistent with the notion that
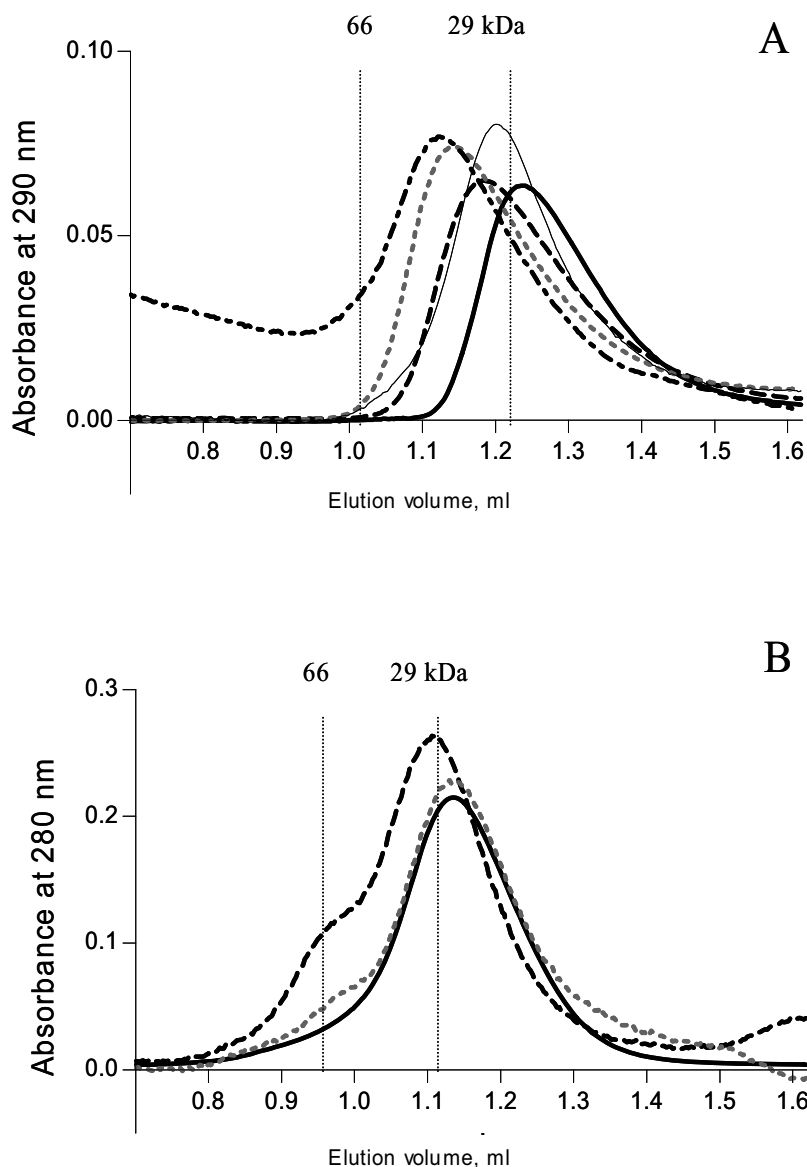
Figure 73. Analytical size-exclusion chromatography of wt HlyB-NBD or H662A HlyB-NBD in the presence of nucleotides in the running buffers

A. Protein mobility in 50 mM malonate pH 5.8, 100 mM sodium acetate, 20% glycerol with or without ATP in the running buffer: H662A mutant without ATP (the same protein mobility was observed for the wild type HlyB-NBD without ATP or for both proteins with ADP), black solid bold line; H662A mutant with 1 mM ATP, black dashed line; H662A mutant with 2 mM ATP, gray dotted line; H662A mutant with 5 mM ATP, black dash-dotted line; wild type HlyB-NBD with 5 mM ATP, gray thin line. The elution profiles of proteins were recorded at 290 nm.

B. Protein mobility in 100 mM CAPS pH 10.4 and 20% glycerol with or without ATP in the running buffer: H662A mutant without ATP (the same protein mobility was observed for the wild type HlyB-NBD without ATP or for both protein with ADP), black solid line; wild type HlyB-NBD with 5 mM ATP, gray dotted line; H662A mutant with 5 mM ATP, black dashed line. The elution profiles of proteins were recorded at 280 nm. Note different protein mobility in CAPS buffer, compared to malonate buffer. The reason for that is a non-ideal behavior of the gel filtration matrix at pH 10.4 of CAPS.

observed protein peaks reveal a rapid equilibrium between dimeric and monomeric forms. Difference in the mobility presumably reflects a difference in the kinetic characteristics of the monomer/dimer equilibrium for two proteins upon ATP binding, with the equilibrium shifted to the dimeric form for the mutated enzyme and with predominantly monomeric species for the wild type HlyB-NBD. Yet, the need for permanently high ATP concentrations ($\geq$ 1mM) in the running buffer and the dependence of the eluted peak position on the ATP-concentration indicates that the affinity of ATP to H662A-HlyB-NBD in the malonate column buffer is not significantly higher than that to the wild type protein.

Inclusion of 10 mM $MgCl_2$ along with ATP into the column buffer had no effect on the elution profile of H662A protein (data not shown). Addition of EDTA-ATP also didn't modify the elution pattern of the H662A-HlyB-NBD protein, compared to ATP alone (data not shown). We also did not observe changes for the wild type protein upon addition of EDTA or Mg^{2+} to the running buffer, although is would be difficult to reliably assess their effect, since ATP alone didn't cause significant changes in the elution profile of the protein.

While a single protein peak was observed for the wild type and mutant HlyB-NBD as a result of SEC in the ATP-supplemented malonate buffer pH 5.8, two peaks were detected in the elution profiles of both proteins studied in CAPS buffer with 5 mM ATP (Figure 73B). An appearance of the major peaks in 'CAPS + ATP' resembled the elution pattern observed for two proteins in malonate with ATP, while the minor peaks corresponded to the precise position of the dimeric protein species, being the most apparent at the highest ATP concentration (5 mM). The major peak for the wild type enzyme appeared to be a monomer, corresponding to the position of 29 kDa standard protein. The position of the lower molecular weight peak for the mutant H662A protein deviated from the 28 kDa monomer, although this difference was not as significant as in the malonate buffer pH 5.8 at the same ATP concentration. Two protein peaks in the elution profile might indicate the existence of a slow monomer-dimer equilibrium. This assumption seems to be true for the wild type HlyB-NBD, where the major peak corresponds to the monomer, and the minor to the dimer species of enzyme. Yet, the shift of the lower molecular weight peak detected in 'CAPS + ATP' for H662A-HlyB-NBD, similar to the one observed in 'malonate + ATP', is most likely an indication of a rapid monomer-dimer equilibrium. To explain the co-existence of two types of equilibria in CAPS buffer with ATP, we are forced to postulate two different forms for His-mutant protein: a form D rapidly equilibrating with the monomeric form (M) and a form incapable of the rapid equilibration (D*) (Figure 74). The rapid equilibrium seems to be favored by 'malonate + ATP', the buffer where HlyB-NBD demonstrates ATPase activity,
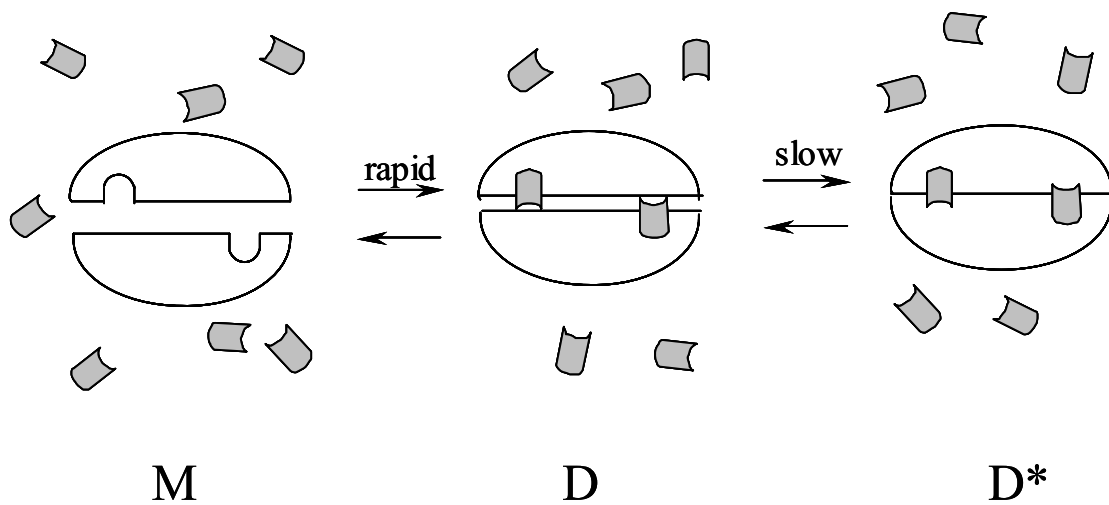
Figure 74. Hypothetical model for dimerization of HlyB-NBD

ATP molecules are colored gray. M designates a monomer form of the protein, D and D* - different forms of a dimer.

For further details see text.

while the slow equilibrium is supported by CAPS with ATP, the buffer where no activity was detected for the protein.

Formation of the aforementioned dimeric peaks in CAPS, as well as the elution shift for the H662A mutant protein in CAPS and malonate buffers, were detectable only in the presence of ATP in the column buffer with freshly purified enzyme. The same protein samples were always eluted as single monomeric peaks upon ATP removal from the running buffer (data not shown). Thus, the ATP-dependent reversible formation of the dimeric species implies that we have observed native conformational/oligomeric changes of the protein state upon ATP addition and not the process of protein denaturation.

7.5. Discussion

The SEC analysis demonstrated that the H662A- and wild type HlyB-NBD proteins are capable to bind ATP and as a result, form dimers in the tested buffers, including CAPS, pH 10.4, which protects the protein from precipitation without disturbing the ATP-binding capability of the protein. Binding of ATP and not Mg^{2+}-ATP seems to play the primary role in the observed changes, since neither Mg^{2+}-ATP nor EDTA-ATP modified the elution pattern of the H662A-HlyB-NBD protein, compared to ATP alone.

The results of our studies detected two ATP-induced dimeric forms for HlyB-NBD and its H662A mutant (Figures 73 and 74). One of them is D form of HlyB-NBD, which exists in a rapid equilibrium with its monomeric form M, and another is the D* form, which results in a slow equilibrium with D- or M-species. The presence of the D-form was readily apparent for the H662A-mutant in the two tested buffers. For the wild type protein it was only detectable in one of the tested buffers, malonate (Figure 73A). We attribute this to the shift of the wild type HlyB-NBD M-D equilibrium to the predominantly monomeric species even at the highest ATP concentration studied (5 mM).

Only the rapidly equilibrating ATP-induced form D of dimer was observed in malonate buffer, where HlyB-NBD displayed ATPase activity. The slowly equilibrating D* dimer form of HlyB-NBD was detected for both the wt and HA proteins in CAPS buffer, where no activity for the wild protein was detected. The specific ability of CAPS to protect the unstable nucleotide-free HlyB-NBD from precipitation during storage is likely to be based on the limitation of protein flexibility in its monomeric form (Zaitseva *et al.*, 2004), which might also be true for the dimeric form of enzyme. It is possible that CAPS inhibits ATPase activity of the wild type protein by locking the protein in its dimeric D* ATP-bound form for the prolonged periods of time, while the enzymatic activity requires a rapid M-D equilibrium.

The D* form might have biological relevance and mimic inactive ATP-bound dimer form of the complete membrane-associated complex that awaits signal from the allocrite to switch ATPase activity on. Tight specific interaction of NBDs with TMDs in the absence of the allocrite might play a role of the stabilizing factor, which limits flexibility of the protein. The existence of such membrane complex would serve as an example of the rational energy-preserving mechanism of ABC transporters.

7.6. Conclusions

Proper storage conditions and adjustment of the pre-assay procedure for isolated HlyB-NBD significantly optimized the kinetic characteristics of the enzyme by maximally excluding the precipitated and inactive protein from the assay. The analysis of protein ATPase activity and SEC experiments demonstrated that a dimer is the functional form of HlyB-NBD. Our studies also indicate that the ATP-promoted dimerization of HlyB-NBD might involve formation of two interconvertible forms: a readily dissociable dimer and a more stable dimer form. Finally, we also showed that HlyB-NBD activity and stability are inversely related.

Chapter 8

Conformational and oligomeric changes of HlyB-NBD within the ATP-hydrolytic cycle

The crystal structures of HlyB-NBD with different bound substrates, such as ADP, ATP-Mg^{2+}-, and ATP, were solved in this study. Thus, HlyB-NBD is the first member of ABC-protein family, for which the nucleotide-free (Schmitt *et al.*, 2003), and nucleotide-loaded pre- and post-hydrolysis crystal structures are available. The obtained structural information for one single NBD in different functional states allows a detailed analysis of the conformational/oligomeric alternations during the complete hydrolytic cycle and makes it possible to postulate a mechanism of action of ABC-proteins.

8.1. Comparison of the nucleotide-free and ATP-loaded structures

The most obvious difference between the nucleotide-free and the ATP-Mg^{2+}- or ATP-loaded structures of HlyB-NBD is their oligomeric state. While the former was crystallized as a monomer (Schmitt *et al.*, 2003), the latter formed dimers upon crystallization. A structural comparison of the nucleotide-free HlyB-NBD and individual subunit of the ATP-Mg^{2+}-bound dimer reveals an rmsd of 2.19 Å and 2.02 Å over 241 Cα atoms (entire NBD) for the A and B subunits, respectively (Figure 75). A similar structural deviation is observed between the nucleotide-free HlyB-NBD and each of the two subunits in the ATP-bound state without Mg^{2+}, 2.00 Å and 2.20 Å over 241 Cα atoms. Since overall structures of the ATP- and ATP-Mg^{2+}- proteins are very similar (Chapter 6), hereafter only the ATP-Mg^{2+}-HlyB-NBD will be discussed, unless otherwise stated. The entire protein structure is re-adjusted upon ATP binding to fit a molecule of ATP (Figures 75, 76). Thus, in the helical domain, the region of residues 564-606 undergoes the most significant conformational changes. This region includes the C-terminal end of helix 3, helix 4, the loop
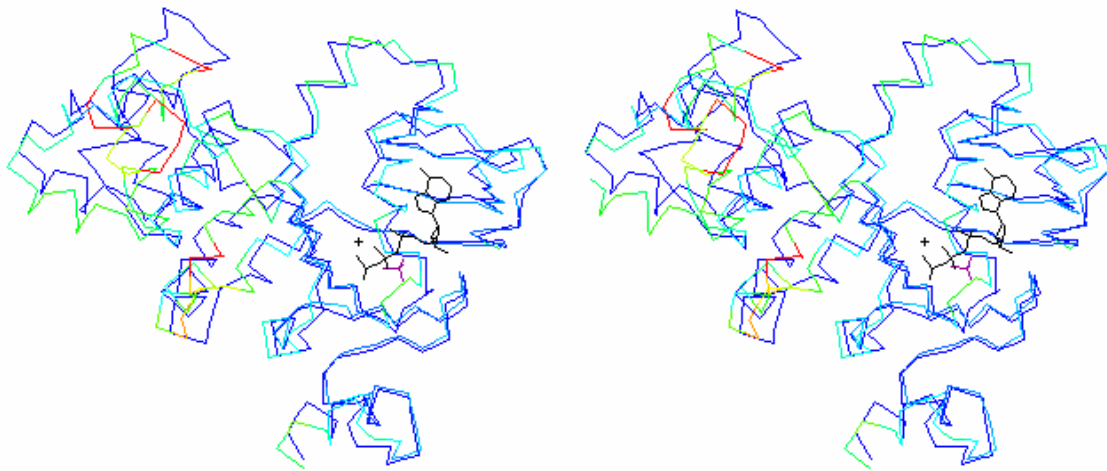
Figure 75. Stereoview of the superposition of the Cα traces of the nucleotide-free HlyB-NBD and the ATP-Mg^{2+}-loaded A subunit of the HlyB-NBD H662A dimer based on the least-squares alignment, rmsd of 1.43 Å^2 for 204 Cα atoms

The view of the dimer interface for each monomer is shown with the C-terminal part facing the cytoplasm at the bottom of figure and the top of the monomer facing the TMDs. The catalytic domain is shown on the right side of each monomer, and the helical domain on the left. The nucleotide-free protein is shown in dark blue. The color of the ATP-Mg^{2+}-bound protein is based on rmsd, where the blue color corresponds to the lowest structural deviation and red to the highest deviation. The ATP molecule and Mg-ion are colored black; the sulfate ion in the active site of the nucleotide-free HlyB-NBD is colored purple.
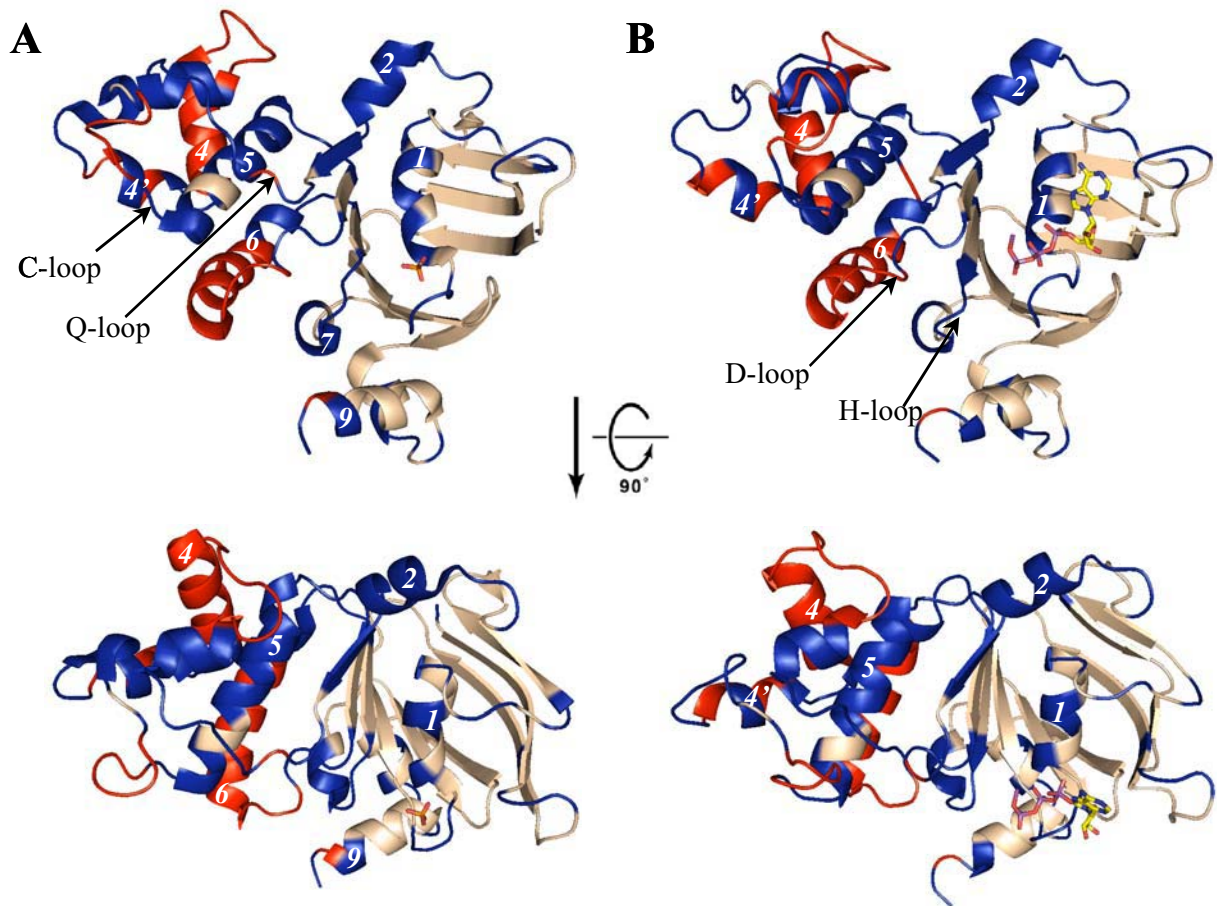
Figure 76. The ribbon diagrams of the nucleotide-free HlyB-NBD and the ATP-Mg^{2+}-loaded A subunit of the HlyB-NBD H662A dimer

Blue color indicates the structural deviations of 1.0-2.7 Å^2 between two proteins based on the least-squares alignment, rmsd of 1.43 Å^2 for 204 Cα atoms. The red color shows rmsd of 2.7 Å^2 and higher between two structures. The secondary structure elements, α-helices, involved in the structural rearrangement, are labeled with white numbers.

A. The nucleotide-free HlyB-NBD.

B. The ATP-Mg^{2+}-loaded A subunit of the HlyB-NBD H662A dimer.

   Top figure: The side view of the protein; the upper part of the monomer is facing the TMDs of the transporter and the lower part is facing the cytoplasm.

   Bottom figure: The view of the protein facing the TMDs, obtained by a 90° rotation of the top figure.

between helices 3 and 4, and the N-terminal sequence of the extended C-loop. All those major conformational alterations in the helical domain (highlighted in red in Figure 76) concern the surface of the protein, which is potentially capable to interact with the transmembrane domain of the complete transporter. The induced fit motion in the helical domain relative to the catalytic one has been described for MJ1267 (Karpowich *et al.*, 2001) and other NBD monomer structures and proposed to be a general feature of ABC-NBDs. In MalK, for example, binding of ATP to the protein results in the inward movement of the helical domain toward the nucleotide-binding site of the same subunit, generating a more compact monomer packing (Chen *et al.*, 2003). In HlyB-NBD, however, conformational alterations in the helical domain upon ATP binding appear to be more complex than a simple inward movement of the helical domain. The structural changes in the helical domains of HlyB-NBD could be described rather as diverse conformational modifications in order to create the complimentary surfaces for NBD-dimerization as well as for the proper interaction with the TMDs of the transporter (Figures 75 and 76). Helix 4, for instance, moves farther from both nucleotide-binding sites of the dimer, while helix 4' seems to get closer to the active site.

Apart from the helical domain, significant conformational changes occur in the orientation of helix 6, which is a structural component of the catalytic domain and located in a close proximity to the helical domain. Helix 6 moves along its axes, perpendicular to the surface, into the interior of the subunit and bends its N-terminal part by 15° to the helical domain (Figures 75 and 76). The D-loop, adjacent to helix 6, also adjusts the position upon ATP-binding. Furthermore, the Q-loop and Pro-loop connecting the helical and catalytic domains also experience some conformational changes as result of ATP-binding.

Moreover, binding of ATP results in noticeable rearrangement of the residues surrounding the nucleotide-binding pocket of HlyB-NBD. Thus, the loop connecting β-strands 1 and 2 adopts a new conformation to provide the π-π interaction between Y477 and adenine group of ATP. Additionally the Walker A undergoes structural changes to accommodate ATP molecule in the active site and provide its specific binding. In particular, the C-terminal residues of the Walker A motif (residues 508- 510) adopt a canonical α-helical conformation in the ATP- and ATP-Mg^{2+} bound form of HlyB-NBD, while a 3_{10} helical conformation for those residues is observed in the nucleotide-free state of the protein (Schmitt *et al.*, 2003). Modest conformational alterations in helix 2, the His-loop, and the C-terminal end of the protein complete a general picture of the ATP-induced structural changes in HlyB-NBD (Figure 76).

Overall, the β-core of the structure is mostly unaffected by binding of ATP or ATP-Mg^{2+}, while all the helices and the majority of the loops of HlyB-NBD are re-arranged to adopt an active protein conformation. Helix 6 of the catalytic domain and helix 4 of the helical domain deviate by more than 3 Å from their position upon ligand binding (Figure 76). The conformational changes involve almost all the conserved motifs, such as the Walker A motif, H-, and D-loop of the catalytic domain, the Q- and Pro-loop connecting the catalytic and helical domains, the C-loop of the helical domain, and the residues of the C-terminus. The Walker B motif, as a part of the β-core, is affected to a lower extend by ATP-binding.

Importantly, HlyB-NBD transition from the nucleotide-free to the ATP-bound state involves two events, ATP binding and NBD dimerization. Thus, all structural modifications observed in the monomer structure of HlyB-NBD loaded with ATP or ATP-Mg^{2+}, reflect the binding of two ATP molecules along the dimer interface *and* association of two protein subunits. That may explain a distribution of the ligand-induced alterations over the entire structure of HlyB-NBD monomer. Strikingly, while every ATP contacts two ABC-subunits simultaneously with the Walker A motifs providing a majority of the interactions, the main conformational changes upon ATP-binding/NBD-dimerization occur in the vicinity of the C-loop (Figure 76). Such a phenomenon can be explained by a greater flexibility of the helical domain and helix 6 relative to the more rigid core of the catalytic domain in HlyB-NBD and other ABC-proteins.

Substantial conformation rearrangements between nucleotide-free and ATP- or ATP-Mg^{2+}-bound structures most likely take place in two steps. The first step, binding of ATP to the Walker A motif, may readjust the catalytic domain of NBD in the vicinity of the active site and propagate the changes throughout the whole protein. Such alterations may create complimentary surfaces for the intersubunit interactions. The shape complementarity (Sc) coefficient of the HlyB-NBD-ATP-Mg^{2+} dimer interface is 0.69 as determined by the shape utility of the ccp4 suite. For comparison, the complementarity for the ATP-bound dimer of MJ0769 is 0.72 (Smith *et al.*, 2002a). Normally a tightly packed interface typical of those found in oligomeric protein structures has S_c coefficients that range from 0.70 to 0.76 (Lawrence and Colman, 1993). Subsequent dimerization of the HlyB-NBD, as a second step, involves the C-loops of each monomer in the ATP-binding that allows the nucleotide to directly contact the helical region of the opposing subunit. Such ATP-protein interactions may generate the structural rearrangement, concerning mainly the helical domains of the NBDs.

It's possible that the presence of TMDs in the complete transporter may restrict these secondary conformational changes of NBDs, thus preventing formation of the active

ABC-dimer. The signal from the bound substrate may permit functional dimerization of the NBD subunits and formation of the transporter channel, resulting in coupled ATP-hydrolysis and substrate translocation. The two-step hypothesis can be supported by our data, demonstrating formation of the inactive wt HlyB-NBD dimers under certain conditions (Zaitseva *et al.*, 2005a). However, the possibility that ATP-bound NBDs are held apart by TMDs in the assembled transporter cannot be ruled out.

8.2. Comparison of the ATP- and ADP-loaded structures

While the ATP-Mg^{2+}-loaded HlyB-NBD was crystallized as a dimer, crystals of the ADP-bound protein contain one molecule per asymmetric unit. Superposition of each nucleotide-binding domain of the ATP-Mg^{2+}- and ADP-bound structures results in rmsd of 2.18-2.45 Å between 241 Cα atoms of HlyB-NBD, depending on the monomer of the ATP-dimer selected for the comparison. The least square deviation for the above structural alignment generates 1.10 Å and 1.13 Å for 176 and 188 Cα atoms of the A and B subunits, respectively (Figure 77).

In contrast to the widespread conformational changes observed upon binding ATP to the nucleotide-free HlyB-NBD, the structural difference between ATP-Mg^{2+}- and ADP-loaded structures mainly concerns the helical domain (Figures 77 and 78). As a result of ATP hydrolysis and dissociation of NBD dimer, flexibility for the residues G600-G605, located N-terminal to the C-loop sequence, drastically increases. In the ATP-Mg^{2+} protein, the B-factor for this region is approximately 60 Å^2, which is just slightly above the average of 51.1 Å^2 for the whole protein, while in the ADP-bound conformation the B-factor values are 90 Å^2 and 30.2 Å^2, respectively. Such a significant difference in the flexibility can be explained by the existence of nucleotide-protein interactions in the dimer structure. In the ATP-Mg^{2+}-HlyB-NBD, residues A604-Q610 are involved in the interaction with bound nucleotide, apparently fixing the extended C-loop sequence in a defined orientation. In the ADP-state, as a result of the missing connection between the C-loop and nucleotide, the G600-G605-loop moves down into the dimer interface, clashing with the nucleotide position in the ATP-Mg^{2+}-bound dimer. Such movement shifts one of the residues of the aforementioned region, Q602, by more than 9.7 Å from the position in the ATP-Mg^{2+} dimer.

It's likely that conformational changes in the G600-G605 loop are propagated throughout the whole helical domain. Thus, 4' helix moves outward from the dimer
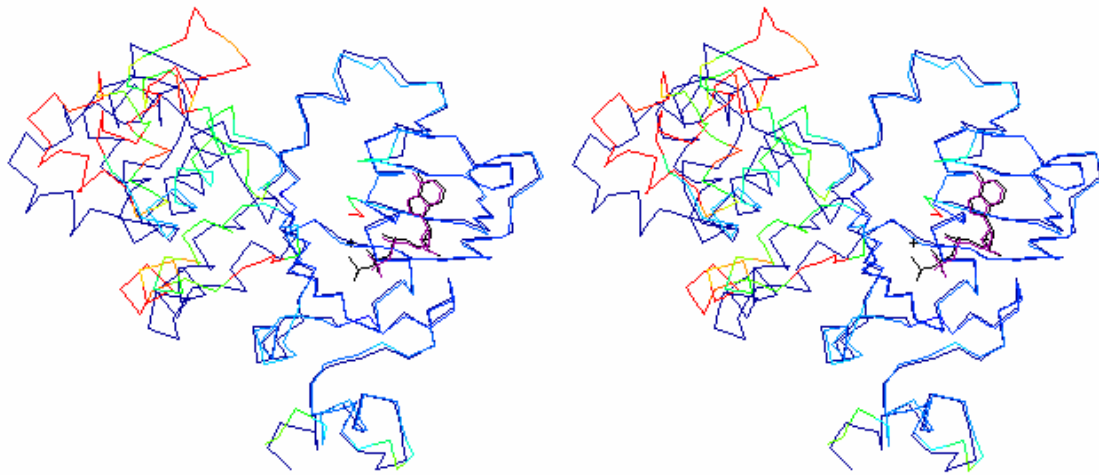
Figure 77. Stereoview of the superposition of the Cα traces of the ATP-Mg^{2+}-loaded A subunit of the HlyB-NBD H662A dimer and the ADP-loaded wild type HlyB-NBD based on the least-squares alignment, rmsd of 1.10 Å^2 for 176 Cα atoms

The view of the dimer interface for each monomer is shown with the C-terminal part facing the cytoplasm at the bottom of figure and the top of the monomer facing the TMDs. The catalytic domain is shown on the right side of each monomer, and the helical domain on the left. The ATP-Mg^{2+}-bound protein is shown in dark blue. The color of the ADP-bound protein is based on rmsd, where the blue color corresponds to the lowest structural deviation and red to the highest deviation. The ATP molecule and Mg-ion are colored black, the ADP - purple.
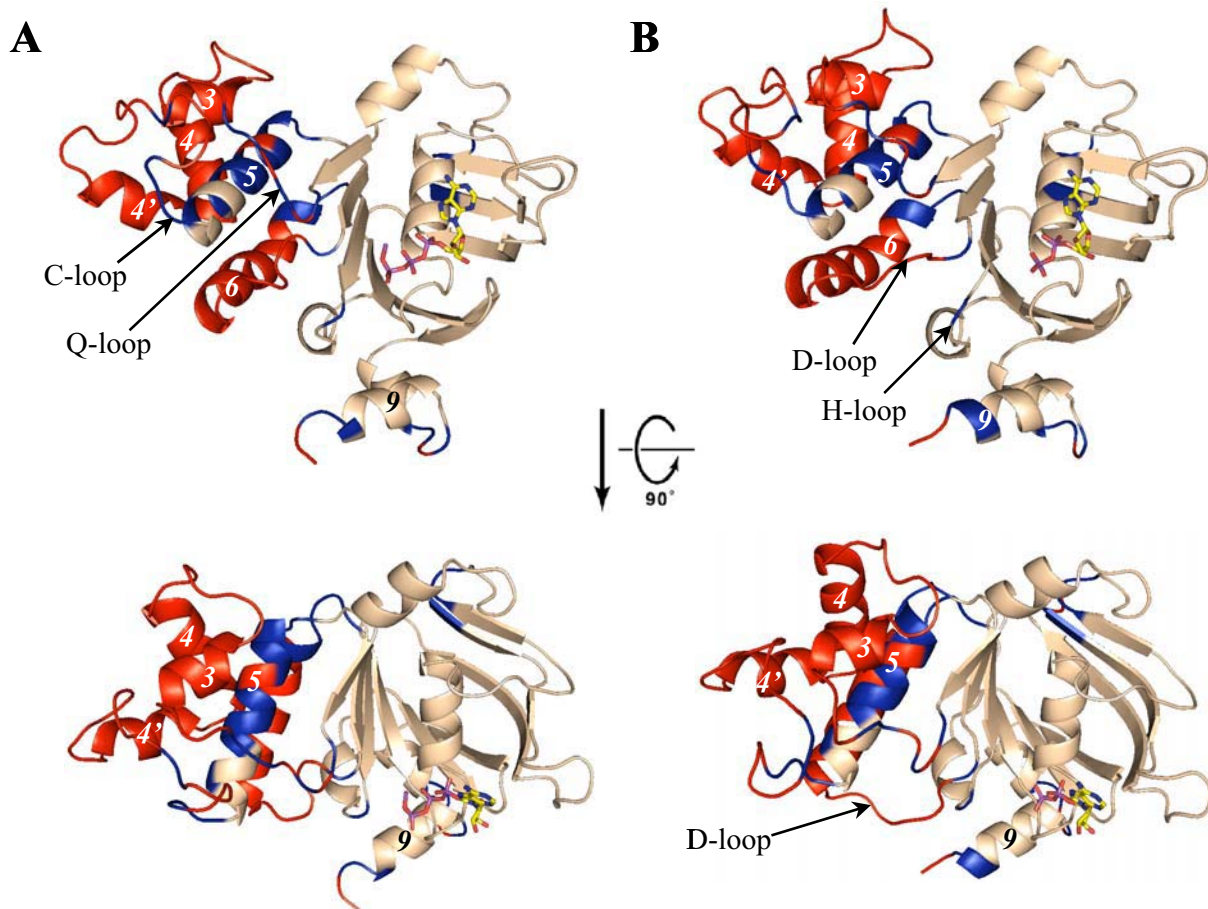
Figure 78. The ribbon diagrams of the ATP-Mg^{2+}-loaded A subunit of the HlyB-NBD H662A dimer and the ADP-loaded HlyB-NBD structure

Blue color indicates the structural deviations of 1.0-2.7 $Å^2$ between two proteins based on the least-squares alignment, rmsd of 1.10 $Å^2$ for 176 Cα atoms. The red color shows rmsd of 2.7 $Å^2$ and higher between two structures. The secondary structure elements, α-helices, involved in the structural rearrangement, are labeled.

A. The ATP-Mg^{2+}-loaded A subunit of the HlyB-NBD H662A dimer.

B. The ADP-loaded HlyB-NBD protein.

Top figure: The side view of the protein; the upper part of the molecule is facing the TMDs of the transporter and the lower part is facing the cytoplasm.

Bottom figure: The view of the protein facing the TMDs, obtained by a 90° rotation of the top figure.

interface (Figure 78), while the peripheral helices 3 and 4 follow the same path as helix 4',
simultaneously rotating toward to ADP bound in the active site. All the loops of the helical
domain also change their orientation upon ATP hydrolysis and dimer dissociation of
HlyB-ND, while the position of the C-loop (residues 606-610) remains rather unaltered. The
Q-loop, which connects the helical and catalytic domains of HlyB-NBD, also distinctly
changes its position (Figures 81, 88). Thus, the conserved Q550, being exposed on the TMD
facing surface in the ATP-bound state of protein, is buried inside of the HlyB-NBD monomer
in the ADP-loaded structure. On the other hand, helix 5 of the helical domain and the Pro-loop
between the catalytic and helical domains only moderately change their positions.

A further comparative analysis of the ATP-Mg^{2+}- and ADP-bound structures of
HlyB-NBD demonstrates that the catalytic domain is also involved in the conformational
changes. Thus, helix 6 is noticeably dislocated, bending toward the helical domain (Figure 78).
The D-loop preceding helix 6 also changes its orientation (Figure 90). While in the
ATP-Mg^{2+}-structure, the residues of the D-loop form the complementary surface between two
NBD subunits and actively participate in the intersubunit contacts, in the ADP-bound
HlyB-NBD the D-loop protrudes into the interface between two subunits (Figure 78, bottom).
Such a conformational alteration will introduce a steric clash and may stimulate dissociation
of HlyB-NBD dimer into the individual subunits.

The C-terminal end of the protein also re-adjusts its position and re-arranges an
interaction pattern with other residues of HlyB-NBD (see details in Chapter 8.4.7 and
Figures 92, 93).

Thus, comparison of the ATP-Mg^{2+}- and ADP-bound HlyB-NBD demonstrates that
ATP hydrolysis and dissociation of the protein dimer generate significant conformational
changes of the helical domain and helix 6 of the catalytic domain, while the major part of the
catalytic domain, including the nucleotide-binding pocket, is virtually unaffected.
Nevertheless, the drastic alterations in the helical domain, the D-loop, and helix 6 entirely
modify the potential TMD-NBD surface in the assembled transporter and interface between
two NBD-subunits of the HlyB-NBD dimer. In particular, modeling of an ADP-bound dimer
of the HlyB-NBD on the structure of the BtuD dimer revealed severe steric clashes between
the D-loops of both monomers (data not shown).

8.3. Comparison of the ADP-bound and nucleotide-free structures

The superposition of the ADP-bound and nucleotide-free structures results in rmsd of 1.64 $Å^2$ for all 241 Cα atoms of HlyB-NBD. The least root-mean-square deviation between two structures of HlyB-NBD involves 223 Cα atoms and produces the value of 1.13 $Å^2$. This structural alignment of the ADP-loaded and nucleotide-free HlyB-NBD is illustrated in Figure 79.

Structural comparison of the two aforementioned functional states of HlyB-NBD demonstrates that ADP dissociation modifies the overall protein structure; yet, most of those changes are moderately expressed and stay within a limited rmsd-range of 1.0-2.7 $Å^2$ (Figure 80). The D-loop and the adjacent N-terminal end of helix-6 of the catalytic domain undergo the most drastic structural transition, being displaced by at least 6 Å. In the ADP-bound HlyB-NBD structure, the N-terminal part of the helix-6 noticeably bends towards the helical domain. Such conformational change allows the residues of the catalytic domain, D637, E639, and S640, and residue R613 of helix 5 to establish an extensive interaction via their side chains (Figure 91). In the nucleotide-free structure, where helix 6 is sprung back to the catalytic domain, a single water mediated link between the side chain amino-group of R613 and the main chain carbonyl of S640 connects the extended D-loop region with the helical domain. Simultaneously, the side chain carbonyl OE2 of Glu639 is displaced by 12.7 Å in the transition from the ADP-bound to nucleotide-free structure of HlyB-NBD (Figure 90).

The C-terminal end of the protein seems also to sense the release of the nucleotide from the active site, slightly displacing the helices 8 and 9 and relocating the loop between these helices by 4-6 Å.

The helical domain responds to the release of ADP by slight adjustment of its secondary structural elements with relatively unchanged orientation of the C-loop. However, other surface exposed loops of the helical domain experience significant structural alterations (Figure 80, red-colored loops). Substantial differences are also observed in the conformation of the Q-loop, connecting the helical and catalytic domains of HlyB-NBD. Residues D551, N552, and L555, which follow the conserved Q550 in the Q-loop sequence, entirely change their orientation, thus, modifying the external surface of NBD (Figures 81, 88).

Thus, ADP dissociation generates a variety of conformational changes, which include local and distant structural alterations. Importantly, the transition between the nucleotide-free and ADP-bound states of HlyB-NBD involves a single event of nucleotide dissociation but
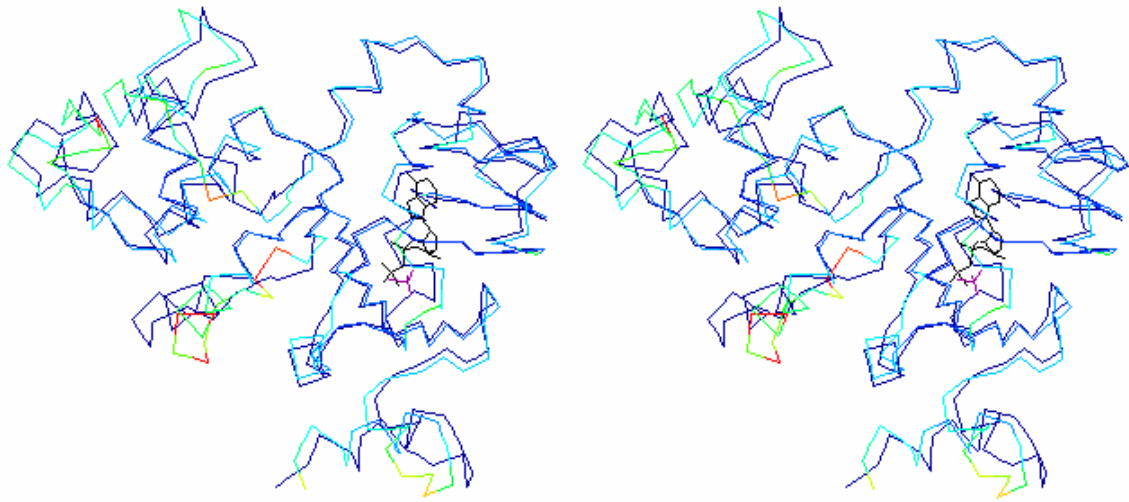
Figure 79. Stereoview of the superposition of the Cα traces of the nucleotide-free and the ADP-bound states of HlyB-NBD based on the least-squares alignment, rmsd of 1.13 Å^2 for 223 Cα atoms

The view of the dimer interface for each monomer is shown with the C-terminal part facing the cytoplasm at the bottom of figure and the top of the monomer facing the TMDs. The catalytic domain is shown on the right side of each monomer, and the helical domain on the left. The ADP-bound protein is shown in dark blue. The color of the nucleotide-free protein is based on rmsd, where the blue color corresponds to the lowest structural deviation and red to the highest deviation. The ADP molecule is colored black and the sulfate ion in the active site of the nucleotide-free HlyB-NBD is colored purple.
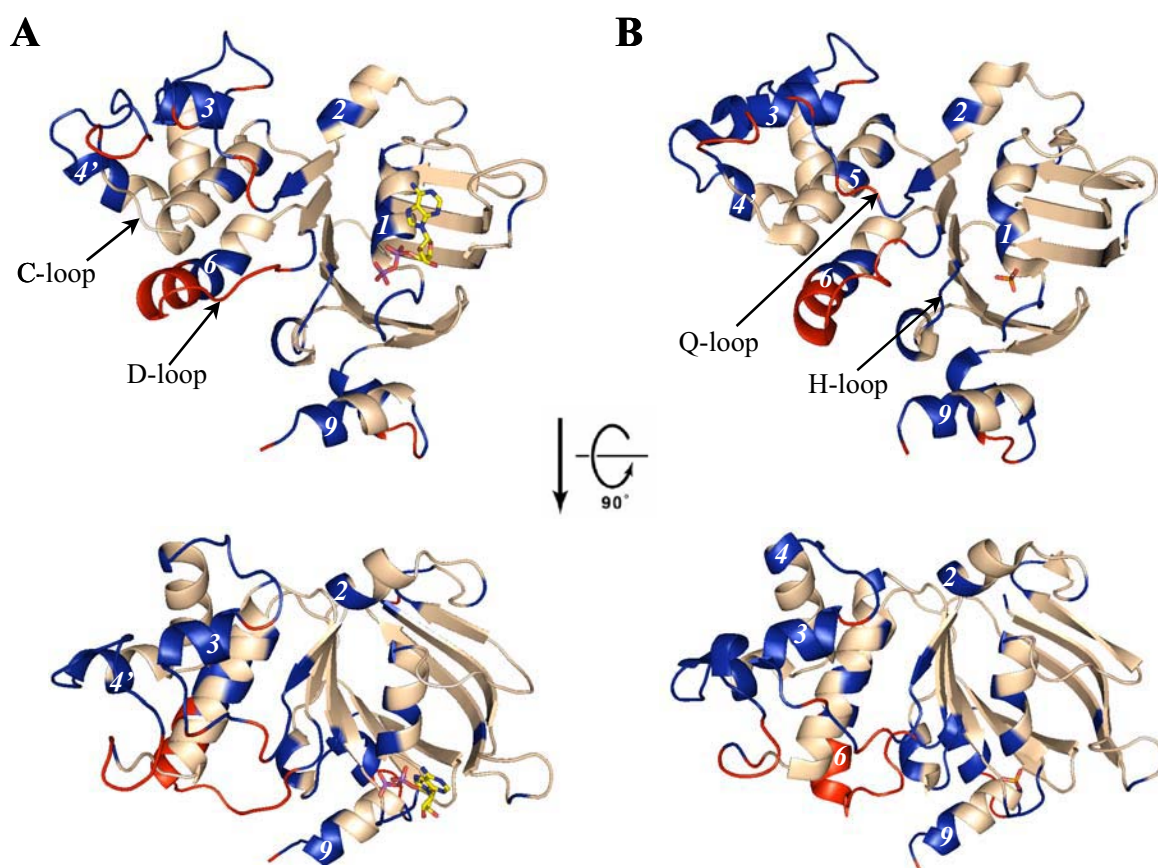
Figure 80. The ribbon diagrams of the ADP-loaded and the nucleotide-free structures of HlyB-NBD

Blue color indicates the structural deviations of 1.0-2.7 $Å^2$ between two proteins based on the least-squares alignment, rmsd of 1.13 $Å^2$ for 223 Cα atoms. The red color shows rmsd of 2.7 $Å^2$ and higher between two structures. The secondary structure elements, α-helices, involved in the structural rearrangement, are labeled with numbers.

    A. The ADP-loaded HlyB-NBD protein.

    B. The nucleotide-free state of HlyB-NBD.

Top figure: The side view of the protein; the upper part of the molecule is facing theTMDs of the transporter and the lower part is facing the cytoplasm.

Bottom figure: The view of the protein facing the TMDs, obtained by a 90° rotation of the top figure.

not the oligomeric changes. Thus, the direct comparison of two functional states suggests that association/dissociation of the nucleotide in HlyB-NBD is capable to produce significant distant conformational changes which are propagated throughout the protein.

8.4. Characteristic motifs of ABC proteins in HlyB-NBD

8.4.1. Walker A

The conformation of the Walker A motif in HlyB-NBD noticeably modifies upon nucleotide binding, switching from 3_{10} helical conformation to the classical α-helix (Figures 81, 82). Neither ATP hydrolysis nor oligomeric changes of protein seems to alter the position of the main chain of the Walker A motif as judged by comparison of the ADP-, ATP-Mg^{2+}-, and ATP-bound states of HlyB-NBD. The only requirement for the traditional α-helical conformation of the Walker A is the bound nucleotide.

8.4.2. Walker B

The positions and interactions of the conservative D630 and E631 residues of the Walker B motif in various functional states of HlyB-NBD are illustrated in Figures 81, 83-85. Both residues are located in relative proximity to the active site of the NBD, establishing a contact between the Walker B motif and nucleotide. Comparison of the nucleotide-free and ATP-Mg^{2+}-bound states of HlyB-NBD shows that the conserved aspartate and glutamate do not change their orientation upon ATP binding and protein dimerization, while both residues significantly modify their positions in the ADP-bound protein state (Figures 81, 83).

In the active ATP-Mg^{2+}-bound state, D630 established multiple contacts with the nucleotide, the Mg-ion, the Walker A motif, and the Q-loop (Figure 84). Interestingly, the conserved D630 of the Walker B always maintains the connection with the Q-loop via Q550 and V548, regardless of the overall protein conformational changes within the hydrolytic cycle (Figure 84). Noteworthy, the main chains of V548 and D630 invariably preserve the same link between carbonyl and amide group, respectively. The strength of the interaction between D630 and Q550 varies in the different functional states of HlyB-NBD, changing
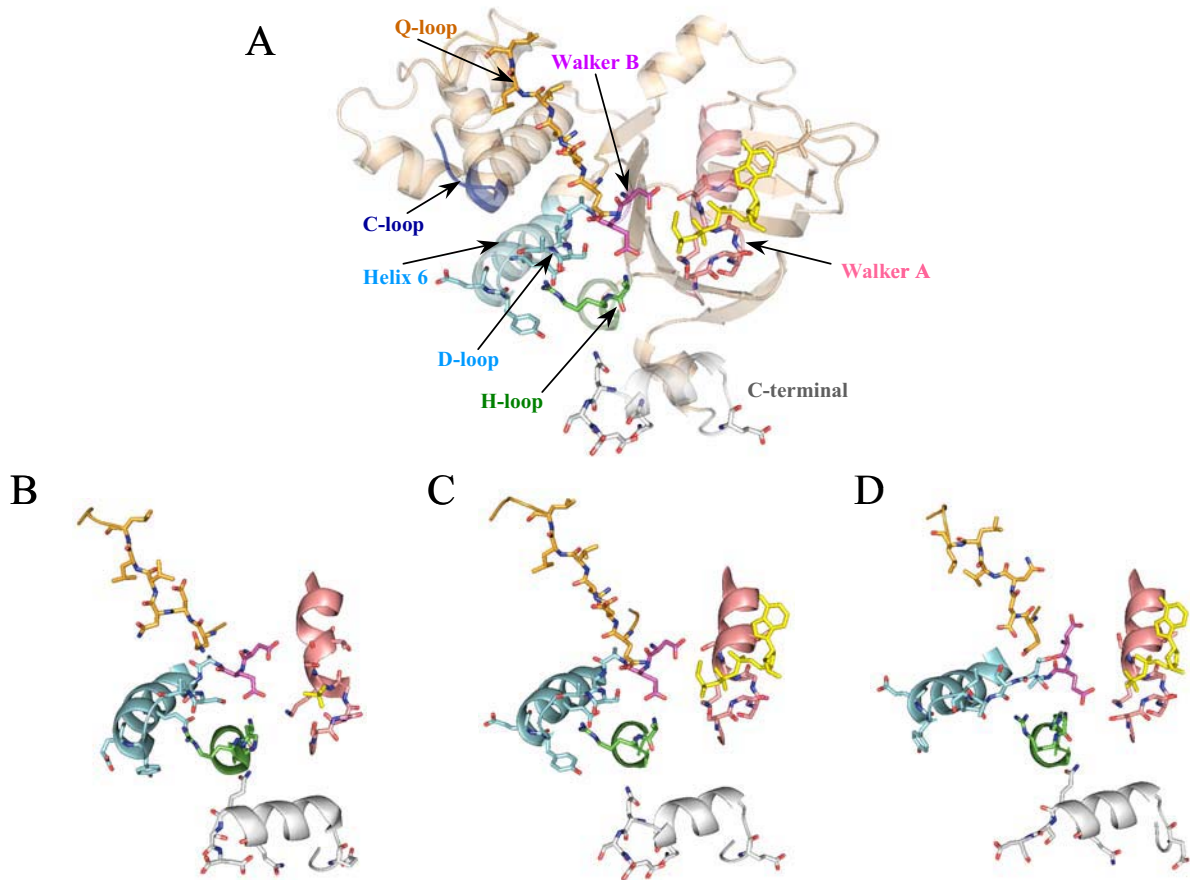
Figure 81. Conformations of the conserved motifs of ABC proteins in various functional states of HlyB-NBD

A. The ribbon diagram of HlyB-NBD monomer with bound ATP-Mg^{2+}. The top of the molecule is facing the TMDs of the transporter; the bottom part is facing the cytoplasm. The conserved motifs of ABC-transporters are indicated and colored; the Walker A motif – pink; the Walker B motif – magenta; the C-loop or ABC-motif – blue; the His-loop – green; the D-loop and helix 6 – cyan; the Q-loop – orange; the C-terminal end – gray. The selected residues and bound molecules of ADP or ATP-Mg^{2+} are shown in stick presentation. ADP and ATP-Mg^{2+} are colored yellow; the oxygen atoms of the residues are colored red, and nitrogen atoms – blue.

B. The nucleotide-free state of HlyB-NBD. Close-up view of the conserved motifs and the C-terminus.

C. The ATP-Mg^{2+}-bound state of HlyB-NBD. The close-up view of the conserved motifs and the C-terminus.

D. The ADP-bound state of HlyB-NBD. The close-up view of the conserved motifs and the C-terminus.
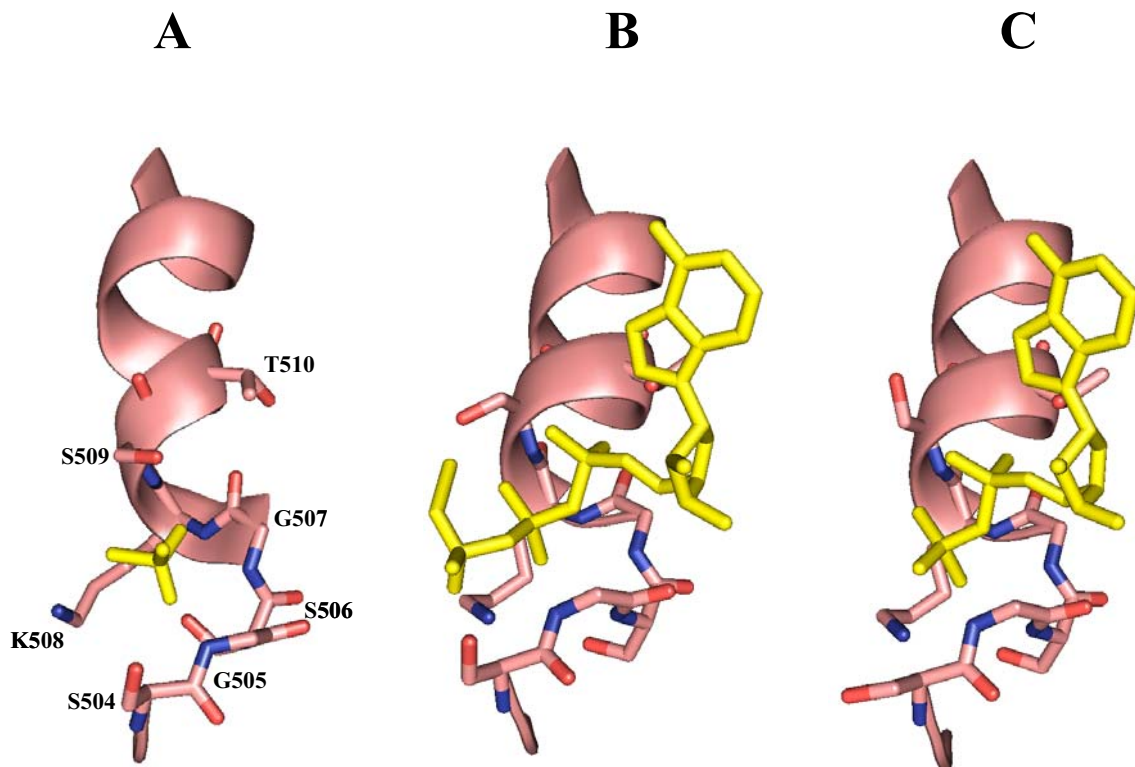
Figure 82. Conformations of the Walker A motif in various functional states of HlyB-NBD

The color scheme and the motif positioning are the same as in Figure 80. See text for details.

    A. The nucleotide-free state of HlyB-NBD.

    B. The ATP-Mg^{2+}-bound state of HlyB-NBD.

    C. The ADP-bound state of HlyB-NBD.
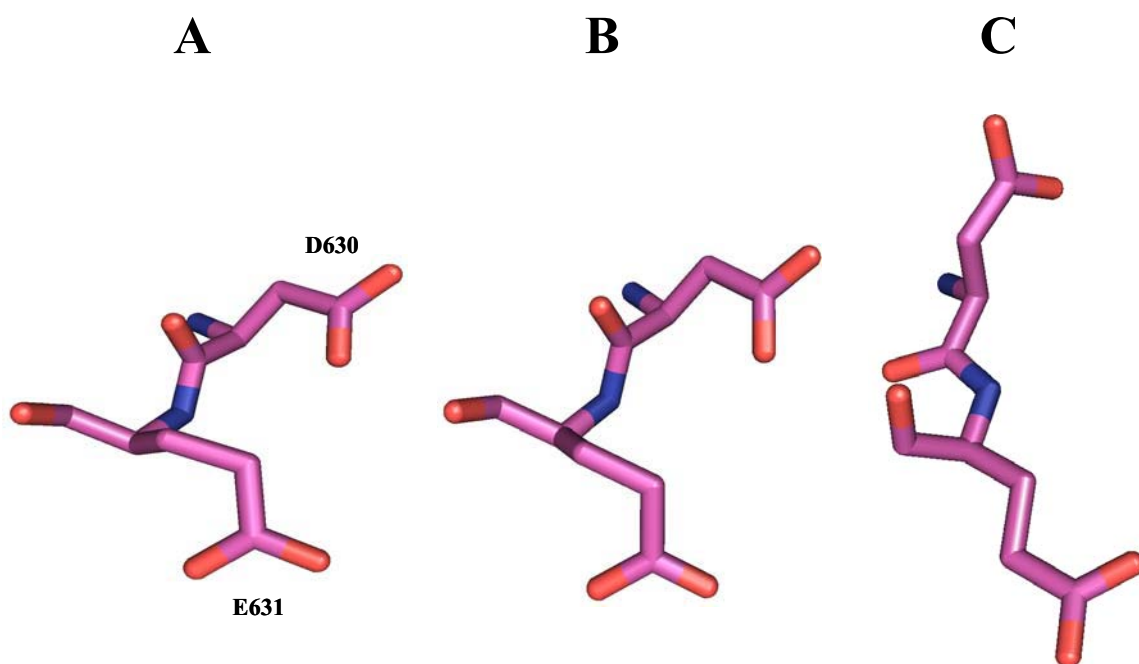
Figure 83. Orientations of the Asp630 and Glu631 residues of the Walker B motif in various functional states of HlyB-NBD

The color scheme and the motif positioning are the same as in Figure 80. See text for details.

  A. The nucleotide-free state of HlyB-NBD.
  B. The ATP-Mg^{2+}-bound state of HlyB-NBD.
  C. The ADP-bound state of HlyB-NBD.
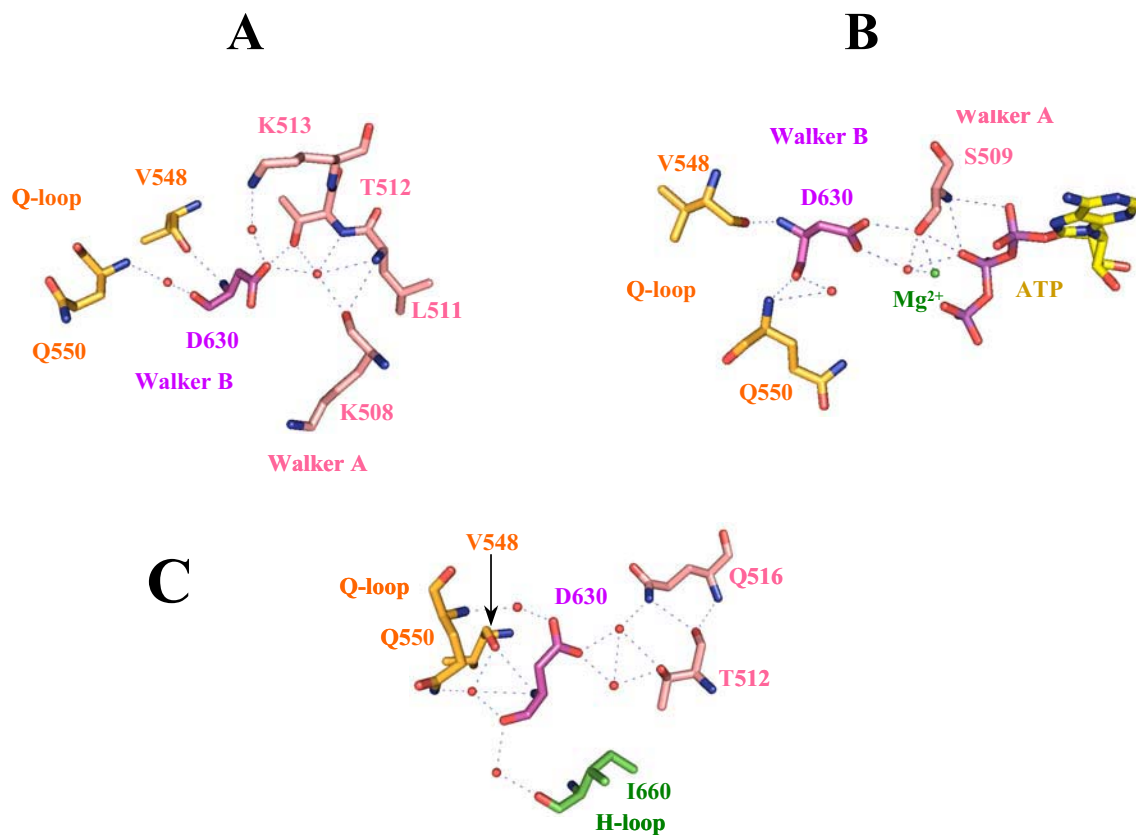
Figure 84. Polar interactions of the conserved aspartate-630 of the Walker B motif in various functional states of HlyB-NBD

The color scheme is the same as in Figure 80, except for ATP-Mg^{2+}. The carbon atoms of ATP are colored yellow, the phosphorus atoms – magenta, oxygen – red, and nitrogen – blue. The Mg-ion is shown as a green sphere. Red spheres indicate water molecules. The positioning of the residues is slightly different from Figure 80 to better demonstrate links between the residues. See text for details.

- A. The nucleotide-free state of HlyB-NBD.
- B. The ATP-Mg^{2+}-bound state of HlyB-NBD.
- C. The ADP-bound state of HlyB-NBD
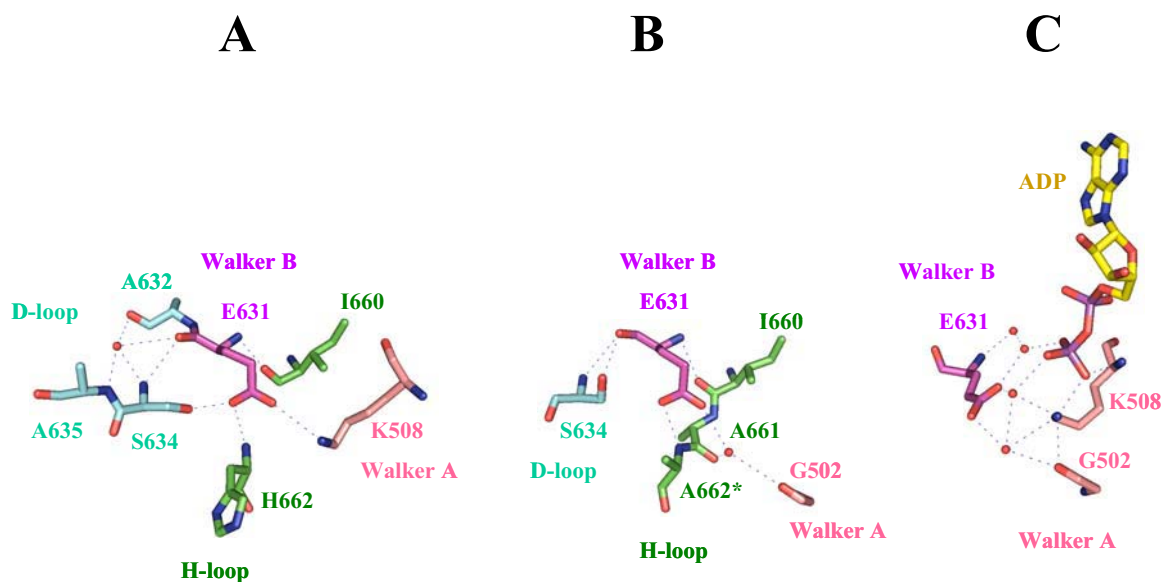
Figure 85. Polar interactions of the conserved glutamate-631of the Walker B motif in various functional states of HlyB-NBD

The color scheme is the same as in Figure 80, except for ADP. The carbon atoms of ADP are colored yellow, the phosphorus atoms – magenta, oxygen – red, and nitrogen – blue. Red spheres indicate water molecules. The positioning of the residues is slightly different from Figure 80 to better demonstrate links between the residues. See text for details.

- A. The nucleotide-free state of HlyB-NBD.
- B. The ATP-Mg^{2+}-bound state of HlyB-NBD.
- C. The ADP-bound state of HlyB-NBD

from a single water-mediated link in the nucleotide-free state to the direct main-to-main-chain interaction in the ATP- or ATP-Mg^{2+}-loaded protein (3.16 - 3.26 Å), transforming to the multiple water-mediated connections in the ADP-bound HlyB-NBD. The conserved 'Walker B – Q-loop' link seems to result in a strong dependence of the D630-orientation on the position of the conserved Gln550 in the HlyB-NBD structure. Thus, in the ADP-bound state of HlyB-NBD, both the conserved residues, D630 and Q550, are withdrawn from the active site followed by significant alterations in the Q-loop conformation.

The position of E631 of the Walker B motif in HlyB-NBD structure seems to depend on the conformation of the two conserved motifs, the His-loop and the Walker A (Figures 81, 85). Particularly, the side chain of Glu631 always maintains a connection with either G502 or K508, or both residues of the Walker A motif, depending on the functional state of the protein (Figure 85). Such a link seems to keep the conserved glutamate in the vicinity of the active site in various HlyB-NBD conformations, yet, not necessarily in contact with a bound nucleotide. Formation of the link between E631 and H662 seems to depend on the orientation of the conserved histidine, which changes within the hydrolytic cycle. In the nucleotide-free and ATP-Mg^{2+}-bound structures of HlyB-NBD, the side chain of the conserved E631 directly contacts the main-chain amide group of the His662/Ala662* residue. Notably, the position of Glu631 in the active ATP-Mg^{2+}-bound state of HlyB-NBD permits more extensive contacts between Glu631 and His662, involving backbone and side-chain links with the histidine. However, in the ADP-bound structure the conserved H662 is flipped out of the active site altering an orientation of the main chain, which apparently results in the disruption of the E631-H662 bond. As a consequence, the side chain of E631 changes its orientation and establishes extensive interactions with residues of the Walker A motif, Gly502 and Lys508, and with bound ADP (Figure 85).

8.4.3. His-loop

The conserved histidine of the His-loop demonstrates a variety of positions and molecular contacts in the different functional states of HlyB-NBD (Figures 81, 86, 87). In the nucleotide-free protein state, the main chain of H662 supports connections between the H-loop and the conserved residues of the Walker A and Walker B motifs, glycine-502 and glutamate-631, respectively, and also with the C-terminal glutamine-705 residue. In the ATP-Mg^{2+}-loaded state of HlyB-NBD, alanine-662 substituted for the conserved histidine

Figure 86. Conformations of the H-loop in various functional states of HlyB-NBD

The color scheme and the motif positioning are the same as in Figure 80. See text for details.

    A. The nucleotide-free state of HlyB-NBD.

    B. The ATP-Mg^{2+}-bound state of HlyB-NBD.

    C. The ADP-bound state of HlyB-NBD
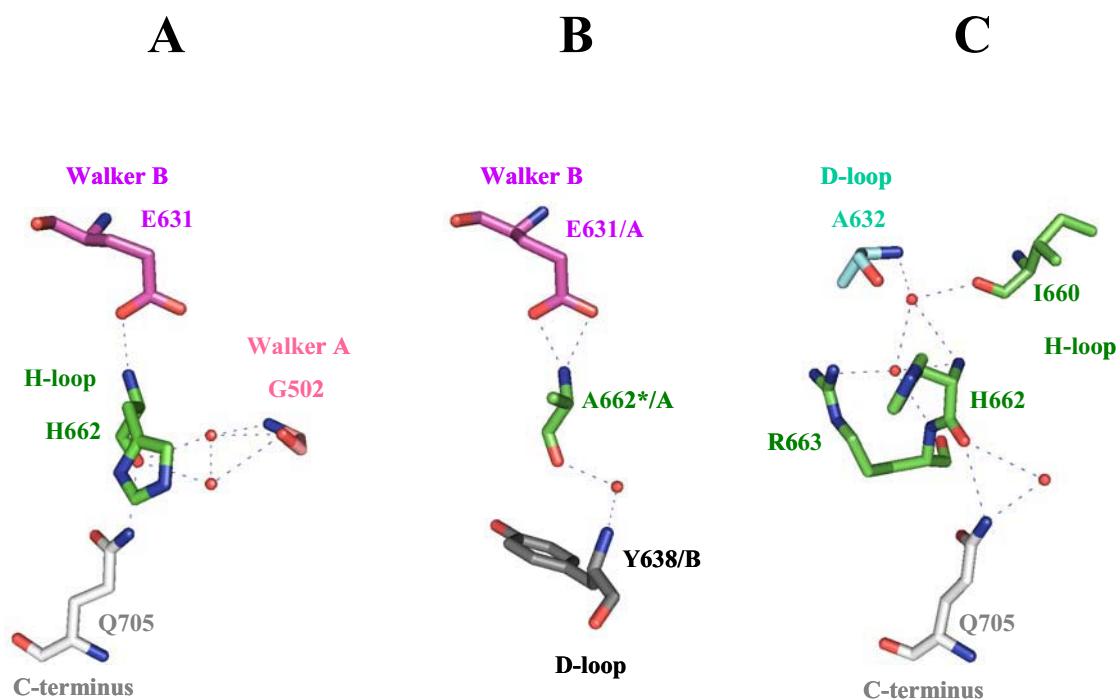
Figure 87. Polar interactions of the conserved histidine-662 (alanine-662 in the ATP-Mg^{2+}-state) of the H-loop in various functional states of HlyB-NBD

The color scheme is the same as in Figure 80. Red spheres indicate water molecules. The positioning of the residues is slightly different from Figure 80 to better demonstrate links between the residues. See text for details.
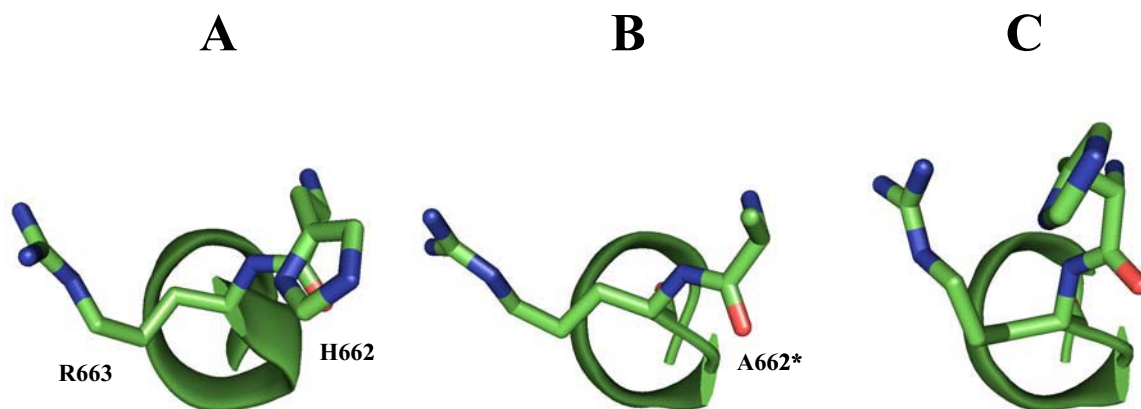
A. The nucleotide-free state of HlyB-NBD.

B. The ATP-Mg^{2+}-bound state of HlyB-NBD. Dark gray color indicates residue of the opposite subunit in ATP-Mg^{2+}-dimer.

C. The ADP-bound state of HlyB-NBD

also participates in the interaction with the side chain of Glu-631. Simultaneously, the main chain of A662* contributes to the intersubunit communication between two NBD monomers, contacting Y638 of the D-loop of the opposite molecule. The main chain of A662 seems to slightly move toward the active site of HlyB-NBD in the ATP-Mg^{2+}-loaded state, and orientation of A662 provides an opportunity for the heterocyclic imidazole ring of the native histidine to directly contact nucleotide (Figures 86, 87, and 47), the same way as it is accomplished in MJ1096- and MalK-ATP-bound dimer structures. In the ADP-bound state, the histidine-662 is withdrawn from the active site of NBD (Figures 81, 86, 87), establishing a new net of interactions with the neighboring residues, R663 and I660, and the A632 residue of the D-loop, and restoring the link with the C-terminal Gln705.

Notably, the side-chain imidazole group of histidine-662 is not involved in the intramolecular contacts neither in the nucleotide-free nor in the ADP-bound state of protein. In fact, the side chain of the histidine forms a bulge at the NBD-dimer interface in both aforementioned structures, which is more prominent in the ADP-bound form. In the ATP-bound state of HlyB-NBD, the γ-phosphate seems to pull the side chain of the histidine towards the active site, while NBD dimerization stabilizes this transition state by holding the flexible histidine in place. Such orientation of the histidine seems to initiate ATPase activity of HlyB-NBD. Thus, the conserved histidine may serve as a mechanical molecular switch, which turns on and off ATPase activity.

Thus, location of the conserved histidine His662, its structural flexibility, and wide participation in the functionally important intra- and intermolecular contacts notably distinguish this residue from other conserved residues of ABC-transporters. The above structural observations are supported by biochemical investigations of the H-loop of various ABC proteins *in vivo* and *in vitro* (Davidson and Sharma, 1997; Nikaido and Ames, 1999; Shyamala *et al.*, 1991; Walter *et al.*, 1992; Zaitseva *et al.*, 2005a). Such studies display the deleterious effect of the histidine mutations on ATPase activity and substrate transport in ABC transporters emphasizing the functional importance of the conserved histidine in the family of ABC- proteins.

8.4.4. Q-loop

The Q-loop of HlyB-NBD demonstrates a remarkable structural plasticity upon ATP-binding and particularly upon ATP-hydrolysis (Figures 81, 88). Thus, ATP-binding and NBD dimerization result in extending of the Q-loop, which brings the conserved Q-550 in close proximity to the active site (Figures 81, 88). The orientation of the other residues of the Q-loop is also re-arranged, reflecting a new conformational and oligomeric state of the HlyB-NBD. While the aforementioned link between the Q-loop and D630 of the Walker B motif is consistently preserved, the structural transformation of HlyB-NBD within the hydrolytic cycle significantly modifies other contacts of the conserved Q550 (Figure 89). A water-mediated link of Q550 with the neighboring N552 residue in the nucleotide-free state is substituted with multiple intra- and intersubunit connections in the active state of HlyB-NBD. Thus, in the ATP-Mg^{2+}-bound protein conformation, Q550 mediates intramolecular communication between the helical domain (via Q612 of helix 5), the D-loop (via S634), and the Walker B motif (via D630), and also intermolecular communication between two NBD subunits via their Q- and D-loops (Figure 89).

ATP-hydrolysis and dissociation of the NBD dimer lead to retraction of the Q-loop along with significant rearrangement of its residues (Figure 81, 88). In fact, all Q550-L555 residues drastically change the orientation. As a result, the conserved Gln550 is completely withdrawn form the active site of the ADP-bound protein, yet, it maintains the link with D630 of the Walker B. Simultaneously, Q550 establishes contacts with V548 residue of the preceding region and T633 of the D-loop (Figure 89).

Thus, the Q-loop of HlyB-NBD seems to fulfill a unique signal transition role, which is favored by the specific localization at the interface between NBD-NBD and NBD-TMD subunits, its high flexibility, and participation in the formation of the active site as well as in the intermolecular communication. Such an observation is consistent with the previously proposed role for the Q-loop based on the molecular dynamics simulation model (Jones and George, 2002).
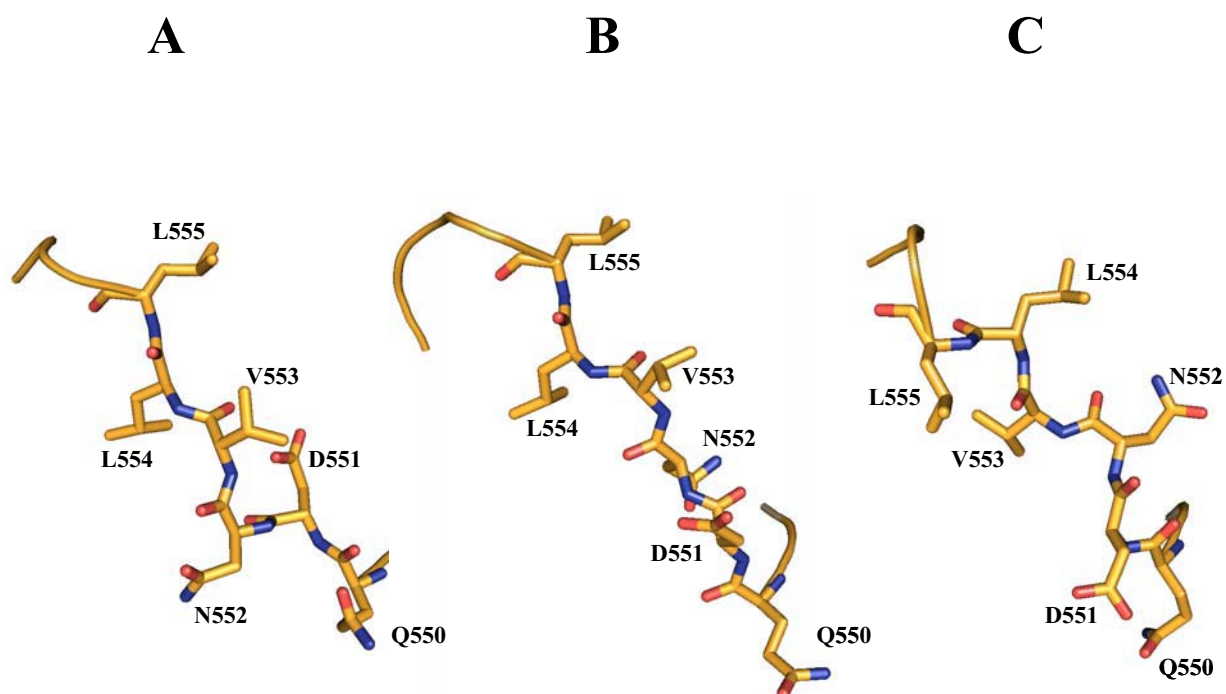
Figure 88. Conformations of the Q-loop in various functional states of HlyB-NBD

The color scheme and the motif positioning are the same as in Figure 80. See text for details.

    A. The nucleotide-free state of HlyB-NBD.

    B. The ATP-Mg^{2+}-bound state of HlyB-NBD.

    C. The ADP-bound state of HlyB-NBD.
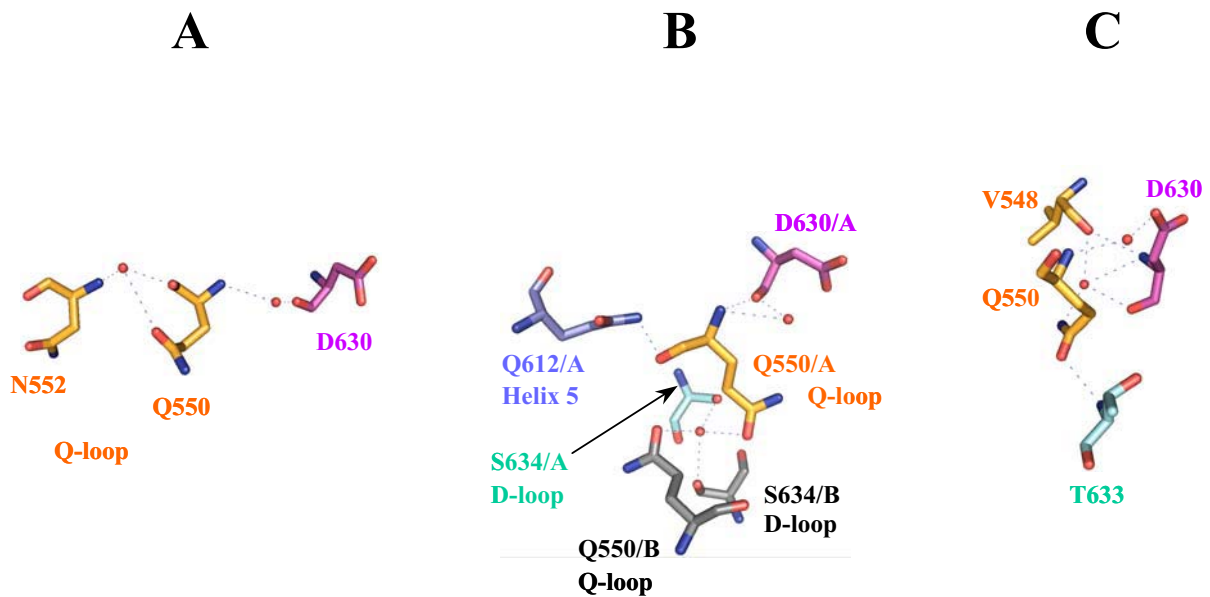
Figure 89. Polar interactions of the conserved glutamine-550 of the Q-loop in various functional states of HlyB-NBD

The color scheme is the same as in Figure 80, except for Q612 residue of helix 5, which is colored slate blue. Red spheres indicate water molecules. The positioning of the residues is slightly different from Figure 80 to better demonstrate links between the residues. See text for details.

A. The nucleotide-free state of HlyB-NBD.

B. The ATP-Mg^{2+}-bound state of HlyB-NBD.

C. The ADP-loaded HlyB-NBD protein.

8.4.5. D-loop and helix 6

Helix 6 is the only secondary structural element of HlyB-NBD, which inevitably responds to every change in the functional protein state by a radical conformational change (Figures 75-81, 90). Helix 6 and the adjacent D-loop are located at the periphery of the catalytic domain, distant from the nucleotide-binding site of the monomer and in close proximity to the helical domain. In the nucleotide-free state, helix 6 is slightly bended towards the catalytic domain. ATP binding and presumably NBD dimerization lead to structural transformation of helix 6 and the D-loop, moving them towards the helical domain. Moreover, in the ATP-bound dimer, both helix 6 and the D-loop are positioned in the vicinity of the newly created ATP-binding site and participate in the formation of the compatible intersubunit surfaces and communication between two monomers.

However, even more significant conformational changes of the D-loop and helix 6 are detected in the protein structure upon transition from the ATP- to ADP-bound HlyB-NBD (Figures 81, 90). As result of the ATP-hydrolysis and NBD-dissociation, the N-terminus of helix 6 is distinctly bended toward the helical domain. The orientation of residues of helix 6 and the D-loop also substantially changes (Figure 90). The next catalytic step, ADP dissociation, recoils helix 6 from the tight connection with the helical domain to the relaxed conformation (Figures 81, 90). Such mechanical movement of helix 6 within the hydrolytic cycle may play an important role in the mechanism of action of ABC-transporters. In agreement with models proposed for various biomolecular motors, such as F1-ATPase and bacteriophage phi 29 portal protein, the chemical energy of ATP-binding/hydrolysis can be converted into elastic strain and stored within the protein (Liao and Oster, 2004). In HlyB, the chemical energy of the ATP-binding and NBD dimerization may be directly propagated to conformational changes in the TMDs via the helical domain to perform the mechanical work of the allocrite transport. However, a part of the binding energy and energy of ATP-hydrolysis can be stored as elastic energy in helix 6, which can be subsequently used for Pi- and ADP-release (the Kd of ADP is 90 µM; that means that 17 kJ/mol is required for ADP dissociation) and also to energize the conformational changes to promote dissociation of the NBD-dimer or full transporter.
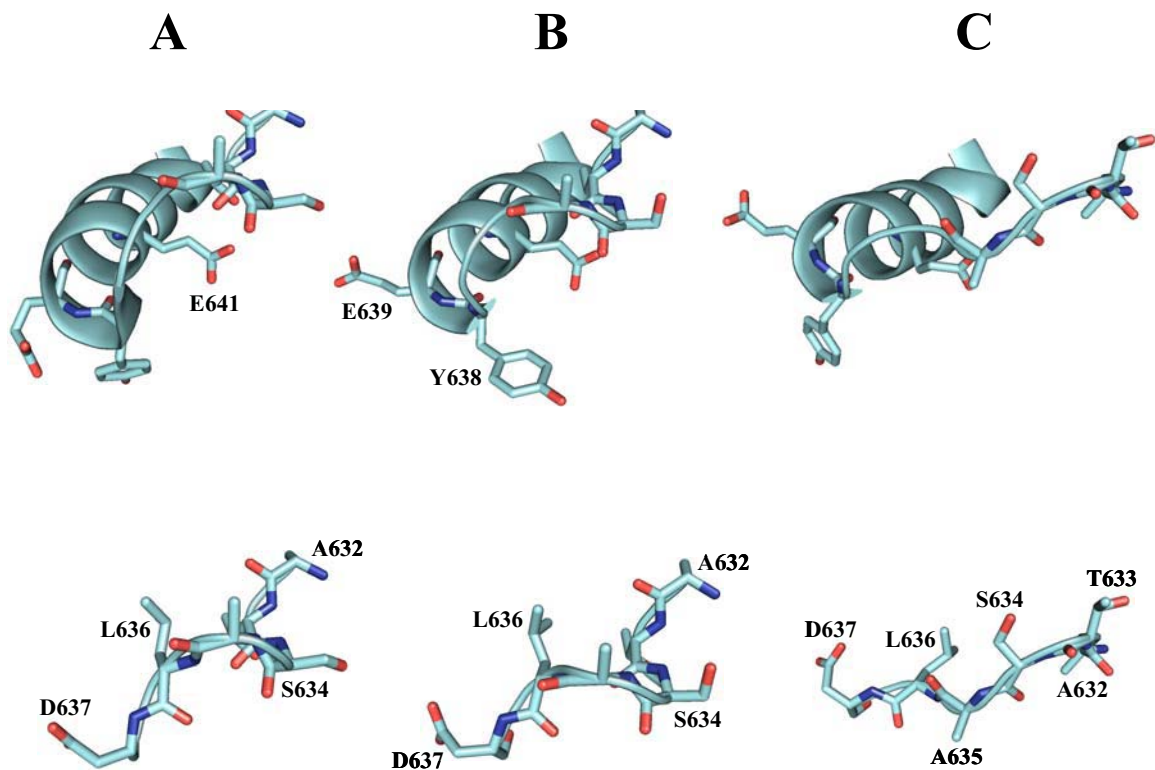
Figure 90. Conformations of helix 6 and the D-loop in various functional states of HlyB-NBD

The color scheme and the motif positioning are the same as in Figure 80. Both helix 6 and the D-loop are shown at the top of the figure. The D-loop alone is depicted at the bottom of the figure. See text for details.

A. The nucleotide-free state of HlyB-NBD.

B. The ATP-Mg^{2+}-bound state of HlyB-NBD.

C. The ADP-loaded HlyB-NBD protein.

8.4.6. Helical domain: C-loop and helix 5

While the C-loop directly participates in nucleotide binding upon the ATP-induced formation of the NBD dimer, neither the C-loop nor the adjacent helix 5 undergoes significant conformational changes within the catalytic cycle (Figures 75-80). An analysis of potential hinges revealed that C-terminus of helix 5 might act as a mechanical hinge in the first step of the catalytic cycle, e.g. upon ATP-binding/NBD dimerization. Moreover, helix 5 might serve as a transducer of the chemical ATP-binding energy into the conformational changes in the helical domain and into elastic energy stored in helix 6 (Figure 91). Thus, in the nucleotide-free state, relatively conserved residues of helix 5, such as Q612, R613, and R618, provide communication of helix 5 with the Q-loop, the loop between helices 4 and 4' of the helical domain, and helix 6 of the catalytic domain (Figure 91). The ATP-Mg^{2+}-binding further expands intramolecular contacts of helix 5, involving additional residues of helix 5. The interactions of Q610, R611, Q612, R613, and R618 of helix 5 include the residues of the D-loop (A632), the Q-loop (L549-N552), helix 3 (N562), the loop connecting 4 and 4'' helices (G583), the ATP molecule, and also the Walker A motif of the opposite NBD subunit (S504). Such wide net of the interactions of helix 5 along with direct nucleotide contact allows transferring the ATP-hydrolysis signal to various protein regions. As a result of ATP hydrolysis and dimer disassembly, the pattern of the intramolecular contacts in the ADP-bound HlyB-NBD resembles pattern in the nucleotide-free protein. Helix 5 consistently preserves the interaction with the loop between helices 4 and 4'(G583) and the Q-loop (N552), while it establishes more extensive connections with the D-loop (D637) and helix 6 (E639, S640), which results from the extreme bending of helix 6 towards the helical domain (Figure 91).

8.4.7. C-terminal end

The C-terminal region of HlyB-NBD does not belong to the highly conserved consensus sequences of ABC proteins; yet, it is essential in NBD dimerization and intersubunit communication (Chapter 6). A structural comparison of the individual states of the catalytic cycle of the HlyB-NBD also reveals noticeable flexibility of the C-terminal end

Figure 91. Selected polar interactions of helix 5 in various functional states of HlyB-NBDThe color scheme is the same as in Figure 80, except for helix 5, ATP-Mg^{2+}, and G583 residue. Helix 5 and its selected residues are colored gray; the glycine-583 of the helical domains is green. The carbon atoms of ATP are colored yellow, the phosphorus atoms and Mg-ion – magenta, oxygen – red, and nitrogen – blue. Red spheres indicate water molecules. The positioning of the residues is different from Figure 80 to better demonstrate links between the residues. See text for details.

A. The nucleotide-free state of HlyB-NBD.

B. The ATP-Mg^{2+}-bound state of HlyB-NBD.

C. The ADP-bound state of HlyB-NBD

of the protein (Figures 75-80, 92, 93). In the inactive nucleotide-free or ADP-bound state, Q705 provides communication between the C-terminal residues facing the cytoplasm and the region of the extended His-loop, including the conserved histidine (Figures 81, 93). While in the active ATP-Mg^{2+} bound protein state, the Gln705 residue is disengaged from the His-loop and involved in the intersubunit interactions (Figures 81, 93). Thus, conformational changes of the C-terminal end of HlyB-NBD may play an important role in the protein communication with the outside world and particularly in the mechanism of allocrite recognition and/or allocrite sensing by the NBD molecule.

8.5. Mechano-chemical model of the catalytic cycle

Structural analysis of HlyB-NBD in various functional states judged by the rmsd values demonstrates that all steps of the hydrolytic cycle involve significant conformational changes. Thus, ATP hydrolysis and dissociation of the protein dimer induces the most prominent structural alterations, represented by rmsd of 2.2-2.5 Å^2 between the ATP- and ADP- bound states. The ATP binding promotes both intrasubunit conformational changes and dimerization of the NBDs resulting in rmsd of 2.0-2.2 Å^2 between the nucleotide-free and ATP-bound structures, while ADP dissociation produces small yet noticeable change in HlyB-NBD conformation with rmsd of 1.6 Å^2. Interestingly, although no significant difference in the rmsd values (0.63 Å for 474 Cα atoms and 0.94 Å for all 482 Cα atoms) was detected for the ATP-dimer upon Mg^{2+}-binding, the presence of this divalent metal in the active site leads to the evident re-arrangement of the protein-nucleotide and inter-subunit interaction, leading to clear asymmetry between the subunits and consequently to the active protein state.

Thus, from a structural point of view, all the steps of the catalytic cycle of HlyB-NBD, such as ATP-binding, ATP-hydrolysis, and ADP-dissociation, seem to be capable to generate a 'power stroke', though ATP-binding and ATP-hydrolysis have a greater potential to initiate significant conformational modifications. The thermodynamic analysis of all the functional steps for HlyB-NBD is in agreement with the structural evaluation (Zaitseva *et al.*, 2005c).

The following mechano-chemical model is proposed to describe the catalytic cycle of ABC transporter, using different conserved sequence motifs as key players (Figure 94). The first step involves ATP-binding and NBD dimerization of ABC subunits/domains. The produced conformational changes in NBDs are propagated into mechanical movement of
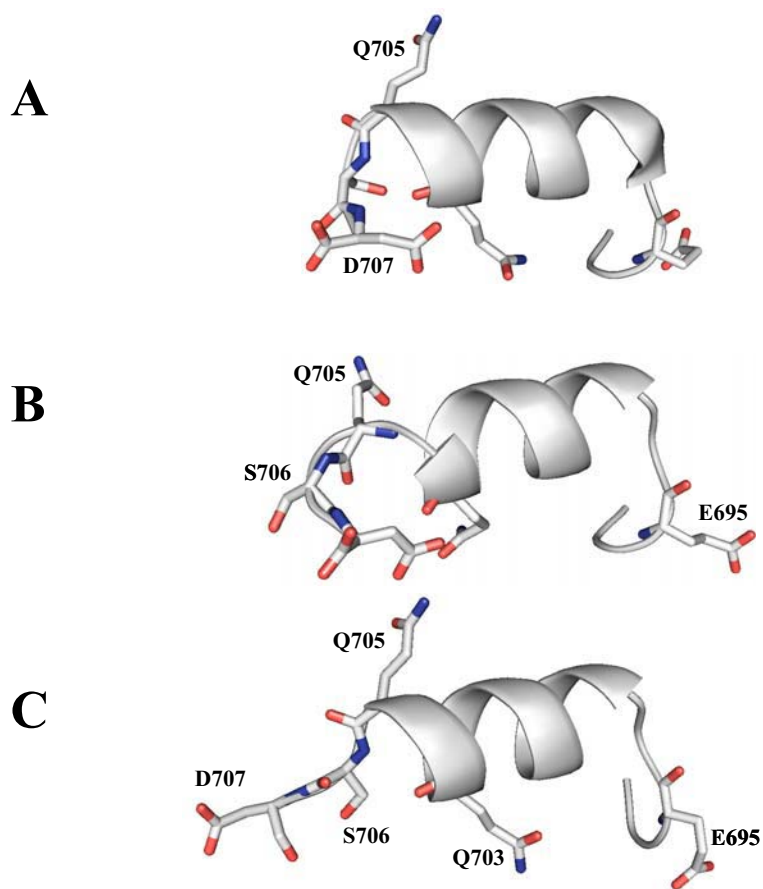
Figure 92. Conformations of the C-terminus in various functional states of HlyB-NBD

The color scheme and the motif positioning are the same as in Figure 80. See text for details.

A. The nucleotide-free state of HlyB-NBD.

B. The ATP-Mg^{2+}-bound state of HlyB-NBD.
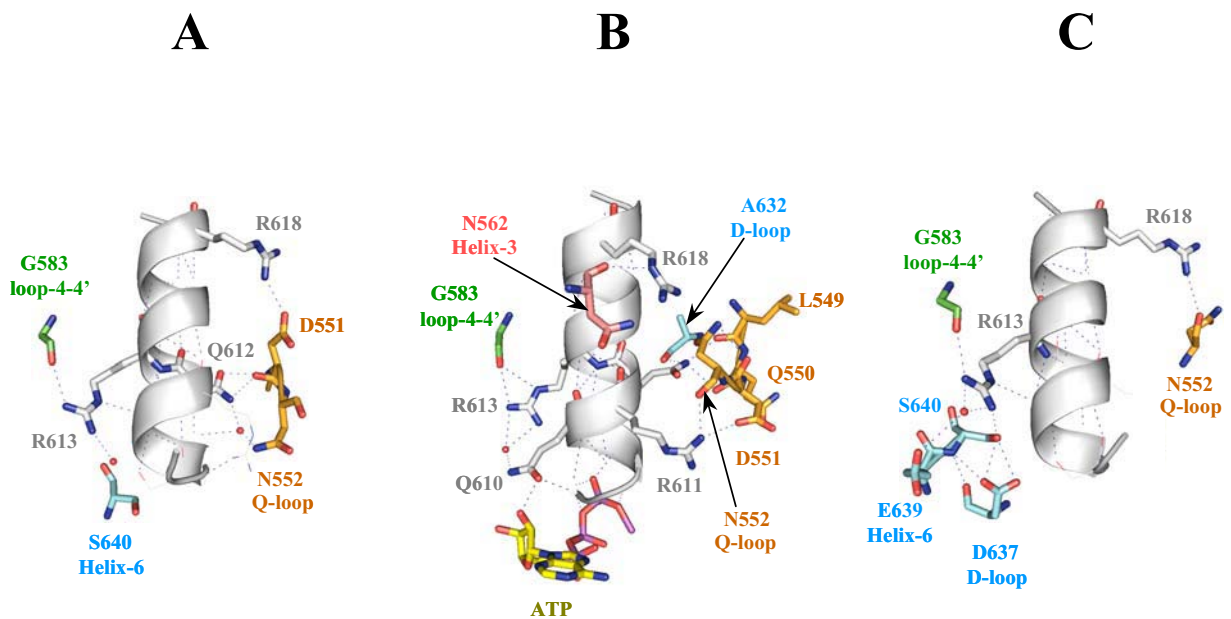
C. The ADP-bound state of HlyB-NBD.
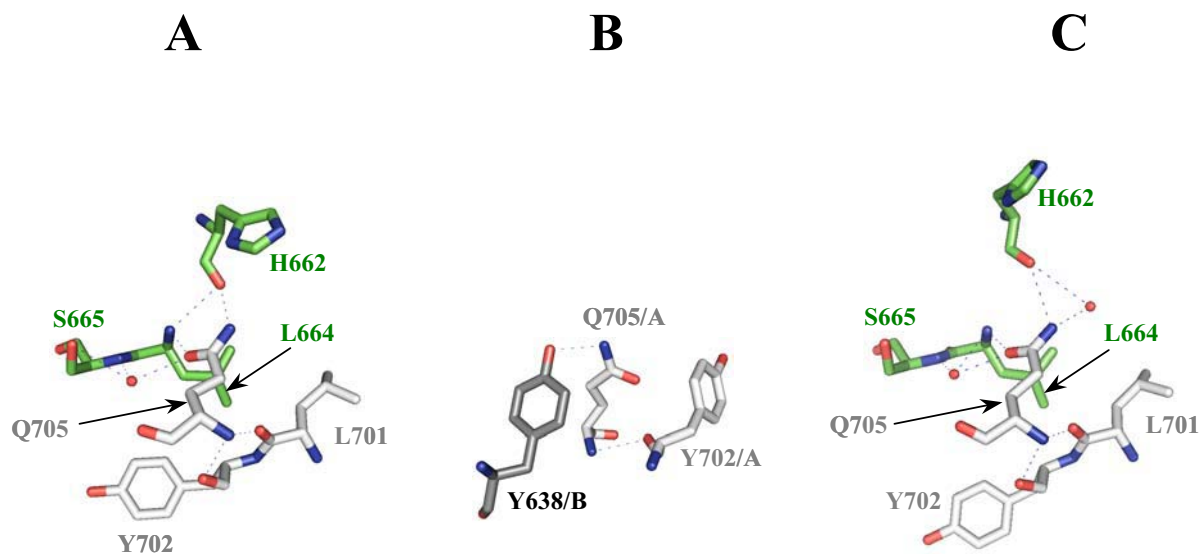
Figure 93. Polar interactions of the Gln705 of the C-terminus in various functional states of HlyB-NBDThe color scheme is the same as in Figure 80. Red spheres indicate water molecules. The positioning of the residues is different from Figure 80 to better demonstrate links between the residues. See text for details.

A. The nucleotide-free state of HlyB-NBD.

B. The ATP-Mg^{2+}-bound state of HlyB-NBD. Dark gray color indicates residue of the opposite subunit in ATP-Mg^{2+}-dimer.

C. The ADP-bound state of HlyB-NBD.

TMDs, producing pre-active conformation of the transporter waiting for the allocrite signal. Alternatively, allocrite recognition permits two NBD subunits to form the ATP-bound sandwich, whose structural modifications induce conformational changes in TMDs of the transporter. As a result of ATP-binding, NBD dimerization, and allocrite binding, the transporter adopts the active conformation. It is likely that a channel for the allocrite transport is already open at this point. Therefore, an allocrite can be transported simultaneously with ATP hydrolysis in one of the active sites of the NBD dimer.

The next step of the catalytic cycle includes release of the γ-phosphate from the nucleotide-binding pocket. This event completes the ATP-hydrolysis step and results in the next round of the conformational changes within the helical domain and helix 6 of the NBD. This step is also converted into mechanical movement of the TMD-helices, closing the transport channel and restoring the ground state conformation of the TMDs. It's possible that the conformational changes in one of the NBD subunits also result in NBD-dimer disassembly. Yet, another alternative is that the elastic energy accumulated in helix 6 is utilized for ADP-dissociation and NBD-dimer disassembly.

Based on this model (Figure 94) one can also assign distinct functions to the conserved motifs of NBDs: the Walker A and B motifs as well as the C-loop and H-loop are required for ATP-binding and hydrolysis, while the Pro-, Q- and D-loop are central for NBD-NBD and NBD-TMD communication.
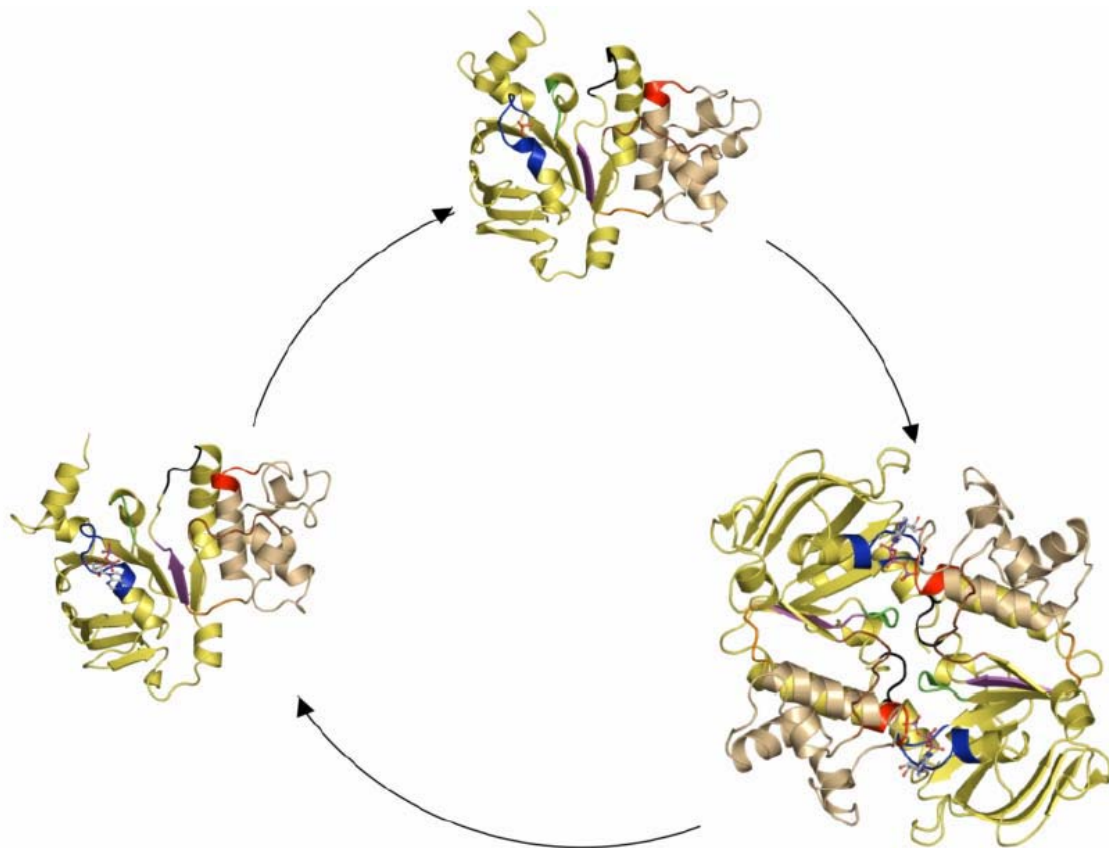
Figure 94. The catalytic cycle of the HlyB-NBD

Crystal structures of the monomeric nucleotide-free, dimeric ATP-bound, and monomeric ADP-bound forms are shown. The catalytic domain is colored in light yellow and the helical domain in light tan. Conserved motifs are highlighted and color-coded as follows: the Walker A (residues 502-510, blue), the Q-loop (residues 549-556, brown), the C-loop (residues 606-610, red), the Pro-loop (residues 621-625, orange), the Walker B (residues 626-630, magenta), the D-loop (residues 634-637, black), and the H-loop (residues 661-663, green). Bound ligands are shown in ball-and-stick representation.

References

Abele, R., and Tampe, R. (2004). The ABCs of immunology: structure and function of TAP, the transporter associated with antigen processing. Physiology (Bethesda) *19*, 216-224.

Abrahams, J. P., Leslie, A. G., Lutter, R., and Walker, J. E. (1994). Structure at 2.8 A resolution of F1-ATPase from bovine heart mitochondria. Nature *370*, 621-628.

Ames, G. F., Nikaido, K., Wang, I. X., Liu, P. Q., Liu, C. E., and Hu, C. (2001). Purification and characterization of the membrane-bound complex of an ABC transporter, the histidine permease. J Bioenerg Biomembr *33*, 79-92.

Andersen, C., Koronakis, E., Bokma, E., Eswaran, J., Humphreys, D., Hughes, C., and Koronakis, V. (2002). Transition to the open state of the TolC periplasmic tunnel entrance. Proc Natl Acad Sci U S A *99*, 11103-11108.

Andrews, A. T. (1981). Electrophoresis: Theory, techniques and biochemical and clinical application (New York, Oxford University Press).

Annereau, J. P., Ko, Y. H., and Pedersen, P. L. (2003). Cystic fibrosis transmembrane conductance regulator: the NBF1+R (nucleotide-binding fold 1 and regulatory domain) segment acting alone catalyses a Co2+/Mn2+/Mg2+-ATPase activity markedly inhibited by both Cd2+ and the transition-state analogue orthovanadate. Biochem J *371*, 451-462.

Balakrishnan, L., Hughes, C., and Koronakis, V. (2001). Substrate-triggered recruitment of the TolC channel-tunnel during type I export of hemolysin by Escherichia coli. J Mol Biol *313*, 501-510.

Barroga, C. F., Zhang, H., Wajih, N., Bouyer, J. H., and Hermodson, M. A. (1996). The proteins encoded by the rbs operon of Escherichia coli: I. Overproduction, purification, characterization, and functional analysis of RbsA. Protein Sci *5*, 1093-1099.

Baumann, U., Wu, S., Flaherty, K. M., and McKay, D. B. (1993). Three-dimensional structure of the alkaline protease of Pseudomonas aeruginosa: a two-domain protein with a calcium binding parallel beta roll motif. Embo J *12*, 3357-3364.

Baykov, A. A., Evtushenko, O. A., and Avaeva, S. M. (1988). A malachite green procedure for orthophosphate determination and its use in alkaline phosphatase-based enzyme immunoassay. Anal Biochem *171*, 266-270.

Benabdelhak, H., Kiontke, S., Horn, C., Ernst, R., Blight, M. A., Holland, I. B., and Schmitt, L. (2003). A specific interaction between the NBD of the ABC-transporter HlyB and a C-terminal fragment of its transport substrate haemolysin A. J Mol Biol *327*, 1169-1179.

Benabdelhak, H., Schmitt, L., Horn, C., Jumel, K., Blight, M. A., and Holland, I. B. (2005). Positive co-operative activity and dimerization of the isolated ABC ATPase domain of HlyB from Escherichia coli. Biochem J *386*, 489-495.

Berchtold, H., Reshetnikova, L., Reiser, C. O., Schirmer, N. K., Sprinzl, M., and Hilgenfeld, R. (1993). Crystal structure of active elongation factor Tu reveals major domain rearrangements. Nature *365*, 126-132.

Bergfors, T. (2003). Seeds to crystals. J Struct Biol *142*, 66-76.

Biswas-Fiss, E. E. (2003). Functional analysis of genetic mutations in nucleotide binding domain 2 of the human retina specific ABC transporter. Biochemistry *42*, 10683-10696.

Blight, M. A., Pimenta, A. L., Lazzaroni, J. C., Dando, C., Kotelevets, L., Seror, S. J., and Holland, I. B. (1994). Identification and preliminary characterization of temperature-sensitive mutations affecting HlyB, the translocator required for the secretion of haemolysin (HlyA) from Escherichia coli. Mol Gen Genet *245*, 431-440.

Blott, E. J., Higgins, C. F., and Linton, K. J. (1999). Cysteine-scanning mutagenesis provides no evidence for the extracellular accessibility of the nucleotide-binding domains of the multidrug resistance transporter P-glycoprotein. Embo J *18*, 6800-6808.

Boehm, D. F., Welch, R. A., and Snyder, I. S. (1990). Calcium is required for binding of Escherichia coli hemolysin (HlyA) to erythrocyte membranes. Infect Immun *58*, 1951-1958.

Bolhuis, H., van Veen, H. W., Molenaar, D., Poolman, B., Driessen, A. J., and Konings, W. N. (1996). Multidrug resistance in Lactococcus lactis: evidence for ATP-dependent drug extrusion from the inner leaflet of the cytoplasmic membrane. Embo J *15*, 4239-4245.

Brunger, A. T. (1993). Assessment of phase accuracy by cross validation: the free R value. Methods and applications. Acta Crystallogr D Biol Crystallogr *49*, 24-36.

Brunger, A. T., Adams, P. D., Clore, G. M., DeLano, W. L., Gros, P., Grosse-Kunstleve, R. W., Jiang, J. S., Kuszewski, J., Nilges, M., Pannu, N. S., Read, R. J., Rice, L. M., Simonson, T., and Warren, G. L. (1998). Crystallography & NMR system: A new software suite for macromolecular structure determination. Acta Crystallogr D Biol Crystallogr *54 (Pt 5)*, 905-921.

Burns, D. L. (2003). Type IV transporters of pathogenic bacteria. Curr Opin Microbiol *6*, 29-34.

Calderone, V., Berni, R., and Zanotti, G. (2003). High-resolution structures of retinol-binding protein in complex with retinol: pH-induced protein structural changes in the crystal state. J Mol Biol *329*, 841-850.

Carter, C. W., Jr., and Carter, C. W. (1979). Protein crystallization using incomplete factorial experiments. J Biol Chem *254*, 12219-12223.

Chang, G. (2003). Structure of MsbA from Vibrio cholera: a multidrug resistance ABC transporter homolog in a closed conformation. J Mol Biol *330*, 419-430.

Chang, G., and Roth, C. B. (2001). Structure of MsbA from E. coli: a homolog of the multidrug resistance ATP binding cassette (ABC) transporters. Science *293*, 1793-1800.

Chang, X. B., Hou, Y. X., and Riordan, J. R. (1997). ATPase activity of purified multidrug resistance-associated protein. J Biol Chem *272*, 30962-30968.

Charkowski, A. O., Huang, H. C., and Collmer, A. (1997). Altered localization of HrpZ in Pseudomonas syringae pv. syringae hrp mutants suggests that different components of the type III secretion pathway control protein translocation across the inner and outer membranes of gram-negative bacteria. J Bacteriol *179*, 3866-3874.

Chen, C. A., and Cowan, J. A. (2003). Characterization of the soluble domain of the ABC7 type transporter Atm1. J Biol Chem *278*, 52681-52688.

Chen, J., Lu, G., Lin, J., Davidson, A. L., and Quiocho, F. A. (2003). A tweezers-like motion of the ATP-binding cassette dimer in an ABC transport cycle. Mol Cell *12*, 651-661.

China, B., and Goffaux, F. (1999). Secretion of virulence factors by Escherichia coli. Vet Res *30*, 181-202.

Christie, P. J., and Vogel, J. P. (2000). Bacterial type IV secretion: conjugation systems adapted to deliver effector molecules to host cells. Trends Microbiol *8*, 354-360.

Collaborative computational project, N. (1994). The CCP4 suite: programs for protein crystallography. Acta Crystallographica Section D *50*, 760-763.

Coote, J. G. (1992). Structural and functional relationships among the RTX toxin determinants of gram-negative bacteria. FEMS Microbiol Rev *8*, 137-161.

Cotten, J. F., Ostedgaard, L. S., Carson, M. R., and Welsh, M. J. (1996). Effect of cystic fibrosis-associated mutations in the fourth intracellular loop of cystic fibrosis transmembrane conductance regulator. J Biol Chem *271*, 21279-21284.

Crameri, A., Whitehorn, E. A., Tate, E., and Stemmer, W. P. (1996). Improved green fluorescent protein by molecular evolution using DNA shuffling. Nat Biotechnol *14*, 315-319.

Csanady, L., and Gadsby, D. C. (1999). CFTR channel gating: incremental progress in irreversible steps. J Gen Physiol *114*, 49-53.

Cserzo, M., Wallin, E., Simon, I., von Heijne, G., and Elofsson, A. (1997). Prediction of transmembrane alpha-helices in prokaryotic membrane proteins: the dense alignment surface method. Protein Eng *10*, 673-676.

Cudney, R., Patel, S., Weisgraber, K., Newhouse, Y., and McPherson, A. (1994). Screening and optimization strategies for macromolecular crystal growth. Acta Crystallogr D Biol Crystallogr *50*, 414-423.

Currier, S. J., Kane, S. E., Willingham, M. C., Cardarelli, C. O., Pastan, I., and Gottesman, M. M. (1992). Identification of residues in the first cytoplasmic loop of P-glycoprotein involved in the function of chimeric human MDR1-MDR2 transporters. J Biol Chem *267*, 25153-25159.

Dall'Acqua, W., and Carter, P. (2000). Substrate-assisted catalysis: molecular basis and biological significance. Protein Sci *9*, 1-9.

Datta, S., Ganesh, N., Chandra, N. R., Muniyappa, K., and Vijayan, M. (2003). Structural studies on MtRecA-nucleotide complexes: insights into DNA and nucleotide binding and the structural signature of NTP recognition. Proteins *50*, 474-485.

Dauter, Z. (2002). New approaches to high-throughput phasing. Curr Opin Struct Biol *12*, 674-678.

Davidson, A. L. (2002). Mechanism of coupling of transport to hydrolysis in bacterial ATP-binding cassette transporters. J Bacteriol *184*, 1225-1233.

Davidson, A. L., and Chen, J. (2004). ATP-binding cassette transporters in bacteria. Annu Rev Biochem *73*, 241-268.

Davidson, A. L., Laghaeian, S. S., and Mannering, D. E. (1996). The maltose transport system of Escherichia coli displays positive cooperativity in ATP hydrolysis. J Biol Chem *271*, 4858-4863.

Davidson, A. L., and Sharma, S. (1997). Mutation of a single MalK subunit severely impairs maltose transport activity in Escherichia coli. J Bacteriol *179*, 5458-5464.

Davidson, A. L., Shuman, H. A., and Nikaido, H. (1992). Mechanism of maltose transport in Escherichia coli: transmembrane signaling by periplasmic binding proteins. Proc Natl Acad Sci U S A *89*, 2360-2364.

Diederichs, K., Diez, J., Greller, G., Muller, C., Breed, J., Schnell, C., Vonrhein, C., Boos, W., and Welte, W. (2000). Crystal structure of MalK, the ATPase subunit of the trehalose/maltose ABC transporter of the archaeon Thermococcus litoralis. Embo J *19*, 5951-5961.

Doudna, J. A., Grosshans, C., Gooding, A., and Kundrot, C. E. (1993). Crystallization of ribozymes and small RNA motifs by a sparse matrix approach. Proc Natl Acad Sci U S A *90*, 7829-7833.

Drenth, J. (1999). Principles of Protein X-ray Crystallography (Heidelberg, Springer Verlag Publishing).

Ehrmann, M., Ehrle, R., Hofmann, E., Boos, W., and Schlosser, A. (1998). The ABC maltose transporter. Mol Microbiol *29*, 685-694.

Ferre-D'Amare, A. R., and Burley, S. K. (1994). Use of dynamic light scattering to assess crystallizability of macromolecules and macromolecular assemblies. Structure *2*, 357-359.

Fersht, A. (1999). Structure and Mechanism in Protein Science: A Guide to Enzyme Catalysis and Protein Folding (New York, WH Freeman and Company).

Fetsch, E. E., and Davidson, A. L. (2002). Vanadate-catalyzed photocleavage of the signature motif of an ATP-binding cassette (ABC) transporter. Proc Natl Acad Sci U S A *99*, 9685-9690.

Fitzgerald, P. (1988). MERLOT, an integrated package of computer programs for the determination of crystal structures by molecular replacement. Journal of Applied Crystallography *21*, 273-278.

Fortelle, E. L., and Bricogne, G. (1997). Maximum-Likelihood Heavy-Atom Parameter Refinement for Multiple Isomorphous Replacememt and Multiwavelength Anomalous Diffraction Methods. Methods in Enzymology *276*, 472-494.

Furey, W., and Swaminathan, S. (1997). PHASES-95: A program package for the processing and analysis of diffraction data from macromolecules. In Methods Enzymol: Macromolecular Crystallography Part B, C. Carter, and R. Sweet, eds. (Orlando, Fl., Academic Press).

Gaudet, R., and Wiley, D. C. (2001). Structure of the ABC ATPase domain of human TAP1, the transporter associated with antigen processing. Embo J *20*, 4964-4972.

Geourjon, C., Orelle, C., Steinfels, E., Blanchet, C., Deleage, G., Di Pietro, A., and Jault, J. M. (2001). A common mechanism for ATP hydrolysis in ABC transporter and helicase superfamilies. Trends Biochem Sci *26*, 539-544.

Gottesman, M. M., and Pastan, I. (1993). Biochemistry of multidrug resistance mediated by the multidrug transporter. Annu Rev Biochem *62*, 385-427.

Groeger, W., and Koster, W. (1998). Transmembrane topology of the two FhuB domains representing the hydrophobic components of bacterial ABC transporters involved in the uptake of siderophores, haem and vitamin B12. Microbiology *144 (Pt 10)*, 2759-2769.

Guan, Y., Manuel, R. C., Arvai, A. S., Parikh, S. S., Mol, C. D., Miller, J. H., Lloyd, S., and Tainer, J. A. (1998). MutY catalytic core, mutant and bound adenine structures define specificity for DNA repair enzyme superfamily. Nat Struct Biol *5*, 1058-1064.

Hacker, J., Hughes, C., Hof, H., and Goebel, W. (1983). Cloned hemolysin genes from Escherichia coli that cause urinary tract infection determine different levels of toxicity in mice. Infect Immun *42*, 57-63.

Hardie, K. R., Issartel, J. P., Koronakis, E., Hughes, C., and Koronakis, V. (1991). In vitro activation of Escherichia coli prohaemolysin to the mature membrane-targeted toxin requires HlyC and a low molecular-weight cytosolic polypeptide. Mol Microbiol *5*, 1669-1679.

Henderson, I. R., and Nataro, J. P. (2001). Virulence functions of autotransporter proteins. Infect Immun *69*, 1231-1243.

Hendrickson, W. A., Horton, J. R., and LeMaster, D. M. (1990). Selenomethionyl proteins produced for analysis by multiwavelength anomalous diffraction (MAD): a vehicle for direct determination of three-dimensional structure. Embo J *9*, 1665-1672.

Hendrickson, W. A., and Ogata, C. M. (1997). Phase determination from multiwavelength anomalous diffraction measurements. In Meth. Enzymol, pp. 494-523.

Higgins, C. F. (1992). ABC transporters: from microorganisms to man. Annu Rev Cell Biol *8*, 67-113.

Higgins, C. F., Hiles, I. D., Salmond, G. P., Gill, D. R., Downie, J. A., Evans, I. J., Holland, I. B., Gray, L., Buckel, S. D., Bell, A. W., and Hermodson, M. A. (1986). A family of related ATP-binding subunits coupled to many distinct biological processes in bacteria. Nature *323*, 448-450.

Hobson, A. C., Weatherwax, R., and Ames, G. F. (1984). ATP-binding sites in the membrane components of histidine permease, a periplasmic transport system. Proc Natl Acad Sci U S A *81*, 7333-7337.

Hodel, A., Kim, S.-H., and Brunger, A. T. (1992). Model bias in macromolecular crystal structures. Acta Crystallographica Section A *48*, 851-858.

Hofmann, K., and Stoffel, W. (1993). TMbase - A database of membrane spanning proteins segments. Biological chemistry *374*, 166.

Holland, I. B. (2003). Introduction to Bacterial ABC proteins. In ABC proteins: from bacteria to man, I. B. Holland, S. P. C. Cole, K. Kuchler, and C. F. Higgins, eds. (London, Academic Press (Elsevier Science)), pp. 149-155.

Holland, I. B., Benabdelhak, H., Young, J., Pimenta, A. L., Schmitt, L., and Blight, M. (2003). Bacterial ABC transporters involved in protein translocation. In ABC proteins: from bacteria to man, I. B. Holland, S. P. C. Cole, K. Kuchler, and C. F. Higgins, eds. (London, Academic Press (Elsevier Science)), pp. 209-241.

Holland, I. B., and Blight, M. A. (1999). ABC-ATPases, adaptable energy generators fuelling transmembrane movement of a variety of molecules in organisms from bacteria to humans. J Mol Biol *293*, 381-399.

Hopfner, K. P., Karcher, A., Shin, D. S., Craig, L., Arthur, L. M., Carney, J. P., and Tainer, J. A. (2000). Structural biology of Rad50 ATPase: ATP-driven conformational control in DNA double-strand break repair and the ABC-ATPase superfamily. Cell *101*, 789-800.

Horn, C., Bremer, E., and Schmitt, L. (2003). Nucleotide dependent monomer/dimer equilibrium of OpuAA, the nucleotide-binding protein of the osmotically regulated ABC transporter OpuA from Bacillus subtilis. J Mol Biol *334*, 403-419.

Hosfield, D. J., Guan, Y., Haas, B. J., Cunningham, R. P., and Tainer, J. A. (1999). Structure of the DNA repair enzyme endonuclease IV and its DNA complex: double-nucleotide flipping at abasic sites and three-metal-ion catalysis. Cell *98*, 397-408.

Hueck, C. J. (1998). Type III protein secretion systems in bacterial pathogens of animals and plants. Microbiol Mol Biol Rev *62*, 379-433.

Hung, L. W., Wang, I. X., Nikaido, K., Liu, P. Q., Ames, G. F., and Kim, S. H. (1998). Crystal structure of the ATP-binding subunit of an ABC transporter. Nature *396*, 703-707.

Hunke, S., Mourez, M., Jehanno, M., Dassa, E., and Schneider, E. (2000). ATP modulates subunit-subunit interactions in an ATP-binding cassette transporter (MalFGK2) determined by site-directed chemical cross-linking. J Biol Chem *275*, 15526-15534.

Issartel, J. P., Koronakis, V., and Hughes, C. (1991). Activation of Escherichia coli prohaemolysin to the mature toxin by acyl carrier protein-dependent fatty acylation. Nature *351*, 759-761.

Janas, E., Hofacker, M., Chen, M., Gompf, S., van der Does, C., and Tampe, R. (2003). The ATP hydrolysis cycle of the nucleotide-binding domain of the mitochondrial ATP-binding cassette transporter Mdl1p. J Biol Chem *278*, 26862-26869.

Jancarik, J., and Kim, S.-H. (1991). Sparse matrix sampling: a screening method for crystallization of proteins. Journal of Applied Crystallography *24*, 409-411.

Jones, P. M., and George, A. M. (2002). Mechanism of ABC transporters: a molecular dynamics simulation of a well characterized nucleotide-binding subunit. Proc Natl Acad Sci U S A *99*, 12639-12644.

Jones, T. A., Zou, J. Y., Cowan, S. W., and Kjeldgaard (1991). Improved methods for building protein models in electron density maps and the location of errors in these models. Acta Crystallogr A *47 (Pt 2)*, 110-119.

Juranka, P., Zhang, F., Kulpa, J., Endicott, J., Blight, M., Holland, I. B., and Ling, V. (1992). Characterization of the hemolysin transporter, HlyB, using an epitope insertion. J Biol Chem *267*, 3764-3770.

Kaplan, W., and Littlejohn, T. G. (2001). Swiss-PDB Viewer (Deep View). Brief Bioinform *2*, 195-197.

Karcher, A., Buttner, K., Martens, B., Jansen, R. P., and Hopfner, K. P. (2005). X-ray structure of RLI, an essential twin cassette ABC ATPase involved in ribosome biogenesis and HIV capsid assembly. Structure (Camb) *13*, 649-659.

Karpowich, N., Martsinkevich, O., Millen, L., Yuan, Y. R., Dai, P. L., MacVey, K., Thomas, P. J., and Hunt, J. F. (2001). Crystal structures of the MJ1267 ATP binding cassette reveal an induced-fit effect at the ATPase active site of an ABC transporter. Structure (Camb) *9*, 571-586.

Kerr, I. D. (2002). Structure and association of ATP-binding cassette transporter nucleotide-binding domains. Biochim Biophys Acta *1561*, 47-64.

Kerr, I. D., Berridge, G., Linton, K. J., Higgins, C. F., and Callaghan, R. (2003). Definition of the domain boundaries is critical to the expression of the nucleotide-binding domains of P-glycoprotein. Eur Biophys J *32*, 644-654.

Kissinger, C. R., Gehlhaar, D. K., and Fogel, D. B. (1999). Rapid automated molecular replacement by evolutionary search. Acta Crystallogr D Biol Crystallogr *55 (Pt 2)*, 484-491.

Kleywegt, G. J. (1996). Use of Non-crystallographic Symmetry in Protein Structure Refinement. Acta Crystallogr D Biol Crystallogr *52*, 842-857.

Koronakis, E., Hughes, C., Milisav, I., and Koronakis, V. (1995). Protein exporter function and in vitro ATPase activity are correlated in ABC-domain mutants of HlyB. Mol Microbiol *16*, 87-96.

Koronakis, V., Andersen, C., and Hughes, C. (2001). Channel-tunnels. Curr Opin Struct Biol *11*, 403-407.

Koronakis, V., and Hughes, C. (1996). Synthesis, maturation and export of the E. coli hemolysin. Med Microbiol Immunol (Berl) *185*, 65-71.

Koronakis, V., Hughes, C., and Koronakis, E. (1993). ATPase activity and ATP/ADP-induced conformational change in the soluble domain of the bacterial protein translocator HlyB. Mol Microbiol *8*, 1163-1175.

Koronakis, V., Sharff, A., Koronakis, E., Luisi, B., and Hughes, C. (2000). Crystal structure of the bacterial membrane protein TolC central to multidrug efflux and protein export. Nature *405*, 914-919.

Koshland, D. E., Jr., Nemethy, G., and Filmer, D. (1966). Comparison of experimental binding data and theoretical models in proteins containing subunits. Biochemistry *5*, 365-385.

Kranitz, L., Benabdelhak, H., Horn, C., Blight, M. A., Holland, I. B., and Schmitt, L. (2002). Crystallization and preliminary X-ray analysis of the ATP-binding domain of the ABC transporter haemolysin B from Escherichia coli. Acta Crystallogr D Biol Crystallogr *58*, 539-541.

Kraulis, P. (1991). Molscript: a program to produce both detailed and schematic plots of proteins. J Appl Crystallogr *24*, 946–950.

Kruh, G. D., Zeng, H., Rea, P. A., Liu, G., Chen, Z. S., Lee, K., and Belinsky, M. G. (2001). MRP subfamily transporters and resistance to anticancer agents. J Bioenerg Biomembr *33*, 493-501.

Laemmli, U. K. (1970). Cleavage of structural proteins during the assembly of the head of bacteriophage T4. Nature *227*, 680-685.

Lamzin, V. S. (1993). Automated refinement of protein models. Acta Crystallogr D Biol Crystallogr *49*, 129-147.

Laskowski, R. A., MacArthur, M. W., Moss, D. S., and Thornton, J. M. (1993). PROCHECK: a program to check the stereochemical quality of protein structures. J Appl Crystallogr *26*, 283-291.

Lawrence, M. C., and Colman, P. M. (1993). Shape complementarity at protein/protein interfaces. J Mol Biol *234*, 946-950.

Lebbink, J. H., and Sixma, T. K. (2005). Variations on the ABC. Structure (Camb) *13*, 498-500.

Lee, V. T., and Schneewind, O. (2001). Protein secretion and the pathogenesis of bacterial infections. Genes Dev *15*, 1725-1752.

Lewis, H. A., Buchanan, S. G., Burley, S. K., Conners, K., Dickey, M., Dorwart, M., Fowler, R., Gao, X., Guggino, W. B., Hendrickson, W. A., Hunt, J. F., Kearins, M. C., Lorimer, D., Maloney, P. C., Post, K. W., Rajashankar, K. R., Rutter, M. E., Sauder, J. M., Shriver, S., Thibodeau, P. H., Thomas, P. J., Zhang, M., Zhao, X., and Emtage, S. (2004). Structure of nucleotide-binding domain 1 of the cystic fibrosis transmembrane conductance regulator. Embo J *23*, 282-293.

Liao, J.-C., and Oster, G. (2004). The engines of biomolecular motors. Proceedings of NANO2004 Integrated Nanosystems: Design, Synthesis and Applications.

Lim, K. B., Walker, C. R., Guo, L., Pellett, S., Shabanowitz, J., Hunt, D. F., Hewlett, E. L., Ludwig, A., Goebel, W., Welch, R. A., and Hackett, M. (2000). Escherichia coli alpha-hemolysin (HlyA) is heterogeneously acylated in vivo with 14-, 15-, and 17-carbon fatty acids. J Biol Chem *275*, 36698-36702.

Linton, K. J., and Higgins, C. F. (1998). The Escherichia coli ATP-binding cassette (ABC) proteins. Mol Microbiol *28*, 5-13.

Litman, T., Druley, T. E., Stein, W. D., and Bates, S. E. (2001). From MDR to MXR: new understanding of multidrug resistance systems, their properties and clinical significance. Cell Mol Life Sci *58*, 931-959.

Liu, C. E., Liu, P. Q., and Ames, G. F. (1997). Characterization of the adenosine triphosphatase activity of the periplasmic histidine permease, a traffic ATPase (ABC transporter). J Biol Chem *272*, 21883-21891.

Lobo, A. L., and Welch, R. A. (1994). Identification and assay of RTX family of cytolysins. Methods Enzymol *235*, 667-678.

Locher, K. P. (2004). Structure and mechanism of ABC transporters. Curr Opin Struct Biol *14*, 426-431.

Locher, K. P., and Borths, E. (2004). ABC transporter architecture and mechanism: implications from the crystal structures of BtuCD and BtuF. FEBS Lett *564*, 264-268.

Locher, K. P., Lee, A. T., and Rees, D. C. (2002). The E. coli BtuCD structure: a framework for ABC transporter architecture and mechanism. Science *296*, 1091-1098.

Loo, T. W., and Clarke, D. M. (1996). Inhibition of oxidative cross-linking between engineered cysteine residues at positions 332 in predicted transmembrane segments (TM) 6 and 975 in predicted TM12 of human P-glycoprotein by drug substrates. J Biol Chem *271*, 27482-27487.

Ludwig, A., Vogel, M., and Goebel, W. (1987). Mutations affecting activity and transport of haemolysin in Escherichia coli. Mol Gen Genet *206*, 238-245.

McPherson, A. (1985). Crystallization of macromolecules: general principles. Methods Enzymol *114*, 112-120.

McPherson, A. (1999). Crystallization of Biological Macromolecules (New York, Cold Spring Harbor Laboratory Press).

McPherson, A. (2001). A comparison of salts for the crystallization of macromolecules. Protein Sci *10*, 418-422.

McRee, D. E. (1999). XtalView/Xfit--A versatile program for manipulating atomic coordinates and electron density. J Struct Biol *125*, 156-165.

Mendez, C., and Salas, J. A. (2001). The role of ABC transporters in antibiotic-producing organisms: drug secretion and resistance mechanisms. Res Microbiol *152*, 341-350.

Menestrina, G., Moser, C., Pellet, S., and Welch, R. (1994). Pore-formation by Escherichia coli hemolysin (HlyA) and other members of the RTX toxins family. Toxicology *87*, 249-267.

Mikael, L. G., Pawelek, P. D., Labrie, J., Sirois, M., Coulton, J. W., and Jacques, M. (2002). Molecular cloning and characterization of the ferric hydroxamate uptake (fhu) operon in Actinobacillus pleuropneumoniae. Microbiology *148*, 2869-2882.

Mitaku, G. Classification and Secondary Structure Prediction of Membrane Proteins (Tokyo).

Monod, J., Wyman, J., and Changeux, J. P. (1965). On the Nature of Allosteric Transitions: A Plausible Model. J Mol Biol *12*, 88-118.

Moody, J. E., Millen, L., Binns, D., Hunt, J. F., and Thomas, P. J. (2002). Cooperative, ATP-dependent association of the nucleotide binding cassettes during the catalytic cycle of ATP-binding cassette transporters. J Biol Chem *277*, 21111-21114.

Mourez, M., Hofnung, M., and Dassa, E. (1997). Subunit interactions in ABC transporters: a conserved sequence in hydrophobic membrane proteins of periplasmic permeases defines an important site of interaction with the ATPase subunits. Embo J *16*, 3066-3077.

Murshudov, G. N., Vagin, A. A., and Dodson, E. (1997). Refinement of macromolecular structures by the maximum-likelihood method. Acta Crystallogr D Biol Crystallogr *53*, 240-255.

Navaza, J. (1994). AMoRe: an automated package for molecular replacement. Acta Crystallographica Section A *50*, 157-163.

Nicaud, J. M., Mackman, N., Gray, L., and Holland, I. B. (1985). Characterisation of HlyC and mechanism of activation and secretion of haemolysin from E. coli 2001. FEBS Lett *187*, 339-344.

Nikaido, K., and Ames, G. F. (1999). One intact ATP-binding subunit is sufficient to support ATP hydrolysis and translocation in an ABC transporter, the histidine permease. J Biol Chem *274*, 26727-26735.

Nikaido, K., Liu, P. Q., and Ames, G. F. (1997). Purification and characterization of HisP, the ATP-binding subunit of a traffic ATPase (ABC transporter), the histidine permease of Salmonella typhimurium. Solubility, dimerization, and ATPase activity. J Biol Chem *272*, 27745-27752.

Orelle, C., Dalmas, O., Gros, P., Di Pietro, A., and Jault, J. M. (2003). The conserved glutamate residue adjacent to the Walker-B motif is the catalytic base for ATP hydrolysis in the ATP-binding cassette transporter BmrA. J Biol Chem *278*, 47002-47008.

Otwinowski, Z. (1991). Maximum likelihood refinement of heavy atom parameters. In Isomorphous Replacement and Anomalous Scattering. Proceedings of the CCP4 Study Weekend., W. Wolf, P. R. Evans, and A. G. W. Leslie, eds. (Warrington, UK, Warrington: Daresbury Laboratory), pp. 80-85.

Otwinowski, Z., and Minor, W. (1997). Processing of X-ray diffraction data collected in oscillation mode. In Methods in Enzymology, C. J. Carter, and R. Sweet, eds. (New York, Academic Press), pp. 307-326.

Padilla, J. E., and Yeates, T. O. (2003). A statistic for local intensity differences: robustness to anisotropy and pseudo-centering and utility for detecting twinning. Acta Crystallogr D Biol Crystallogr *59*, 1124-1130.

Pai, E. F., Krengel, U., Petsko, G. A., Goody, R. S., Kabsch, W., and Wittinghofer, A. (1990). Refined crystal structure of the triphosphate conformation of H-ras p21 at 1.35 A resolution: implications for the mechanism of GTP hydrolysis. Embo J *9*, 2351-2359.

Perrakis, A., Sixma, T. K., Wilson, K. S., and Lamzin, V. S. (1997). wARP: improvement and extension of crystallographic phases by weighted averaging of multiple-refined dummy atomic models. Acta Crystallogr D Biol Crystallogr *53*, 448-455.

Pflugrath, J. W. (1999). The finer things in X-ray diffraction data collection. Acta Crystallogr D Biol Crystallogr *55 (Pt 10)*, 1718-1725.

Pimenta, A. L., Young, J., Holland, I. B., and Blight, M. A. (1999). Antibody analysis of the localisation, expression and stability of HlyD, the MFP component of the E. coli haemolysin translocator. Mol Gen Genet *261*, 122-132.

Poelarends, G. J., Mazurkiewicz, P., and Konings, W. N. (2002). Multidrug transporters and antibiotic resistance in Lactococcus lactis. Biochim Biophys Acta *1555*, 1-7.

Read, R. (1986). Improved Fourier coefficients for maps using phases from partial structures with errors. Acta Crystallographica Section A *42*, 140-149.

Read, R. J., and Schierbeek, A. J. (1988). A phased translation function. Journal of Applied Crystallography *21*, 490-495.

Reyes, C. L., and Chang, G. (2005). Structure of the ABC transporter MsbA in complex with ADP.vanadate and lipopolysaccharide. Science *308*, 1028-1031.

Riordan, J. R., Rommens, J. M., Kerem, B., Alon, N., Rozmahel, R., Grzelczak, Z., Zielenski, J., Lok, S., Plavsic, N., Chou, J. L., and et al. (1989). Identification of the cystic fibrosis gene: cloning and characterization of complementary DNA. Science *245*, 1066-1073.

Rodgers, D. W. (1994). Cryocrystallography. Structure *2*, 1135-1140.

Rosenberg, M. F., Callaghan, R., Ford, R. C., and Higgins, C. F. (1997). Structure of the multidrug resistance P-glycoprotein to 2.5 nm resolution determined by electron microscopy and image analysis. J Biol Chem *272*, 10685-10694.

Russel, M. (1998). Macromolecular assembly and secretion across the bacterial cell envelope: type II protein secretion systems. J Mol Biol *279*, 485-499.

Saridakis, E., Dierks, K., Moreno, A., Dieckmann, M. W., and Chayen, N. E. (2002). Separating nucleation and growth in protein crystallization using dynamic light scattering. Acta Crystallogr D Biol Crystallogr *58*, 1597-1600.

Sauna, Z. E., Muller, M., Peng, X. H., and Ambudkar, S. V. (2002). Importance of the conserved Walker B glutamate residues, 556 and 1201, for the completion of the catalytic cycle of ATP hydrolysis by human P-glycoprotein (ABCB1). Biochemistry *41*, 13989-14000.

Sauna, Z. E., Smith, M. M., Muller, M., Kerr, K. M., and Ambudkar, S. V. (2001). The mechanism of action of multidrug-resistance-linked P-glycoprotein. J Bioenerg Biomembr *33*, 481-491.

Sawaya, M. R., Guo, S., Tabor, S., Richardson, C. C., and Ellenberger, T. (1999). Crystal structure of the helicase domain from the replicative helicase-primase of bacteriophage T7. Cell *99*, 167-177.

Scheffel, F., Demmer, U., Warkentin, E., Hulsmann, A., Schneider, E., and Ermler, U. (2005). Structure of the ATPase subunit CysA of the putative sulfate ATP-binding cassette (ABC) transporter from Alicyclobacillus acidocaldarius. FEBS Lett *579*, 2953-2958.

Schlor, S., Schmidt, A., Maier, E., Benz, R., Goebel, W., and Gentschev, I. (1997). In vivo and in vitro studies on interactions between the components of the hemolysin (HlyA) secretion machinery of Escherichia coli. Mol Gen Genet *256*, 306-319.

Schmees, G., Honer zu Bentrup, K., Schneider, E., Vinzenz, D., and Ermler, U. (1999). Crystallization and preliminary X-ray analysis of the bacterial ATP-binding-cassette (ABC) protein MalK. Acta Crystallogr D Biol Crystallogr *55 (Pt 1)*, 285-286.

Schmitt, L., Benabdelhak, H., Blight, M. A., Holland, I. B., and Stubbs, M. T. (2003). Crystal structure of the nucleotide-binding domain of the ABC-transporter haemolysin B: identification of a variable region within ABC helical domains. J Mol Biol *330*, 333-342.

Schmitt, L., and Tampe, R. (2000). Affinity, specificity, diversity: a challenge for the ABC transporter TAP in cellular immunity. Chembiochem *1*, 16-35.

Schmitt, L., and Tampe, R. (2002). Structure and mechanism of ABC transporters. Curr Opin Struct Biol *12*, 754-760.

Senior, A. E., al-Shawi, M. K., and Urbatsch, I. L. (1995). The catalytic cycle of P-glycoprotein. FEBS Lett *377*, 285-289.

Sharff, A., Fanutti, C., Shi, J., Calladine, C., and Luisi, B. (2001). The role of the TolC family in protein transport and multidrug efflux. From stereochemical certainty to mechanistic hypothesis. Eur J Biochem *268*, 5011-5026.

Sharma, S., and Davidson, A. L. (2000). Vanadate-induced trapping of nucleotides by purified maltose transport complex requires ATP hydrolysis. J Bacteriol *182*, 6570-6576.

Sheldrick, G. (1990). Phase annealing in SHELX-90: direct methods for larger structures. Acta Crystallographica Section A *46*, 467-473.

Sheldrick, G. M. (1996). High resolution structure refinement. In Proceedings from the Macromolecular Crystallography Computing School: Crystallographic Computing 7, P. E. Bourne, and K. Watenpaugh, eds. (Western Washington University, WA, USA).

Sheldrick, G. M. (1998). SHELX: applications to macromolecules. In Direct methods for solving macromolecular structures, S. Fortier, ed. (Dordrecht, Kluwer Academic Publishers), pp. 401-411.

Shyamala, V., Baichwal, V., Beall, E., and Ames, G. F. (1991). Structure-function analysis of the histidine permease and comparison with cystic fibrosis mutations. J Biol Chem *266*, 18714-18719.

Smith, B. J., Lawrence, M. C., and Colman, P. M. (2002a). Modelling the structure of the fusion protein from human respiratory syncytial virus. Protein Eng *15*, 365-371.

Smith, P. C., Karpowich, N., Millen, L., Moody, J. E., Rosen, J., Thomas, P. J., and Hunt, J. F. (2002b). ATP binding to the motor domain from an ABC transporter drives formation of a nucleotide sandwich dimer. Mol Cell *10*, 139-149.

Smith, P. K., Krohn, R. I., Hermanson, G. T., Mallia, A. K., Gartner, F. H., Provenzano, M. D., Fujimoto, E. K., Goeke, N. M., Olson, B. J., and Klenk, D. C. (1985). Measurement of protein using bicinchoninic acid. Anal Biochem *150*, 76-85.

Soloaga, A., Veiga, M. P., Garcia-Segura, L. M., Ostolaza, H., Brasseur, R., and Goni, F. M. (1999). Insertion of Escherichia coli alpha-haemolysin in lipid bilayers as a non-transmembrane integral protein: prediction and experiment. Mol Microbiol *31*, 1013-1024.

Stanley, P., Koronakis, V., and Hughes, C. (1998). Acylation of Escherichia coli hemolysin: a unique protein lipidation mechanism underlying toxin function. Microbiol Mol Biol Rev *62*, 309-333.

Steinke, A., Grau, S., Davidson, A., Hofmann, E., and Ehrmann, M. (2001). Characterization of transmembrane segments 3, 4, and 5 of MalF by mutational analysis. J Bacteriol *183*, 375-381.

Story, R. M., and Steitz, T. A. (1992). Structure of the recA protein-ADP complex. Nature *355*, 374-376.

Stoscheck, C. M. (1990). Quantitation of protein. Methods Enzymol *182*, 50-68.

Sun, H., and Nathans, J. (2001). Mechanistic studies of ABCR, the ABC transporter in photoreceptor outer segments responsible for autosomal recessive Stargardt disease. J Bioenerg Biomembr *33*, 523-530.

Terwilliger, T. C., and Berendzen, J. (1999). Automated MAD and MIR structure solution. Acta Crystallogr D Biol Crystallogr *55 (Pt 4)*, 849-861.

Thanabalu, T., Koronakis, E., Hughes, C., and Koronakis, V. (1998). Substrate-induced assembly of a contiguous channel for protein export from E.coli: reversible bridging of an inner-membrane translocase to an outer membrane exit pore. Embo J *17*, 6487-6496.

Thomas, P. J., and Hunt, J. F. (2001). A snapshot of Nature's favorite pump. Nat Struct Biol *8*, 920-923.

Tombline, G., Bartholomew, L. A., Tyndall, G. A., Gimi, K., Urbatsch, I. L., and Senior, A. E. (2004). Properties of P-glycoprotein with mutations in the "catalytic carboxylate" glutamate residues. J Biol Chem *279*, 46518-46526.

Tong, L., and Rossmann, M. G. (1997). Rotation function calculations with GLRF program. Methods Enzymol *276*, 594-611.

Trent, M. S., Worsham, L. M., and Ernst-Fonberg, M. L. (1998). The biochemistry of hemolysin toxin activation: characterization of HlyC, an internal protein acyltransferase. Biochemistry *37*, 4644-4652.

Tronrud, D. E., Ten Eyck, L. F., and Matthews, B. W. (1987). An efficient general-purpose least-squares refinement program for macromolecular structures. Acta Crystallographica Section A *43*, 489-501.

Urbatsch, I. L., Julien, M., Carrier, I., Rousseau, M. E., Cayrol, R., and Gros, P. (2000). Mutational analysis of conserved carboxylate residues in the nucleotide binding sites of P-glycoprotein. Biochemistry *39*, 14138-14149.

Uson, I., and Sheldrick, G. M. (1999). Advances in direct methods for protein crystallography. Curr Opin Struct Biol *9*, 643-648.

Vagin, A., and Teplyakov, A. (2000). An approach to multi-copy search in molecular replacement. Acta Crystallogr D Biol Crystallogr *56 Pt 12*, 1622-1624.

Van Duyne, G. D., Standaert, R. F., Karplus, P. A., Schreiber, S. L., and Clardy, J. (1993). Atomic structures of the human immunophilin FKBP-12 complexes with FK506 and rapamycin. J Mol Biol *229*, 105-124.

van Gunsteren, W. F., and Berendsen, H. J. C. (1990). Computer simulation of molecular dynamics: Methodology, applications and perspectives in chemistry. Angewandte Chemie International Edition in English *29*, 992–1023.

Verdon, G., Albers, S. V., Dijkstra, B. W., Driessen, A. J., and Thunnissen, A. M. (2003a). Crystal structures of the ATPase subunit of the glucose ABC transporter from Sulfolobus solfataricus: nucleotide-free and nucleotide-bound conformations. J Mol Biol *330*, 343-358.

Verdon, G., Albers, S. V., van Oosterwijk, N., Dijkstra, B. W., Driessen, A. J., and Thunnissen, A. M. (2003b). Formation of the productive ATP-Mg2+-bound dimer of GlcV, an ABC-ATPase from Sulfolobus solfataricus. J Mol Biol *334*, 255-267.

Vergani, P., Lockless, S. W., Nairn, A. C., and Gadsby, D. C. (2005). CFTR channel opening by ATP-driven tight dimerization of its nucleotide-binding domains. Nature *433*, 876-880.

Vetter, I. R., and Wittinghofer, A. (1999). Nucleoside triphosphate-binding proteins: different scaffolds to achieve phosphoryl transfer. Q Rev Biophys *32*, 1-56.

Walker, J. E., Saraste, M., Runswick, M. J., and Gay, N. J. (1982). Distantly related sequences in the alpha- and beta-subunits of ATP synthase, myosin, kinases and other ATP-requiring enzymes and a common nucleotide binding fold. Embo J *1*, 945-951.

Walter, C., Wilken, S., and Schneider, E. (1992). Characterization of site-directed mutations in conserved domains of MalK, a bacterial member of the ATP-binding cassette (ABC) family [corrected]. FEBS Lett *303*, 41-44.

Wang, D. N., Safferling, M., Lemieux, M. J., Griffith, H., Chen, Y., and Li, X. D. (2003). Practical aspects of overexpressing bacterial secondary membrane transporters for structural studies. Biochim Biophys Acta *1610*, 23-36.

Weeks, C. M., and Miller, R. (1999). The design and implementation of SnB version 2.0. Journal of Applied Crystallography *32*, 120-124.

Westlake, C. J., Payen, L., Gao, M., Cole, S. P., and Deeley, R. G. (2004). Identification and characterization of functionally important elements in the multidrug resistance protein 1 COOH-terminal region. J Biol Chem *279*, 53571-53583.

Wiechelman, K. J., Braun, R. D., and Fitzpatrick, J. D. (1988). Investigation of the bicinchoninic acid protein assay: identification of the groups responsible for color formation. Anal Biochem *175*, 231-237.

Winn, M. D., Isupov, M. N., and Murshudov, G. N. (2001). Use of TLS parameters to model anisotropic displacements in macromolecular refinement. Acta Crystallogr D Biol Crystallogr *57*, 122-133.

Yang, J., Yu, M., Jan, Y. N., and Jan, L. Y. (1997). Stabilization of ion selectivity filter by pore loop ion pairs in an inwardly rectifying potassium channel. Proc Natl Acad Sci U S A *94*, 1568-1572.

Yao, J.-X. (1981). On the application of phase relationships to complex structures. XVIII. RANTAN-random MULTAN. Acta Crystallographica Section A *37*, 642-644.

Yuan, Y. R., Blecker, S., Martsinkevich, O., Millen, L., Thomas, P. J., and Hunt, J. F. (2001). The crystal structure of the MJ0796 ATP-binding cassette. Implications for the structural consequences of ATP hydrolysis in the active site of an ABC transporter. J Biol Chem *276*, 32313-32321.

Zaitseva, J., Holland, I. B., and Schmitt, L. (2004). The role of CAPS buffer in expanding the crystallization space of the nucleotide-binding domain of the ABC transporter haemolysin B from Escherichia coli. Acta Crystallogr D Biol Crystallogr *60*, 1076-1084.

Zaitseva, J., Jenewein, S., Jumpertz, T., Holland, I. B., and Schmitt, L. (2005a). H662 is the linchpin of ATP hydrolysis in the nucleotide-binding domain of the ABC transporter HlyB. Embo J *24*, 1901-1910.

Zaitseva, J., Jenewein, S., Wiedenmann, A., Benabdelhak, H., Holland, I. B., and Schmitt, L. (2005b). Functional Characterization and ATP-Induced Dimerization of the Isolated ABC-Domain of the Haemolysin B Transporter. Biochemistry *44*, 9680-9690.

Zaitseva, J., Oswald, C., Jenewein, S., Wiedenmann, A., Holland, I. B., and Schmitt, L. (2005c). The catalytic cycle of the nucleotide-binding domain of the ABC-transporter HlyB. Manuscript in preparation.

Zaitseva, J., Zhang, H., Binnie, R. A., and Hermodson, M. (1996). The proteins encoded by the rbs operon of Escherichia coli: II. Use of chimeric protein constructs to isolate and characterize RbsC. Protein Sci *5*, 1100-1107.

Conclusions and outlook

A simple screening test was utilized to search for the optimal conditions that stabilized the purified NBD in solution. The most optimal buffer, 100 mM CAPS pH 10.4 and 20% glycerol, protected HlyB-NBD from precipitation and allowed to attain high concentration (20-50 mg/ml and higher) of the homogenous and substrate-free HlyB-NBD in solution. The resulting protein sample was suitable for the long term storage on ice and for the reproducible functional assays and provided a starting point for crystallization of HlyB-NBD in the various states of the hydrolytic cycle. The described procedure may also be readily adaptable for other precipitation-prone proteins providing an important prerequisite for their structural studies and functional analysis (Zaitseva *et al.*, 2004).

The nucleotide-binding domain of HlyA transporter, NBD-HlyB, was characterized in regard to its uncoupled ATPase activity, oligomeric state, and stability in solution (Zaitseva *et al.*, 2005b). Experimental data have shown that both the nature and pH of an assay buffer influenced the level of protein activity. The highest ATPase activity was detected in HEPES buffer pH 7.0. Kinetic analysis of ATPase activity in this buffer revealed ATP-induced protein dimerization. Assuming that the dimer is the active form of the protein, at least half of the purified HlyB-NBD was estimated to be a dimer at 1.2 μM enzyme concentration in the most optimal conditions for ATP hydrolysis. The maximum reaction velocity of 0.7 μmol/mg*min and the apparent kinetic constant $K^{app}_{0.5}$ of 0.26 mM for ATP were obtained for the fully dimerized HlyB-NBD. Comparative analysis of protein stability and ATPase activity in various buffers suggested an inverse relationship between the two. Gel-filtration experiments with the H662A-mutant HlyB-NBD and the wild type protein allowed to monitor protein stability and provided further evidence of ATP-induced protein dimerization. In the future, similar gel-filtration experiments could also be employed to monitor specific binding of the allocrite and nucleotides to the target protein and to detect the corresponding changes in stability/oligomeric state of the protein. In particular, a stoichiometry of protein-substrate or protein-allocrite complexes could be tested using fluorescent or radioactive-labeled ATP/ADP and/or HlyA/C-terminal fragment of HlyA. Varying experimental conditions, a correlation for the allocrite and nucleotide effects on the protein could be established. In regard to the target protein, both the NBD-component of HlyB, including the wild type version as well as its

various mutants, and the entire HlyB protein could be studied by SEC experiment to examine protein-protein and protein-substrate interactions.

The wild type HlyB-NBD and the H662A- and E631Q-mutants of HlyB-NBD were crystallized with bound ADP (Zaitseva *et al.*, 2004; Zaitseva *et al.*, 2005c). The wild type protein and its mutants produced crystals diffracting to 1.6 Å-1.9 Å. The phase information for all three proteins with bound ADP was obtained by molecular replacement (MR), using the known structure of apo-HlyB-NBD (Schmitt *et al.*, 2003). All three structures were very similar and represented the monomeric enzyme species. Crystals of H662A-HlyB-NBD dimer were obtained in two other states, with bound ATP and with ATP-Mg^{2+} (Zaitseva *et al.*, 2004; Zaitseva *et al.*, 2005a). Diffraction data were collected for the ATP- and ATP-Mg^{2+}-bound crystals to 2.6 Å and 2.5 Å, respectively. Since initial MR approach failed for these crystals, the phase problem for the ATP-Mg^{2+}-bound protein was solved by a combination of single-wavelength anomalous diffraction (SAD) with seleno-methionine derivative of H662A protein and MR, using the catalytic and the helical domains of the nucleotide-free structure of HlyB-NBD simultaneously. The structure of the HlyB-NBD H662A protein revealed a symmetrical head-to-tail NBD dimer with two ATP- or two ATP-Mg^{2+} molecules sandwiched between the Walker A motif of one subunit and the ABC-signature motif of the other subunit.

Overall structures of the ADP-, ATP-, and ATP-Mg^{2+}-bound states of HlyB-NBD and/or its mutant versions are described. The implications of structural and functional results are discussed with relation to the mechanism of ABC transporters. Another approach to broaden our knowledge of the structure-functional relationships in ABC transporters would be co-crystallization/crystal soaking experiments of HlyB-NBD with the C-terminal binding sequence of the allocrite in the presence/absence of nucleotides. Such studies, which seem straightforward based on the specific binding of HlyB-NBD and HlyA (Benabdelhak *et al.*, 2003), may provide a valuable insight into mechanism of coupling the allocrite transport and ATP hydrolysis in ABC transporters. The results obtained by gel-filtration analysis could be employed to deduce the most promising crystallization experiments. To further expand our understanding of the molecular mechanism of action of ABC proteins, crystallization of various mutant proteins of HlyB-NBD/HlyB in the presence of ATP/ADP/ATP + vanadate/ADP + vanadate/allocrite would be highly desirable.

The most interesting mutations of HlyB-NBD comprise the substitutions in the conserved amino acids, which participate in the intersubunit protein-protein interactions (NBD-NBD and NBD-TMD) and closely approach ATP-binding sites of the transporter, such as the Q-, D-, H-loops, and the Walker B motif. The replacements in the H-loop and the

Walker B motif were described in this work; yet they deserve further investigation to unravel protein-allocrite interactions. The dimer structure of HlyB-NBD protein suggests that the D-loop seems to be an interesting objective when testing NBD dimerization and NBD-NBD communication, since the residues of the D-loop are buried into the NBD-dimer interface contacting all conserved motifs and the C-terminus of the opposite subunit (Chapter 6). Besides, replacement of the conserved aspartate in the D-loop was shown to affect ATPase activity of the NBD component of the histidine transporter (Nikaido and Ames, 1999). Hence, mutation of D637 and of the neighboring amino acids could be useful for the HlyB-NBD investigation as well as for the HlyB study. The Q-loop also participates in the NBD-NBD communication of the HlyB-NBD dimer (Chapter 6). Moreover, the Q-loop was shown to face the transmembrane component of the BtuCD transporter (Locher *et al.*, 2002). Since the Q-loop is located on the dimer surface of HlyB-NBD (Chapter 6), the substitution of Q551 and of the following amino acids of the Q-loop may be primarily essential for NBD-TMD communications being attractive target for crystallization and gel-filtrations studies of the whole HlyB protein.

Zusammenfassung

Der ABC-(<u>A</u>TP-<u>b</u>inding <u>c</u>assette) Transporter Haemolysin B (HlyB) aus *Escherichia coli* (*E coli*) ist ein zentrales Element einer Typ I Sekretionsmaschinerie, die unter Verbrauch von ATP, das Toxin HlyA in einem Schritt über beide Membranen von *E. coli* transportiert. Neben dem Toxin HlyA werden in Gram-negativen Bakterien z. B. Proteasen, Lipasen und S-Layerproteine in diesem von der Sec-Maschinerie unabhängigen Sekretionsmechanismus über biologische Membranen transportiert. In allen Typ I Substraten ist die Information, die für die Sekretion notwendig und ausreichend ist, in den letzten 50 bis 60 C-terminalen Aminosäuren kodiert. Neben dem ABC-Transporter wird das Transportsystem von HlyD, einem Membranfusionsprotein, das wie HlyB in der inneren Membran von *E. coli* lokalisiert ist, und TolC, das sich in der äußeren Membran befindet, gebildet. Deletion einer dieser drei Komponenten verhindert die Substrattranslokation und impliziert, das diese drei Komponenten einen kontinuierlichen Kanal durch die beiden Membranen von *E. coli* und das Periplasma bilden. Ein derartiger Kanal erklärt auch die Abwesenheit periplasmatischer Transportintermediate.

ABC-Transporter sind ATP-abhängige Transporter, Kanäle und Rezeptoren, die in allen Bereichen des Lebens gefunden werden. Seit ihrer Entdeckung im Jahre 1982 ist die Familie dieser Membranproteine kontinuierlich gestiegen. So werden z. B. in *E. coli* 78, in Hefe 31 und im menschlichen Genom 49 ABC-Transporter kodiert. Die Klassifizierung der ABC-Transporter basiert einzig und allein auf ihrer Primärsequenz. Im Falle von ABC-Transportern müssen die folgenden konservierten Bereiche vorhanden sein. Erstens das Walker A und B Motiv, Konsensussequenz GXXGX(G)KST, wobei X jede beliebige Aminosäure darstellt (Walker A) und ΦΦΦΦD, wobei Φ jede hydrophobe Aminosäure darstellt (Walker B). Zweitens die C-Schleife oder das Signaturmotiv, Konsensussequenz LSGGQ und die D-Schleife, Konsensussequenz SALD. Des Weiteren muss eine hydrophobe Domäne oder Untereinheit vorhanden sein. Die C-Schleife stellt hierbei das wichtigste diagnostische Motiv für ABC-Transporter dar.

Trotz der Vielzahl von Substraten, die von ABC-Transportern importiert oder exportiert werden, besitzen alle Vertreter dieser Familie denselben modularen Aufbau aus zwei <u>T</u>rans<u>m</u>embran<u>d</u>omänen (TMD) und zwei <u>N</u>ukleotid<u>b</u>indenden <u>D</u>omänen (NBD). Diese Module treten entweder separat, als Fusion einer TMD und einer NBD („*half-size*

transporter") oder aber als Fusion aller vier Module („*full-size transporter* ") auf. HlyB ist ein Beispiel für einen „*half-size transporter*", d.h. für eine Fusion einer TMD und einer NBD. In Analogie zu anderen ABC-Transportern wird davon ausgegangen, dass ein Homodimer des HlyB die funktional aktive Form bildet. Die NBDs oder Motordomänen der ABC-Transporter können, basierend auf bereits publizierten Kristallstrukuren anderer Systeme, in zwei weitere Subdomänen, der katalytischen und der helikalen Subdomäne, unterteilt werden. Die katalytische Subdomäne, die strukturelle Ähnlichkeit zur F_1-ATPase oder RecA besitzt, beinhaltet das Walker A und B Motiv, die D- und H-Schleife, während die helikale Subdomäne die C-Schleife enthält. Beide Subdomänen werden durch die Q- und Pro-Schleife verbunden.

In der hier vorliegenden Arbeit wurde die isolierte NBD von HlyB (HlyB-NBD) biochemisch und strukturbiologisch analysiert. Im ersten Schritt wurde ein Puffersystem etabliert, die die NBD in Lösung stabilisierten, so dass selbst bei Konzentrationen von 50 mg/ml keine Aggregation für diese NBD nachgewiesen werden konnte. Dadurch konnte der Grundstein für die detaillierte biochemische Charakterisierung gelegt werden. Hier wurde die NBD und funktional relevante Mutanten im Bezug auf ihren oligomeren Zustand und ihre basale ATPase Aktivität untersucht. Gleichzeitig konnten andere Bedingungen bestimmt werden, die die ATPase Aktivität maximal stimulierten. Kinetische Analysen zeigten, dass eine positive Kooperativität sowohl in Abhängigkeit der ATP-Konzentration als auch in Abhängigkeit der Proteinkonzentration auftritt, deren kinetische Parameter bestimmt wurden. Durch die Abhängigkeit der ATPase Aktivität von der Proteinkonzentration konnte der bestimmte $K_{0.5}^{app}$ mit der apparenten Dissoziationskonstante des Dimers (K_D^{app}) gleichgesetzt werden und lieferte somit zum ersten Mal eine thermodynamische Größe für die ATP-induzierte Dimerisierung einer isolierten NBD eines ABC-Transporters. Die Existenz eines Dimers als funktional aktive Einheit während der ATP-Hydrolyse konnte durch Gelpermeationschromatographie eindeutig belegt werden. Neben der detaillierten, biochemischen Charakterisierung der ATPase Aktivität der NBD wurden zwei essentielle Aminosäuren identifiziert, E631 und H662. Durch Untersuchungen an anderen Systemen wurde dem Glutamat an Position 631 der HlyB-NBD die Rolle einer „allgemeinen Base" zugeordnet. Im Falle der HlyB-NBD, zeigte die entsprechende E631Q Mutanten eine deutlich reduzierte, aber immer noch vorhandene ATPase Aktivität, die das Postulat der „allgemeinen Base" in Frage stellte. Im Gegensatz hierzu konnte für die H662A Mutante keinerlei ATPase Aktivität mehr festgestellt werden. Dies implizierte eine essentielle Rolle

dieser Aminosäure während der ATP-Hydrolyse. Die Konservierung dieses Histidins in anderen ABC-Transportern untermauerte dieses Postulat.

Parallel zu den biochemischen Untersuchungen gelang es die Kristallstrukturen des ATP, ATP/Mg^{2+} und ADP-gebundenen Zustandes für die HlyB-NBD zu bestimmen. Somit ist es zum ersten Mal möglich alle katalytischen Zustände der NBD eines ABC-Transporters zu vergleichen. Für den ATP und ATP/Mg^{2+} gebundenen Zustand wurde die H662A Mutante verwendet, da trotz großer Anstrengungen keine Bedingung bestimmt werden konnte, die für das Wildtyp Enzym röntgentaugliche Kristalle lieferte. Die Auflösung der ATP-gebundenen- sowie des ATP/Mg^{2+}-gebundenen Zustandes beträgt 2.6 Å bzw. 2.5 Å. Die Struktur des ATP/Mg^{2+}-gebundenen HlyB-NBD H662A Mutante konnte nicht durch den Ansatz des molekularen Ersatzes mit der bekannten Nukleotid-freien Struktur der HlyB-NBD gelöst werden. Daher wurden Bedingungen entwickelt, die es ermöglichten, Selenomethionin markierte Kristalle der HlyB-NBD zu vermessen. Nach Aufnahme eines Datensatzes nach der Methode der anomalen Streuung musste jedoch festgestellt werden, das diese Kristalle nicht für die Lösung des Phasenproblems verwendet werden konnten. Trotzdem konnten dieser Datensatz verwendet werden, um mittels der Methode des molekularen Ersatzes das Phasenproblem zu lösen. Diese Lösung konnte auf native Kristalle der HlyB-NBD H662A in Komplex mit ATP/Mg^{2+} transferiert werden, und ermöglichte die Bestimmung der dreidimensionalen Kristallstruktur. Der in der asymmetrischen Einheit vorhandene Dimer der HlyB-NBD zeigte eine „*head-to-tail*" Anordnung, welche einen universellen Aufbau der NBD-Dimere der ABC-Transporter darstellt. Hier wird ATP zwischen dem Walker A Motiv des einen Monomers und der C-Schleife des anderen Monomers gebunden. Diese Anordnung wird durch eine ATP-induzierte Bewegung der helikalen Domäne um 18° in Richtung der katalytischen Domäne ermöglicht. Drei von vier molekularen Wechselwirkungen zwischen der C-Schleife und dem gebunden ATP finden mit der γ-Phosphatgruppe des ATP statt. Dies erklärt die ATP-induzierte Dimerisierung auf molekularer Ebene und belegt, dass eine derartige Dimerisierung nur mit ATP aber nicht ADP möglich ist. Im Gegensatz zu den beiden anderen im Verlaufe dieser Arbeit publizierten Kristallstrukturen, MJ0796 und MalK aus *E. coli*, die ebenfalls ATP enthielten und eine analoge Dimerarchitektur aufwiesen, konnten im Falle der HlyB-NBD intensive Protein-Protein Wechselwirkungen im Dimer nachgewiesen werden. So tragen zum Beispiel die C-Termini wesentlich zur Stabilität des Dimers bei. Dies untermauert die Bedeutung des C-Terminus und erklärt experimentelle Befunde an anderen NBDs, die auf eine funktionale Rolle des C-Terminus hindeuteten.

Gleichzeitig konnte basierend auf der ATP bzw. ATP/Mg^{2+} gebundenen Struktur der HlyB-NBD, der D-Schleife eine funktionale Rolle zugewiesen werden. Schon die ersten Sequenzen, die für ABC-Transporter publiziert worden sind, belegten die hohe Konservierung dieser Schleife. In der ATP/Mg^{2+} gebundenen Struktur der HlyB-NBD interagiert die D-Schleife mit der H-Schleife und dem Walker A Motivs des anderen Monomers. Dies impliziert eine Sensorfähigkeit, die es ermöglicht, Informationen aus einer ATP-Bindungsstelle über die D-Schleife in die andere Bindungsstelle zu übertragen. Basierend auf den Kristallstrukturen der HlyB-NBD im ATP und ATP/Mg^{2+} gebundenen Zustand und den oben beschriebenen biochemischen Daten, wurde das „Achsnagel"-Modell postuliert, in dem H662 die essentielle Rolle für die Stabilisierung des Übergangszustandes der ATP-Hydrolyse und für die Monomer-Monomer Kommunikation im Dimer zu ordnet. In diesem Modell kommt E631, das auf Grund eines bisher angenommenen Mechanismus als „allgemeine Base" fungieren sollte, die Rolle einer Plattform zu, die durch Wechselwirkung seiner Seitenkette mit H662 die aktive Konformation der Imidazolseitenkette stabilisiert. Mutationen des E631 würden in diesem Modell die Flexibilität des H662 erhöhen und somit die Stabilisierung des Übergangszustandes der ATP-Hydrolyse reduzieren.

Der ADP gebundene Zustand der HlyB-NBD wurde für das Wildtypenzym, die E631Q und die H662A Mutanten bei 1.6 Å, 1.7 Å bzw. 1.9 Å bestimmt. Das Phasenproblem all dieser Strukturen konnte durch die Methode des molekularen Ersatzes mit der Kristallstruktur des Nukleotid-freien Zustandes als Leitstruktur gelöst werden. Wie für die Nukleotid-freie Struktur, die bei einer Auflösung von 2.6 Å bereits zuvor bestimmt worden war, stellen die ADP-gebunden Strukturen der HlyB-NBD einen Monomer dar. Durch die hohe Auflösung dieser Kristallstrukturen konnte nicht nur strukturelle Analyse der einzelnen Strukturen durchgeführt werden, sondern auch eine detaillierte Analyse der B-Faktoren und des Wassernetzwerkes. Die Ergebnisse dieser Untersuchungen belegten eindeutig, dass die funktionalen Mutationen E631Q und H662A, die die ATPase Aktivität des Enzyms drastisch reduzieren (E631Q) bzw. völlig auslöschen (H662A), keine strukturellen Konsequenzen für den ADP-gebunden Zustand besitzen. Da nun alle Kristallstrukturen des katalytischen Zyklus der HlyB-NBD bestimmt worden sind, konnten die konformationellen Änderungen im Detail untersucht werden. Gleichzeitig konnten die strukturellen Ergebnisse mit der detaillierten biochemischen Analyse verglichen und verifiziert werden.

Im ersten Schritt wurden die konformationellen Änderungen der konservierten Sequenzmotive der NBD, Walker A und B Motiv, Q-, C-, D- und H-Schleife, während des katalytischen Zyklus bestimmt und mit ihrer postulierten Rolle in Beziehung gesetzt. Gleichzeitig konnte ein Modell entwickelt werden, das erklärt wie die Energie, die durch die Hydrolyse von ATP freigesetzt wird, innerhalb des Proteins gespeichert wird, um eine optimale Effizienz zu gewährleisten. Weiterhin gelang es durch die Identifizierung der katalytisch relevanten Aminosäuren der NBD und ihrem Wechselspiel, einen Mechanismus etablieren, den die HlyB-NBD verwendet, um ATP zu hydrolysieren. Dieser Mechanismus, „*substrate assisted cataylsis*" wird ebenfalls in Ras[p21], einer GTPase oder EcoRI und EcoRV angewendet, um die entsprechenden Nukleotidtriphosphate zu hydrolysieren. In diesem Mechanismus abstrahiert das Substrat ATP ein Proton des katalytischen Wassermoleküls und generiert das Hydroxidion, das im nächsten, geschwindigkeitsbestimmenden Schritt die Bindung zwischen der β- und y-Phosphatgruppe des ATP spaltet. Basierend auf dieser Arbeit konnte ein detailliertes Modell entwickelt werden, das beschreibt wie auf molekularer Ebene die chemische Energie, freigesetzt durch die Hydrolyse des ATP, in mechanische Energie, verantwortlich für die Substrattranslokation, umgesetzt wird.

E R K L Ä R U N G

Ich erkläre hiermit, dass ich mich bisher keiner Doktorprüfung unterzogen habe.

Frankfurt am Main, den....................................

....

(Jelena Zaitseva)

Eidesstattliche Versicherung

Ich erkläre hiermit an Eides Statt, dass ich die vorgelegte Dissertation über

"The catalytic cycle of the nucleotide-binding domain of the ABC transporter HlyB"

selbständig angefertigt und mich anderer Hilfsmittel als der in ihr angegebenen nicht bedient habe, insbesondere, dass aus Schriften Entlehnungen, soweit sie in der Dissertation nicht ausdrücklich als solche mit Angabe der betreffenden Schrift bezeichnet sind, nicht stattgefunden haben.

Frankfurt am Main, den...

(Jelena Zaitseva)

JELENA ZAITSEVA

Home address:
3924 Spring Hill Dr
Lawrence, KS 66049, USA
Home phone: (785)-331-3626

Citizenship: Estonia
(U.S. permanent resident)

EDUCATION

M.S. in Biochemistry, Moscow State University, Moscow, Russia – 1988
B.S. in Biochemistry, Moscow State University, Moscow, Russia – 1987

RESEARCH EXPERIENCE

2001- 2005   Ph.D. student, Institute of Biochemistry, Biocenter, Johann-Wolfgang Goethe
University Frankfurt, Germany
Laboratory head – Prof. Dr. R Tampé; head of research group – Dr. L. Schmitt
Study of HlyA-toxin secretion transmembrane complex in *E.coli*
- Functional and structural characterization of ATP-binding cassette (ABC) of HlyA transporter
- Purification and crystallization of ABC-protein in various functional states
- Studying the structure-functional relationships in the ABC-protein
- Elucidation of HlyA transport mechanism

1994 - 2001   Research Associate, Biochemistry Department, Purdue University, USA
Laboratory headed by Prof. M. Hermodson
Study of high affinity membrane transport of ribose in *E.coli*
- Use of chimeric protein constructs for purification and characterization of hydrophobic constituent of the transporter
- Solubilization and purification of membrane proteins in the presence of various detergents
- Functional reconstitution of membrane proteins in liposomes
- Study of protein-protein interactions in the transporter
- Development of assays for evaluation of membrane transport and enzymatic activity *in vitro*
- Site-directed mutagenesis
- PCR-based cloning
- Construction of vectors for protein overexpression
- Raising and purification of polyclonal antibodies
- Protein crystallization

1992 - 1994   Laboratory technician, Biochemistry Department, Purdue University, USA
Laboratory headed by Prof. M. Hermodson
- Variety of laboratory tests on bacteria
- Cultivation and maintaining of bacterial strains
- DNA recombination and cloning

- Overproduction of bacterial soluble and integral membrane proteins
- Protein purification and analysis (SDS-PAGE, Western blot, isoelectric focusing, enzymatic methods, column chromatography, 2D-electrophoresis, circular dichroism)

1988 - 1992   Senior Laboratory Technician, Cosmetology Research Institute, Moscow, Russia
New Cosmetic Products R&D Laboratory headed by Prof. N.B. Koroleva
- Toxicity evaluation of specific cosmetic compounds on various laboratory animals
- Study of the effect of those compounds on intracellular metabolism of skin cells (DNA and RNA level, qualitative-quantitative lipid composition, protein synthesis)
- Activity measurements of skin enzymes (tyrosinase, collagenase and other proteases)

1987 - 1988   Graduate Research Assistant, Cosmetology Research Institute, Moscow, Russia
New Cosmetic Products R&D Laboratory headed by Prof. N.B. Koroleva
Impact of α-tocopherol derivatives and their permeation through the skin barrier after external application

1986 - 1987   Graduate Research Assistant, Shemyakin Institute of Bioorganic Chemistry, USSR Academy of Sciences, Moscow, Russia. Protein Research Laboratory headed by Prof. Yu.A. Ovchinnikov
Extraction and purification of adenylate cyclase from bovine brain

OTHER PROFESSIONAL EXPERIENCE

- Teaching Assistant for Biochemistry Lab Courses; top rank among all TA's based on students' teaching evaluations – Institute of Biochemistry, Goethe University Frankfurt, Germany; Spring 2003

- Supervising laboratory technicians, rotation graduate students, and graduate students involved in M.S. and Ph.D. projects in Biochemistry, Purdue University, 1994 - 2001

- Computer skills: gene/protein analysis, database search, crystallographic data processing

PUBLICATIONS

Zaitseva, J., Jenewein, S., Jumpertz, T., Holland, I. B., and Schmitt, L. (2005). H662 is the linchpin of ATP hydrolysis in the nucleotide-binding domain of the ABC transporter HlyB. *Embo J 24*, 1901-1910.

Zaitseva, J., Jenewein, S., Wiedenmann, A., Benabdelhak, H., Holland, I. B., and Schmitt, L. (2005). Functional characterization and ATP-induced dimerization of the isolated ABC-domain of the haemolysin B transporter. *Biochemistry 44,* 9680-9690.

Zaitseva, J., Jenewein, S., Oswald, C., Jumpertz, T., Holland, I. B., and Schmitt, L. (2005). A molecular understanding of the catalytic cycle of the nucleotide-binding domain of the ABC transporter HlyB. *Biochem Soc Trans 33, part 5,* 990-995.

Hanekop, N., **Zaitseva, J.,** Jenewein, S., Holland, I. B., and Schmitt, L. (2005). Molecular insights into the mechanism of ATP hydrolysis by the NBD of the ABC-transporter HlyB. *FEBS Lett.* In Press.

Zaitseva, J., Holland, I. B., and Schmitt, L. (2004). The role of CAPS buffer in expanding the crystallization space of the nucleotide-binding domain of the ABC transporter haemolysin B from *Escherichia coli. Acta Crystallogr D Biol Crystallogr 60*, 1076-1084.

Zaitseva, J., Zhang, H., Binnie, R. A., and Hermodson, M. A. (1996). The proteins encoded by the *rbs* operon of *Escherichia coli*: II. Use of chimeric protein constructs to isolate and characterize RbsC. *Protein Science 5*: 1100-1107.

Koroleva N. B., and **Zaitseva, J. V.** (1992) Liposomes in cosmetology. *Sbornik Trudov Moskovskogo Instituta Cosmetologii* (in Russian).

Zaitseva, J. V. (1990). Effect of D,L-α-tocopheryl phosphate and acetate on the skin of various age animals. *Sbornik Trudov Moskovskogo Instituta Cosmetologii* (in Russian).

Gurochkina, L. P, and **Zaitseva, J. V.** (1990) Effect of vitamin E and its derivatives on animal skin after external application. *Sbornik Trudov Moskovskogo Instituta Cosmetologii* (in Russian).

Zaitseva, J. V. (1988). Impact of D, L-α-tocopherol derivatives and their permeation through the skin barrier after external application, *M.Sc. thesis, Moscow State University* (in Russian).

MANUSCRIPTS IN PREPARATION

Zaitseva, J., Oswald, C., Jumpertz, T., Jenewein, S., Wiedenmann, A., Holland, I. B., and Schmitt, L. (2005). A structural analysis of hinges, springs, and inherent asymmetry required for functional activity of an ABC ATPase domain. Manuscript in preparation.

Zaitseva, J., and Hermodson, M.A. (2005). Reconstitution studies on the membrane transport complex for ribose in *Escherichia coli*. Manuscript in preparation.

ABSTRACTS / PRESENTATIONS

Zaitseva J., I.B. Holland, and L. Schmitt, 2003, "The ATP-bound sandwich dimer of the ATP-binding domain of the ABC-transporter haemolysin B from *E. coli*," *DESY Annual Report*, Germany.

Zaitseva J., A. Wiedenmann, I.B. Holland, and L. Schmitt, 2003, "Structure-function analysis of the ATP-binding domain of the ABC-transporter haemolysin B from *E. coli*," *DESY Annual Report*, Germany.

Zaitseva J., I.B. Holland, and L. Schmitt, 2002, "Structure of the ABC-domain of the HlyB-NBD in a complex with ADP," *DESY Annual Report*: 489-490, Germany.

Zaitseva, J., and M. Hermodson, October 2000, "Investigation of the ribose transporter components of *E.coli*: Part I. Purification and crystallization of RbsD. Part II. Testing of various detergents for the preparation of active proteoliposomes," presented at the Biochemistry Department Research Seminar, Purdue University, West Lafayette, Indiana, USA.

Zaitseva, J., and M. Hermodson, November 1998, "Functional reconstitution of the *Escherichia coli* ribose transporter into lipid vesicles," presented at the Fourth Annual Purdue University Biophysics Symposium, West Lafayette, Indiana, USA.

Zaitseva, J., and M. Hermodson, July 1998, "Functional and structural characterization of the membrane-associated ribose transporter in *Escherichia coli,*" Poster Presentation at the 12th Annual Symposium of the Protein Society, San Diego, California, USA.

Zaitseva, J., and M. Hermodson, May 1997, "Functional reconstitution of the membrane-associated ribose transporter of *E.coli*," presented at the Biochemistry Department Research Seminar, Purdue University, West Lafayette, Indiana, USA.

Hermodson M., H. Zhang, S. Armstrong, **J. Zaitseva,** and C. Stauffacher, October 1996, "Structural analysis of the ribose membrane transporter of *E.coli*," presented at the Second Annual Biophysics Symposium, Department of Biological Sciences, Purdue University, West Lafayette, Indiana, USA.